Mass Spectrometry Imaging to inform on the pathology of Age-Related Macular Degeneration

Joshua Millar

A thesis submitted in partial fulfilments of the requirements of Sheffield Hallam University for the degree of Doctor of Philosophy

in collaboration with Trinity College Dublin, University of Dublin

April 2024

Candidate Declaration

I hereby declare that:

- I have not been enrolled for another award of the University, or other academic or professional organisation, whilst undertaking my research degree.

- None of the material contained in the thesis has been used in any other submission for an academic award.

- I am aware of and understand the University's policy on plagiarism and certify that this thesis is my own work. The use of all published or other sources of material consulted have been properly and fully acknowledged.

- The work undertaken towards the thesis has been conducted in accordance with the SHU Principles of Integrity in Research and the SHU Research Ethics Policy. The µPIXE work carried out in Chapter 4 was carried out in part by staff at the UK National Ion Beam Centre, the work of which is attributed to them in the Author Contribution section of the chapter. I played a major role in the preparation of these samples; in addition, the data analysis and interpretation are entirely my own work.

- The word count of this thesis is 52876

Name	Joshua Millar
Award	PhD
Date of Submission	16/04/2024
Faculty	Health & Wellbeing
Director of Studies	Laura Cole

Acknowledgements

Having first stepped foot in Sheffield in 2015 for my undergraduate degree, little did I know that I'd still be enrolled at Hallam almost 9 years later. In that time, and most vitally in the years of my PhD I have found great comfort in a wildly vibrant and interesting research community made up of wonderful people who I owe so much to.

It would be wrong not to start these acknowledgements with my supervisor Laura, who not only decided (whether it be advisable or not) to believe in me and encourage me to pursue a career in research but has stuck with me all these years! As a mentor, and as a friend she has been infallible in her support for me, she most definitely has solidified my passion for MSI.

I also owe a great deal to the technical staff at Hallam, namely Mick Cox, who, despite perhaps helping me to delay my work through idle chat over a plasma torch, has supplied his experience and expertise consistently and without complaint.

I also would like to thank a great number of people within the field for their time taken to share their knowledge with me and help me grow as an individual researcher; Rob Hutchinson (Horton) for endless laser ablation & burrito days, David Price for his ICP guidance and can-do attitude, Malcolm Clench for his 'no-nonsense' advice, & Simona Francese for sharing her research (and some media training) with me.

There are almost too many individuals to name within the student offices at the BMRC, for all their help, and companionship, that thankfully has continued. It would be amiss to not mention the endless trips for bananas with Sam, Greggs with Chloe, pints with Joe, long drinks with Alex, coffees with Katie & squash with Lucy. I'll miss forced hugs from Andrea, and having Tim as a reliable companion in the Red Lion.

Thanks also must go to the rest of my supervisory team; Catherine (who rightly jumped ship) for inspiring some amazing ICP-MS work, Sue, for helping with endless drafts, and to Sarah for welcoming me into her lab group.

Finally, to Shannon, my partner in life, who is currently pulling her hair out over her own thesis, who has consistently, and patiently supported me through an era of life so turbulent and unstable it makes James Cameron's *Titanic* seem like a pleasant film about a cruise.

Table of Abbreviations

Abbreviation	Phrase
1,5-DAN	1,5-Diaminonaphthalene
2D	Two-Dimensional
9AA	9-Aminoacridine
AAS	Atomic Absorption Spectrometry
ACN	Acetonitrile
AEM	Analytical Electron Microscopy
AMD	Age-Related Macular Degeneration
AREDS	Age Related Eye Disease Study
AU	Arbitrary Units
BrM	Brusch's Membrane
C3	Complement Component Three
C5a	Complement Component 5a
CARD	Caspase Recruitment Domains
CC	Chorio Capillaris
CCS	Chaperone For Superoxide Dismutase
CHCA	A-Hydroxycinnamic Acid
CHCl3	Chloroform
ClCCA	4-Chloro-A-Cyano-Cinnamic Acid
CLIC4	Chliride Intracellular Channel 4
CLMC	Continuous Lock Mass Correction
CLR	C-Type Lectin
CMC	Carboxymethylcellulose
CRP	C-Reactive Protein
Da	Dalton
DAMPS	Damage Associated Molecular Patterns
DESI	Desorption Electrospray Ionisation
DHB	2,5-Dihydroxybenzoic Acid
EFP	Encoded Frequent Pulsing
ELISA	Enzyme-Linked Immunosorbent Assay
ESI	Electrospray Ionisation
ESL	Elemental Scientific Lasers
EtOH	Ethanol
FCM	Flow Cytometry
FWHM	Full-Width At Half Maximum
gAcOH	Glacial Acetic Acid
HABA	2-(4-Hydrocyhenylazo) Benzoic Acid
HDMS	High Definition Mass Spectrometer
HFIP	1,1,1,3,3,3-Hexafluoropropanol
HMDB	Human Metabolome Database
Hz	Hertz
IBA	Ion Beam Analysis
ICP	Inductively Coupled Plasma
IL-6	Interleukin 6
IL-8	Interleukin 8

INL	Inner Nuclear Layer
IPL	Inner Plexiform Layer
IPL	Inner Plexiform Layer
IS	Inner Segment
ITO	Indium Tin Oxide
KED	Kinetic Energy Discriminatory
LA	Laser Ablation
LESA	Liquid Extraction Surface Analysis
LRR	Leucine-Rich Repeat
m/z	Mass To Charge Ratio
MALDI	Matrix Assisted Laser Desorption Ionisation
MeOH	Methanol
mL	Millilitres
MRT	Multi-Reflecting TOF
MS	Mass Spectrometry
MSI	Mass Spectrometry Imaging
MYD88	Myeloid Differentiation Primary Response 88
NA	Nicotinic Acid
NACHT	NAIP (Neuronal Apoptosis Inhibitor Protein), C2TA (Class 2 Transcription Activator), of the MHC, HET-E (Heterokaryon Incompatibility) and TP1 (Telomerase-Associated Protein 1)
NAD+	Nicotinamide Adenine Dinucleotide
NB	Nanobeam
ND	Neutral Density
Nd:YAG	Neodymium-Doped Yttrium Aluminium Garnet NIH National Institutes of Health
NF-κB	Nuclear Factor Kappa-Light-Chain-Enhancer of Activated B Cells
NIBC	National Ion Beam Centre
NIH	National Institute of Health
NLR	NOD Like Receptor
NLRC4	NLR Family CARD Domain-Containing Protein 4 Complex (NAIP-NLRC4)
NLRP1	NACHT, LRR And PYD Domains-Containing Protein 1
NLRP3	NACHT, LRR And PYD Domains-Containing Protein 3
NMNAT1	Nicotinamide Mononucleotide Adenylyltransferase 1
OA	Orthogonal Acceleration
OcGlc	Octyl-A/B-Glucoside
ONL	Outer Nuclear Layer
OPL	Outer Plexiform Layer
OS	Outer Segment
PAMPs	Pattern Associated Molecular Patterns
PC	Phosphatidylcholine
PCA	Principle Component Analysis
PET	Polyethylene Terephthalate
PET	Polyethylene Terephthalate

PIPS	Passivated Implanted Planar Silicon
PIXE	Particle Induced X-Ray Emission
PLS-DA	Partial Least Squares- Discriminant Analysis
ppm	Parts Per Million
ppq	Parts Per Quadrillion
Proteasome assembly chaperone 4	Proteasome Assembly Chaperone 4
PRR	Pattern Recognition Receptors
psi	Pounds Per Square Inch
PYD	PYRIN Domain
QID	Quadrupole Ion Deflector
qToF	Quadrupole Time-Of Flight
RFLPs	Restriction Fragment Length Polymorphism
RHO	Rhodopsin
RLRs	RIG-I-Like
ROI	Region Of Interest
ROS	Reactive Oxygen Species
RP	Retinis Pigmentosa
RPE	Retinal Pigment Epithelium
RT-PCR	Reverse Transcription Polymerase Chain Reaction
SA	3,5-Dimethoxy-4- Hydroxycinnamic Acid
SARM1	Sterile Alpha and Toll/Interleukin-1 Receptor Motif–Containing 1
SDD	Silicon Drifted Detector
SOD1	Superoxide Dismutase
STD	Standard Mode
TFA	Trifluoroacetic Acid
TLR2	Toll Like Receptor 2
TLR3	Toll Like Receptor 3
TLR4	Toll Like Receptor 4
TOF	Time-of-Flight
UKNIBC	United Kingdom National Ion Beam Centre
UMAP	Uniform Manifold Approximation And Projection
VIP	Variable Importance In Projection
WB	Western Blot
WHO	World Health Organisation
WT	Wildtype
µg	Microgram
µL	Microlitres
µm	Micrometres

Table of Contents

Table of Figures

1.0. Chapter 1 Figures

2.0. Chapter 2 Figures

3.0. Chapter 3 Figures

4.0. Chapter 4 Figures

5.0. Chapter 5 Figures

6.0. Chapter 6 Figures

7.0. Chapter 1 Tables

8.0. Chapter 2 Tables

9.0. Chapter 3 Tables

10.0. Chapter 6 Tables

Abstract

Mass Spectrometry Imaging (MSI) has been developed significantly in the past few decades and has been transformed into a technique that not only allows for spatial mapping of analytes of interest but is a key tool in biomarker and medicinal discovery. At Sheffield Hallam University, research using matrix-assisted laser desorption ionisation (MALDI-MSI) has propelled ocular research, oncological research, and many other fields. Additionally, the use of laser ablation inductively coupled plasma mass spectrometry imaging (LA-ICP-MSI) has been fruitful for investigations into the ocular pathology of uveal melanoma, and desorption electrospray ionisation mass spectrometry imaging (DESI-MSI) has aided research into certain cancers through biomarker research. These techniques however are seldom combined to create multifaced datasets and had yet to be applied to age-related macular degeneration (AMD) research. Furthermore, the field of ocular pathology has benefitted greatly from decades of extensive immunological research into age-related macular degeneration. More recently, Doyle et al. at Trinity College Dublin have been using immunological techniques to investigate AMD and its pathology, in addition to the wider innate immune system. However, there have been few studies in AMD research that have built upon these works with MS.

The work conducted herein offers a platform on which further ocular research can be built. Through utilisation of DESI-MSI for the detection of lipids, MALDI-MSI for the detection of peptides, LA-ICP-MSI for the detection of metals, and micro-particle induced X-ray emission (μPIXE) for the detection of other elements this work has developed a multimodal workflow whereby a rich dataset can be obtained from ocular tissue.

The aforementioned immunological techniques have provided great insight into the ocular proteome but reply heavily on antibody specificity. There have been instances where this specificity has been called into question, undermining otherwise reputable research, which has intimated there may be a role for untargeted techniques such as MS in ocular pathology. The development of a high-resolution peptide imaging strategy using tailored sample preparation techniques and employment of modern sample preparation apparatus has provided key initial steps for the discovery of biomarkers of AMD in the ocular proteome (Chapter 2,3). Within this study, employment of this strategy aided the research into the human ocular proteome (Chapter 5) through the tentative identification of NLRP3 peptides within the human retina, which has been subject to ongoing debate as a result of immunological reagent specificity.

Literature data has clearly linked the metallome to the onset of AMD, and has recommended supplementation of zinc and copper to protract AMD onset, but there is no clear role for these metals in AMD pathology. With existing studies infrequently using high resolution imaging, and rarely applying quantitative dimensions, there is adequate appeal for clarity on the involvement of essential trace elements in the ocular anatomy. Development and deployment of a semi quantitative imaging strategy for copper and zinc within the ocular anatomy (Chapters 3,4) was able to demonstrate the high spatial resolution imaging capacities achievable using biological tissue by LA-ICP-MSI. Furthermore, the application of this strategy to wildtype and transgenic ocular mouse tissues was able to give an insight into the ocular metallome, and when combined with µPIXE

(Chapter 4) could show how trace elements interact with the substructures of the ocular structure in the context of retinal degeneration.

With an increasing number of studies utilising untargeted lipidomic data to identify potential biomarkers of disease, there was also scope to include the use of MSI to investigate lipidomics. Using DESI-MSI (Chapter 5) lipid profiles of multiple wildtype and transgenic mouse ocular tissue was characterised and processed using statistical analysis. Additionally, through use of the ‘soft’ ionisation provided by DESI, MALDI-MSI experiments were able to take place in tandem with DESI analysis, allowing 2 datasets to be obtained from a single tissue. With the previous demonstration (Chapter 2) of the efficacy of LA-ICP-MSI on biological tissues previously analysed by MALDI-MSI, this body of work has provided the tools necessary for a 3-technique multimodal approach to imaging of ocular tissue. Consequently, through method development and optimisation for multiple imaging strategies, and the demonstration thereof, this body of work has contributed significantly to the field of ocular pathology by MSI.

Chapter 1

Introduction

Introduction

1.0. The Eye and Ocular Disease

Ocular tissue is a complex anatomical system constituted by multiple tissue types, organised in a highly structured, and highly privileged manner. It consists primarily of distinct layers, starting with the bloody supply, in the choriocapillaris (CC), which provides the eye with the necessary nutrients and oxygen from the blood. The layers that constitute the outer blood-retinal barrier follow from this; the Bruch's membrane (BrM), a fibrous membrane that in part forms a basement membrane of the choriocapillaris, and the retinal pigment epithelium (RPE) a monolayer of pigmented hexagonal epithelial cells which are highly ordered in their structure.[1] The inner blood retinal barrier contains the photoreceptors: the outer segment (OS) and inner segment (IS); the outer nuclear layer (ONL) and outer plexiform layer (OPL), the inner nuclear layer (INL) and inner plexiform layer (IPL), all which kay a crucial role in ocular function.

Disruption of this otherwise balanced structure can lead to the onset of ocular diseases, that without viable treatment may lead to visual impairment.[2] There are many kinds of ocular disease, but those which affect the retina can be devastating to ocular health, resulting in irreversible loss in vision. Diseases such as diabetic retinopathy, age-related macular degeneration, and retinitis pigmentosa all affect this region of the eye and can manifest as reduced vision or localised blindness.[3-5] Depending on the severity, ocular disease can lead to progressive blindness, meaning patients can suffer from great decreases in

quality of life, and may become legally blind.[6-8] If the prognosis of the disease is poor, the risk of these outcomes becomes every increased. Many ocular disease types are increasingly preventable as advances in medicine help to understand these diseases, but in some cases, modern medicine has led to an increase in instances of disease as the privilege of advanced age is considered a risk factor.[6-9]

1.1. Age-related macular degeneration

1.1.1. What is AMD?

Age-related macular degeneration remains one of the greatest threats to ocular health within industrialised countries. It is an ocular degenerative disease, affecting the macular region of the eye, which is the region situated directly opposite the pupil, and is densely populated with cones and rods. Though the symptoms can be similar, there are two types of AMD, wet, and dry. Wet AMD is caused by neovasculature within the macula region, which invades the chorio-retinal microanatomy, breaking the blood-retinal barrier (BRB) and rupturing, causing damage to receptors (Figure 1). Dry AMD causes retinal damage through build-up of extracellular material known as drusen and is characterised by retinal pigment epithelium (RPE) degradation, choriocapillaris (CC) drop-out and thickening of the Brusch's membrane (BrM) (Figure 1).[4,5,10]

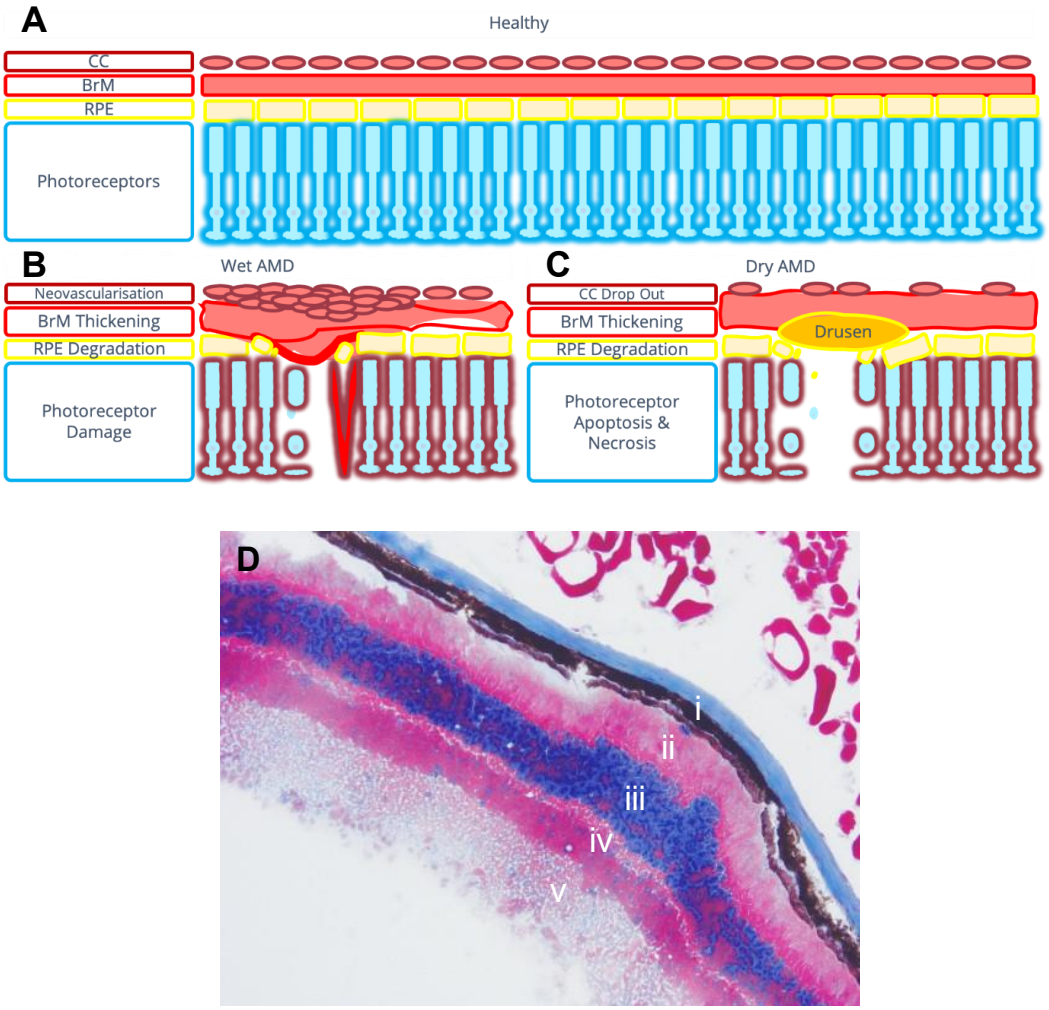

Figure 1 (A) ***Healthy****: the microanatomy of a healthy retinal region, with a highly conserved structure, uniformity and healthy exchange of blood & nutrients in the otherwise highly privileged anatomy of the retina. (B)* ***Wet AMD****: invading choroidal neovasculature that subsequently disrupts and degrades the RPE, and can invade even further to the photoreceptors, breaking down the blood-retinal barrier, causing damage to photoreceptors. (C)* ***Dry AMD****: Build-up of extracellular matter known as drusen, breakdown of the RPE, and photoreceptor apoptosis and necrosis, with BrM thickening and dropout of the CC (D)* ***Histological stain*** *showing mouse ocular tisssues & the i. choriocapillaris ii. Photoreceptors iii. Outer nuclear layer iv. Inner nuclear layer v. inner plexiform layer.*[4,5]

1.1.2. Prevalence

AMD is an age-related disease, and predominately affects over 60s.[11] Currently, there are over 200 million patients worldwide, affecting 8.7% of the population. However, as industrialised countries experience ageing populations, and a greater number if people benefit from improved healthcare, populations around the world will start to experience higher incidences of age-related ocular diseases such as AMD.[11] As indicated by a study in 2013., the incidence of AMD in England and Wales is so prevalent that AMD accounts for over half of legal blindness (Figure 2).[12] AMD can be seen in other industrialised countries, with European studies indicating that the occurrence of AMD in those over 70 years old to be 16.2%. The same study also concluded that by 2050, incidences of AMD will increase from 400,000 to 700,000 per year.

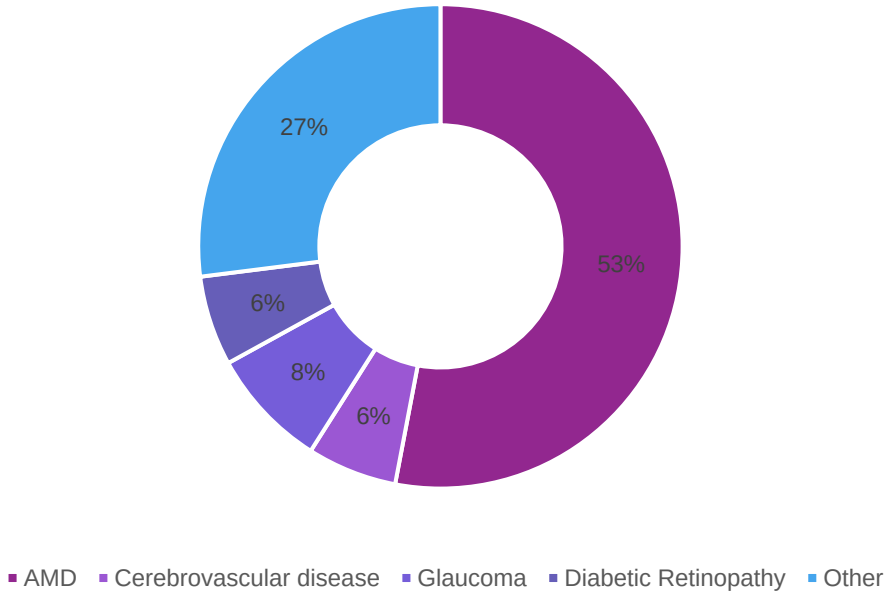

Figure 2 A figure representing the ocular diseases that are responsible for legally recognised blindness in England and Wales as part of a 2013 study by Quartihlo et al. showing the prevalence of AMD in the population of England and Wale in comparison to other diseases such as diabetic retinopathy or glaucoma.[12]

S

1.1.3. Prognoses

Prognoses for AMD patients can be poor, and treatment limitations often lead to poorer outcomes. Though the outcomes are similar, the prognoses difference between wet and dry AMD is appreciable. For those patients with wet AMD, though the disease is relatively slow to progress, treatments are available in the form of intravitreal injection.[13,14] Typically administered by a general practitioner on a monthly basis, these injections, primarily containing antiangiogenics such as bevacizumab, are effective at slowing or even stopping the further progression of wet AMD.[7,13] Despite their efficacy in preventing the generation of neovasculature, treatment is not prescribed to reverse damage which may impact vision.[7] Additionally, as intravitreal injections are known to cause discomfort in patients, there have been cases where patients elect not to proceed with treatment, as though AMD can greatly reduce quality of life, it is not considered life threatening.[6,15]

However, dry AMD represents 10-15% of all AMD cases however has a poorer prognosis.[16,17] Dry AMD can be slow to progress, however preventing or halting the progression of dry AMD is considered vital to the conservation of vision. Due to the complexity and relative differences in the aetiology between dry and wet AMD, dry AMD cannot be treated by the same means. Moreover, there is currently no pharmaceuticals on the market for the treatment of dry AMD, meaning those diagnosed are encouraged to maintain the best quality of life, however, cannot have their vision preserved nor restored.[8]

1.2. The Innate Immune System

The pathology of both wet and dry AMD is poorly understood, however one of the most heavily implicated factors in AMD pathology is the innate immune system.[18] The innate immune system contains phagocytic cells, epithelial and endothelial cells to help combat stimuli. The phagocytic cells consist of granulocytes, monocytes/macrophages, and dendritic cells. Through expression of different proteins, the cells can be involved in not only phagocytosis but in the inflammatory process as well.[19] Unlike the adaptive immune system which uses B-cells and T-cells to recognise foreign bodies, the innate immune system reacts to stimuli in a less specific manner.[19] One of the ways the innate immune system provides protection from harmful stimuli is by controlling the expression of a class of proteins known as pattern-recognition receptors (PRRs) which recognise danger associated molecular patterns (DAMPs) and pathogen associated molecular patterns (PAMPs) and trigger the inflammatory response that helps to mitigate harmful stimuli.[18,20,21] However, chronic sterile inflammation as a result of an overactive innate immune system has been identified as a factor in AMD pathogenesis (Figure 3).[18,22,23] PRRs consist mainly of toll-like (TLRs), NOD-like (NLRs), C-Type Lectin (CLRs) and RIG-I-like (RLRs) receptors, which are expressed mostly within cells pertaining to the innate immune system. Specific PRRs within the innate immune system have further been implicated in the onset of AMD, such as NACHT, LRR and PYD domains-containing protein 1 and 3 (NLRP1/3), NLR family of apoptosis inhibitory protein inflammasome and NLR family CARD domain-containing protein 4 complex (NAIP-NLRC4), TLRs 2-4, and Sterile alpha and Toll/interleukin-1 receptor motif–containing 1 (SARM1).

However, the specific role they play remains elusive, limiting their viability as therapeutic targets as the field remains in infancy[18,24,25]

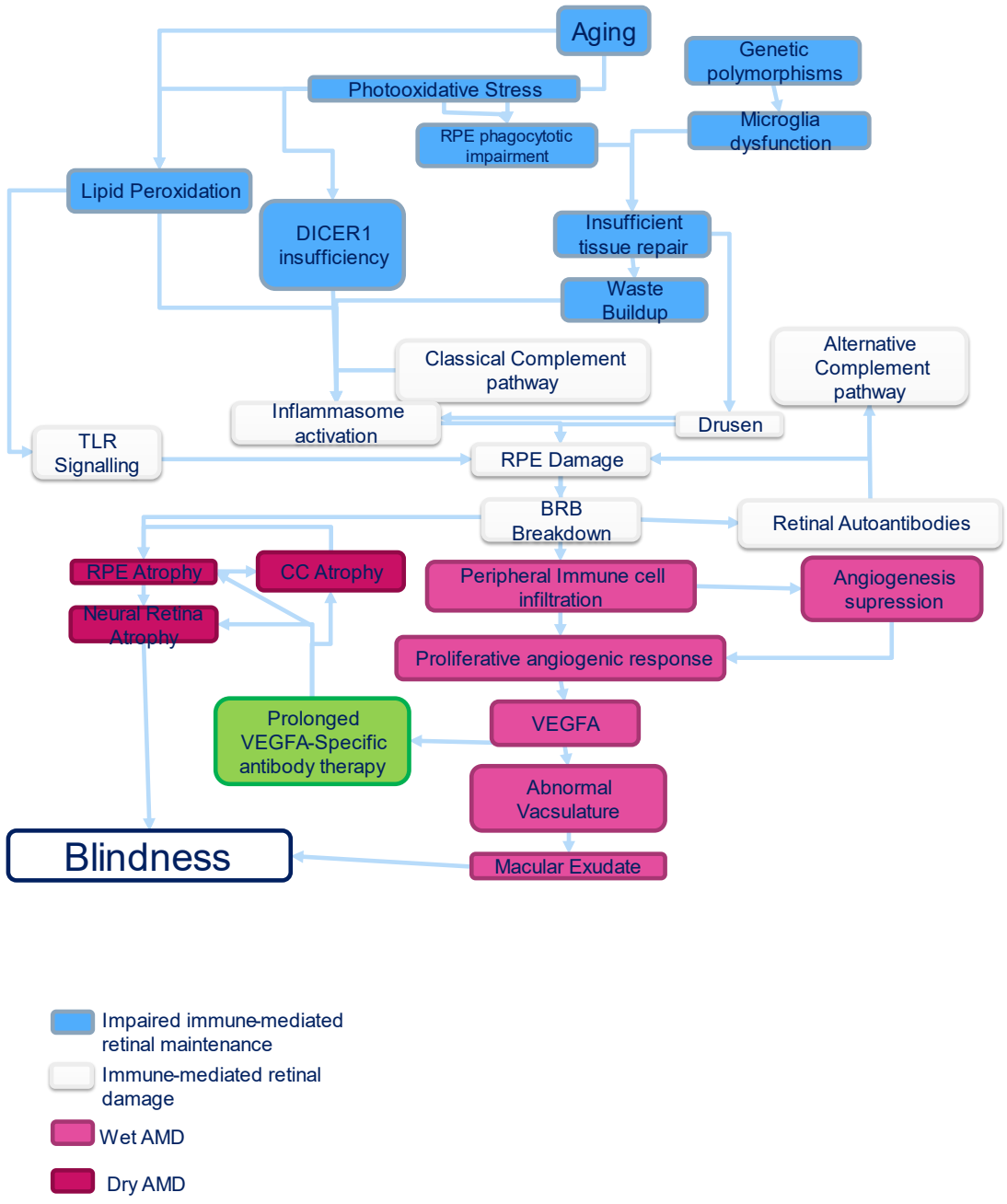

Figure 3 A scheme adapted from Ambati et al. showing how age and innate immunity are related within the context of age-related macular degeneration.[23]

TLRs are membrane spanning PRRs, 10 of which are expressed in humans.[26] They span the membranes of immune cells such as monocytes, macrophages, dendritic cells, B-cells, T-cells and mast cells however have also been recorded in the RPE.[27,28] Through their ability to recognise PAMPs and DAMPs, TLRs act as a prerequisite for the innate immune response (

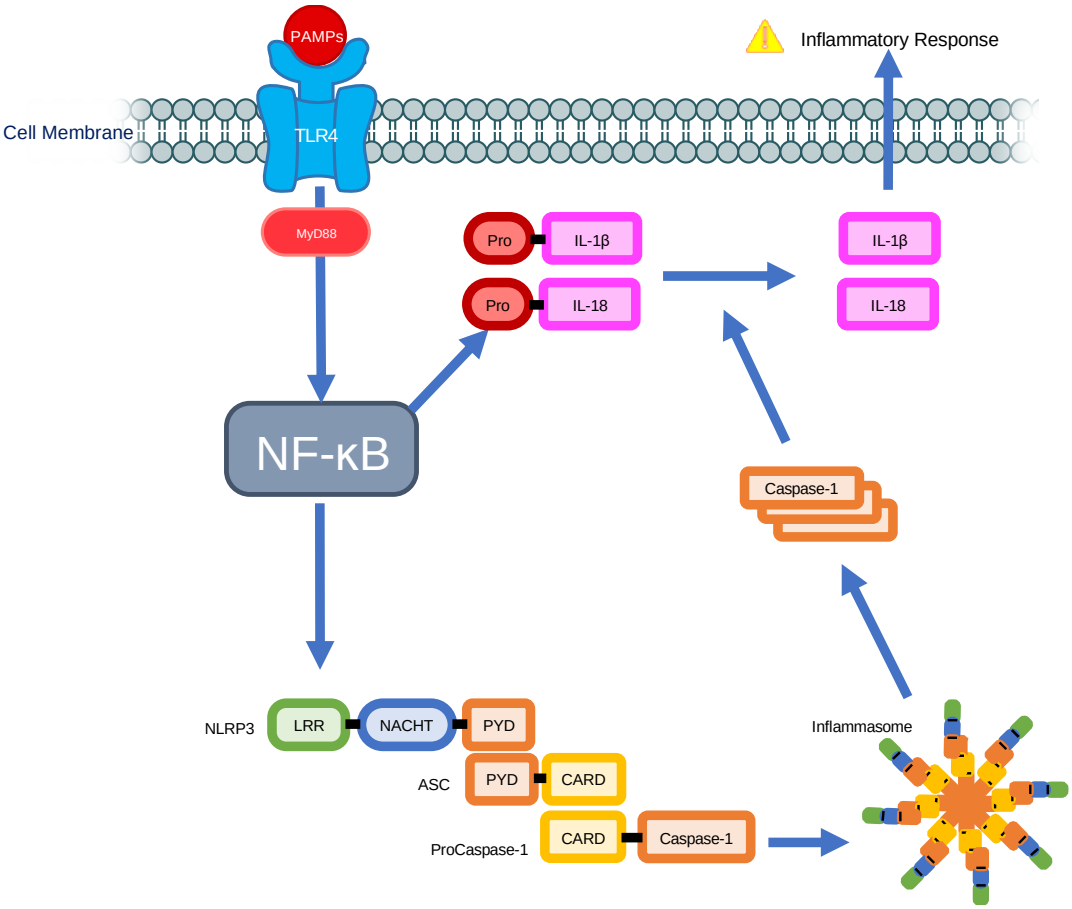

Figure 4). Using MyD88 and NF-κB mediated pathways, they are responsible for the release of proinflammatory cytokines, induction of autophagy, and assembly of the inflammasome.[29]

TLR response to tissue injury, repair and regeneration is crucial to physiological function, and so dysregulation of TLRs in people over 60 as a result of inferior metabolic function, or genetic predisposition could be crucial

to the onset of chronic inflammation and photoreceptor death within AMD patients.[30] Indeed, in diseases such as atherosclerosis and tuberculosis, the functions of TLRs can be damaging through induction of autophagy via activating the expression of DNA damage-regulated autophagy modulator 1 (DRAM-1) expression, or chronic inflammation through release of cytokine, chemokine, and matrix metalloproteinase-1.[21,29]

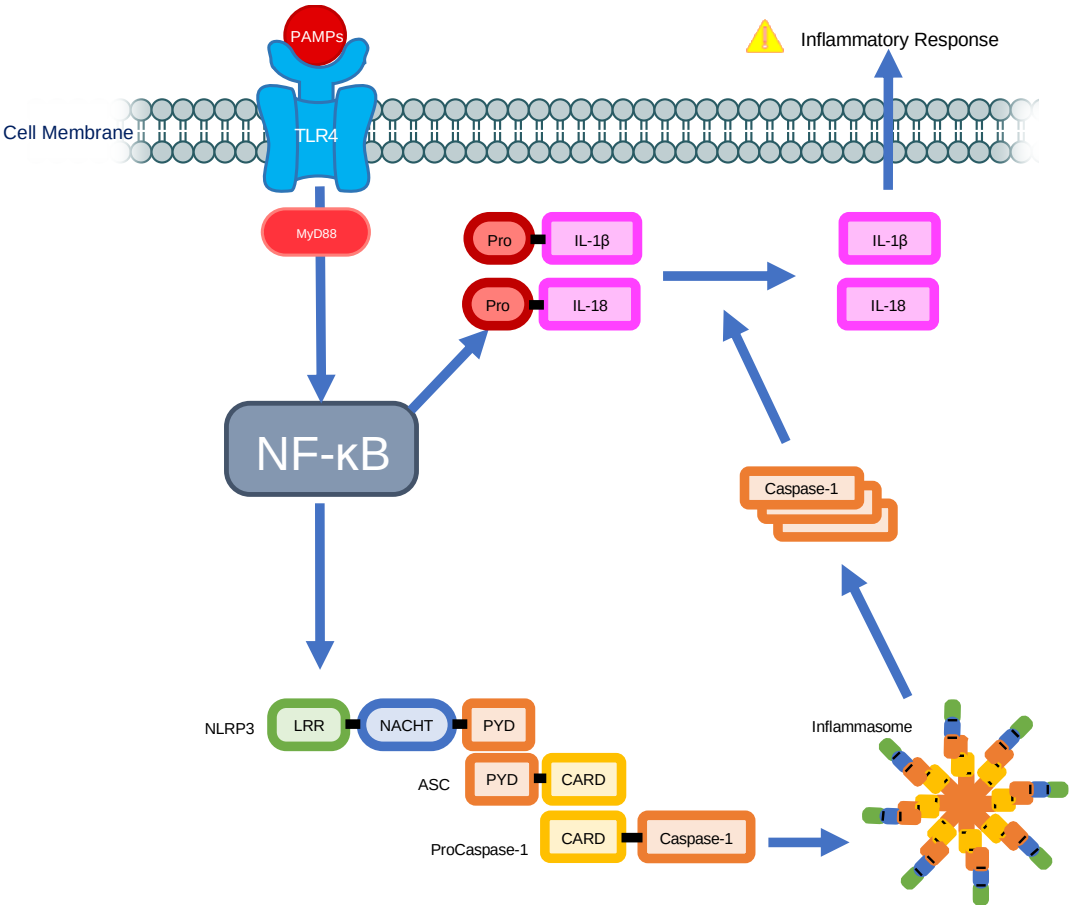

Figure 4 A schematic adapted from Guo et al.. exhibiting the relationship between the detection of pattern associated molecular patterns (PAMPs) and the inflammatory response, via a MyD88 and NF-κB mediated pathway that forms the NLRP3 inflammasome.[22]

Studies have linked certain TLR genetic polymorphisms to AMD susceptibility, such as TLR2[31], TLR3[32,33] and TLR4 [31,32,34-36]. In addition to their genetic association, there are studies that link TLRs to the symptoms of AMD, such as a 2010 study by Fujimoto *et al.* which found that *Chlamydia pnemoniae* infection produced choroidal neovascularisation (CNV) in a TLR2 (and MyD88) dependent manner.[37] Similarly, West *et al.* found that TLR2 caused CNV in a MyD88-dependant manner in reaction to ω-(2-carboxyethyl) Pyrrole (CEP). The findings of West *et al.* could be significant as CEP and other carboxyalkylpyrroles are a product of oxidative stress, which is known to occur in AMD.[38]

TLR2 has also been implicated in the mediation on oxidative damage and complement-mediated AMD, with TLR2 deficiency providing protection from opsonizing fragments of complement component 3 (C3) in the outer retina and oxidative stress induced degeneration.[39,40] Additionally, the same study showed that TLR2 deficiency also helped protect the RPE from fragmentation and ultimately conserve the privilege provided by the BRB. [40]

It has also been shown that in AMD, microglia necroptosis-mediated inflammation was dependant on TLR4 signalling, meaning that TLR4 may contribute to the production of DAMPs in AMD.[41,42] Furthermore, as elevated complement component 5a (C5a) levels are associated with AMD, the finding that C5a could upregulate TLR4 in the RPE and cause the subsequent

production of cytokines interleukin (IL) 6&8 adds to the potential involvement of TLR4 in AMD.[43]

There have however been contradictory conclusions, Elner *et al.* for example found TLR4 to be involved with IL-6 and IL-8 production, supported by Zhu *et al* who found IL-8 production was reduced in the presence of a TLR-blocking monoclonal antibody. [43-46] However, Monaco *et al.* and Campbell *et al.* found that blocking of TLR4, or the use of $TLR4^{-/-}$ tissue did not affect the production of inflammatory cytokines (IL-6, and IL-8 respectively), instead suggesting the process could occur independently of the receptor.[47,48]

SARM1, which is a TLR adaptor protein, has also been key to some pathological findings relating to AMD, with multiple sources supporting the postulation that SARM1 is involved in retinal damage. Ozaki *et al.* show that SARM1 deficiency can protect against photoreceptor degeneration, and Sasaki *et al.* showed that NAD+ synthesis enzyme NMNAT1-dependent retinal cell death was facilitated by SARM1 in retinal degeneration.[49-51]

In addition to TLRs, NLRs are also key to the inflammatory response. NLRP3, a key component of the inflammasome is a NLR which has been heavily implicated in the pathology of AMD. Studies highlighted in Table 1 demonstrate how the role of NLRP3 and other NLRs are disputed, with *in vitro* studies demonstrating the involvement of NLRP3 in the pathology of AMD, but ultimately disputing whether NLRP3 has a causative or preventative role in AMD. A study by Kosmidou *et al.* suggests the discrepancies between studies

can be accounted for by a lack of specificity and/or sensitivity of anti-NLRP3 antibodies. The study goes on to claim that not only is the perceived role of NLRP3 affected by this inherent lack of specificity, but also call in to question whether NLRP3 is present at all within the human retina.

Given the association of the innate immune system, inflammasome and pattern recognition receptors within the inflammatory process, the involvement of inflammation in AMD, and ultimately the individual ways in which the innate immune system can contribute to AMD pathology, the intricacies of the relationship between the innate immune system and AMD suggest that the key to therapeutics may lie within the physiological processes associated with the innate immune system.

Table 1 Predicted preventative and causative pathological roles of PRRs within AMD.

PRR	Causative/Preventative	Method	Reference	Year	Gene	AMD Tissue
NLCR1	Causative	FCM	Kasimsetty [52]	2020		No
NLRP3	Preventative	WB/ELISA	Doyle [53]	2012		*in vitro*
NLRP3	Causative	RT-PCR	Tarallo [54]	2012		*in vitro*
NLRP3	Causative	WB/ELISA	Tseng [55]	2013		*in vitro*
NLRP3	Causative	RT-PCR	Liu [56]	2020		*in vitro*
NLRP3	Causative	WB/ELISA	Wu [57]	2020		No
NLRP3	Causative	PCR/WB	Liao [58]	2019		*in vitro*
NLRP3	Causative	PCR/ELISA	Kauppinen [4]	2012		*in vitro*
TLR2	Causative	RT-PCR	Güven [31]	2016	TLR2-rs5743708	Both
TLR2	Causative	Cell	West [38]	2010		*in vitro*
TLR2	Causative	Mice	Fujimoto [37]	2010		No
TLR2	Causative	Cell	Monaco [48]	2009		No
TLR2	Causative	FCM	Kasimsetty [52]	2020		No
TLR2	Causative	WB/ELISA	Wu [57]	2020		No
TLR3	Preventative	DNASeq.	Yang [59]	2008	TLR3-rs3775291	*in vitro*
TLR3	Causative	TaqMan	Edwards [32]	2008	TLR3-rs3775291	Dry
TLR3	Causative	TaqMan	Edwards [32]	2008	TLR7-rs179008	Dry
TLR3	No Result	TaqMan	Edwards [32]	2008	TLR4-rs4986790	Dry
TLR4	Preventative	PCR-RFLPs	Ling [60]	2019	TLR4-rs1927914	Both
TLR4	No Result	PCR-RFLPs	Ling [60]	2019	TLR4-rs1927907	Both
TLR4	No Result	RT-PCR	Güven [31]	2016	TLR4-rs4986790	Both
TLR4	Preventative	PCR	Kiechl [61]	2002	TLR4-rs4986790	No
TLR4	Causative	PCR	Zareparsi	2005	TLR4-rs4986790	Both
TLR4	Causative	Meta	Liu [35]	2020	TLR4-rs4986790	Both
TLR4	No Result	Meta	Liu [35]	2020	TLR4-rs4986791	Both
TLR4	Causative	WB/ELISA	Huang [42]	2018		*in vitro*
TLR4	Causative	WB/ELISA	Chen [46]	2016		*in vitro*
TLR4	No Result	PCR	Despriet [36]	2008	TLR4-rs4986790	Both
TLR4	No Result	TaqMan	Cho [62]	2009	TLR4-rs4986790	Both
TLR3	No Result	TaqMan	Cho [62]	2009	TLR3-rs3775291	Both

1.3. Essential & Non-essential Elements in AMD

For as long as two decades, the association between the buildup of essential and non-essential elements within the plasma and ocular tissue of AMD patients has been linked with the onset of AMD (Table 2). At the turn of the century, the Age-Related Eye Disease Study (AREDS) concluded that essential trace elements are crucial for regulation of inflammation and in the prevention of disease.[63]

NIH AREDS began to recommend supplementation of the essential elements zinc and copper as a precautionary measure for those susceptible to AMD. Though copper was present to avoid hypocupremia, both zinc and copper have a role in the mitigation of inflammation, as part of copper-zinc superoxide dismutase, and deficiencies of zinc can cause an inflammatory response.[64] Additionally, aside from aging, the most common risk factor for AMD is smoking, which is associated with the inhalation of and exposure to heavy metals such as cadmium and lead, which are common non-essential elements.[65-69]

Since the publication of the AREDS, many studies have explored the metallomic changes that have occurred within the ocular tissue of both young and aged retinal tissue. Essential elements such as sulphur, phosphorus and aluminium can be key in ocular function, and in 2008, Wills et al. postulated a correlation between the levels of the essential elements zinc and copper within the choroid, RPE and retina of diseased ocular tissue, citing elevated levels of zinc and copper within the aged choroid, and reduced levels of zinc within

the aged retina.[70] Though the metallome is a vast and complex aspect of ocular pathology, it has been made clear that copper and zinc may play key roles within the pathology of AMD, and more importantly, may hold the key to prevention or even treatment of AMD.

Table 2 A compilation of analyses of essential and non-essential elements and their association with age-related macular degeneration (AMD), along with the method(s) used to measure the concentrations within each study. Each metal can be seen to have increased, decreased or to have exhibited no significant change as a result of AMD.

Element	Matrix	Technique	AMD Δ	Notes	Reference
As	RPE/Choroid Tissue	ICP-MS	Increased		Aberami [71]
As	Plasma	ICP-MS	No Change		Heesterbeek [72]
Ba	Plasma	ICP-MS	Increased		Heesterbeek [72]
Ca	Plasma	ICP-MS	No Change		Heesterbeek [72]
Cd	RPE/Choroid Tissue	ICP-MS	Increased	Early/Late	Aberami [71]
Cd	Neural Retina	ICP-MS	No Change		Erie [73]
Cd	RPE/Choroid Tissue	ICP-MS	No Change		Erie [73]
Cd	Blood	ICP-MS	Increased	Late AMD	Park [74]
Cd	Blood	AAS	No Change		Güngor [69]
Cd	Aqueous Humor	ICP-MS	Increased		Jünemann [75]
Cd	Plasma	ICP-MS	Increased		Heesterbeek [72]
Cd	Urine	ICP-MS	Increased		Wu [68]
Co	RPE/Choroid Tissue	ICP-MS	Increased		Aberami [71]
Co	Aqueous Humor	ICP-MS	Increased		Jünemann
Co	Plasma	ICP-MS	No Change		Heesterbeek [72]
Cr	RPE/Choroid Tissue	ICP-MS	Increased		Aberami [71]
Cr	Plasma	ICP-MS	Decreased		Heesterbeek [72]
Cu	RPE/Choroid Tissue	ICP-MS	Decreased		Erie [76]
Cu	Aqueous Humor	ICP-MS	Decreased		Jünemann [75]
Cu	Serum	ICP-MS	No Change		Aranaz [77]
Cu	Plasma	ICP-MS	No Change		Heesterbeek [72]
Cu	Serum	ICP-MS	Increased		Cardinault [78]
Fe	Aqueous Humor	ICP-MS	Increased		Jünemann [75]
Fe	Bruch's Membrane	AEM	Increased		Biesemeier [79]
Fe	Serum	ICP-MS	No Change		Biesemeier [79]
Fe	Plasma	ICP-MS	No Change		Heesterbeek [72]
Fe	Serum	QuantiChrom	No Change		Wysokinski [80]

Hg	Blood	ICP-MS	Increased	Late AMD	Park [74]
K	Serum	ICP-MS	No Change		Aranaz [77]
Mg	Serum	ICP-MS	No Change		Aranaz [77]
Mg	Plasma	ICP-MS	No Change		Heesterbeek [72]
Mn	Blood	ICP-MS	Decreased		Park [74]
Mn	Aqueous Humor	ICP-MS	No Change		Jünemann [75]
Mn	Plasma	ICP-MS	No Change		Heesterbeek [72]
Mo	Plasma	ICP-MS	No Change		Heesterbeek [72]
Na	Serum	ICP-MS	No Change		Aranaz [77]
Ni	RPE/Choroid Tissue	ICP-MS	Increased		Aberami [71]
P	Serum	ICP-MS	Increased		Aranaz [77]
Pb	RPE/Choroid Tissue	ICP-MS	Increased		Aberami [71]
Pb	Neural Retina	ICP-MS	Increased		Erie [81]
Pb	RPE/Choroid Tissue	ICP-MS	No Change		Erie [81]
Pb	Blood	ICP-MS	Increased		Park [74]
Pb	Blood	AAS	No Change		Güngor [69]
Pb	Plasma	ICP-MS	No Change		Heesterbeek [72]
Sb	Plasma	ICP-MS	No Change		Heesterbeek [72]
Se	RPE/Choroid Tissue	ICP-MS	Increased		Aberami [71]
Se	Aqueous Humor	ICP-MS	No Change		Jünemann [75]
Se	Plasma	ICP-MS	No Change		Heesterbeek [72]
Se	Blood	AAS	Decreased		Mayer [82]
V	Plasma	ICP-MS	No Change		Heesterbeek [72]
Zn	RPE/Choroid Tissue	ICP-MS	Decreased		Erie [76]
Zn	Blood	ICP-MS	Decreased		Park [74]
Zn	Aqueous Humor	ICP-MS	Increased		Jünemann [75]
Zn	Serum	ICP-MS	Increased		Aranaz [77]
Zn	Plasma	ICP-MS	No Change		Heesterbeek [72]

1.3.1. Zn

Zinc is the most abundant trace metal in the retina and is essential to many of the physiological processes of the eye, such as antioxidant defence, cell metabolism, retinal development and ocular function such as phototransduction, rhodopsin recovery, and neurotransmission.[83,84] However, zinc is not easily stored in the body, and must be replenished though diet. Due to age-related physiological changes involving metabolism, proteostasis, macromolecular damage, and inflammation, people over the age of 60 are more susceptible to zinc deficiency, which has been shown to affect these zinc mediated ocular functions, and has been implicated in the onset of AMD.[9,64,84] Consequently, following a large scale clinical trial as part of the Age-Related Eye Disease Study (AREDS), zinc has been in use as a supplement alongside antioxidants, as it was reported to inhibit the release of pro-inflammatory cytokines, and reduce the amount of CRP and oxidative stress markers, and slow the progression of early AMD to late-stage AMD.[85-87]

Consequently, inductively coupled plasma mass spectrometry (ICP-MS) has been used to study concentrations of zinc within various matrices in the context of AMD. Many studies aim to associate trace metal blood concentrations using ICP-MS.[74,88] Some have also qualitatively characterised zinc distribution within the chorio-retinal microanatomy of ocular tissues of healthy patients in the context of AMD.[84] Additionally, some studies have utilised both healthy and diseased ocular tissues to compare the concentrations of zinc within ocular tissues such as a study

by Erie *et al.* which compared zinc levels within AMD and healthy donor eyes.[76] To date, a significant number of studies conclude a negative association of zinc concentration and AMD, consistent with the evidence from AREDS & AREDS 2 that zinc deficiency is a risk factor in the onset of AMD.[75] In contrast some studies note higher levels of zinc within AMD patients; notably in blood/serum studies.[75,77] Elevated zinc levels in AMD patients could be explained by the release of intracellular deposits of zinc from photoreceptors following apoptosis, resulting in a high extracellular concentration of zinc despite the overall zinc deficiency experienced by the patient. As extracellular or 'free' zinc has been shown to activate microglia, and can aggravate inflammation, this increase in free zinc from photoreceptors could lead to exacerbation of AMD. It is clear that zinc can play a role in AMD, whether it be through protective roles in the innate immune system, or as a pro-inflammatory species released in the diseased state.[89]

1.3.2. Cu

AREDS also recommended the supplementation of copper in the form of Cupric oxide to AMD patients due to the risk of hypocupraemia that occurs with large doses of zinc as part of the AREDS supplementation programme.[90] However, copper has been investigated outside of AREDS, separately to zinc in the context of AMD.[76,90] Like zinc, copper is involved in essential ocular processes, and acts as a cofactor for multiple ocular enzymes, including copper-zinc superoxide dismutase, an enzyme involved in regulation of oxidative stress.[76,83] However, despite

its role in the regulation of oxidative stress, copper can initiate oxidative stress if present in large enough quantities, meaning that regulation of copper levels is essential to ocular health.[70,91] Copper has been investigated though the use of multiple analytical methodologies, most of which conclude a relationship with AMD and inflammation, however, disagree on the causative role of copper in AMD. [70,91]

The present study aimed to explore the past decades findings related to essential and non-essential elements and AMD, and to focus on the essential elements copper and zinc, and how the perceived duplicity of their role in ocular pathology can be explained.

2.0. Analytical techniques within Ocular pathology

Mass Spectrometry (MS) has been used for a variety of pathological investigations in recent history. Notably, the use of mass spectrometry in the study of biomarkers and other key species relating to disease pathology.[92-94] Current techniques used to investigate the innate immune system and related proteins within the context of AMD predominantly rely on the use of immunological techniques to study the presence of proteins.[17,50,53,95] The specificity and accuracy at which these methods can operate, in combination with high resolution imaging techniques have forged a path through ocular research, facilitating the discovery of novel therapeutics in ocular research that has helped to improve ocular health outcomes. However, the power of immunological techniques is reliant on the efficacy or specificity of the antibodies used within the assay.[96] Despite successes within the field of ocular research, there are disputes

within the literature that can compromise the influence of some of the existing research.[96] In addition, immunological techniques are limited to targeted research, which can breed insular research. With the ever-growing relevance of mass spectrometry within the field of biomarkers, and in combinations with its ability to perform untargeted experiments, without the need for specific reagents, there is adequate scope to employ mass spectrometry in conjunction with immunological research.[97] The untargeted and multiplexing nature of mass spectrometry has long been able to offer a great deal of information to pathological investigations, however with the development of modern mass spectrometry imaging (MSI) techniques, new dimensions have been added to the capabilities within mass spectrometry. With the ability to compare spatial information from multiple disciplines, there is potential to make meaningful contributions to ocular pathology.

In addition to bolstering research into the innate immune system, the work investigating the role of essential and non-essential elements within ocular pathology can be supported by the suite of analytical techniques used to study metallomics. Techniques such as Ion beam analysis (IBA) are long established within the field of metallomic research, offering immense multiplexing and high spatial resolution of elements from multiple matrices. However, their power is only matched by their relative inaccessibility. However, with modern advances in LA-ICP-MS, there is now high throughput, fast, accessible and high sensitivity techniques for the detection, quantification, and spatial characterisation of metals within biological tissue.

Whilst mass spectrometry could hold great potential within the field of ocular pathology, its success is dependent on the successful ionisation and transport of ions related to the target analyte. Additionally, when performing untargeted analyses, the identification of species within biological tissue can heavily rely on mass resolution. Herein the different methods and the theory on which they operate is discussed, with a how new technologies have revolutionised the capabilities of analytical research.

2.1. Matrix assisted laser desorption ionisation (MALDI)

Matrix assisted laser desorption ionisation (MALDI), developed in the 1980s by Karas *et al.* and Tanaka *et al..* is an ionisation technique used for mass spectrometry.[98,99] MALDI is a 'soft' ionisation technique that relies on the co-crystallisation of the analytes of interest with a chemical compound known as a matrix. In 'soft' ionisation techniques the number of intact, ionised species produced in the source is significantly greater that the number of fragment ions.[100] The role of the matrix is to absorb energy at the wavelength of the laser (*e.g.* a 355 nm Nd:YAG or a N_2 337 nm laser) converting the energy from the laser into heat, causing sample disintegration. In addition, for positive polarity analysis, the ability for the matrix ion to be readily protonated is desirable. As a result, the choice matrix, in addition to the way in which the matrix is incorporated into the sample can be crucial to the success of the analysis, with different preparations producing different results (Table 3). For this study, α-

cyano-4-hydroxycinnamic acid (CHCA) was used as MALDI analysis was primarily used for peptide analysis, and in addition, a number of application techniques were explored.

Table 3 Different matrix compounds have historically been used in ultraviolet matrix assisted laser desorption ionisation (UV-MALDI). Below, common analytes and their corresponding matrices..

Analyte	**Matrices**	**Acronyms**	**References**
Peptides	Nicotinic acid	NA	[101]
	2-(4-Hydrocyhenylazo) benzoic acid	HABA	[101]
	4-Chloro-α-cyano-cinnamic acid	ClCCA	[101]
	α-Cyano-4-hydroxycinnamic acid	CHCA	[101,102]
Proteins	Nicotinic acid	NA	[101]
	2,5-Dihydroxybenzoic acid	DHB	[101]
	α-Cyano-4-hydroxycinnamic acid	CHCA	[101]
	3,5-Dimethoxy-4-hydroxycinnamic acid	SA	[101]
	2-(4-Hydrocyhenylazo) benzoic acid	HABA	[101]
Lipids/Metabolites	1,5-Diaminonaphthalene	1,5-DAN	[103]
	9-aminoacridine	9-AA	[103]

2.1.1. MALDI Ionisation Theory

How the matrix facilitates ion production is complex, and remains unclear, with two predominantly accepted models for ionisation. In the Gas phase production model, the heat transfer induced by the absorption of laser energy allows the matrix and the analyte molecules to enter the gas phase. Once in the gas phase, the gas phase protonation model postulates the transfer of a proton from the matrix ion to the analyte

molecules, allowing them to be transferred and analysed by the mass spectrometer [104].

The second model for MALDI ionisation is called the lucky survivor model, proposed by Karas *et al.* in 2000.[105] Revised in 2011, the model relies on the theory that the analyte is ionised prior to analysis, as part of the matrix application process whereby the solvent allows the analyte to form a negative ion by co-crystallisation with the matrix.[105,106] In its first iteration, the analyte ions are then desorbed and analysed without further aid from the matrix. The revised lucky survivor model accounts for the formation of doubly charged species with the matrix being desorbed with the analyte, as counterions.[106]

2.2. Desorption Electrospray Ionisation

Desorption electrospray ionisation (DESI) is another form of soft ionisation technique used in mass spectrometry. DESI, like MALDI has been utilised for both profiling and imaging applications.[107,108] Conceived in the early 2000s to alleviate the need to expose samples to a high vacuum, DESI, as the name implies, relies on some of the same principles as ESI.[109] A solvent, typically a mixture of aqueous and organic solvents is incident upon the sample at an angle, nebulised by a flow of N_2 gas and a voltage (Figure 5). The solvent aerosol then interacts with the sample source, and the analyte is desorbed into the solvent. The solvent (now charged droplets containing the analyte) is transported into the mass spectrometer in the form of secondary ions through a transfer line. Through this methodology, DESI is able to analyse the analytes on

the surface of some tissues whilst causing minimal damage to the sample surface. The analysis is rapid and non-invasive, and the lack of vacuum makes it ideal for samples that will degrade easily. In addition to these benefits, DESI requires little to no sample preparation. DESI-MS does however require method optimisation as different parameters, including θ_α, θ_β, d_1 and d_2 (Figure 5) can greatly influence the efficacy of ionisation. The angles of incidence and desorption can be finely tuned in order to bias the class of desired species entering the mass spectrometer.

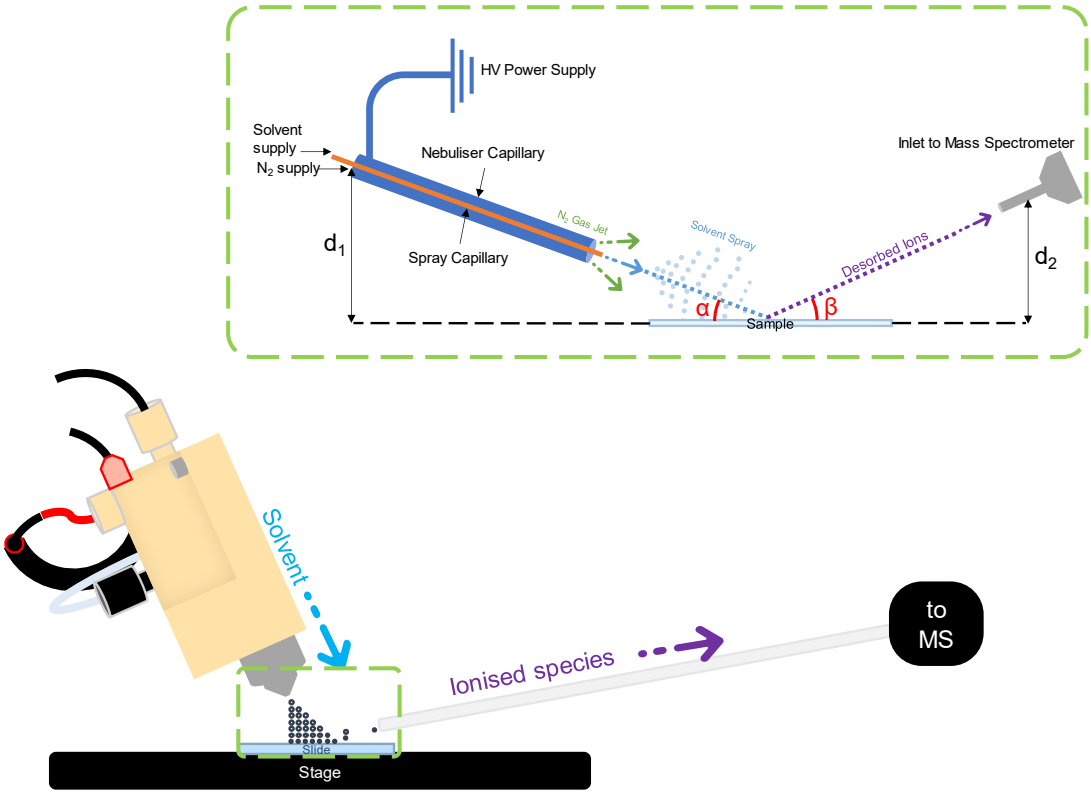

Figure 5 A schematic showing the mechanism by which desorption electrospray ionisation (DESI) produces ions in DESI mass spectrometry (MS). A zoomed view (green dashed box) shows the intricacies of the DESI source, including angle α, the angle of the incident DESI source cone, β, the angle of the capillary connected to the MS, and the heights at which the source cone (d_1) and the transfer line (d_2) are from the sample stage.[108]

2.3. Inductively Coupled Plasma

Inductively coupled plasma (ICP) was first conceptualised in the early 1960s, with commercial instruments developed in the 1970s and 1980s.[110] ICP is a form of ion source used most in the field of metallomics, or the study of metals. ICP relies on the principle of using a high temperature ionised argon gas (plasma), which is stabilised by a high frequency electric field, and contained by an N_2 sheath gas. Depending on the application, sampling can range from the introduction of solutions through a nebuliser chamber to analysis of dry aerosol particles by laser ablation. The plasma retains energy created by the radiofrequency (RF) field applied to it and atomises the analyte species. Following atomisation, the ionisation steps can occur, which happen as a result of two main processes: charge-transfer ionisation ($Ar^+ + M \rightarrow M^{+*} + Ar$), and Penning ionisation ($Ar^m + M \rightarrow M^{+*} + Ar$).[111] Following ionisation, ions are separated from neutral species by manipulating the ions with an electric field. In the NexION 350X (the instrument used within these works) the ions are deflected 90° by a quadrupole ion deflector (QID) (Figure 6).

When in standard mode, the ions pass through the first quadrupole uninhibited, before passing into the quadrupole mass analyser. The mass analyser will be tuned to multiple masses, which in the 350X can be resolves at 0.2 amu at 10% peak height. The total acquisition time or sweep depends on two factors, dwell time and settling time. The overall dwell time will be determined by the number of masses being scanned for during a sweep, which in turn is determined by the dwell times of each

individual element. Individual dwell times can be crucial for sensitivity, with longer dwell times often used for the least abundant elements. Settling time, which makes up the rest of the acquisition time is determined by the ability of the quadrupole to switch between masses. Whilst most modern ICP-MS instrument can achieve settling times below 200 µs, most have a dynamic settling time, which can increase as the mass difference increases.[112,113] The NexION benefits from settling times of ≤200 µs meaning that less time of an acquisition is spent 'settling' resulting in better sensitivity for routine analysis. When conducting analysis with a transient signal, such as in single particle analysis and laser ablation ICP-MS, settling time can be of paramount importance. Figure 7 exhibits the impact that settling time can have when analysing multiple elements. If settling time is too large, then the efficiency of the acquisition can result in a loss of sensitivity or indeed a loss of a transient signal.

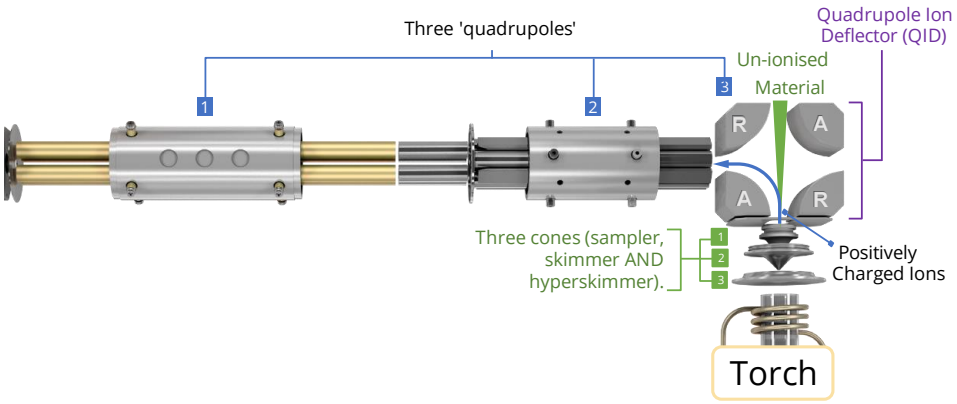

Figure 6 The ion path within a NexION 350 ICP-MS. Wherein the labels 'R' and 'A' on the quadrupole ion deflector (QID) stand for 'repeller' and 'attractor' respectively. The repellers repel the ions using a dynamic voltage, and the attractors attract ions using a static voltage, allowing neutralised ions to pass through uninhibited, and forcing the ionised species around a 90° ion path to the left. Adapted from PerkinElmer [114]

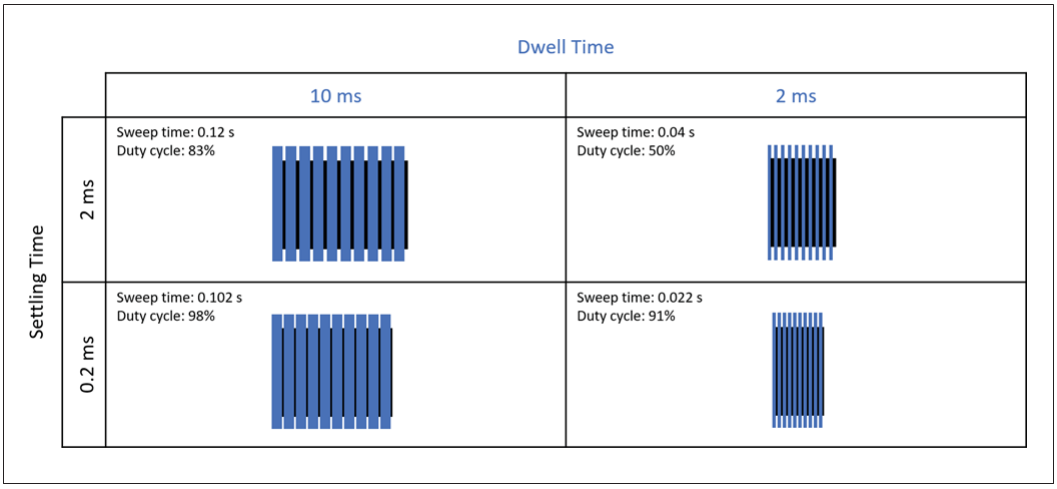

Figure 7 The effect of settling time on the efficiency of duty cycle. Adapted from PerkinElmer [115]

2.4. Laser Ablation

Laser Ablation (LA) is a technique for the analysis of geological and biological materials. LA utilises an incident laser beam to irradiate and ablate samples. The result is the eruption of a plume of material on the surface of the sample, which produces an aerosol cloud containing the constituents of the surface material. In LA-ICP-MS, a carrier gas or mass flow controller (MFC) is used to carry this gas to the ICP source. MFCs have traditionally been argon gas, which not only matches the source gas, but allows the aerosol to be carried by an inert gas towards the ICP source.

In recent years the use of helium as an MFC has gained popularity. ^{2}He is relatively inert, but additionally due to its lightness and low density allows for better aerosol formation within the sample chamber of the LA, meaning less particulate matter falls back to the sample stage.[116] LA is used as a MS imaging technique, and so the MFC is not only important in the production of aerosols within the sample chamber, but also for the delivery of the aerosol particles to the ICP in a singularly, sharp peak, so that each pixel within the MS image is discreet, and that no carry over form the previous pixel is carried to the next. This ‘delivery speed’ is determined by washout time, a function determined by the flow dynamics of the sample chamber. In the LA apparatus used within this piece of work, the ImageBio266, the sample chamber is designed for low washout times, citing a washout of <700 ms. Low washout times are achieved by utilising a reduced internal volume, and a conical cup which transports the aerosol from directly above where the laser is firing. [117]

2.5. Microbeam Particle-Induced X-ray Emission

Particle induced X-ray emission (PIXE) was first conceived in Sweden in 1970, with micro PIXE (μPIXE) being developed in the 1980s. PIXE relies on the Coulomb interaction between the incident ions produced, in this case a proton ($^{1}H^{+}$) and the inner shell electrons.[101] The proton causes vacancies of lower shell electrons, which are then replaced by higher energy electrons. In order to occupy the lower energy vacancy, the higher energy electrons release energy in the form of characteristic X-rays (hv). These characteristic X-rays are detected by a lithium drifted silicon detector (SDD).[118] In combination with a moving sample stage (Figure 8), imaging data from μPIXE can be obtained giving spatial information relating to the elemental information given by the X-rays. Unlike ICP-MS, there is less risk of polyatomic interferences, and fewer instances of matrix effects.[119]

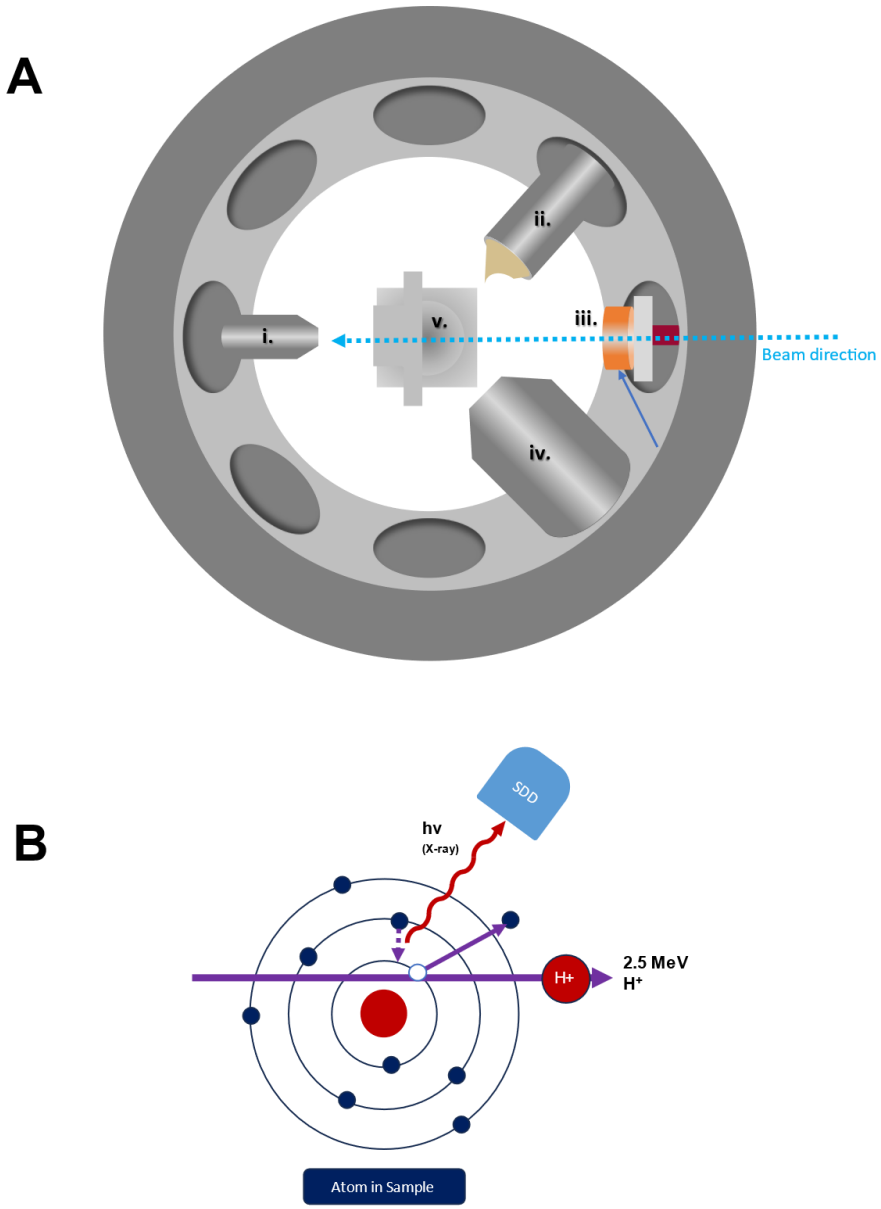

Figure 8 (A) A micro particle induced X-ray emission (μPIXE) sample chamber used for μPIXE imaging. (i) Graphite Faraday Cup (ii) Silicon drifted detector (SDD) (iii) Particle Detector (iv) Video microscope. Adapted from Grime et al. [119] *(B) A Diagram showing the emission of a characteristic X-ray.*

2.6. Mass Analysers

2.6.1. Quadrupole

Quadrupole mass analysers were first conceived in 1960 and have since been a common mass analyser for mass spectrometry.[120] Their versatility allows their application to a number of different techniques, including ICP-MS. The radio frequency (RF) voltage within a quadrupole instrument is applied to four diametrically opposed rods or 'poles' which then create a frequency with which ions can be resonant or non-resonant. By tuning ratio of these voltages, you can tune a quadrupole for mass filtering and selection.[121]

2.6.2. TOF

Time-of-flight (TOF) mass analysers are means by which to measure mass used most commonly in mass spectrometry. TOF analysers rely on a measured time period as a function of mass-to-charge ratios to determine the mass of ions. The principle relies on the theory that ions with larger m/z values with the same mass will take a longer period of time to reach a detector at the end of a flight tube from the time of pulse (t_0) to the time where the ion is incident on the detector (t_1) when the same acceleration voltage is applied to each. In mass spectrometry, the use of reflectron TOF instruments has become increasingly popular, as through the use of a reflectron, ions can travel for roughly twice the distance within the same instrument footprint, allowing for improved resolution (Figure 9).[122,123]

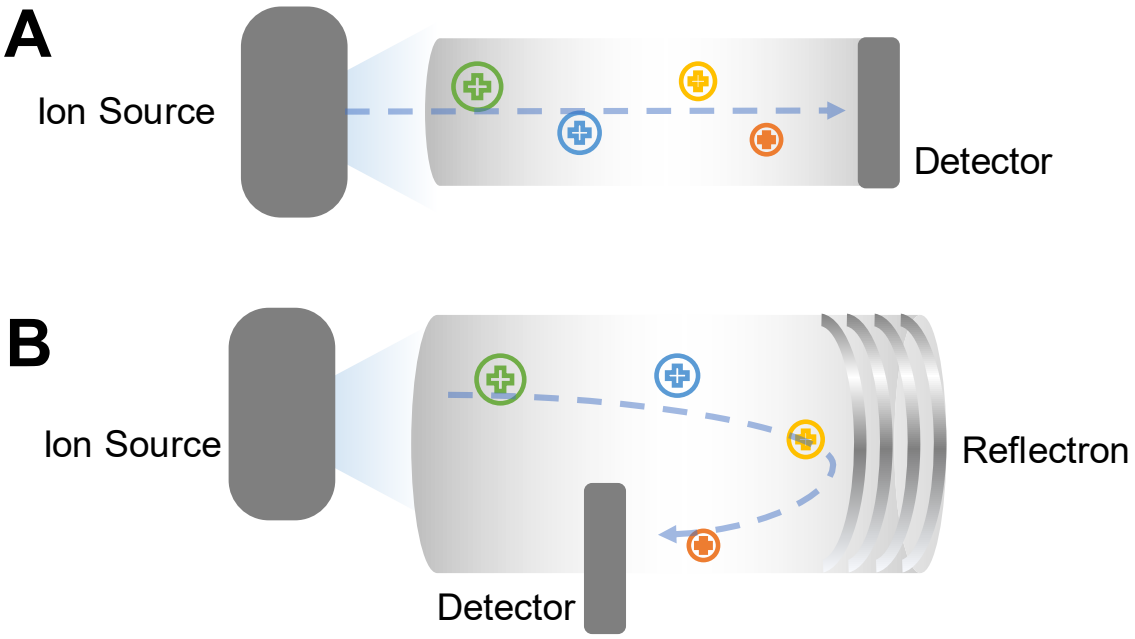

Figure 9 A figure representing the ion paths involved in the measurement of masses in (A) A linear TOF where the time-of-flight is determines over a set distance and (B) a Reflecting TOF, where the time-of-flight is extended within a similar footprint by using a reflectron to change the path of the ions.[122,123]

2.6.3. qTOF

Instruments such as the Waters SYNAPT G2 HDMS rely not only on quadrupole technology but use it in combination with TOF technology. The combination of quadrupole and TOF technology allows for high speed, high mass accuracy mass spectrometry with the ability to fragment compounds.[94] Deviating from a conventional linear TOF, the SYNAPT utilises a double reflection, allowing the instrument to operate in *Sensitivity* (V-mode) or *Resolution* (W-Mode) which allow for resolutions of 10,000 FWHM and 40,000 FWHM respectively (Figure 10).

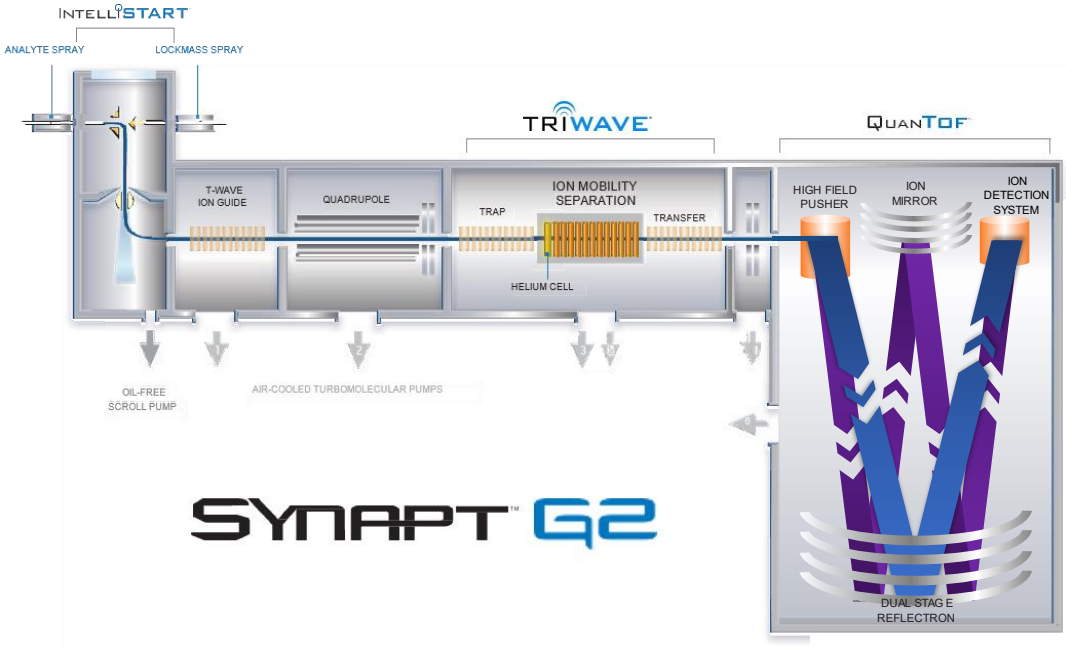

Figure 10 The ion path of a SYNAPT G2 HDMS, when operating in V mode (blue) and W mode (purple) Adapted from Waters Corporation [124]

2.6.4. Multi-reflecting TOF

Multi-reflecting TOF (MRT) analysers rely on the same principles as TOF analysers. Like reflectron TOF instruments they utilise an ion mirror to reflect the ion packets to increase the flight path. Single reflectron mass analysers however often use an electrostatic grid to reflect ions, as first described by Mamyrin in 1973.[123] The model utilises a metal mesh over which an electrostatic charge is applied. The ions pass through these meshes and are reflected by the potential difference applied. Whilst passing through these grids on a traditional reflectron, up to 20% of the ions passing through are lost, with modern reflectrons having around 90% transmission efficiencies.[125,126] Given losses of ions within the beam path are expected in MS instrumentation, this becomes negligible. The SYNAPT series from Waters Corporation, which are qTOF instruments, these losses are compounded with the multiple reflections that occur in

V & W mode (Figure 10). These analysers can offer resolutions of up to 100,000 full width at half maximum (FWHM), but should further reflections take place, there is a risk of further sensitivity loss, and an ever-increasing duty cycle.[125] Loss of sensitivity can be avoided through the use of early gridless mirrors, which utilised a reflectron that doesn't rely on the use of a mesh to exert an electrostatic force, but rather using gridless diaphragm rings, which otherwise resembled a standard reflectron.[126] Gridless mirrors have since improved, offering higher order TOF focusing, and higher resolutions, with some offering up to 500,000 FWHM at a fixed mass range. Whilst this helps mitigate loss of sensitivity, there are still issues with increasing duty cycle.

Traditional TOF systems utilise a pulse-wait system, whereby the time between orthogonal acceleration (OA) pulses is determined by the TOF of the heaviest species within the mass range. With each reflection, the time taken for the largest species to reach the detector will increase, increasing duty cycle, and loss of ions. As the time spent by the ions in the flight tube increases, the time between OA pulses becomes extremely large. To enable more packets of ions may be entering the flight tube at any one time, the use of encoded frequent pulsing (EFP) has been utilised, wherein the 'pulses' take place in an encoded sequence, whereby the time intervals are unique allowing the mass spectrometer to deconvolute signals from multiple ion packets simultaneously. [127] This EFP technology allows a 25% improvement in duty cycles for sequences of 100 pulses, and allows an increase in sensitivity, dynamic range and speed of analysis by up to two orders of magnitude.

This results in the culmination of multiple technological advances allowing for the manufacture of multi-reflecting TOF MS. The Waters MRT, which is the first to commercialised these technologies together, is able to have a flight path of ~50 m, with 47 reflections. This enhanced flight path allows for routine analyses to take place at a mass resolution of 200,000 FWHM, whilst maintaining a scan time of 0.1 s.[125] Additionally, when used in resolution enhancement mode (REM) mode, the instrument allows for a further 47 reflections to occur by pushing the ions though the MRT flight path an additional time, increasing the resolution to 300,000 FWHM. In this research, the instrument was used in MRT mode, with one pass through the flight tube, and thereby a resolution of >200,000 FWHM.

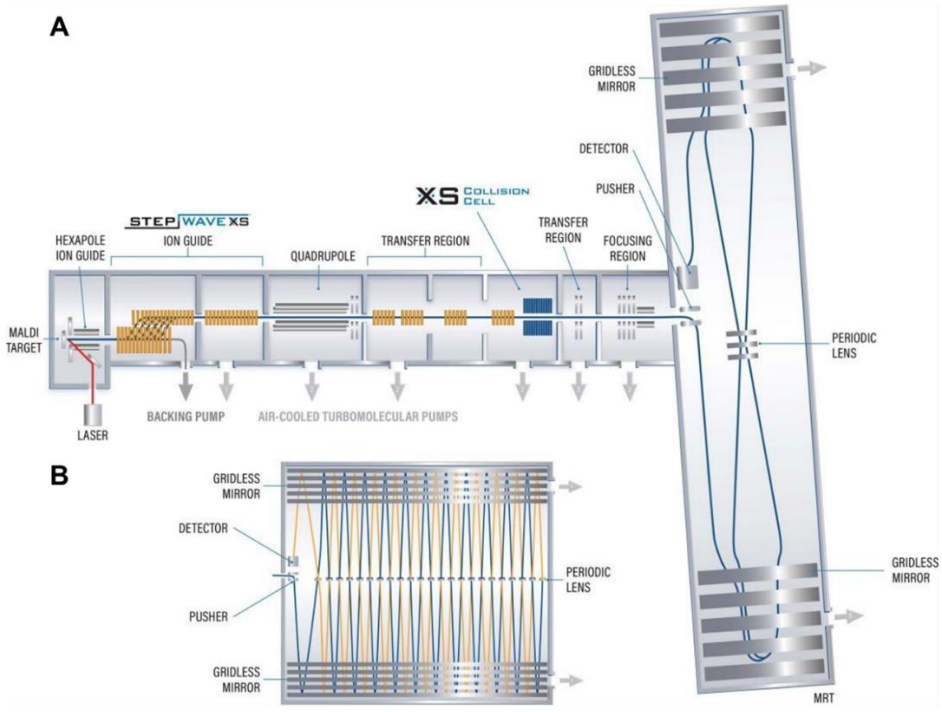

Figure 11 The ion path found in the Waters SELECT SERIES MRT (A) the ion path when operating in Diamon d Mode (10,000 FWHM) (B) An expanded view of the ion path within the MRT flight tube when operating in MRT mode (200,000 FWHM).[128]

2.7. Mass Spectrometry Imaging

Mass spectrometry imaging relies on a compatible technique such as MALDI, DESI or LA-ICP to produce mass spectra containing m/z and intensity values for each 2D x & y coordinate within a determined area. The spectra for each m/z can then be viewed as a 2D heatmap, showing spatial distribution and relative intensity at each point within a sample. (Figure 12) In this programme of research, a pixel size of 50 µm or less, with a lower limit of 10 µm was utilised when using LA. This means, using the correct sample preparation to accentuate analytes of interest, mass spectrometry experiments can be used to create heatmaps showing the content and two-dimensional arrangement of analyte species within a sample. Additionally, by utilising co-registration techniques, the data can be compared to histological stains, and associate species, and their relative intensity with structures within biological tissue.

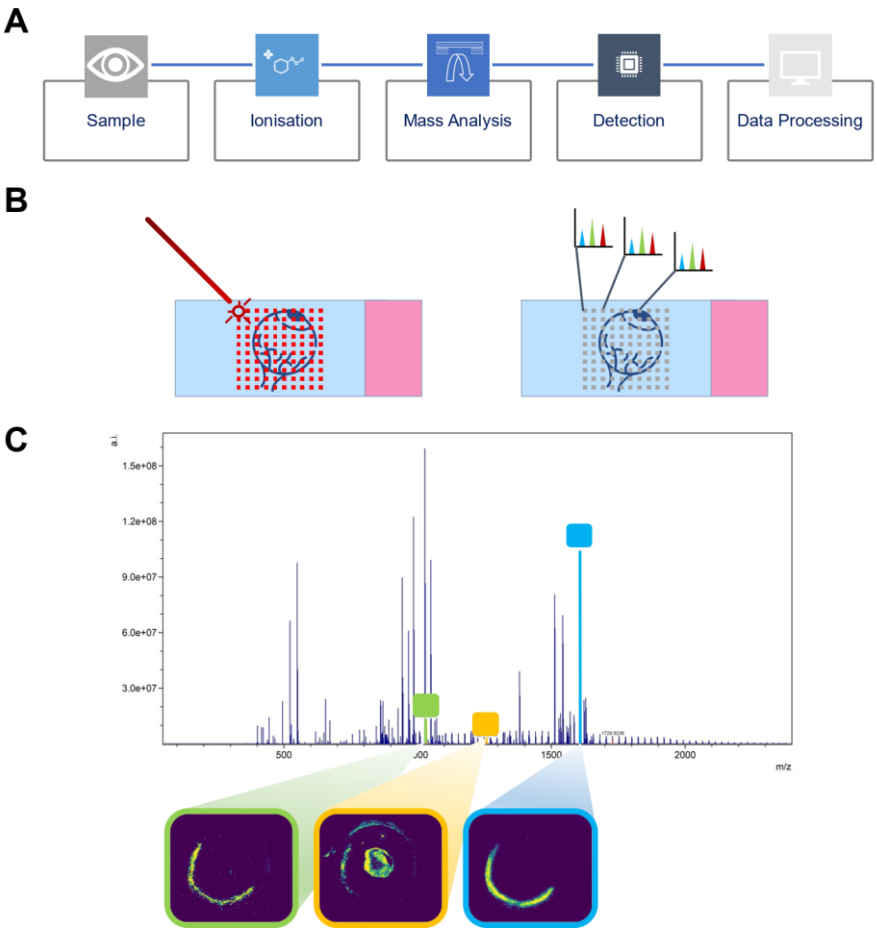

Figure 12 A figure representing the workflow involved when performing mass spectrometry imaging (MSI); (A) the workflow which helps to produce mass spectrometry imaging experiments (B) A representation of the collection of individual spectra from each xy coordinate within a same region using a laser as an ion source. (C) MSI data once processed; with each m/z value in the spectrum providing a heatmap that contains information relating to the m/z value, its coordinates in a 2D array, and the relative intensity at each coordinate.

Using the analytical strategies described herein, and the context of the research being completed into the age-related macular degeneration, a number of aims for this project were conceptualised, in order to begin a novel approach to age-related macular degeneration.

3.0. Aims & Objectives

This PhD project aimed to inform on the pathology of AMD by utilising mass spectrometry imaging in a multifaceted and multimodal fashion. The main aims are outlined below:

1) ***Optimisation of strategies aimed to study ocular disease through multimodal workflows***

This initial study of the project was designed to cultivate a set of basic methodologies on which further research and optimisation could be built. The study was designed to demonstrate a proof of concept for the analysis of peptides from proteins related to ocular pathology and aimed to develop individual imaging workflows using MALDI-MSI and LA-ICP-MSI, taking into consideration the complexities of sample preparation within each of the workflows. This work aimed to prove the utility of both MSI modalities for the application within ocular pathology.

2) Development of a multiomic workflows for the high resolution imaging of ocular tissue metals and peptides related to the onset of AMD

Building on the methodologies in Aim 1, this section of the research aimed to refine the workflows set out in the first part of this project. One aspect of this aim was to improve the sample preparation procedures for MALDI-MSI through the utility of more sophisticated techniques. In addition, it was proposed that the LA-ICP-MSI work developed in the

initial study could be improved upon through the use of a quantitative strategy.

3) ***Deployment of a multimodal metal imaging strategy to investigate the relationship between essential and non-essential metals within a retinal degeneration model.***

Further to the metallomic studies, this aspect of the research programme aimed to develop the ideas set out as part of the research into the relationship between trace elements and ocular pathology. Utilising the developed workflows, it was proposed that LA-ICP-MSI could be used to further probe the relationship between ocular tissue and trace elements, using a transgenic tissue to map changes to the elemental landscape of ocular tissue. Furthermore, validation, and expansion of the datasets produced by LA-ICP-MSI was proposed to be undertaken using μPIXE, a powerful technique for the analysis of trace elements.

4) Development of a multimodal workflow for the analysis of mouse and human ocular tissue in the context of ocular pathology.

This final aspect of the research aimed to stand as a culmination of the methodologies an techniques developed in the previous chapter, with the addition of DESI-MSI, this phase of the research aimed to combine the MALDI-MSI and LA-ICP-MSI techniques employed earlier into a unified and integrated workflow, wherein lipidomic, peptidomic, and metallomic data could be obtained from single tissue sections using a large suite of techniques. Additionally, there was an aspiration to apply some of the

aforementioned techniques to human tissue, in order to contextualise the facility of the previously developed imaging strategies.

4.0. References

1 A. Tisi, M. Feligioni, M. Passacantando, M. Ciancaglini and R. Maccarone, The Impact of Oxidative Stress on Blood-Retinal Barrier Physiology in Age-Related Macular Degeneration *Cells (Basel, Switzerland),* 2021, **10**, 64.

2 J. D. Ash, C. Grimm, J. G. Hollyfield, R. E. Anderson, M. M. LaVail and C. Bowes Rickman, *Retinal Degenerative Diseases*, Springer New York, Cham, 2014.

3 J. K. Phelan and D. Bok, A brief review of retinitis pigmentosa and the identified retinitis pigmentosa genes *Molecular vision,* 2000, **6**, 116–124.

4 A. Kauppinen, J. Paterno, J. Blasiak, A. Salminen and K. Kaarniranta, Inflammation and its role in age-related macular degeneration *Cell Mol. Life Sci.,* 2016, **73**, 1765–1786.

5 R. P. Danis, J. A. Lavine and A. Domalpally, Geographic atrophy in patients with advanced dry age-related macular degeneration: current challenges and future prospects *Clinical ophthalmology (Auckland, N.Z.),* 2015, **9**, 2159–2174.

6 J. Mitchell and C. Bradley, Quality of life in age-related macular degeneration: a review of the literature *Health and Quality of Life Outcomes,* 2006, **4**, 97.

7 N. Rayess, Houston Steven, O. Gupta, A. Ho and C. Regillo, Treatment Outcomes After 3 Years in Neovascular Age-Related Macular Degeneration Using a Treat-and-Extend Regimen *Am. J. Ophthalmol.,* 2015, **159**, 3–8.e1.

8 M. Fleckenstein, P. Mitchell, K. B. Freund, S. Sadda, F. G. Holz, C. Brittain, E. C. Henry and D. Ferrara, The Progression of Geographic Atrophy Secondary to Age-Related Macular Degeneration *Ophthalmology,* 2018, **125**, 369–390.

9 B. K. Kennedy, S. L. Berger, A. Brunet, J. Campisi, A. M. Cuervo, E. S. Epel, C. Franceschi, G. J. Lithgow, R. I. Morimoto, J. E. Pessin, T. A. Rando, A. Richardson, E. E. Schadt, T. Wyss-Coray and F. Sierra, Geroscience: Linking Aging to Chronic Disease *Cell,* 2014, **159**, 709–713.

10 V. Chichagova, D. Hallam, J. Collin, D. Zerti, B. Dorgau, M. Felemban, M. Lako and D. H. Steel, Cellular regeneration strategies for macular degeneration: past, present and future *Eye,* 2018, **32**, 946–971.

11 W. L. Wong, X. Su, X. Li, C. M. G. Cheung, R. Klein, C. -. Cheng and T. Y. Wong, Global prevalence of age-related macular degeneration and disease burden projection for 2020 and 2040: A systematic review and meta-analysis 2014, .

12 A. Quartilho, P. Simkiss, A. Zekite, W. Xing, R. Wormald and C. Bunce, Leading causes of certifiable visual loss in England and Wales during the year ending 31 March 2013 *Eye,* 2016, **30**, 602–607.

13 D. F. Martin, M. G. Maguire, G. Ying, J. E. Grunwald, S. L. Fine and G. J. Jaffe, Ranibizumab and Bevacizumab for Neovascular Age-Related Macular Degeneration *The New England journal of medicine,* 2011, **364**, 1897–1908.

14 L. M. Khachigian, G. Liew, K. Y. C. Teo, T. Y. Wong and P. Mitchell, Emerging therapeutic strategies for unmet need in neovascular age-related macular degeneration *Journal of translational medicine,* 2023, **21**, 133.

15 K. Henriksen and S. Adhami, Patient experience of intravitreal injections in AMD *International journal of ophthalmic practice,* 2010, **1**, 68–72.

16 Z. Papadopoulos, Recent Developments in the Treatment of Wet Age-related Macular Degeneration *CURR MED SCI,* 2020, **40**, 851–857.

17 L. Celkova, S. L. Doyle and M. Campbell, NLRP3 Inflammasome and Pathobiology in AMD *Journal of clinical medicine,* 2015, **4**, 172–192.

18 K. L. Rock, E. Latz, F. Ontiveros and H. Kono, The Sterile Inflammatory Response *Annual Review of Immunology,* 2009, **28**, 321–342.

19 A. C. Shaw, D. R. Goldstein and R. R. Montgomery, Age-dependent dysregulation of innate immunity *Nature reviews. Immunology,* 2013, **13**, 875–887.

20 C. Franceschi, P. Garagnani, P. Parini, C. Giuliani and A. Santoro, Inflammaging: a new immune–metabolic viewpoint for age-related diseases *Nature reviews. Endocrinology,* 2018, **14**, 576–590.

21 K. Dolasia, M. K. Bisht, G. Pradhan, A. Udgata and S. Mukhopadhyay, TLRs/NLRs: Shaping the landscape of host immunity *International reviews of immunology,* 2017, **37**, 3–19.

22 H. Guo, J. B. Callaway and J. P. Ting, Inflammasomes: mechanism of action, role in disease and therapeutics *Nature medicine,* 2015, **21**, 677–687.

23 J. Ambati, J. P. Atkinson and B. D. Gelfand, Immunology of age-related macular degeneration *Nature reviews. Immunology,* 2013, **13**, 438–451.

24 Y. Wooff, N. Fernando, J. H. C. Wong, C. Dietrich, R. Aggio-Bruce, J. Chu-Tan, A. A. B. Robertson, S. L. Doyle, S. M. Man and R. Natoli, Caspase-1-dependent inflammasomes mediate photoreceptor cell death in photo-oxidative damage-induced retinal degeneration *Scientific Reports,* 2020, **10**, 2263.

25 S. M. Man and T. Kanneganti, Regulation of inflammasome activation *Immunological Reviews,* 2015, **265**, 6–21.

26 F. X. Yu and L. D. Hazlett, Toll-like Receptors and the Eye *Invest. Ophthalmol. Vis. Sci.,* 2006, **47**, 1255–1263.

27 K. Mai, J. J. Chui, N. Di Girolamo, P. J. McCluskey and D. Wakefield, Role of toll-like receptors in human iris pigment epithelial cells and their response to pathogen-associated molecular patterns *Journal of inflammation (London, England),* 2014, **11**, 20.

28 A. Klettner and J. Roider, Retinal Pigment Epithelium Expressed Toll-like Receptors and Their Potential Role in Age-Related Macular Degeneration *International journal of molecular sciences,* 2021, **22**, 8387.

29 T. Kawasaki and T. Kawai, Toll-like receptor signaling pathways *Frontiers in immunology,* 2014, **5**, 461.

30 A. C. Shaw, A. Panda, S. R. Joshi, F. Qian, H. G. Allore and R. R. Montgomery, Dysregulation of human Toll-like receptor function in aging *Ageing research reviews,* 2011, **10**, 346–353.

31 M. Güven, B. Batar, T. Mutlu, M. Bostancı, M. Mete, C. Aras and M. Ünal, Toll-Like Receptors 2 and 4 Polymorphisms in Age-Related Macular Degeneration *Curr. Eye Res.,* 2016, **41**, 856–861.

32 A. O. Edwards, D. Chen, B. L. Fridley, K. M. James, Y. Wu, G. Abecasis, A. Swaroop, M. Othman, K. Branham, S. K. Iyengar, T. A. Sivakumaran, R. Klein, B. E. K. Klein and N. Tosakulwong, Toll-like Receptor Polymorphisms and Age-Related Macular Degeneration *Investigative ophthalmology & visual science,* 2008, **49**, 1652–1659.

33 Toll-like Receptor 3 and Geographic Atrophy in Age-Related Macular Degeneration *The New England Journal of Medicine,* 2009, **361**, 431.

34 S. ZAREPARSI, M. BURACZYNSKA, H. R. PETTY, J. E. RICHARDS, G. R. ABECASIS, V. M. ELNER, A. SWAROOP, K. E. H. BRANHAM, S. SHAH, D. ENG, MINGYAO LI, H. PAWAR, B. M. YASHAR, S. E. MOROI and P. R. LICHTER, Toll-like receptor 4 variant D299G is associated with susceptibility to age-related macular degeneration *Human molecular genetics,* 2005, **14**, 1449–1455.

35 X. Liu, X. Guo, X. Chen and Y. Yao, Toll-like receptor 4 gene polymorphisms rs4986790 and rs4986791 and age-related macular degeneration susceptibility: a meta-analysis *Ophthalmic Genetics,* 2020, **41**, 31–35.

36 D. D. G. Despriet, A. A. B. Bergen, J. E. Merriam, J. Zernant, G. R. Barile, R. T. Smith, I. A. Barbazetto, S. van Soest, A. Bakker, P. T. V. M. de Jong, R. Allikmets and C. C. W. Klaver, Comprehensive Analysis of the Candidate Genes CCL2, CCR2, and TLR4 in Age-Related Macular Degeneration *Investigative ophthalmology & visual science,* 2008, **49**, 364–371.

37 T. Fujimoto, K. Sonoda, K. Hijioka, K. Sato, A. Takeda, E. Hasegawa, Y. Oshima and T. Ishibashi, Choroidal Neovascularization Enhanced by Chlamydia pneumoniae via Toll-like Receptor 2 in the Retinal Pigment Epithelium *Investigative ophthalmology & visual science,* 2010, **51**, 4694–4702.

38 X. Z. West, N. L. Malinin, A. A. Merkulova, M. Tischenko, B. A. Kerr, E. C. Borden, E. A. Podrez, R. G. Salomon and T. V. Byzova, Oxidative stress induces angiogenesis by activating TLR2 with novel endogenous ligands *Nature (London),* 2010, **467**, 972–976.

39 S. Doyle, K. Mulfaul, N. Fernando, K. Chirco, E. Connolly, T. Ryan, E. Ozaki, K. Brennan, A. Maminishkis and R. Salomon, TLR2 bridges oxidative damage and complement-associated pathology and is a therapeutic target for age-related macular degeneration *Invest. Ophthalmol. Vis. Sci.,* 2018, **59**, 3475.

40 K. Mulfaul, E. Ozaki, N. Fernando, K. Brennan, K. R. Chirco, E. Connolly, C. Greene, A. Maminishkis, R. G. Salomon, M. Linetsky, R. Natoli, R. F. Mullins, M. Campbell and S. L. Doyle, Toll-like Receptor 2 Facilitates Oxidative Damage-Induced Retinal Degeneration *Cell reports (Cambridge),* 2020, **30**, 2209–2224.e5.

41 A. Kaczmarek, P. Vandenabeele and D. Krysko, Necroptosis: The Release of Damage-Associated Molecular Patterns and Its Physiological Relevance *Immunity (Cambridge, Mass.),* 2013, **38**, 209–223.

42 Z. Huang, T. Zhou, X. Sun, Y. Zheng, B. Cheng, M. Li, X. Liu and C. He, Necroptosis in microglia contributes to neuroinflammation and retinal degeneration through TLR4 activation *Cell death and differentiation,* 2018, **25**, 180–189.

43 Y. Zhu, B. Dai, Y. Li and H. Peng, C5a and toll-like receptor 4 crosstalk in retinal pigment epithelial cells *Molecular vision,* 2015, **21**, 1122–1129.

44 S. G. Elner, H. R. Petty, V. M. Elner, A. Yoshida, Z. Bian, D. Yang and A. L. Kindzelskii, TLR4 Mediates Human Retinal Pigment Epithelial Endotoxin Binding and Cytokine Expression *Investigative ophthalmology & visual science,* 2005, **46**, 4627.

45 K. Kaarniranta and A. Salminen, Age-related macular degeneration: activation of innate immunity system via pattern recognition receptors *J. Mol. Med.,* 2009, **87**, 117–123.

46 L. CHEN, Y. BAI, M. ZHAO and Y. JIANG, TLR4 inhibitor attenuates amyloid-β-induced angiogenic and inflammatory factors in ARPE-19 cells: Implications for age-related macular degeneration *Molecular Medicine Reports,* 2016, **13**, 3249–3256.

47 J. S. Campbell, K. J. Riehle, J. T. Brooling, R. L. Bauer, C. Mitchell and N. Fausto, Proinflammatory Cytokine Production in Liver Regeneration Is Myd88 -Dependent, but Independent of Cd14 , Tlr2 , and Tlr4 *The Journal of immunology (1950),* 2006, **176**, 2522–2528.

48 C. Monaco, S. M. Gregan, T. J. Navin, B. M. J. Foxwell, A. H. Davies and M. Feldmann, Toll-Like Receptor-2 Mediates Inflammation and Matrix Degradation in Human Atherosclerosis *Circulation,* 2009, **120**, 2462–2469.

49 M. Djidja, S. Francese, P. M. Loadman, C. W. Sutton, P. Scriven, E. Claude, M. F. Snel, J. Franck, M. Salzet and M. R. Clench, Detergent addition to tryptic digests and ion mobility separation prior to MS/MS improves peptide yield and

protein identification for in situ proteomic investigation of frozen and formalin-fixed paraffin-embedded adenocarcinoma tissue sections *Proteomics (Weinheim),* 2009, **9**, 2750–2763.

50 E. Ozaki, L. Gibbons, N. G. Neto, P. Kenna, M. Carty, M. Humphries, P. Humphries, M. Campbell, M. Monaghan, A. Bowie and S. L. Doyle, SARM1 deficiency promotes rod and cone photoreceptor cell survival in a model of retinal degeneration *Life science alliance,* 2020, **3**, e201900618.

51 Y. Sasaki, H. Kakita, S. Kubota, A. Sene, T. J. Lee, N. Ban, Z. Dong, J. B. Lin, S. L. Boye, A. DiAntonio, S. E. Boye, R. S. Apte and J. Milbrandt, SARM1 depletion rescues NMNAT1-dependent photoreceptor cell death and retinal degeneration *eLife,* 2020, **9**.

52 S. G. Kasimsetty, A. Hawkes, K. Barekatain, E. Soo, A. K. Welch and D. B. McKay, TLR2 and NODs1 and 2 cooperate in inflammatory responses associated with renal ischemia reperfusion injury *Transplant immunology,* 2020, **58**, 101260.

53 L. D. Sarah, M. Campbell, E. Ozaki, G. S. Robert, A. Mori, F. K. Paul, J. F. Gwyneth, Anna-sophia Kiang, M. H. Marian, C. L. Ed, A. J. O. Luke, G. H. Joe and P. Humphries, NLRP3 has a protective role in age-related macular degeneration through the induction of IL-18 by drusen components *Nat. Med.,* 2012, **18**, 791–798.

54 V. Tarallo, Y. Hirano, B. Gelfand, S. Dridi, N. Kerur, Y. Kim, W. Cho, H. Kaneko, B. Fowler, S. Bogdanovich, R. C. Albuquerque, W. Hauswirth, V. Chiodo, J. Kugel, J. Goodrich, S. Ponicsan, G. Chaudhuri, M. Murphy, J. Dunaief, B. Ambati, J. Ambati, Y. Ogura, J. Yoo, D. Lee, P. Provost, D. Hinton, G. Núñez, J. Baffi and M. Kleinman, DICER1 Loss and Alu RNA Induce Age-Related

Macular Degeneration via the NLRP3 Inflammasome and MyD88 *Cell,* 2012, **149**, 847–859.

55 W. A. Tseng, T. Thein, K. Kinnunen, K. Lashkari, M. S. Gregory, P. A. D'Amore and B. R. Ksander, NLRP3 Inflammasome Activation in Retinal Pigment Epithelial Cells by Lysosomal Destabilization: Implications for Age-Related Macular Degeneration *Invest. Ophthalmol. Vis. Sci.,* 2013, **54**, 110.

56 R. T. Liu, J. Gao, S. Cao, N. Sandhu, J. Z. Cui, C. L. Chou, E. Fang and J. A. Matsubara, Inflammatory mediators induced by amyloid-beta in the retina and RPE in vivo: implications for inflammasome activation in age-related macular degeneration *Investigative ophthalmology & visual science,* 2013, **54**, 2225–2237.

57 H. Wu, C. Zhao, Q. Xie, J. Xu and G. Fei, TLR2-Melatonin Feedback Loop Regulates the Activation of NLRP3 Inflammasome in Murine Allergic Airway Inflammation *Frontiers in immunology,* 2020, **11**, 172.

58 Y. Liao, H. Zhang, D. He, Y. Wang, B. Cai, J. Chen, J. Ma, Z. Liu and Y. Wu, Retinal Pigment Epithelium Cell Death Is Associated With NLRP3 Inflammasome Activation by All-trans Retinal *Investigative ophthalmology & visual science,* 2019, **60**, 3034–3045.

59 Z. Yang, C. Stratton, P. J. Francis, M. E. Kleinman, P. L. Tan, D. Gibbs, Z. Tong, H. Chen, R. Constantine, X. Yang, Y. Chen, J. Zeng, L. Davey, X. Ma, V. S. Hau, C. Wang, J. Harmon, J. Buehler, E. Pearson, S. Patel, Y. Kaminoh, S. Watkins, L. Luo, N. A. Zabriskie, P. S. Bernstein, W. Cho, A. Schwager, D. R. Hinton, M. L. Klein, S. C. Hamon, E. Simmons, B. Yu, B. Campochiaro, J. S. Sunness, P. Campochiaro, L. Jorde, G. Parmigiani, D. J. Zack, N. Katsanis, J.

Ambati and K. Zhang, Toll-like Receptor 3 and Geographic Atrophy in Age-Related Macular Degeneration *The New England Journal of Medicine,* 2008, **359**, 1456–1463.

60 Y. Ling and F. Xiong, Associations of TLR4 gene polymorphisms with the risk of age-related macular degeneration in a Chinese Han population *Medicine,* 2019, **98**, e15583.

61 S. Kiechl, E. Lorenz, M. Reindl, C. J. Wiedermann, F. Oberhollenzer, E. Bonora, J. Willeit and D. A. Schwartz, Toll-like Receptor 4 Polymorphisms and Atherogenesis *The New England Journal of Medicine,* 2002, **347**, 185–192.

62 Y. Cho, J. J. Wang, E. Y. Chew, F. L. Ferris III, P. Mitchell, C. Chan and J. Tuo, Toll-like Receptor Polymorphisms and Age-Related Macular Degeneration: Replication in Three Case-Control Samples *Investigative ophthalmology & visual science,* 2009, **50**, 5614–5618.

63 A Randomized, Placebo-Controlled, Clinical Trial of High-Dose Supplementation With Vitamins C and E, Beta Carotene, and Zinc for Age-Related Macular Degeneration and Vision Loss: AREDS Report No. 8 *Arch. Ophthalmol.,* 2001, **119**, 1417–1436.

64 C. P. Wong, N. A. Rinaldi and E. Ho, Zinc deficiency enhanced inflammatory response by increasing immune cell activation and inducing IL6 promoter demethylation *Molecular Nutrition & Food Research,* 2015, **59**, 991–999.

65 A. Repić, P. Bulat, B. Antonijević, M. Antunović, J. Džudović, A. Buha and Z. Bulat, The influence of smoking habits on cadmium and lead blood levels in the

Serbian adult people *Environmental science and pollution research international,* 2020, **27**, 751–760.

66 J. THORNTON, R. EDWARDS, P. MITCHELL, R. A. HARRISON, I. BUCHAN and S. P. KELLY, Smoking and age-related macular degeneration: a review of association *Eye (London),* 2005, **19**, 935–944.

67 C. Rubio Armendáriz, T. Garcia, A. Soler, Á J. Gutiérrez Fernández, D. Glez-Weller, G. Luis González, A. H. de la Torre and C. Revert Gironés, Heavy metals in cigarettes for sale in Spain *Environmental research,* 2015, **143**, 162–169.

68 E. W. Wu, D. A. Schaumberg and S. K. Park, Environmental cadmium and lead exposures and age-related macular degeneration in U.S. adults: The National Health and Nutrition Examination Survey 2005 to 2008 *Environmental research,* 2014, **133**, 178–184.

69 E. Damar Güngör, F. Yülek, U. Serkant, Y. Toklu, A. Hocaoğlu and Ş Şimsek, Blood lead and cadmium in age related macular degeneration in a Turkish urban population *Journal of trace elements in medicine and biology,* 2018, **48**, 16–19.

70 N. K. Wills, V. M. Sadagopa Ramanujam, N. Kalariya, J. R. Lewis and F. J. G. M. van Kuijk, Copper and zinc distribution in the human retina: Relationship to cadmium accumulation, age, and gender *Experimental eye research,* 2008, **87**, 80–88.

71 S. Aberami, S. Nikhalashree, M. Bharathselvi, J. Biswas, K. N. Sulochana and K. Coral, Elemental concentrations in Choroid-RPE and retina of human eyes with age-related macular degeneration *Experimental eye research,* 2019, **186**, 107718.

72 T. J. Heesterbeek, M. Rouhi-Parkouhi, S. J. Church, Y. T. Lechanteur, L. Lorés-Motta, N. Kouvatsos, S. J. Clark, P. N. Bishop, C. B. Hoyng, A. I. den Hollander, R. D. Unwin and A. J. Day, Association of plasma trace element levels with neovascular age-related macular degeneration *Experimental eye research,* 2020, **201**, 108324.

73 J. C. Erie, J. A. Butz, J. A. Good, E. A. Erie, M. F. Burritt and J. D. Cameron, Heavy Metal Concentrations in Human Eyes *American journal of ophthalmology,* 2005, **139**, 888–893.

74 S. J. Park MD, J. H. Lee MS, Woo, Se Joon, MD, PhD, Kang, Se Woong, MD, PhD and Park, Kyu Hyung, MD, PhD, Five Heavy Metallic Elements and Age-Related Macular Degeneration *Ophthalmology,* 2015, **122**, 129–137.

75 A. G. M. Jünemann, P. Stopa, B. Michalke, A. Chaudhri, U. Reulbach, C. Huchzermeyer, U. Schlötzer-Schrehardt, F. E. Kruse, E. Zrenner and R. Rejdak, Levels of Aqueous Humor Trace Elements in Patients with Non-Exsudative Age-related Macular Degeneration: A Case-control Study *PloS one,* 2013, **8**, e56734.

76 J. C. Erie, J. A. Good, J. A. Butz and J. S. Pulido, Reduced Zinc and Copper in the Retinal Pigment Epithelium and Choroid in Age-related Macular Degeneration *American Journal of Ophthalmology,* 2009, **147**, 276–282.e1.

77 M. Aranaz, M. Costas Rodriguez, L. Lobo, H. González-Iglesias, F. Vanhaecke and R. Pereiro, Pilot study of homeostatic alterations of mineral elements in serum of patients with age-related macular degeneration via elemental and isotopic analysis using ICP-mass spectrometry 2020, .

78 N. Cardinault, J. Abalain, B. Sairafi, C. Coudray, P. Grolier, M. Rambeau, J. Carré, A. Mazur and E. Rock, Lycopene but not lutein nor zeaxanthin decreases in serum and lipoproteins in age-related macular degeneration patients *Clinica chimica acta,* 2005, **357**, 34–42.

79 A. Biesemeier, E. Yoeruek, O. Eibl and U. Schraermeyer, Iron accumulation in Bruch's membrane and melanosomes of donor eyes with age-related macular degeneration *Experimental Eye Research,* 2015, **137**, 39–49.

80 D. Wysokinski, K. Danisz, J. Blasiak, M. Dorecka, D. Romaniuk, J. Szaflik and J. P. Szaflik, An association of transferrin gene polymorphism and serum transferrin levels with age-related macular degeneration *Experimental eye research,* 2013, **106**, 14–23.

81 J. C. Erie, J. A. Good and J. A. Butz, Excess Lead in the Neural Retina in Age-Related Macular Degeneration *American Journal of Ophthalmology,* 2009, **148**, 890–894.

82 M. Mayer and J. G. M. Frederik, Whole blood selenium in exudativeage-related maculopathy 1998, **76**, 62–67.

83 Ugarte, Marta, DPhil, FRCOphth, N. N. Osborne PhD, L. A. Brown PhD and Bishop, Paul N., FRCOphth, PhD, Iron, zinc, and copper in retinal physiology and disease *Survey of ophthalmology,* 2013, **58**, 585–609.

84 S. Rodríguez-Menéndez, B. Fernández, M. García, L. Álvarez, M. Luisa Fernández, A. Sanz-Medel, M. Coca-Prados, R. Pereiro and H. González-Iglesias, Quantitative study of zinc and metallothioneins in the human retina and

RPE cells by mass spectrometry-based methodologies *Talanta,* 2018, **178**, 222–230.

85 F. Virgili, R. Ambra, J. McCormack, Ellen E.A. Simpson, D. Ciarapica, L. Barnaba, E. Azzini and A. Polito, Genetic Polymorphisms and Zinc Status: Implications for Supplementation in Metabolic Diseases *Curr. Pharm. Des.,* 2018, **24**, 4131–4143.

86 M. Maywald and L. Rink, Zinc homeostasis and immunosenescence *Journal of Trace Elements in Medicine and Biology,* 2015, **29**, 24–30.

87 Age-Related Eye Disease Study Research Group, *A randomized, placebo-controlled, clinical trial of high-dose supplementation with vitamins C and E, beta carotene, and zinc for age-related macular degeneration and vision loss: AREDS report no. 8*, 119, United States, 2001.

88 T. N. Abduljabbar, B. L. Sharp, H. J. Reid, N. Barzegar-Befroeid, T. Peto and I. Lengyel, Determination of Zn, Cu and Fe in human patients' serum using micro-sampling ICP-MS and sample dilution *Talanta (Oxford),* 2019, **204**, 663–669.

89 M. A. Aras and E. Aizenman, Redox Regulation of Intracellular Zinc: Molecular Signaling in the Life and Death of Neurons *Antioxidants & redox signaling,* 2011, **15**, 2249–2263.

90 The Age-Related Eye Disease Study Research Group, The effect of five-year zinc supplementation on serum zinc, serum cholesterol and hematocrit in persons randomly assigned to treatment group in the age-related eye disease study: AREDS Report No. 7 *The Journal of nutrition,* 2002, **132**, 697–702.

91 T. N. Abduljabbar, B. L. Sharp, H. J. Reid, N. Barzegar-Befroeid, T. Peto and I. Lengyel, Determination of Zn, Cu and Fe in human patients' serum using micro-sampling ICP-MS and sample dilution *Talanta (Oxford),* 2019, **204**, 663–669.

92 H. Jin, P. Goossens, P. Juhasz, W. Eijgelaar, M. Manca, J. M. H. Karel, E. Smirnov, C. J. J. M. Sikkink, B. M. E. Mees, O. Waring, K. van Kuijk, G. E. Fazzi, M. J. J. Gijbels, M. Kutmon, C. T. A. Evelo, U. Hedin, M. J. A. P. Daemen, J. C. Sluimer, L. Matic and E. A. L. Biessen, Integrative multiomics analysis of human atherosclerosis reveals a serum response factor-driven network associated with intraplaque hemorrhage *Clinical and Translational Medicine,* 2021, **11**, e458–n/a.

93 C. Keller, P. Wei, B. Wancewicz, T. L. Cross, F. E. Rey and L. Li, Extraction optimization for combined metabolomics, peptidomics, and proteomics analysis of gut microbiota samples *Journal of mass spectrometry.,* 2021, **56**, e4625–n/a.

94 H. I. Wettersten, A. A. Hakimi, D. Morin, C. Bianchi, M. E. Johnstone, D. R. Donohoe, J. F. Trott, O. A. Aboud, S. Stirdivant, B. Neri, R. Wolfert, B. Stewart, R. Perego, J. J. Hsieh and R. H. Weiss, Grade-Dependent Metabolic Reprogramming in Kidney Cancer Revealed by Combined Proteomics and Metabolomics Analysis *Cancer research (Chicago, Ill.),* 2015, **75**, 2541–2552.

95 L. Gibbons, E. Ozaki, C. Greene, A. Trappe, M. Carty, J. A. Coppinger, A. G. Bowie, M. Campbell and S. L. Doyle, SARM1 Promotes Photoreceptor Degeneration in an Oxidative Stress Model of Retinal Degeneration *Frontiers in neuroscience,* 2022, **16**, 852114.

96 C. Kosmidou, N. E. Efstathiou, M. V. Hoang, S. Notomi, E. K. Konstantinou, M. Hirano, K. Takahashi, D. E. Maidana, P. Tsoka, L. Young, E. S. Gragoudas, T. W. Olsen, Y. Morizane, J. W. Miller and D. G. Vavvas, Issues with the

Specificity of Immunological Reagents for NLRP3: Implications for Age-related Macular Degeneration *Scientific reports,* 2018, **8**, 461–12.

97 H. E. Bowrey, D. M. Anderson, P. Pallitto, D. B. Gutierrez, J. Fan, R. K. Crouch, K. L. Schey and Z. Ablonczy, Imaging mass spectrometry of the visual system: Advancing the molecular understanding of retina degenerations *Proteomics. Clinical applications,* 2016, **10**, 391–402.

98 M. Karas, D. Bachmann and F. Hillenkamp, Influence of the wavelength in high-irradiance ultraviolet laser desorption mass spectrometry of organic molecules *Analytical chemistry (Washington),* 1985, **57**, 2935–2939.

99 K. Tanaka, H. Waki, Y. Ido, S. Akita, Y. Yoshida, T. Yoshida and T. Matsuo, Protein and polymer analyses up to m/z 100 000 by laser ionization time-of-flight mass spectrometry *Rapid communications in mass spectrometry,* 1988, **2**, 151–153.

100 V. Lopez-Avila, P. J. Roach and R. Urdahl, in *Comprehensive Analytical Chemistry*, ed. nonymous , Elsevier Science & Technology, 2013, p. 325–346.

101 E. Koltay, in *Encyclopedia of Analytical Science*, ed. nonymous , p. 456–466.

102 C. Zhang, H. Zhang, D. W. Litchfield and K. K. -. Yeung, *CHCA or DHB? Systematic comparison of the two most commonly used matrices for peptide mass fingerprint analysis with MALDI-MS*, Advanstar Communications, Inc, Monmouth Junction, 2010.

103 J. H. Gross, in *Mass Spectrometry: A Textbook*, ed. J. H. Gross, Springer International Publishing, Cham, 2017, p. 651–720.

104 R. Knochenmuss, Ion formation mechanisms in UV-MALDI *Analyst,* 2006, **131**, 966–986.

105 M. Karas, M. Glückmann and J. Schäfer, Ionization in matrix-assisted laser desorption/ionization: singly charged molecular ions are the lucky survivors *Journal of mass spectrometry.,* 2000, **35**, 1–12.

106 T. W. Jaskolla and M. Karas, Compelling Evidence for Lucky Survivor and Gas Phase Protonation: The Unified MALDI Analyte Protonation Mechanism *J. Am. Soc. Mass Spectrom,* 2011, **22**, 976–988.

107 L. E. Flint, G. Hamm, J. D. Ready, S. Ling, C. J. Duckett, N. A. Cross, L. M. Cole, D. P. Smith, R. J. A. Goodwin and M. R. Clench, Characterization of an Aggregated Three-Dimensional Cell Culture Model by Multimodal Mass Spectrometry Imaging *Analytical chemistry (Washington),* 2020, **92**, 12538–12547.

108 Z. Miao and H. Chen, Direct Analysis of Liquid Samples by Desorption Electrospray Ionization-Mass Spectrometry (DESI-MS) *J Am Soc Mass Spectrom,* 2009, **20**, 10–19.

109 Takáts Takáts, W. Wiseman, G. Gologan and C. Cooks, Mass Spectrometry Sampling Under Ambient Conditions with Desorption Electrospray Ionization *Science,* 2004, **306**, 471–473.

110 K. Ohls and B. Bogdain, History of inductively coupled plasma atomic emission spectral analysis: from the beginning up to its coupling with mass spectrometry *Journal of analytical atomic spectrometry,* 2016, **31**, 22–31.

111 J. Mermet, in *Inductively Coupled Plasma Spectrometry and its Applications*, ed. nonymous , Blackwell Publishing Ltd, Oxford, UK, 2006, p. 27–60.

112 K. Newman, C. Metcalfe, J. Martin, H. Hintelmann, P. Shaw and A. Donard, Improved single particle ICP-MS characterization of silver nanoparticles at environmentally relevant concentrations *Journal of analytical atomic spectrometry,* 2016, **31**, 2069–2077.

113 J. W. Olesik and P. J. Gray, Considerations for measurement of individual nanoparticles or microparticles by ICP-MS: determination of the number of particles and the analyte mass in each particle *Journal of analytical atomic spectrometry,* 2012, **27**, 1143–1155.

114 , https://resources.perkinelmer.com/corporate/pdfs/downloads/bro_nexion350icpmsbrochure.pdf, (accessed January 2024).

115 PerkinElmer Inc., *Advantages of Short Settling Times for Quadrupole-Based ICP-MS Laser Ablation Imaging*, 2020.

116 D. Günther and C. Heinrich, Enhanced sensitivity in laser ablation-ICP mass spectrometry using helium-argon mixtures as aerosol carrier *Journal of Analytical Atomic Spectrometry,* 1999, **14**, 1363–1368.

117 L. Elemental Scientific Lasers, The TwoVol3 Ablation Cell for ESL Platform 2018, .

118 C. J. Greenhalgh, E. Karekla, G. J. Miles, I. R. Powley, C. Costa, J. de Jesus, M. J. Bailey, C. Pritchard, M. MacFarlane, J. H. Pringle and A. J. Managh, Exploration of Matrix Effects in Laser Ablation Inductively Coupled Plasma Mass

Spectrometry Imaging of Cisplatin-Treated Tumors *Analytical chemistry (Washington),* 2020, **92**, 9847–9855.

119 G. W. Grime, O. B. Zeldin, M. E. Snell, E. D. Lowe, J. F. Hunt, G. T. Montelione, L. Tong, E. H. Snell and E. F. Garman, High-Throughput PIXE as an Essential Quantitative Assay for Accurate Metalloprotein Structural Analysis: Development and Application *Journal of the American Chemical Society,* 2020, **142**, 185–197.

120 PAUL WOLFGANG and STEINWEDEL HELMUT, *Apparatus for separating charged particles of different specific charges*, 1960.

121 F. A. Mellon, MASS SPECTROMETRY | Principles and Instrumentation *Encyclopedia of Food Sciences and Nutrition, Ten-Volume Set,* , 3739–3749.

122 B. A. Mamyrin, Time-of-flight mass spectrometry (concepts, achievements, and prospects) *International journal of mass spectrometry,* 2001, **206**, 251–266.

123 B. A. Mamyrin, V. I. Karataev, D. V. Shmikk and V. A. Zagulin, The mass-reflectron, a new nonmagnetic time-of-flight mass spectrometer with high resolution *Zh.Eksp.Teor.Fiz,* 1973, **64**, 82–89.

124 Waters, waters.com, (accessed January 2024).

125 D. A. Cooper-Shepherd, J. Wildgoose, B. Kozlov, W. J. Johnson, R. Tyldesley-Worster, M. E. Palmer, J. B. Hoyes, M. McCullagh, E. Jones, R. Tonge, E. Marsden-Edwards, P. Nixon, A. Verenchikov and J. I. Langridge, Novel Hybrid Quadrupole-Multireflecting Time-of-Flight Mass Spectrometry System *Journal of the American Society for Mass Spectrometry,* 2023, **34**, 264–272.

126 M. I. Yavor, T. V. Pomozov, S. N. Kirillov, Y. I. Khasin and A. N. Verenchikov, High performance gridless ion mirrors for multi-reflection time-of-flight and electrostatic trap mass analyzers *International journal of mass spectrometry,* 2018, **426**, 1–11.

127 A. Verenchikov, S. Kirillov, Y. Khasin, V. Makarov, M. Yavor and V. Artaev, Multiplexing in Multi-Reflecting TOF MS *Journal of Applied Solution Chemistry and Modeling,* 2017, **6**, 1–22.

128 Waters, https://www.waters.com/nextgen/us/en/products/mass-spectrometry/mass-spectrometry-systems/select-series-mrt.html, (accessed January 2024).

Chapter 2

Joshua Millar, Ema Ozaki [2], Susan Campbell [1], Catherine Duckett [1], Sarah Doyle [2] and Laura M. Cole [1]*

Optimisation of strategies aimed to study ocular disease through multimodal workflows

1. Centre for Mass Spectrometry Imaging, Biomolecular Research Centre, Sheffield Hallam University, Sheffield S1 1WB, UK
2. Immunobiology Research Group, Department of Clinical Medicine, Trinity College Institute of Neuroscience (TCIN), School of Medicine, Trinity College Dublin (TCD), D02 R590 Dublin 2, Ireland

Author Contribution: J. Millar conducted all analysis, sample preparation & data processing

Other Contributions: E. Ozaki sectioned & mounted the mouse ocular tissue used in this study

Abstract

The prevalence of ocular disease is rising, especially as our populations begin to age. Diseases of the eye that occur in the elderly such as age-related macular degeneration (AMD), diabetic retinopathy, and retinitis pigmentosa have required more attention due to increasing demands on healthcare systems aiming to aid our goring and ageing populations. Many of the studies investigating ocular disease have been fruitful but reach difficulties where the limit of techniques is reached. In order to make progress in ocular disease research, a multidisciplinary approach must be taken. Mass Spectrometry Imaging (MSI) is often overlooked for ocular disease pathology, with the majority of studies being undertaken using histological or liquid chromatography-based techniques. With every application and tissue type, special considerations must be made in the sample preparation steps in order to ensure quality data is produced. The following study outlines the sample preparation optimisations used in consideration of ocular tissue to study the peptides relating to the innate immune system and the field of ocular pathology.

1.0. Introduction

Ocular disease affects over 2.2 billion people worldwide, and the World Health Organisation (WHO) estimates almost half of cases are preventable or have not been addressed.[1] Part of the unsustainable growth in ocular disease can be attributed to the lack of understanding of some of the ocular diseases, such as with age-related macular degeneration (AMD), a disease which effects around 196 million people worldwide and has a poor prognosis for the majority of patients, with only 15% able to receive treatment due to lack of viable drug targets.[1,2] Key to the success in finding viable drug targets is the investigation of ocular pathology. Recently, studies have claimed that mass spectrometry (MS)

is the “choice” method for the analysis of the drugs, metabolites and disease biomarkers within ocular disease.[3] Moreover, recent research has stimulated further interests into specific pathways and biological systems within the ophthalmological community through the utilisation of MS methods. For example, studies investigating presbyopia and the microcirculation within the lens of the eye have identified aquaporins as potential viable drug targets for use in the future.[4] In addition to this, studies ranging over the past couple of decades have identified key proteins relating to the complement and innate immune systems.[5-7] Whilst genetic and immunological studies have produced potential investigative targets, few studies have utilised the mass spectrometric approach to disease biology.

Recent studies have investigated the involvement of the innate immune system within ocular biology, namely the association with AMD.[5-9] The studies name a class of proteins known as toll-like receptors, of which there are 13, with 10 being expressed within the human genome.[10] Their association with damage-associated molecular patterns, pathogen associated molecular patterns and chronic inflammatory pathways have made them crucial targets of interest within AMD and wider ocular pathology.[2,8,11,12]

One key, yet occasionally overlooked aspect of mass spectrometry is the intricacy involved in sample preparation. Whilst it is generally acknowledged that sample preparation is a fundamental aspect to the process, little care is noted to the minutiae that can be associated with each class of target analytes. Aquaporins and toll-like receptors for example, are membrane bound proteins, so often to make the proteins accessible for enzymatic digestion, solubilisation steps may

diverge from those related to other proteins being digested. Equally, classes of compounds such as lipids and metabolites, though they share many chemical qualities, must be considered individually for the optimal results to be achieved.

Sample preparation and method optimisation are crucial steps when evaluating a workflow for the analysis of a sample by mass spectrometry imaging (MSI).[13-15] For decades, the development of methods and techniques to be applied to mass spectrometry, namely MSI have been ever growing, yet despite the exponential growth of publications relating to MSI there is little consensus of the preparation of samples, nor the utilisation of matrix assisted laser desorption ionisation MS imaging (MALDI-MSI) for their analyses.[13,16,17] As MSI methods and techniques become more established, the unique combination of analytes and sample matrices can be infinite, and each combination of analyte and matrix can come with nuances and challenges which require optimisation of analytical procedure.

Multimodal workflows are becoming increasingly more prevalent, and as they become more popular their use in high-value studies may increase. Therefore, for the multimodal workflow to work, they must be truly multimodal, and allow for multiple methodologies to work sequentially on the same tissue or sample section. Thereby, work herein explores the initial sample preparation of MALDI-MSI, and the targeting of spatially localised peptides within ocular tissue, in addition to laser ablation inductively coupled plasma mass spectrometry (LA-ICP-MSI), and the initial sample preparation that not only underpins LA-ICP-MSI, but the multimodal approach.

2.0. Materials

2.1. Instrumentation & Parameters

2.1.1. MALDI-MS

Profiles and imaging data were acquired using a SYNAPT G2 MALDI HDMS (Waters Corporation, Manchester, UK), in positive ion sensitivity mode at a mass resolution of 10,000 FWHM in ion mobility mode, within the mass range 700 to 2000Da. The Nd:YAG laser was set to 1 kHZ repetition rate with a laser power of 250 a.u. IMS wave velocity parameters applied were ramped over the full IMS cycle with a start velocity of 700 ms^{-1} and end velocity of 200 ms^{-1}.

2.1.2. MALDI Imaging

Images were acquired at 100 µm spatial resolution for porcine tissue, and 50 µm for mouse tissues. Data were processed using Waters HD Imaging software (Waters Corporation, Manchester, UK). Processing was applied to the 2000 most intense peaks at a resolution of 10000, and a low intensity threshold of 50, and a m/z mass window of 0.05 Da. Normalisation was performed through adjustment by total ion count (TIC), and images were compiled on a linear scale, with no image smoothing.

2.1.3. LA-ICP-MS

Analysis was conducted using a NexION 350X ICP-MS (PerkinElmer, Manchester, UK) coupled to an UP-213 LA system (New Wave Research, Freemont, CA, USA). The ICP-MS was run in Kinetic Energy Discriminatory (KED) mode utilising a variable laser spot size, 46% laser energy, a repetition rate of 22 Hz, a scan rate of 25 μms^{-1} warmup time of (6-40 µm), 40 s, washout time of 30 s and an acquisition time of 0.420 s.

2.1.4. Sample Materials

Porcine ocular tissue samples were obtained from MedMeat (Wetlab, Warwick, UK) and 10 µm sagittal sections were mounted onto polylysine slides. Sectioned mouse tissue was obtained from Department of Clinical Medicine, School of Medicine, Trinity College Dublin, where mice were raised and culled in conditions that adhere to the principles laid out by the internal ethics committee at TCD, and all relevant national licences were obtained before commencement of all studies before being processed & sent to Shefield Hallam University. For each analytical experiment 3 technical replicates were performed. Trypsin was obtained from Promega (Southampton, UK). Acetonitrile, methanol, ethanol, chloroform. and glacial acetic acid were obtained from Fisher Scientific (Loughborough, UK). α-hydroxycinnamic acid (CHCA), trifluoroacetic acid (TFA), and octyl-α/β-glucoside (Oc/Glc) were obtained from Sigma Aldrich (Gillingham, UK). Xtra adhesive poly-lysine slides were obtained from Leica Biosystems (Newcastle, UK) and ITO slides were obtained from Visiontek (Chester, UK).

2.1.5. Washing

Wash steps were performed on ocular tissue by submerging slides of tissue in 50 ml of freshly prepared solvents in starting with 70% EtOH (1 min), followed by 90% EtOH (1 min), $CHCl_3$ (30 s) and 90:9:1 EtOH:gAcOH:H_2O (1 min)

2.1.6. Enzymatic Digests

Enzyme was applied using SunChrom SunCollect (Friedrichsdorf, Germany) MALDI Matrix Applicator. For tryptic peptide images, 6 layers of 20 $\mu g ml^{-1}$ trypsin with 0.1% octyl-α/β-glucoside was sprayed at 4 $\mu l min^{-1}$, with an N_2 Pressure 35 psi, in the presence of warm water to prevent drying. Samples were subsequently placed in a humidity chamber filled with 50:50 MeOH:H_2O, sealed and placed in an incubator overnight at 37ºC.

2.1.7. Matrix Application

5 $mgml^{-1}$ α-hydroxycinnamic acid dissolved in 50:50 ACN:H_2O (0.1% TFA) was applied using SunChrom SunCollect (Friedrichsdorf, Germany) in 5 layers at 4 $\mu lmin^{-1}$ with a N_2 pressure of 35 psi. Once matrix was applied, samples were either submitted for analysis or vacuum sealed and placed in -80 ºC storage for ≤1 month prior to analysis.

2.1.8. LA-ICP-MS Methods

All samples used for LA-ICP-MS were dried under a stream of N_2 or placed within a vacuum desiccator overnight prior to analysis.

3.0. Results and Discussion

3.1. Washing Tissue

The ability to detect analytes of interest effectively from biological tissues is highly dependent on sample preparation, one of which is the pre-treatment step, sample washing. Biological tissues are immensely complex, and may contain many unwanted species such as salts, and lipids, which can mask the detection of peptides and proteins.[14] As they are chemically different from proteins, they can be removed in a series of wash steps; most of which employ a sequence of aqueous and organic solvents, ideally with combinations removing lipid and salt interferences.[13-15,18] For MALDI experiments where the target analytes are tryptic peptides, considerations for the enzymatic digest must be made in addition to those steps which remove unwanted species.[19]

Typically, salts and lipids can be eliminated by immersion of the tissue in 70-90% ethanol (EtOH).[15] By applying these washes sequentially from most aqueous to most organic, the washing steps can help to fix the tissue.[15] ‘Standard’ procedures often include a 0.5-1 minute wash in up to three ethanol solutions,

such as 70%, 90%, 95% respectively.[13-15] After a short drying step in ambient conditions, these washes can be seen to improve the signal-to-noise ratio of m/z peaks of peptides. Additionally, more aggressive wash steps have been trialled in the past, with some using chloroform, hexane, acetone, toluene and xylene to remove lipids that may have been left behind. These steps are adapted from lipid extraction methods, operating under the principle that the hydrophobic lipids will be dissolved in the organic solvents more readily, though too harsh a wash step can cause the damage or removal of the target peptides.[13]

In more recent times, more complex solutions have been applied in place of an aggressive solvent, most notably, Carnoy's solution and derivatives thereof. Carnoy's solution (60:30:10 EtOH:$CHCl_3$:gAcOH) includes a mixture of ethanol and one of the strong organic solvents, chloroform, in addition to glacial acetic acid.[15,20] Carnoy's solution, derived in the 19th century, has historically been used as a fixative for various purposes including immunohistochemistry.[21,22] The chloroform and glacial acetic acid within Carnoy's solution, when used as a denaturing fixative is theorised to counteract the collapse of tissue caused by the protein coagulation that results from the alcohol present in the denaturing step by creating hydrogen bonds within the tissue.[21] This preservatory effect could in theory contribute to better preservation of the tissue for use within mass spectrometry imaging (MSI). In addition, it has been theorised that the presence of an acid within the tissue may help with the formation of positive ions within positive mode MALDI-MSI.[23]

Utilising the literature available, an amalgamation of multiple publications and their respective practices for washing tissue were encapsulated in four simplified

methods detailed in Table 1. Form here, the wash methods were applied to porcine ocular tissue in triplicate, and matrix was spotted at a concentration of 5 $mgml^{-1}$ onto the washed tissue, before analysis by MALDI-MS.

Table 1 Wash methods utilised to test the efficacy of reducing interferences from salts and lipids, and to improve signal from peptides.

ID	Step 1	Duration (minutes)	Step 2	Duration(minutes)	Step 3	Duration(minutes)	Step 4	Dur-ation (minutes)
WM01	70 % EtOH	1	90% EtOH	1	$CHCl_3$	1		
WM02	70 % EtOH	1	90% EtOH	1	$CHCl_3$	1	Carnoy's Solution	1
WM03	70 % EtOH	1	Carnoy's Solution	1				
WM04	70 % EtOH	1	EtOH	1				
WM05	H20	10						
WM06	70 % EtOH	1	90% EtOH	1	$CHCl_3$	1	90:9:1 EtOH:gAcOH:H_2O	1

The wash methods showed variability between each replicate, however, the results were clearly able to show the effect that they had on the tissues. Using phosphatidylcholine (PC) (m/z 782) as a marker of the presence of lipids, and histone 2A (m/z 944) and actin (m/z 1198) as an indicator of the presence of tryptic peptides, the effectiveness of the wash methods was assessed. Figure 1 shows how the lipid envelope (600 – 900 Da) can be affected by the different wash methods; with wash method 1, 3, 4 and 6 exhibiting the most diminished lipid envelope in comparison to the rest of the ions within the spectra. The wash method that provided the least amount of PC ions at m/z 782, was wash method 4 (Figure). Whilst the wash proved effective at removing lipid interferences, there was also a diminished result from the measured peptides at m/z 944 and m/z

1198 (Figure). The wash method that provided the best signal-to-noise ratio was wash method 6 (Table). Wash method 6 was most similar to wash methods 1 and 2, however differed in the final step, whereby a final wash with 90:9:1 EtOH:gAcOH:H_2O was added. This final step, similar to the Carnoy's solution was seen to help with the intensity of the peptides, without worsening any interfering lipid masses.

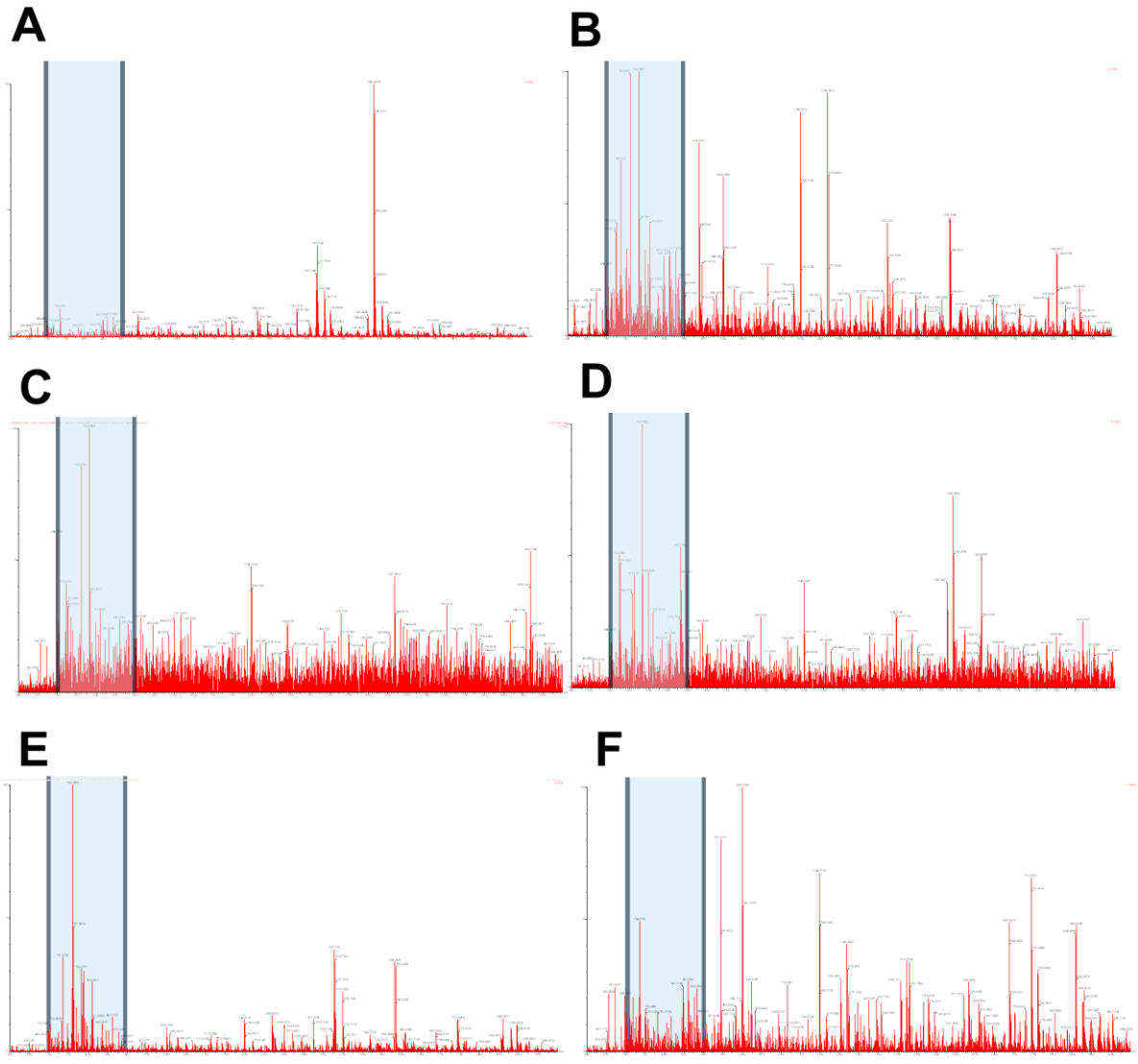

Figure 1 Mass spectra obtained from tissue by MALDI-MS analysis using wash methods; (A) 1, (B) 2, (C) 3, (D) 4, (E) 5, (F) 6. The mass spectrums were obtained using a mass range of 600-2000 Da, with the lipid envelope (700-900 Da) highlighted.

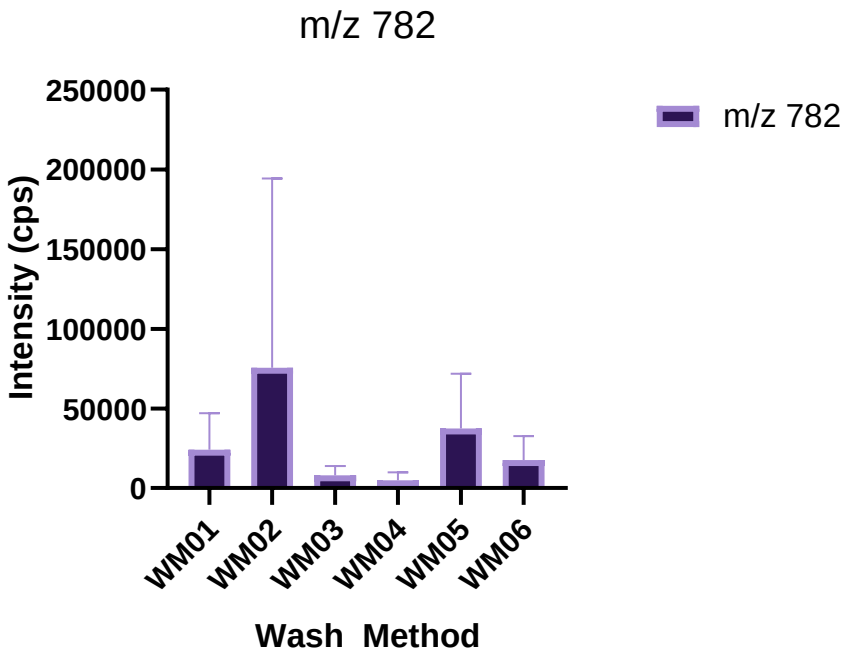

Figure 2 Intensity of phosphatidylcholine (PC) at m/z 782 within the spectra produced from each wash method. Error bars represent standard deviation of the technical replicates (n=3)

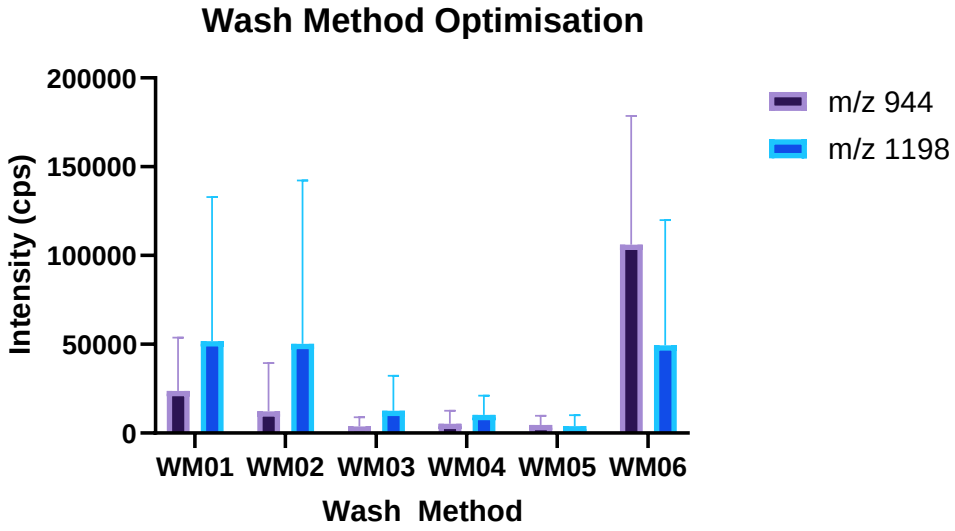

Figure 3 Intensities of peptides histone H2A (m/z 944) and actin (m/z 1198) after each wash method (WM01-WM06) Error bars represent standard deviation of the technical replicates (n=3)

Table 2 Peak ratio of the phospholipid (m/z 782) to the peptide peaks m/z 944 and m/z 1198

	m/z 944	***m/z 1198***
WM01	*1.034693*	*2.01298*
WM02	*0.249781*	*0.958585*
WM03	*0.346381*	*1.100528*
WM04	*0.614897*	*1.409079*
WM05	*0.525355*	*0.638271*
WM06	*9.705669*	*4.019405*

3.2. Tryptic Digestion

In addition to wash steps, crucial to the identification of peptides within MSI is the cleavage of the peptides from the tertiary structures of the proteins. For MALDI-MSI, one of the most used mechanisms for cleavage is the use of trypsin to yield tryptic peptides.[24] This enzyme specifically cleaves peptide bonds at the C-terminal side of lysine and arginine residues. The use of trypsin requires a number of prerequisites for the use with MSI. One key issue is the polar solvent used to dissolve trypsin, which can in turn mobilise the species of interest within the tissue and can be detrimental to the conservation of localisation within the tissue.

The most common way to apply trypsin in a way that disrupts the localisation of species the least is through the use of a robotic sprayer.[19,25] Some robotic sprayers, such as the SunChrom SunCollect rely on low flow rates and a fine

spray of enzyme by utilising a fine N_2 gas. Other sprayers such as the HTX Imaging series of sprayers rely on a similar principle, but by utilising a heated capillary within the sprayer, can apply the enzyme at much higher flow rates.[20,26] In addition to helping the application and subsequent evaporation of the enzyme solvent, the temperatures used to apply the enzyme are typically between 30 and 45 °C, with temperatures over 37 °C allowing the enzyme to become 'pre-activated' allowing for more efficient digestion.[20,26]

Use of surfactants has been reported as beneficial for MALDI-MSI analyses. Surfactants have long been used to aid the development of in-solution digests. By allowing proteins to unfold and reduce the number of cleavage site rendered inaccessible by steric hinderance, the surfactant can increase the number of successful cleavages in the digest, and when applied properly, can give the same effect for MSI. One common surfactant is RapiGest SF, a chemical detergent manufactured and sold by the Waters Corporation. RapiGest is an acid labile surfactant and has been shown to unfold proteins, making them more amenable to proteolytic cleavage.[27] In addition to RapiGest, the commercially available octyl-α-β-glucoside (OcGlc) has been shown to aid with the digestion process. OcGlc is a non-ionic surfactant which aids the digestion process by helping to solubilise the proteins, making them accessible for enzymatic digest.[28-30]

An example of this improved signal can be seen in Figure , wherein images of porcine ocular tissue exhibit the improved signal that can be achieved through the addition of a detergent. However, in order to effectively test the efficacy of the commercially available detergents, both OcGlc and RapiGest were tested on sequential tissues of mouse ocular tissue. Figure shows how, when applied to

the same tissues, that the OcGlc and RapiGest surfactants can have differing effects on the efficacy of the MS image quality. From the images, it is clear that, in the case of histone H2A, there is a marked improvement in the signal of the peak at m/z 944.

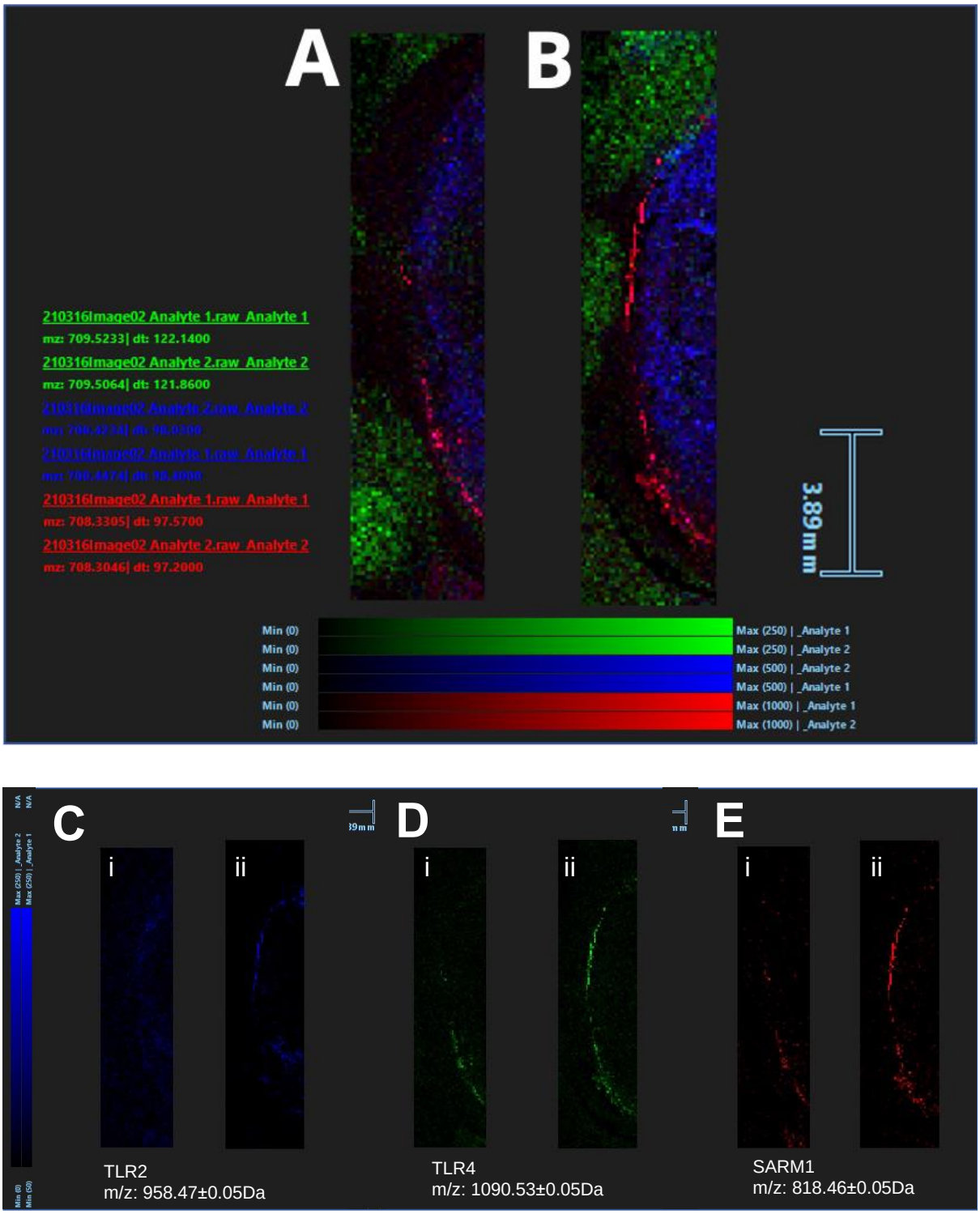

Figure 4 (A) Porcine ocular tissue prepared using 6 layers of trypsin, without the use of a detergent (B) A serial section of porcine ocular tissue prepared with the use of 0.1% octyl-α/β-glucoside in a 20μgml^{-1} trypsin solution (C) Improvement of signal of TLR2 peptide m/z 958.47 (D) Improvement of TLR4 signal m/z*

1090.53 (E) Improvement of signal of SARM1 peptide m/z 818.467* *Tentative peak identifications, within 0.05Da*

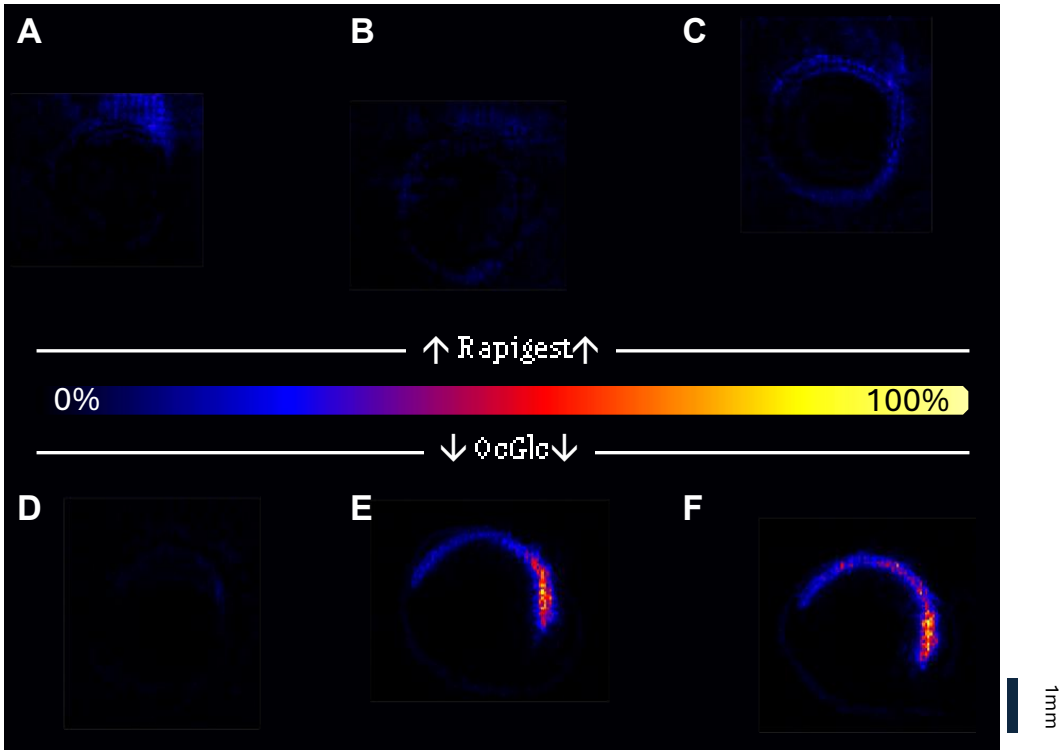

Figure 5 A comparison of a peptide peak m/z 944 (Histone H2A) in mouse ocular tissue prepared with RapiGest (A, B, C) and Octyl-α-β-glucoside (D, E, F) as detergents. For each condition there are 3 technical replicates.

3.1. Matrix Additives

Despite the relative longevity of MALDI-MSI as a technique, matrices used for MALDI-MSI analyses are still subject to issues in the case of inhomogeneous co-crystallisation, interferences from matrix adducts and ions. Homogenous co-crystallisation of the matrix and the analyte of interest is essential for the efficient transport and ionisation of the sample of interest. Peptides are most commonly analysed as $[M+H]^+$ ions, following successful desorption with a MALDI matrix

called α-cyano-hydroxycinnamic acid (CHCA).[31,32] However, unlike some matrices, CHCA has peaks that overlap with the analyte of interest, in this case peptides (Table). Additives to form ionic liquid matrices (ILMs) have become more common due to their proficiency in reducing the detrimental effects caused by interfering matrix peaks.[33] The ILMs help to form adducts with the matrices, in this case CHCA, and thereby reduce the number of peaks within the range that interferes with peptides. Aniline, a phenolic organic compound, has been shown to reduce the number of interfering matrix peaks from CHCA without interfering with the properties of the CHCA which allow it to co-crystallise with and facilitate the transport of the peptides.[33]

Experiments to measure the reduction of the interfering matrix peaks from CHCA were devised, and the highest intensity CHCA peaks were measured within a control and an aniline-CHCA matrix. The results (Figure) show a significant reduction in the presence of m/z 877 ([CHCA-3H+2Na+2K]+) when an equimolar amount of aniline is added to the CHCA mixture. Further experiments (Figure) demonstrated that the addition of aniline did not cause any detriment to image quality. Likewise, when processing images, fewer high intensity peaks were populated by matrix adducts.

Table 3 List of CHCA adducts that are likely to form in MALDI-MS experiments and their corresponding m/z values

Number of CHCA Molecules	***[nCHCA +H]+***	***[nCHCA +Na]+***	***[nCHCA +K]+***	***[nCHCA-H+Na+K]+***	***[nCHCA-2H+2Na+K]+***	***[nCHCA-3H+3Na+K]+***	***[nCHCA-4H+4Na+1K]+***	***[nCHCA-3H+2Na+2K]+***	***[nCHCA-4H+2Na+3K]+***	***[nCHCA-4H+3Na+2K]+***
1	190.0504	212.0324	228.0063	250.9961	271.9703	293.9523	315.9343	309.9262	347.8821	331.9082
2	379.093	401.075	417.0489	440.0387	460.0051	482.9949	504.9769	498.9688	536.9247	520.9508
3	568.1356	590.1176	606.0915	629.0813	648.0399	672.0375	694.0195	688.0114	725.9673	709.9934
4	757.1782	779.1602	795.1341	818.1239	836.0747	861.0801	883.0621	877.054	915.0099	899.036
5	946.2208	968.2028	984.1767	1007.1665	1024.1095	1050.1227	1072.1047	1066.0966	1104.0525	1088.0786
6	1135.2634	1157.2454	1173.2193	1196.2091	1212.1443	1239.1653	1261.1473	1255.1392	1293.0951	1277.1212
7	1324.306	1346.288	1362.2619	1385.2517	1409.2493	1428.2079	1450.1899	1444.1818	1482.1377	1466.1638

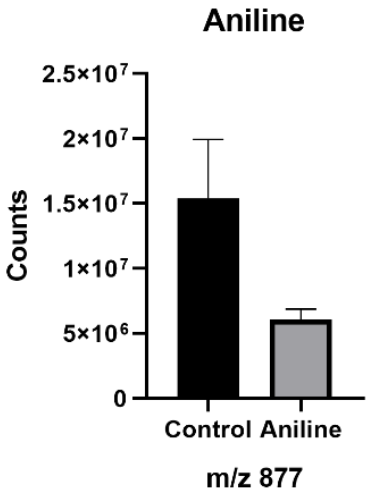

Figure 6 The counts per second of the CHCA peak m/z 877 ([CHCA-3H+2Na+2K]+) within a mouse ocular tissue before when prepared with (aniline) and without (Control) a ionic liquid matrix additive. Error bars represent the standard deviationof the technical replicates (n=3)

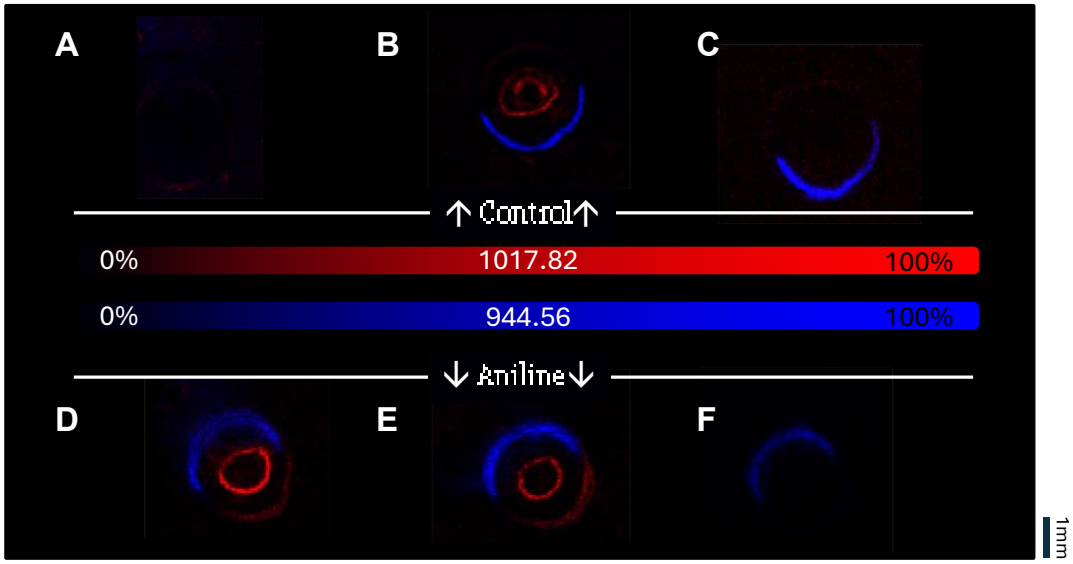

Figure 7 Experiment exhibiting the effects of aniline on image quality of a mouse ocular tissue. The control images (A, B and C) and the images from both the control and the 'aniline' matrix preparations (D,E, F) are represented by overlaid ion images. The image shows m/z 944 in blue (Histone H2A) and a contrasting lens peak in red at m/z 1017. Slight spreading of the retinal species (blue) can be observed in D, E & F. For each condition there are 3 technical replicates.

3.2. ICP-MS

LA-ICP-MS has increasingly become the choice for metallomics, especially for quantitative analysis, with ppq detection limits, some forms of ICP-MS can offer sensitivity unseen in other MS techniques.[34] The method developed herein was required to be able to observe the distribution of essential trace metals to a high spatial resolution and be able to characterise the metals within the chorio-retinal microanatomy, whilst following the sample preparation taken place prior when analysing the same sections by MALDI-MSI.

Some of the key metals of interest to AMD pathology include zinc, copper, cadmium and lead. In addition, there are further elements such as selenium, calcium and iron, however, as these metals are subject to polyatomic interferences from species that share the same mass, and are generated after the atomisation process, they can be difficult to analyse. ^{56}Fe has known interferences with $^{40}Ar^{16}O^{+}$ (MW = 56) caused by oxygen from the atmosphere mixing with the argon fuelled plasma torch.[35-40] This means that for analysis of iron to take place, factors to mitigate the polyatomic interferences must be employed. Figure A shows a trace of ^{63}Cu intensity as a function of time. At the start of the trace (0 – 25 s) the laser is 'off-tissue' and is ablating only glass. The dotted lines (25 – 50 s) show the point at which the tissue was ablated by the laser, and indicate an increase in copper, which can be used to characterise the copper within the tissue. An analysis of ^{56}Fe was executed simultaneously with the copper, seen in Figure B. The intensity plot is however relatively featureless with a slight increase in counts at t=50. This is as the signal-to-noise ratio of the ^{56}Fe to the $^{40}Ar^{16}O$ is too low. Kinetic energy discriminatory (KED) mode is an

optional parameter on the ICP-MS which can help to mitigate these issues perpetuated by polyatomic interferences. KED mode works by introducing a cell gas in Q2 of the ICP-MS. The cell gas, N_2 flows through the cell, opposing the direction of the ion path. There, through use of statistical probability, it will collide with the larger polyatomic species more frequently than with the monoatomic ^{56}Fe, meaning that fewer of the $^{40}Ar^{16}O$ are detected, resulting in an improved signal-to-noise ratio (Figure D). However, as laser ablation has a transient signal, elements must be analysed quickly and simultaneously. Therefore, N_2 which flows through the collision cell will also interact with all of the other elements being analysed at that point. Figure C and Figure show the result of the relative imprecision that KED operated under, exhibiting up to 400-fold reductions intensity being observed for some of the elements. Additionally, the most significant reduction in intensity was that of ^{13}C. The observed loss in signal intensity which could be attributed to loss of some atomic ^{13}C to collisions with He, but is likely due to interference in standard mode from $^{12}C^{1}H$.

Due to the large reduction in an already diminutive signal from low intensity trace metals from copper, further work refrained from the use of KED mode for the detection of problematic elements such as iron. Consequently, for multimodal analysis of elements such as iron, phosphorus, sulphur and chlorine, the recommendation of a non-destructive technique such as particle induced X-ray emission (PIXE) may be considered for use in sequence or in tandem with LA-ICP-MS in future studies.

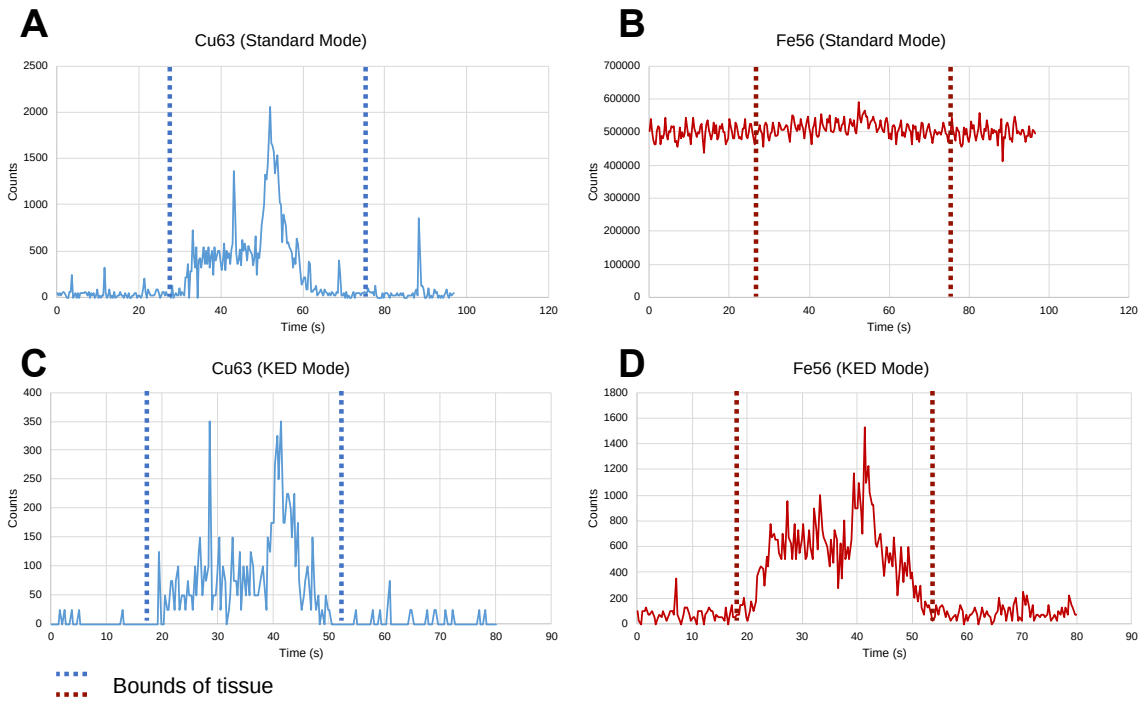

*Figure 8 ICP-MS intensity vs. Time plots of trace metal content within mouse ocular tissue for (**A**)^{63}Cu in standard mode (**B**)^{56}Fe in standard mode (**C**)^{63}Cu in kinetic energy discriminatory (KED) mode and (**D**)^{56}Fe in KED mode. The KED mode allows the filtration of polyatomic interferences, but is here shown to suppress signal of other species.*

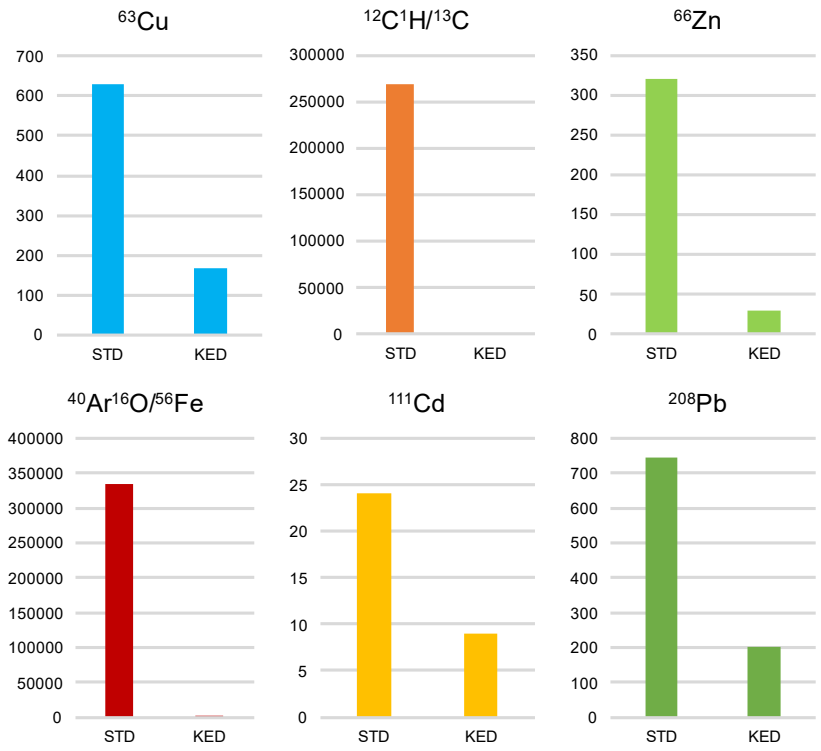

Figure 9 Bar Charts showing the average observed intensities within mouse ocular tissue in both Standard mode (STD) and kinetic energy discrimination (KED) mode. Diminished signal in species such as ^{63}Cu, ^{13}C, ^{66}Zn, ^{111}Cd, and ^{208}Pb will often constitute loss in analyte signal as they experience few interferences. ^{56}Fe has an elevated signal intensity to begin with as interferences cause elevated signal intensity.

Additionally, laser power optimisation can be a key factor for the success of a LA-ICP-MS experiment. Whilst the aim of a laser ablation experiment is to ablate, aerosolise, and atomise all biological material on the slide, leaving nothing behind, it is pertinent to ensure that no glass has been removed with the biological material. Glass, though chiefly constituted of silicon, magnesium and oxygen, can contain a multitude of interfering elements, which may produce interfering atoms or molecules within the ICP-MS, resulting in artefacts that can reduce the quality of the images produced (Figure).

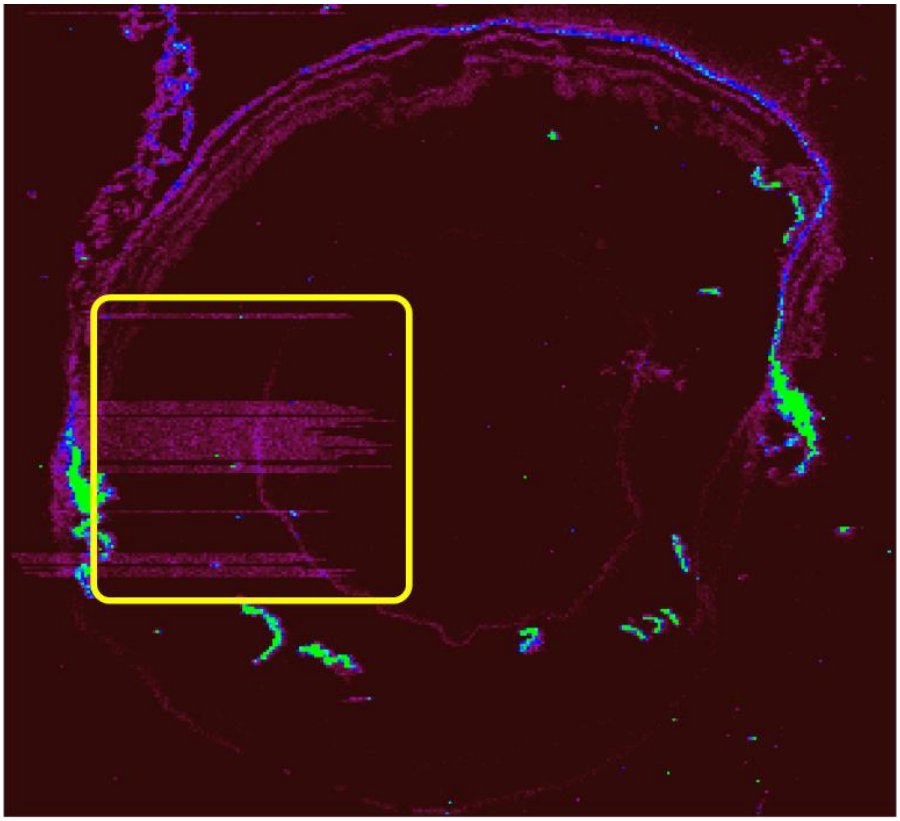

Figure 10 A ^{63}Cu image within a WT mouse ocular tissue, acquired using an ImageBio266 laser ablation unit operating at 1000Hz at a laser energy of 40%. Yellow: An artefact of the experiment caused by increase laser power and repetition rate, resulting in ablation of the glass slide beneath the tissue.

To ascertain the optimal laser energy for the LA-ICP-MS, as too much laser power can be detrimental to the ablation unit, acquiring the surface beneath the sample, and too little can yield unrepresentative data as only the top layer of the sample is acquired. The optimisation took place in 10% intervals between 50-70% which yielded an optimum laser energy between 40-50% (**Error! Reference source not found.**). Further experiments with a laser energy range of 40-50% at

2% intervals yielded an optimum laser energy of 46%, which, when employed at a 100µm spot size, was able to produce an image of a mouse ocular section (**Error! Reference source not found.**) The images obtained from the experiment were able to show distinct localisation within the mouse ocular tissue for ^{13}C, ^{66}Zn, ^{63}Cu and ^{56}Fe.

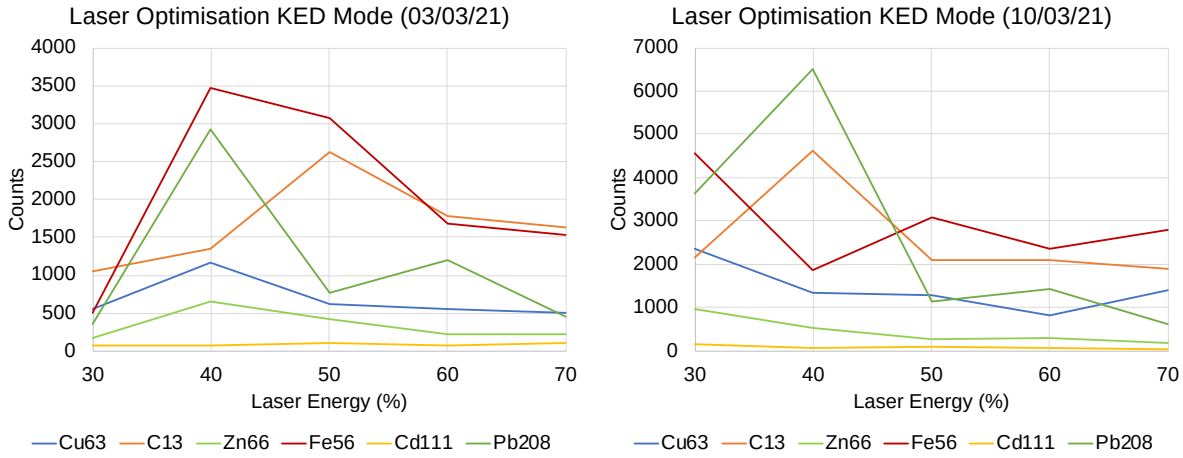

Figure 11 Laser optimisation energy charts, showing the peak intensities from each run obtained. Laser power will often follow a gaussian plot, giving an optimal laser power for any given element. The charts above demonstrate how that optimal power can differ from element to element, and in experimental conditions.

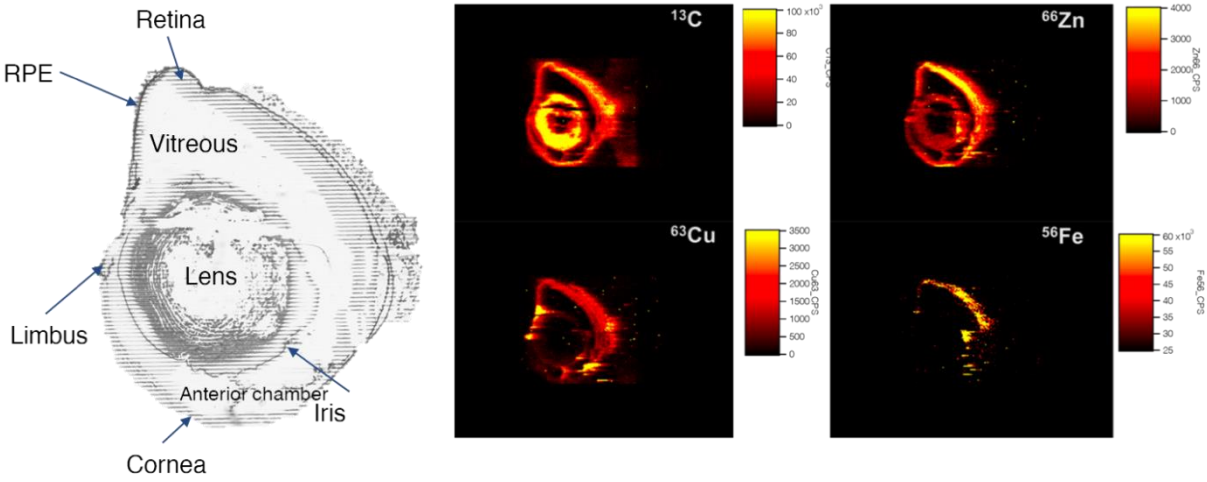

*Figure 12 LA-ICP-MSI images of WT mouse ocular tissue (**A**) The section analysed, labelled with regions of interest (**B**) The ^{13}C reference image (**C**) ^{66}Zn*

*distributions within the ocular tissue (**D**) ^{63}Cu distributions within the mouse ocular tissue (**E**) ^{56}Fe distributions within ocular tissue*

The image showed a localisation for zinc that suggested higher quantities of zinc within the chorio-retinal region of the ocular, tissue, with smaller traces within the lens, the cornea, the iris, and the limbus. Copper, was also observable in small quantities across the tissue but was acutely localised within the limbus, a phenomenon which is known to occur as a symptom Wilson's disease, known as a Kayser-Fleischer Ring, which is a form of copper toxicosis, manifested by an accumulation of tissue copper.[41] Iron, which appeared in much higher quantities, was also observed within the chorio-retinal region of the ocular tissue, where iron plays a key role in RPE65 activity.

Use of tissue previously analysed by MALDI-MSI for LA-ICP-MSI analysis is not well documented, however, as MALDI-MSI is a non-destructive 'soft' ionisation technique, there is sufficient biological matter that can be analysed by LA-ICP-MSI following MALDI analysis. The benefits of analysing the same section over serial or otherwise analogous tissues is predominantly the efficiency that the workflow offers, with fewer sections being used per experiment. Additionally, correlation of species from high spatial resolution MALDI and LA-ICP-MSI analysis done in sequence may offer unique insights into the mechanisms of ocular and other tissue in future.

Though the MALDI analysis is non-destructive, there is a residue of the applied solutions left on the samples, such as the detergents, the enzyme and most predominantly the matrix. As there was no previous literature on the preparation

of LA-IC-MS samples following MALDI analysis, an experiment was devised to ascertain whether a wash step, to remove these deposits, was necessary. Samples that had not been washed had produced successful images (Figure 13), however further experiments to determine the efficacy of a wash step were conducted.

For one set of tissue no alteration in the sample preparation was carried out while the second tissue had been washed in ethanol (70%, 2 × 1min), a standard for CHCA removal. The tissues were then ablated 3 times with the same laser energy (46%) and average peak intensities were taken. The results (Figure) showed that the additional wash step was not necessary, as it was detrimental to the analysis. It is likely that the additional wash step introduced further moisture into the tissue, that caused inefficient aerosol production by the laser. As the samples could be analysed without a wash step, and the wash step was negatively impacting results, the wash step was herein removed from the workflow.

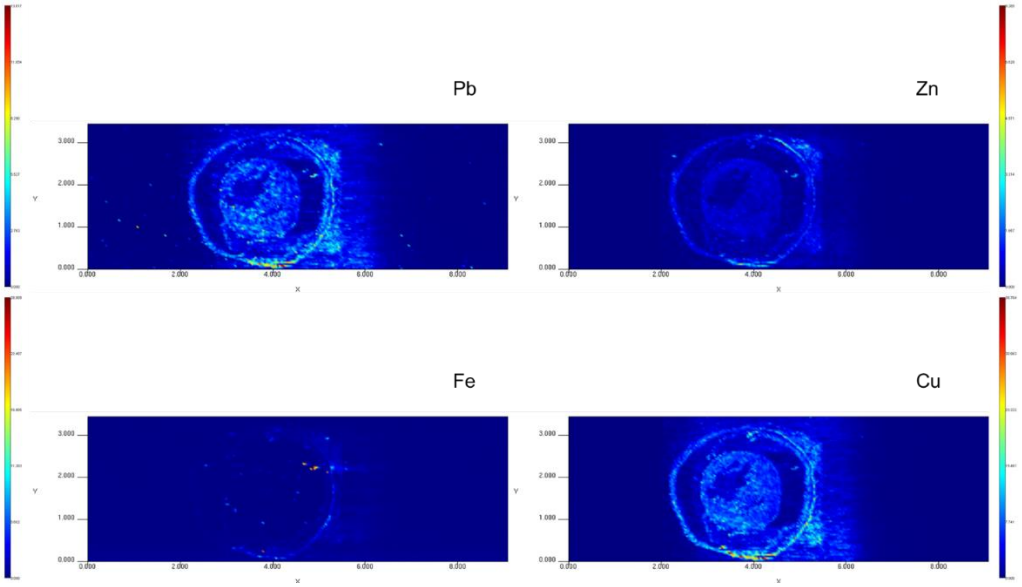

Figure 13 LA-ICP-MS images conducted on mouse ocular tissue that had previously undergone MALDI-MSI analysis, at 40µm spot size, for ^{208}Pb, ^{63}Cu, ^{66}Zn, and ^{56}Fe

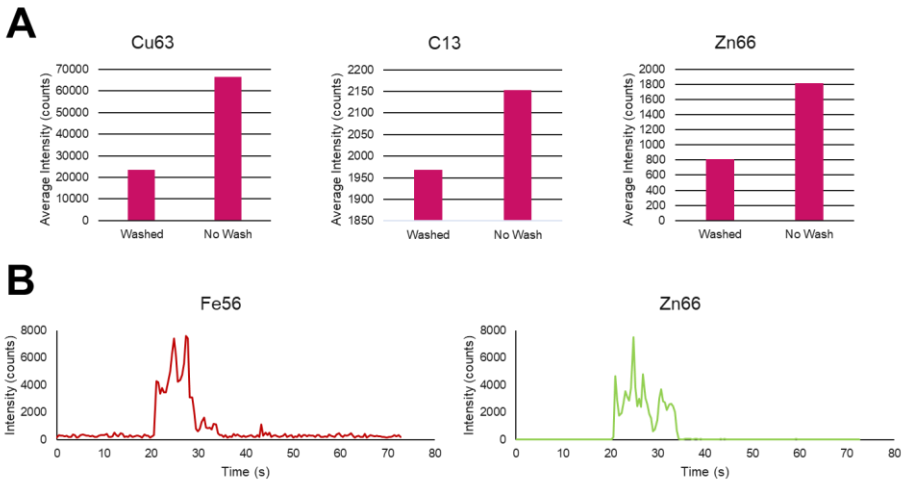

*Figure 14 (**A**) Charts showing the average intensities for both washed and control ocular tissue that had been previously ablated by MALDI-MSI (**B**) Intensity vs Time graphs showing data obtained from previously ablated ocular tissues, showing that metallomic data could be obtained from tissue used in MALDI-MSI studies.*

4.0. Conclusion

Sample preparation methods for modalities such as MALDI have always been of crucial importance to the success of an analytical strategy, with the issue becoming even more pertinent when applied to peptidomics by MALDI-MS.[14,17,20] The study herein set out to achieve an optimised protocol for the analysis of peptides by MALDI-MSI, taking into account the removal of interferences through wash steps and the inclusion of additives, as well as the optimisation of enzymatic digest through the use of surfactants. For washing, following a conventional ethanol fixation and chloroform-based wash, it was found that the use of acidic solution for hydration promoted the ionisation of species by MALDI-MS following enzymatic digestion. Additionally, the use of commercially available detergents showed that the use of OcGlc was more effective at providing peptides than that of RapiGest. Additives to matrix are common for MALDI-MS, and in this case the use of aniline was found not only to promote the suppression of matrix peaks but also was shown to not significantly impact the quality of the MS images. Through the trial of multiple workflows and methodologies, the work herein can be used to highlight just how crucial these methods can be for peptide analysis by MALDI, showing the reduction of suppressing interferences and the intensification of analyte species by combining a multitude of developed workflows.

In addition, this study took the first steps towards multimodal imaging of ocular tissue by MALDI-MSI and LA-ICP-MSI. The LA-ICP-MSI work here in was optimised, in its own right, in addition to in tandem with MALDI-MSI. The analysis of elements subject to spectral interferences is a significant challenge for ICP-MS, and though the use of collision cells is a growing field in ICP-MS, this study

demonstrated the limitations of using such techniques when in tandem with a source providing a transient signal, proving that the acquisition of multiple elements with polyatomic interferences can prove a challenge in spite of modern technologies.[42]

Additionally, as debate surrounds the use of laser wavelengths for use in biological imaging using LA-ICP-MS, this study demonstrated the fine balance of laser intensity when dealing with thin sections of tissue on glass. In addition, experiments aiming to provide the foundation for a multimodal workflow involving MALDI-MSI and LA-ICP-MSI in sequence proved that there is little need for sample preparation prior to analysis by LA-ICP-MS when using the organic matrix CHCA; instead showing that the removal of the residual matrix greatly reduced signal intensity of endogenous metals from the tissues.

The work undertaken to optimise LA-ICP-MSI highlights the importance of experimental design for the effective analysis of elements within biological tissue, and the critical effects caused by polyatomic interferences within the field of ICP analysis. Furthermore, considerations for a future workflow wherein MALDI-MSI and LA-ICP-MSI could be sued in tandem were explored. The work herein found the compatibility of soft ionisation techniques such as MALDI allow for the subsequent analysis of elements by LA-ICP-MSI with little detriment to the results obtained by LA-ICP-MS following the MALDI analysis. The work detailed sought to kickstart the use of multimodal workflows for the study of ocular aetiology, with the aim to support future work in the investigations of ocular omics through the production of rich and multifaceted datasets.

References

1 World Health Organization, *World report on vision*, World Health Organization, 2019.

2 L. Celkova, S. L. Doyle and M. Campbell, NLRP3 Inflammasome and Pathobiology in AMD *Journal of clinical medicine,* 2015, **4**, 172–192.

3 E. M. del Amo, K. Vellonen, A. Urtti, T. Terasaki, A. Hammid, P. Honkakoski and S. Auriola, Mass spectrometry in ocular drug research *Mass spectrometry reviews,* 2023, .

4 K. L. Schey, R. B. Gletten, C. V. T. O'Neale, Z. Wang, R. S. Petrova and P. J. Donaldson, Lens Aquaporins in Health and Disease: Location is Everything *Frontiers in physiology,* 2022, **13**, 882550.

5 S. Kiechl, E. Lorenz, M. Reindl, C. J. Wiedermann, F. Oberhollenzer, E. Bonora, J. Willeit and D. A. Schwartz, Toll-like Receptor 4 Polymorphisms and Atherogenesis *The New England Journal of Medicine,* 2002, **347**, 185–192.

6 L. D. Sarah, M. Campbell, E. Ozaki, G. S. Robert, A. Mori, F. K. Paul, J. F. Gwyneth, Anna-sophia Kiang, M. H. Marian, C. L. Ed, A. J. O. Luke, G. H. Joe and P. Humphries, NLRP3 has a protective role in age-related macular degeneration through the induction of IL-18 by drusen components *Nat. Med.,* 2012, **18**, 791–798.

7 A. O. Edwards, D. Chen, B. L. Fridley, K. M. James, Y. Wu, G. Abecasis, A. Swaroop, M. Othman, K. Branham, S. K. Iyengar, T. A. Sivakumaran, R. Klein, B. E. K. Klein and N. Tosakulwong, Toll-like Receptor Polymorphisms and Age-Related Macular Degeneration *Investigative ophthalmology & visual science,* 2008, **49**, 1652–1659.

8 S. Doyle, K. Mulfaul, N. Fernando, K. Chirco, E. Connolly, T. Ryan, E. Ozaki, K. Brennan, A. Maminishkis and R. Salomon, TLR2 bridges oxidative damage

and complement-associated pathology and is a therapeutic target for age-related macular degeneration *Invest. Ophthalmol. Vis. Sci.,* 2018, **59**, 3475.

9 L. Gibbons, E. Ozaki, C. Greene, A. Trappe, M. Carty, J. A. Coppinger, A. G. Bowie, M. Campbell and S. L. Doyle, SARM1 Promotes Photoreceptor Degeneration in an Oxidative Stress Model of Retinal Degeneration *Frontiers in neuroscience,* 2022, **16**, 852114.

10 F. X. Yu and L. D. Hazlett, Toll-like Receptors and the Eye *Invest. Ophthalmol. Vis. Sci.,* 2006, **47**, 1255–1263.

11 Y. Zhu, B. Dai, Y. Li and H. Peng, C5a and toll-like receptor 4 crosstalk in retinal pigment epithelial cells *Molecular vision,* 2015, **21**, 1122–1129.

12 Y. Wooff, N. Fernando, J. H. C. Wong, C. Dietrich, R. Aggio-Bruce, J. Chu-Tan, A. A. B. Robertson, S. L. Doyle, S. M. Man and R. Natoli, Caspase-1-dependent inflammasomes mediate photoreceptor cell death in photo-oxidative damage-induced retinal degeneration *Scientific Reports,* 2020, **10**, 2263.

13 E. R. Amstalden van Hove, D. F. Smith and R. M. A. Heeren, A concise review of mass spectrometry imaging *Journal of Chromatography A,* 2010, **1217**, 3946–3954.

14 R. Lemaire, M. Wisztorski, A. Desmons, J. C. Tabet, R. Day, M. Salzet and I. Fournier, MALDI-MS Direct Tissue Analysis of Proteins: Improving Signal Sensitivity Using Organic Treatments *Analytical chemistry (Washington),* 2006, **78**, 7145–7153.

15 J. L. Norris and R. M. Caprioli, Analysis of Tissue Specimens by Matrix-Assisted Laser Desorption/Ionization Imaging Mass Spectrometry in Biological and Clinical Research *Chemical reviews,* 2013, **113**, 2309–2342.

16 M. Feucherolles, W. Le, J. Bour, C. Jacques, H. Duplan and G. Frache, A Comprehensive Comparison of Tissue Processing Methods for High-Quality

MALDI Imaging of Lipids in Reconstructed Human Epidermis *Journal of the American Society for Mass Spectrometry,* 2023, **34**, 2469–2480.

17 T. S. Høiem, M. K. Andersen, M. Martin-Lorenzo, R. Longuespée, B. S. R. Claes, A. Nordborg, F. Dewez, B. Balluff, M. Giampà, A. Sharma, L. Hagen, R. M. A. Heeren, T. F. Bathen, G. F. Giskeødegård, S. Krossa and M. Tessem, An optimized MALDI MSI protocol for spatial detection of tryptic peptides in fresh frozen prostate tissue *Proteomics (Weinheim),* 2022, **22**, e2100223–n/a.

18 B. Banstola, E. T. Grodner, F. Cao, F. Donnarumma and K. K. Murray, Systematic assessment of surfactants for matrix-assisted laser desorption/ionization mass spectrometry imaging *Analytica chimica acta,* 2017, **963**, 76–82.

19 E. Patel, in *Imaging Mass Spectrometry*, ed. nonymous , Springer New York, New York, NY, 2017, p. 7–14.

20 P. M. Angel, K. Norris-Caneda and R. R. Drake, In Situ Imaging of Tryptic Peptides by MALDI Imaging Mass Spectrometry Using Fresh-Frozen or Formalin-Fixed, Paraffin-Embedded Tissue *Current Protocols in Protein Science,* 2018, **94**, e65–n/a.

21 H. Puchtler, F. S. Waldrop, H. M. Conner and M. S. Terry, Carnoy fixation: practical and theoretical considerations *Histochemie (Berlin),* 1968, **16**, 361–371.

22 W. J. Howat and B. A. Wilson, Tissue fixation and the effect of molecular fixatives on downstream staining procedures *Methods (San Diego, Calif.),* 2014, **70**, 12–19.

23 K. Chughtai and R. M. A. Heeren, Mass Spectrometric Imaging for Biomedical Tissue Analysis *Chemical reviews,* 2010, **110**, 3237–3277.

24 M. Manea, G. Mező, F. Hudecz and M. Przybylski, Mass spectrometric identification of the trypsin cleavage pathway in lysyl-proline containing oligotuftsin peptides *Journal of peptide science,* 2007, **13**, 227–236.

25 R. J. A. Goodwin, Sample preparation for mass spectrometry imaging: Small mistakes can lead to big consequences *Journal of proteomics,* 2012, **75**, 4893–4911.

26 F. Zubair, P. E. Laibinis, W. G. Swisher, J. Yang, J. M. Spraggins, J. L. Norris and R. M. Caprioli, Trypsin and MALDI matrix pre-coated targets simplify sample preparation for mapping proteomic distributions within biological tissues by imaging mass spectrometry *Journal of mass spectrometry.,* 2016, **51**, 1168–1179.

27 Y. Yu, M. Gilar, P. J. Lee, E. S. P. Bouvier and J. C. Gebler, Enzyme-Friendly, Mass Spectrometry-Compatible Surfactant for In-Solution Enzymatic Digestion of Proteins *Analytical chemistry (Washington),* 2003, **75**, 6023–6028.

28 V. Mainini, P. M. Angel, F. Magni and R. M. Caprioli, Detergent enhancement of on-tissue protein analysis by matrix-assisted laser desorption/ionization imaging mass spectrometry *Rapid communications in mass spectrometry,* 2011, **25**, 199–204.

29 M. Djidja, S. Francese, P. M. Loadman, C. W. Sutton, P. Scriven, E. Claude, M. F. Snel, J. Franck, M. Salzet and M. R. Clench, Detergent addition to tryptic digests and ion mobility separation prior to MS/MS improves peptide yield and protein identification for in situ proteomic investigation of frozen and formalin-fixed paraffin-embedded adenocarcinoma tissue sections *Proteomics (Weinheim),* 2009, **9**, 2750–2763.

30 E. Patel, M. R. Clench, A. West, P. S. Marshall, N. Marshall and S. Francese, Alternative Surfactants for Improved Efficiency of In Situ Tryptic Proteolysis of Fingermarks *J. Am. Soc. Mass Spectrom,* 2015, **26**, 862–872.

31 R. C. Beavis, T. Chaudhary and B. T. Chait, α-Cyano-4-hydroxycinnamic acid as a matrix for matrixassisted laser desorption mass spectromtry *Org. Mass Spectrom.,* 1992, **27**, 156–158.

32 D. J. Harvey, in *Reference Module in Chemistry, Molecular Sciences and Chemical Engineering*, ed. nonymous , Elsevier, 2018.

33 C. Calvano, S. Carulli and F. Palmisano, Aniline/a-cyano-4-hydroxycinnamic acid is a highly versatile ionic liquid for matrix-assisted laser desorption/ionization mass spectrometry *Rapid communications in mass spectrometry,* 2009, **23**, 1659–1668.

34 T. J. Stewart, Across the spectrum: integrating multidimensional metal analytics for in situ metallomic imaging *Metallomics,* 2019, **11**, 29–49.

35 T. W. MAY and R. H. WIEDMEYER, A table of polyatomic interferences in ICP-MS *Atomic spectroscopy,* 1998, **19**, 150–155.

36 J. P. Sang, H. L. Ju, J. W. Se, W. K. Se and H. P. Kyu, Five heavy metallic elements and age-related macular degeneration: Korean National Health and Nutrition Examination Survey, 2008-2011 *Ophthalmology,* 2015, **122**, 129–137.

37 E. W. Wu, D. A. Schaumberg and S. K. Park, Environmental cadmium and lead exposures and age-related macular degeneration in U.S. adults: The National Health and Nutrition Examination Survey 2005 to 2008 *Environmental research,* 2014, **133**, 178–184.

38 J. C. Erie, J. A. Butz, J. A. Good, E. A. Erie, M. F. Burritt and J. D. Cameron, Heavy Metal Concentrations in Human Eyes *American journal of ophthalmology,* 2005, **139**, 888–893.

39 J. C. Erie, J. A. Good and J. A. Butz, Excess Lead in the Neural Retina in Age-Related Macular Degeneration *American Journal of Ophthalmology,* 2009, **148**, 890–894.

40 J. C. Erie, J. A. Good, J. A. Butz and J. S. Pulido, Reduced Zinc and Copper in the Retinal Pigment Epithelium and Choroid in Age-related Macular Degeneration *American Journal of Ophthalmology,* 2009, **147**, 276–282.e1.

41 Hajare Q, Mehdi K. Kayser-Fleischer ring in Wilson's disease. The Pan African medical journal. 2018;30:137.

42 N. Yamada, Kinetic energy discrimination in collision/reaction cell ICP-MS: Theoretical review of principles and limitations *Spectrochimica acta. Part B: Atomic spectroscopy,* 2015, **110**, 31–44.

Chapter 3

Joshua Millar, Ema Ozaki [2], Susan Campbell [1], Catherine Duckett [1], Sarah Doyle [2] and Laura M. Cole [1]*

Metabolites: Multiomic Mass Spectrometry Imaging to Advance Future Pathological Understanding of Ocular Disease

1. Centre for Mass Spectrometry Imaging, Biomolecular Research Centre, Sheffield Hallam University, Sheffield S1 1WB, UK
2. Immunobiology Research Group, Department of Clinical Medicine, Trinity College Institute of Neuroscience (TCIN), School of Medicine, Trinity College Dublin (TCD), D02 R590 Dublin 2, Ireland

Author Contribution: J. Millar conducted all analysis, sample preparation & data processing

Other Contributions: E. Ozaki sectioned & mounted the mouse ocular tissue used in this study

Abstract

Determining the locations of proteins within the eye thought to be involved in ocular pathogenesis is important to determine how best to target them for therapeutic benefits. However, immunohistochemistry is limited by the availability and specificity of antibodies. Additionally, the perceived role of both essential and non-essential metals within ocular tissue has been at the forefront of age-related macular degeneration (AMD) pathology for decades, yet even key metals such as copper and zinc have yet to have their roles deconvoluted. Here, mass spectrometry imaging (MSI) is employed to identify and spatially characterize both proteomic and metallomic species within ocular tissue to advance the application of a multiomic imaging methodology for the investigation of ocular diseases.

1.0. Introduction

Ocular tissue is a complex anatomical system constituted by multiple tissue types and organized in a highly structured and highly privileged manner. Disruption of this otherwise balanced structure can lead to the onset of ocular diseases that, without viable treatment, may lead to visual impairment.[1] Key to therapeutic discovery is a deeper understanding of the underlying mechanisms of disease onset. Age-related macular degeneration (AMD) is one of the most common ocular degenerative diseases, making up over 50% of legal blindness cases in England and Wales.[2] Currently, there are around 200 million patients worldwide, but incidence is expected to rise as populations begin to age.[3] There are presently very limited treatments for AMD, with only 15% of patients having viable treatment available to them.[4-6] This lack of viable therapeutics can be attributed

to inadequate understanding of AMD pathology. Recent studies have linked a class of proteins called pattern recognition receptors (PRRs) and other proteins associated with the innate immune system in AMD pathology, implicating chronic inflammation and immune- mediated retinal damage in AMD.[7,8] Current immunological studies, however, have been limited by factors such as insufficient specificity, leading to disputes within the literature around the involvement of certain PRRs in AMD pathology.[9] Additionally, as highlighted in the Age-Related Eye Disease Study (AREDS) at the turn of the century, essential trace elements are crucial for regulation of inflammation and in the prevention of disease.[10] Following this, the National Eye Institute, began to recommend supplementation of zinc as a precautionary measure for those susceptible to AMD. Though copper was present to avoid hypocupremia, both zinc and copper have a role in the mitigation of inflammation as part of copper-zinc superoxide dismutase, and deficiencies in zinc can cause an inflammatory response.[11] The role of both essential and non-essential metals in ocular tissue in AMD has been associated with AMD onset.

Multiple MS approaches have been utilized in the past few decades to attempt to further the understanding of AMD etiology. MALDI-MS has been applied in the investigation of non-invasive tear analysis[12], proteomic changes in the aqueous humor and retina[13,14] as well as MSI of retinal lipids[15] in the context of AMD. Additionally, ICP-MS investigations into AMD tissue, conducted as early as 2000, have been seen to corroborate the findings within the AREDS.[16.17] Similarly, ICP-MS has mostly been ap- plied to non-invasive matrices[16-23] or through analysis of the aqueous humor[24], with fewer targeting retinal tissue.[17,25,26] Invariably, few

techniques utilize the multiplexing and multi-dimensional nature of 2D MS imaging, with even fewer studies combining techniques in a multimodal fashion.[27]

2.0. Materials & Methods

2.1. Tissue Samples

Tissue was obtained from Trinity College Dublin (Dublin, Ireland) and consisted of fresh frozen C57Bl/6J wildtype mouse ocular tissues sectioned at 10 µm after being embedded in carboxymethylcellulose (CMC).

2.2. Chemicals

Ethanol (200 proof) from Honeywell (Bracknell, UK), glacial acetic acid (Fisher Scientific, Loughborough, UK), acetonitrile (Fisher Scientific, Loughborough, UK), octyl- α-β-glucoside (Sigma-Aldrich, Dorset, UK), trypsin (Promega, Southampton, UK), TFA (Sigma-Aldrich, Dorset, UK), CMC (Merck Group, Darmstadt, Germany), traceCERT® Multielement Standard Solution 6 for ICP (Merck Group, Darmstadt, Germany), HNO3 (VWR, Poole, UK) and gelatin (Merck Group, Darmstadt, Germany) were used in this study.

2.3. MALDI-MSI Sample Preparation

2.3.1. Sample Washing

Salts and lipids were removed using sequential washing with 70% EtOH, 90% EtOH, CHCl3 and 90:9:1 EtOH:AcOH:H2O for 1 min with drying steps in between.

2.3.2. On Tissue Digestion

First, 20 µg/mL of MS-grade trypsin (Promega, Southampton, UK) was prepared in 50 mM NH4HCO3 with 0.1% octyl-α-β-glucoside applied to the tissue via the

use of sequencing grade trypsin. Then, 15 layers of 45°C trypsin were applied at 10 psi N2 pressure and at 20 µLmin−1 using an HTX M3+ Sprayer (HTX Imaging, Chapel Hill, NC, USA). Following application, the samples were placed in a humidity chamber containing 50% methanol before incubation overnight at 37°C. On removal, the samples were allowed to reach room temperature before matrix application.

2.3.3. Matrix Application

A matrix consisting of 5 mgmL^{-1} α-cyano-hydroxycinnamic acid (CHCA) was prepared in a 50% acetonitrile solution with 0.01% TFA. It was then sonicated and syringe- filtered prior to application using an HTX M3+ (HTX Imaging, Chapel Hill, NC, USA) at 80◦C, using a solvent flow rate of 100 µLmin^{-1} and a N2 pressure of 10 psi, in 8 layers. Following matrix application, the samples were either used in MALDI analysis immediately or placed into slide mailers, vacuum sealed and stored at −80 ◦C for a maximum of 1 week.

2.4. MALDI-MSI Analysis

All MALDI-MS analyses were conducted on two instruments: a Waters Corporation (Wilmslow, UK) SELECT SERIES MRT and a SYNAPT G2 HDMS. The SYNAPT was

operated in sensitivity mode with positive polarity using a 1 kHz Nd:YAG laser at a power of 250 a.u. and a spot size of 50 µm. The acquisition mass range was 600–2500 Da. The MRT was operated in MRT mode, wherein the flight path was over 47 m and the resolution was ≥200,000 FWHM. The 2 kHz laser was operated at 1 kHz and was attenuated with 2 ND filters. The primary variable filter was

applied at 300, and the secondary fixed filter was engaged. The laser was rastered over the sample at 125 µms−1, utilizing a 25 µm step size. A quad profile was set for optimum transmission of the analytes between 700 and 2500 Da, and the scan rate was set to 0.2 s, while data acquisition and processing were conducted using MassLynx version 4.2, HDI version 1.7, (Waters Corporation, Wilmslow, UK) and SCiLS Lab MVS version 2022b Pro (Bruker GmbH, Bremen Germany).

2.5. LA-ICP-MSI Sample Preparation

Prior to further analysis by LA-ICP-MS, the MALDI matrix was removed from the samples using a matrix wash step of 70% EtOH (2 × 1 min) before overnight desiccation.

2.5.1. LA-ICP-MSI Calibration Arrays

The calibration standards were prepared using an ICP Standard solution. Serially diluted standards were made in a range between 0–50 ppm by diluting in 1% HNO3, with an 115In internal standard at 1 ppm. Equal parts of each standard were then mixed with 20% (w/v) gelatin from porcine skin and vortexed before spotting 15 µL of each into 4 mm nylon wells. Once in the wells, the standards were allowed to dry overnight in a vacuum desiccator prior to analysis.

Gelatin from the porcine skin, carboxymethyl cellulose (CMC), ICP Standard Solution 6 (100 gL^{-1}) and HNO3 (69%) were used in the preparation of the 1% CMC, 2.5% gelatin, 5% gelatin and 10% gelatin standards.

2.6. LA-ICP-MS Analysis

The LA-ICP-MS experiments were conducted on a UP-213 LA system (New Wave Research, Huntingdon, UK) and an ImageBio266 (Elemental Scientific Lasers, Inc. Hunting- don, UK) connected to a NexION 350x ICP-MS. Data were analyzed using Iolite version 4.4.6 (Elemental Scientific Lasers, Inc. Bozeman, MT, USA). The calibration arrays were analysed prior to imaging and afterward, and they were processed to account for instrumental drift. Additionally, following quantitative imaging, the calibrants were analysed by ICP-MS following a microwave digestion protocol to ascertain their true concentrations.

3.0. Results

3.1. Matrix Application

The MALDI-MSI images acquired of three ions using two different flow rates on the HTX M3+ sprayer can be seen in Figure 1. It can be seen from the images that the same ions in the serial sections of mouse ocular tissue increased in intensity when a higher flow rate of 75 $\mu L min^{-1}$ was used in comparison with a lower rate of 50 $\mu L min^{-1}$. Notably, despite the increase in flow rate, the ions within the MS image seemingly did not suffer from lateral delocalization within the retinal region, allowing better sensitivity within the experiments without compromising the spatial resolution.

3.2. MALDI-MSI Results

Using the optimized matrix application methodology, Figure 2 shows images of SARM1 (m/z 1606.84 ± 1.12 ppm; see Table 1), an innate immune protein with pro- degenerative function known to be expressed mainly in photoreceptors and retinal ganglion cells [28]. The mass-to-charge ratios of SARM1 and other endogenous species such as hi- stone H32, a common tryptic peptide observable in tissue, were tentatively identified using MALDI-MS at a mass resolution of 200,000 FWHM. SARM1 can be seen to localize within the retina, and when comparing to the ion image for histone H32 (m/z 1032.5975± 2.51 ppm; see Table 1), it is clear that the SARM1 peptide appeared to localize more specifically to the outer segment, outer nuclear area and chorio-retinal region, as opposed to histone H32, which localized more specifically to the inner nuclear layer and inner plexiform layer.

Further images at 25 µm were once more able to segment the retinal substructure laterally, but rather than doing so in layers, as observed with SARM1 and histone H32 in Figure 2, through the observation of the copper chaperone for superoxide dismutase (CCS) and proteasome assembly chaperone 4 (PSMG4), MALDI-MSI was able to bisect the retina into anterior and posterior sections (Figure 3). This localization of ions suggests a higher relative intensity of CCS within the posterior region of the eye, meaning any copper observed within the retina may have been transported by CCS. Consequently, the copper observed throughout the rest of the ocular tissue may have been transported by different means, especially if observed in equal or greater quantities than the copper that co-localized with CCS.

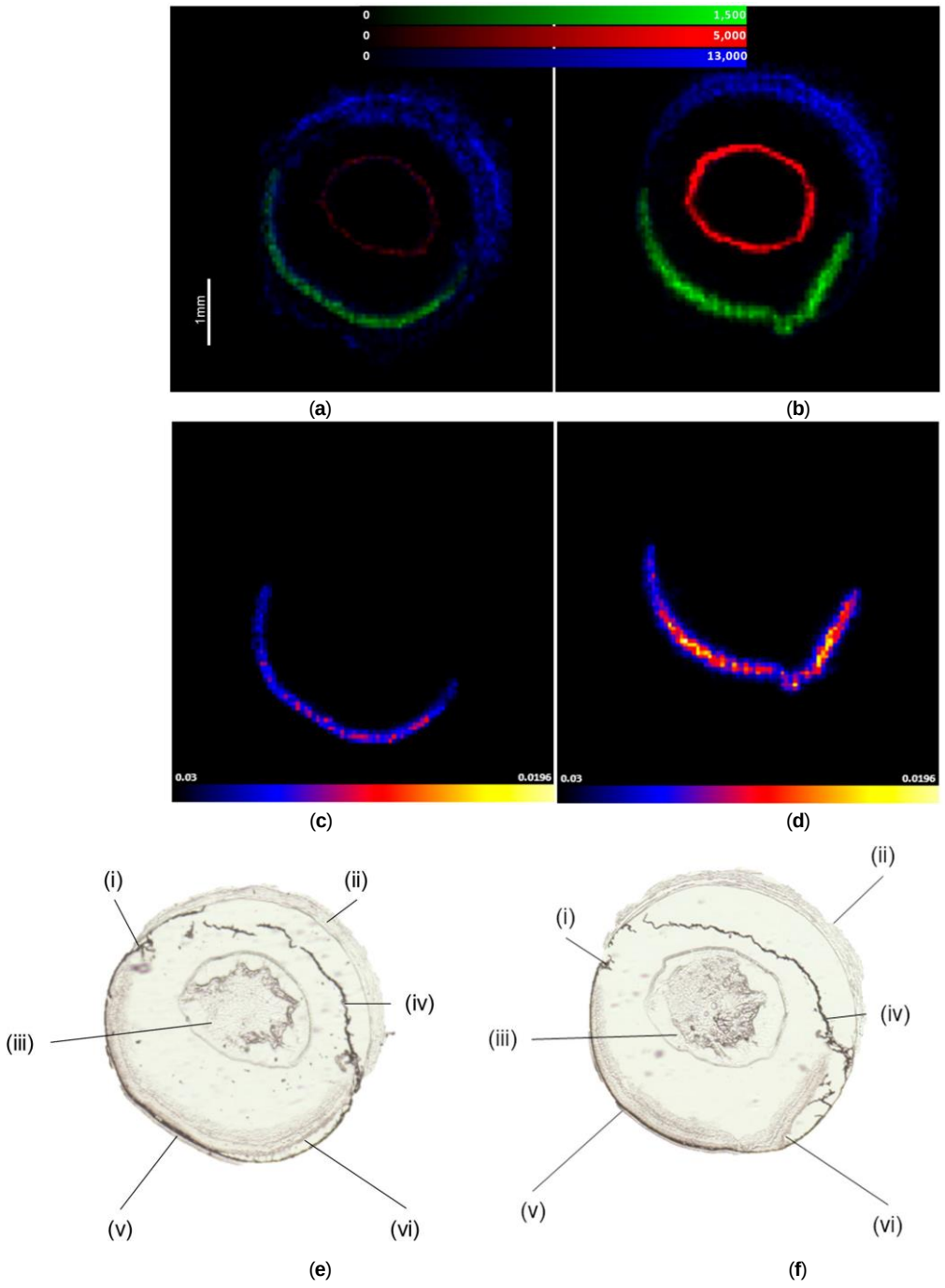

Figure 1 Images of 3 ions in the lens (m/z 1000.45), cornea (m/z 836.44) and retina (m/z 931.55), exhibiting the effects of different matrix application flow rates: (a) 50 µLmin^{-1} application with 3 peptide ions to contrast, (b) 75 µLmin−1 application with 3 ions

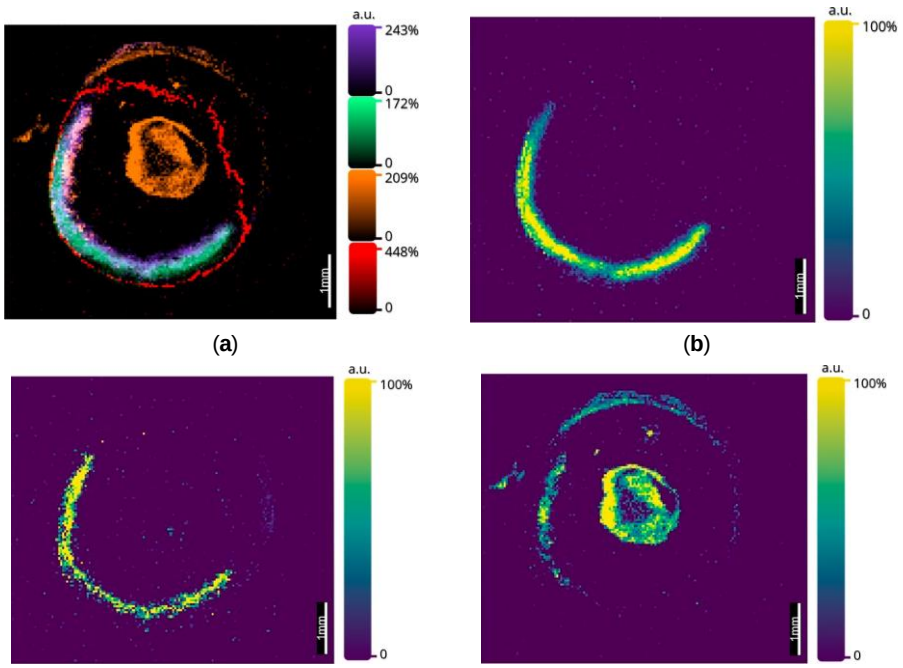

Figure 2 (a) An overlay image of 4 peptides within mouse ocular tissue, acquired by MALDI MS on a SELECT SERIES MRT at 25 µm with leptin m/z 1729.10 (red), lens crystallin m/z 1255.55 (orange), SARM1 m/z 1606.84 (green) and histone H32 m/z 1032.60 (purple). (b) S SARM1 m/z 1606.84. (c) Histone H32 m/z 1032.60. (d) Lens crystallin m/z 1255.55. Data acquired on a Waters SELECT SERIES MRT.

Table 1 Relative error values for those ions observed in Figure 2.

ID	ppm	M_{exp}	M_{calc}	Position	No. of Missed Cleavages
Histone H32	2.51	1032.5975	1032.5949	42–50	**0**
Lens Crystallin	3.02	1255.5487	1255.5429	835–845	**0**
Sarm1	1.12	1606.8428	1606.8410	202–216	**0**
Leptin	**1.44**	**1729.9963**	**1729.9938**	**27–41**	**2**

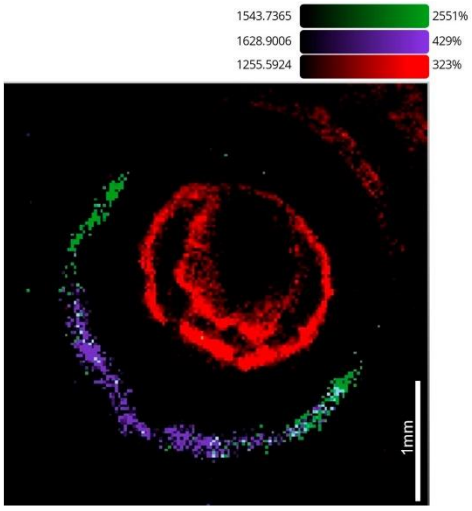

Figure 3 An overlay MALDI MS image acquired on the SELECT SERIES MRT at 25 µm, showing a lens crystallin m/z 1255.55 (red), proteasome assembly chaperone 4 (PSMG4) m/z 1543.73 in the anterior retina and CCS m/z 1628.90 in the posterior retina (purple). Data acquired on a Waters SELECT SERIES MRT.

3.3. LA-ICP-MSI Results

3.3.1. Qualitative LA-ICP-MSI Results

LA-ICP-MS was employed on sections previously examined by MALDI-MSI. Using two different LA units, a variety of spot sizes was utilized to produce ion images. Using an NWR UP-213 laser ablation unit, the 40 µm spot size images shown in Figure 4 were produced, which show that ^{66}Zn and ^{63}Cu were present throughout the ocular tissue, ^{66}Zn was present in the cornea, lens retina and iris, and ^{63}Cu shared a similar distribution, though it was seen to localize more predominantly in the ciliary body and on either side of the iris.

Utilizing the faster washout times of the ESL ImageBio266, the 10 µm spot size images improved in spatial resolution in comparison with the 40 µm images while

maintaining comparable acquisition times. The 10 µm images (Figure 5) show that the observations from the previous images could be corroborated, as 66Zn was observed in the retina and could be seen within the lens and iris. As in Figure 4, the ^{63}Cu can be seen to localize most predominantly in the ciliary body, though this image also shows larger amounts within the iris.

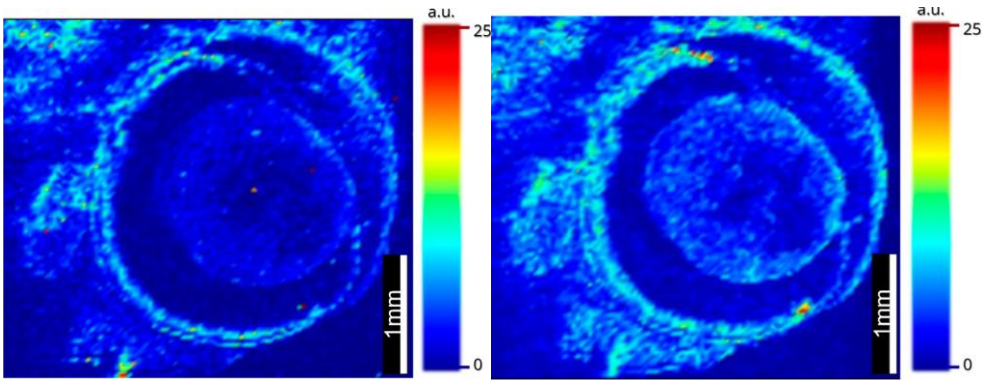

(**a**) (**b**)

Figure 4 LA-ICP-MS images conducted at a 40 µm spot size on a UP-213 coupled to a NexION350x:(a) ^{66}Zn in mouse ocular tissue and (b) ^{63}Cu in mouse ocular tissue.

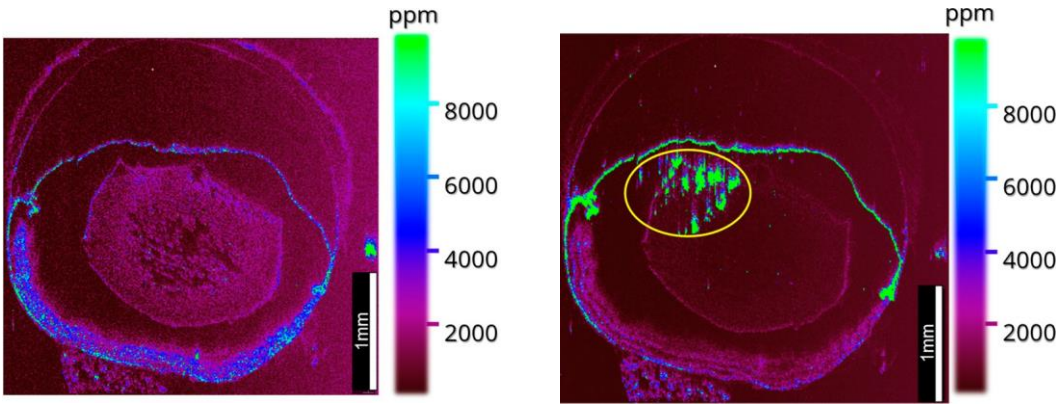

(**a**) (**b**)

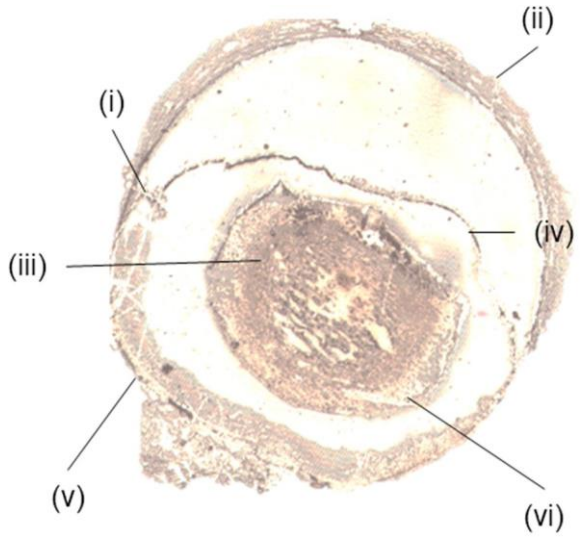

(**c**)

Figure 5 LA-ICP-MS images taken at 10 µm on an ESL ImageBio266 coupled to a NexION 350x: (a) ^{66}Zn distribution within mouse ocular tissue and (b) ^{63}Cu distribution within mouse ocular tissue N.B. The speckled region in the lens (circled in yellow) was identified as an artifact of the experiment and did not appear in subsequent experiments. (c) The anatomy of the mouse ocular tissue: (i) ciliary body, (ii) cornea, (iii) lens, (iv) iris, (v) choroid and (vi) retina.

3.3.2. Quantitative LA-ICP-MS Results

Quantitative ICP-MS was employed in order to add further dimensions to the data. One of the key aspects of this approach is the preparation of reproducible calibration arrays. Table 2 shows how inconsistencies appeared when initially trying to prepare the calibration arrays, as there were statistically significant differences in the repeats of the same elements.

Table 2 Regression figures given by calibration arrays prepared in carboxymethyl cellulose and gelatin from porcine skin

Element	***CMC***	***Gelatin (5%)***	***Gelatin (10%)***
^{63}Cu	*0.9574*	0.9776	*0.9939*
^{66}Zn	*0.9438*	*0.9696*	*0.9637*

In order to ascertain the source of these anomalies in the quantitative calibration arrays, images were taken on the UP-213 at 40 µm to see if the calibration arrays were homogenous. Figure 6a shows how zinc was not being deposited homogenously. Figure 6b–d exhibits how this Marangoni effect can be mitigated through the use of low aqueous calibration arrays.

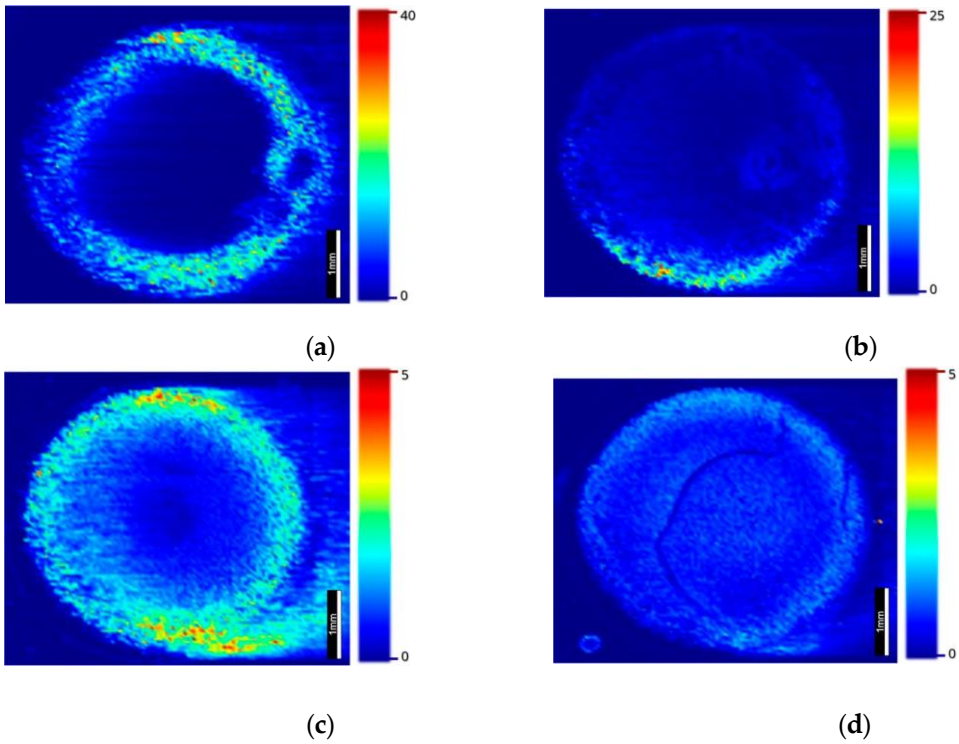

Figure 6 LA-ICP-MS images showing the spatial distribution of zinc in calibration arrays made from (a) 1% CMC, (b) 2.5% gelatin, (c) 5% gelatin and (d) 10% gelatin.

The images produced with the optimized calibration arrays (Figure 7) were similar to those in Figure 5, showing the localization of ^{66}Zn in the retina, lens and iris and ^{63}Cu again localizing within the ciliary body, with smaller amounts in the iris. With the added dimension of quantitative data, analysis showed that ^{66}Zn was localized in higher quantities than ^{63}Cu within the lens, cornea and choroid, whereas ^{63}Cu was observed in higher quantities within the ciliary body of the ocular tissue and in similar quantities to ^{66}Zn within the iris.

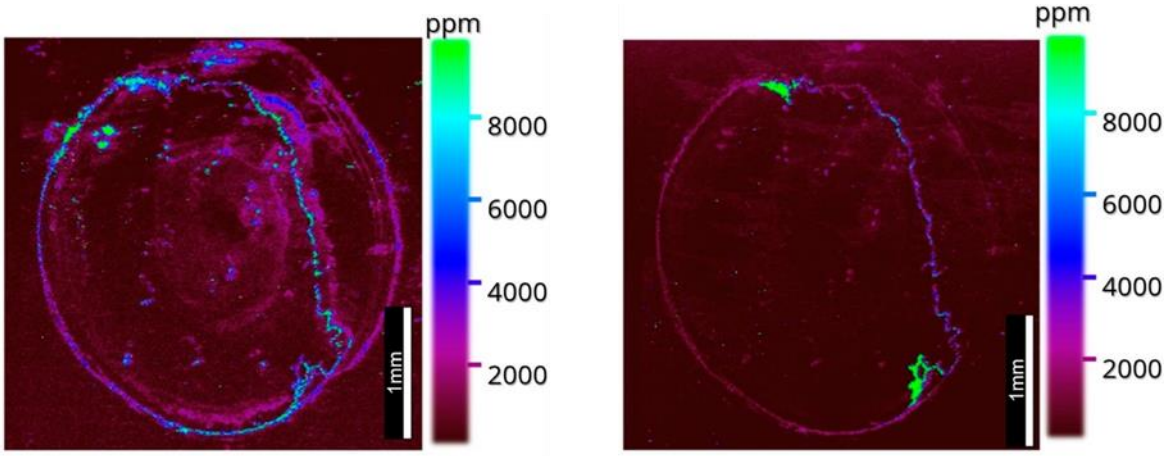

(**a**) (**b**)

Figure 7 Quantitative LA-ICP-MS images taken at 10 µm on an ESL ImageBio266 coupled to a NexION 350x: (a) ^{66}Zn distribution within mouse ocular tissue and (b) ^{63}Cu distribution within mouse ocular tissue.

4.0. Discussion

4.1. MALDI Sample Preparation Optimisation

To ensure the deposition method provides enough spatial resolution, this is most often determined by the crystal size of the matrix, which is heavily dependent on the application methodology.[29] Additionally, the lateral migration of the proteins

must be limited, which can happen when a tissue becomes overly wet or exposed to high volumes of an organic matrix.[30] Generally, with an optimal matrix solvent, matrix concentration and gas flow, robotic sprayers can provide relatively small crystal sizes of around 5–25 µm.[31] The data provided in Figure 1 show the benefit of higher flow rates while simultaneously exhibiting the value of robotic sprayers such as the HTX M3+ and their ability to provide heated solvent deposition, which simultaneously helps reduce the matrix crystal size by allowing high organic matrix solvent composition while preventing lateral delocalization.

4.2. MALDI-MSI

within axonal degeneration, a process key to a variety of retinal degenerative diseases whereby SARM1 regulates the depletion of essential metabolites (NAD) and induces an energy crisis.[28,32,33] Thus, a deeper understanding of the biology of SARM1 within healthy and diseased tissue could prove to be pivotal in finding treatment for retinal degenerative diseases in the future (e.g., SARM1 inhibitors). Here, SARM1 can be seen to localize within the posterior region of the retina, namely the outer nuclear layer adjacent to the RPE and choroid, a region which is key in the onset of both wet and dry AMD[5] and which is supportive of previous localization data for this protein.[28]

Additionally, peptides related to the transport and regulation of metals within the retina were observed. Figure 3 shows the observation of CCS within the posterior region of the ocular tissue. The ability to image proteins related to the regulation and transport of key trace elements may in the future provide unique insight into the role of accumulating essential and non-essential trace metals within diseased

ocular tissue, helping to further understand the co-dependencies that exist in the proteomic and metallomic changes that occur in ocular disease. The mapping of metals as well as the proteins by which they are transported is of great benefit, utilizing a multifaceted and multimodal approach.

4.3. LA-ICP-MSI

4.3.1. Qualitative Imaging

Previous studies that have investigated the accumulation or relation of trace metals to AMD have been both qualitative and quantitative, but fewer have included the added dimension that imaging data can provide to this niche of pathobiology.[17-19,25] Figure 4 shows that zinc and copper were distributed within the choroid and less so in the lens, cornea and iris. These data not only corroborate past reports that cite increased levels of metal within the choroid and RPE but add a further dimension, showing that the metals were evenly distributed throughout the choroid.

The 10 µm images produced in Figure 5 corroborated the findings from the previous images, exhibiting the localization of copper to the ciliary body and choroid.[16] The presence of copper within the ciliary body was most likely associated with the high levels of copper found within muscle tissue, though as the ciliary body is responsible for the production of aqueous humor, and AMD patients are often seen to have a copper deficiency in their aqueous humor, this may prove to be an interesting insight in the future [17–19,24,25,34]. Additionally, copper was seen to localize to the exterior regions of the lens, which constitutes the youngest part of the lens.[34] The observation of copper and zinc within the choroid was, however, most important, as it has previously been reported that

this area of the ocular structure is subject to the most change in the elderly. Wills et al. reported a significant increase in copper and zinc in the choroid but a reduction within the neural retina in aged ocular tissue when compared with younger tissue.[16] Erie et al. further demonstrated the changes that occur in the choroid by showing that of 44 participants, those with AMD had significantly lower amounts of copper and zinc within their choroids, which aligns with the advice provided by the AREDS.[17]

4.3.2. Quanitative Imaging

While quantitative data have provided key information about the wider mechanisms of essential metals within ocular physiology, quantitative ICP is not without its limitations. The reliability of quantitative conclusions drawn from ICP experiments is susceptible to elemental fractionation, a phenomenon that encompasses the effects of the perceived compositions of ICP samples caused by factors such as the preferred ablation of more volatile compounds, the time-dependent changes in the ion beam and the transport efficiency of differently sized aerosol particles.[35] Overcoming these issues can be fundamental in the success of a quantitative study on biological samples. However, the introduction of imaging, and therefore the use of laser ablation, involves additional factors affecting quantitative analysis. The main issue stemming from laser ablation is the effects of the matrix.[35,36]

The problem becomes most pertinent when using quantitative standards, as different matrices will, for example, behave differently when subjected to an incident laser beam and will thereby produce aerosols more or less efficiently,

depending on properties such as the thermal conductivity, absorptivity and reflectivity.[35] As a consequence, when using quantitative standards, the matrix chosen to hold the elemental standards must behave in an analogous manner to the analyte. Gelatin, agarose gel or sol-gel in the past have been the most common matrices for elemental standards used to mimic the carbon content and density of the biological sample without the need for expensive CRMs.[35-37] Herein, the use of gelatin, in addition to an MS-friendly medium of carboxymethyl cellulose, were trialled as potential matrices to house the elemental standards for quantitative ICP imaging. We prepared and mixed 1% CMC and 5%,10% and 20% gelatin in equal parts with 50 ppm of ICP Solution 6, yielding m/v values of 0.5%, 2.5%, 5% and 10%, respectively. The standards were first prepared by spotting 15 µL into M4 metric washers and dried in a vacuum desiccator overnight at room temperature. Regarding the utilized parameters optimized for mouse ocular tissue, the LA standards were acquired by using one line per standard. Using the average intensities from the line scans, calibration curves were produced. The data showed poor regressions (Table 2).

To identify the source of the anomalous regressions given to the samples, images of the gelatin spots were taken to ascertain if uneven distributions were the cause of the anomalous results. The images were taken at 40 µm. The results (Figure 6) showed that the CMC, 2.5% gelatin and 5% gelatin were exhibiting characteristics of the Marangoni effect and producing rings of high concentrations at the periphery of the standards. To avoid this, lower aqueous standards were prepared which, as demonstrated by Šala et al., could help reduce the effects caused by capillary action, as demonstrated in Figure 6d.[36] Then, 10% gelatin was used thereafter within the LA standards which, when acquired alongside an image of mouse ocular tissue at 10 µm (Figure 7), were able to produce a

quantitative LA-ICP-MS image. The images were able to inform of the previously viewed data, which showed what appeared to be lower levels of zinc within the sclera, but by normalizing the scales of copper and zinc to one another, it can be seen that zinc was in higher quantities in the choroid when compared with copper, concurring with previous studies that employed excision as a way to quantify the metal content within the choroid.[16]

The distribution of zinc in ocular tissue is poorly understood in the context of AMD, yet zinc deficiency is one of the hallmarks of AMD and has been attributed to the onset of AMD in later life.[10] Additionally, zinc deficiency is seen to be inflammatory through the induction of IL6 promoter demethylation.[11] Whilst AREDS recognized the importance of zinc deficiency in AMD onset, and the links between zinc and the inflammatory response are well documented, little work has been performed that explores a potential synergy between the proteomic and metallomic changes in the aging eye that may result in chronic inflammation. In Figures 5 and 7, there is a clear demarcation between the metal distribution within the choroid in the outer blood–retinal vascular bed and the inner retina as well as distinct proteomic segments, exhibiting the similar behaviour of metals and proteins within the highly privileged retinal structure.[1]

In summary, the combination of both proteomic analysis by MALDI-MSI and metal analysis by LA-ICP-MSI exhibited the utility of applying the extra dimension of 2D qualitative and quantitative imaging to complex heterogenous ocular tissue. Additionally, the multiplexing nature of the experiments that can be conducted by using these imaging techniques in tandem as part of a multiomic approach was demonstrated. By using a workflow that not only informs of the proteomic

changes within a tissue but also the metallomic changes, a broader understanding of the underlying mechanisms of ocular disease can be achieved.

5.0. Conclusion

The workflow described here invites an opportunity to alter the way in which mass spectrometry is used to study ocular disease. Current methodologies for studying ocular diseases such as AMD risk stagnation without an interdisciplinary and multidimensional approach to their investigation. Studies on the AMD proteome by immunological methods could benefit from complimentary mass spectrometry data and yet further improved with the added dimension of mass spectrometry imaging. Likewise, studies into the essential metals related to AMD stand to gain from the use of quantitative LA-ICP-MS imaging to not only quantify the changes in metal content in healthy and AMD eyes but map the changes of distribution within the ocular tissue in relation to the proteomic changes that occur within the same space in combination with MALDI-MSI. However, though mouse models have long been used for the modelling of disease due to convenience and economy, mouse models offer issues, as they are nocturnal creatures with ocular adaptations different to humans and additionally do not possess a macula.[38,39] As a result, to further the significance of these studies, future work will include investigations of the localization of the aforementioned classes of proteins within the human retina. When used in tandem as described here, these imaging techniques, when applied to diseased ocular tissue, offer multi-dimensional and multifaceted data from a single tissue section, and if applied in an inter-disciplinary manner, they will aid the development of research on a variety of ocular diseases.

6.0. References

1. Ash, J.D.; Grimm, C.; Hollyfield, J.G.; Anderson, R.E.; LaVail, M.M.; Bowes Rickman, C. *Retinal Degenerative Diseases*; Springer: New York, NY, USA; Cham, Switzerland, 2014.
2. Quartilho, A.; Simkiss, P.; Zekite, A.; Xing, W.; Wormald, R.; Bunce, C. Leading causes of certifiable visual loss in England and Wales during the year ending 31 March 2013. *Eye* **2016**, *30*, 602–607. [PubMed]
3. Wong, L.W.; Su, X.; Li, X.; Cheung, G.M.C.; Klein, R.; Cheng, C.; Wong, T.Y. Global prevalence of age-related macular degeneration and disease burden projection for 2020 and 2040: A systematic review and meta-analysis. *Lancet Glob. Health* **2014**, *2*, e106–e116. [CrossRef] [PubMed]
4. Papadopoulos, Z. Recent Developments in the Treatment of Wet Age-related Macular Degeneration. *Curr. Med. Sci.* **2020**, *40*, 851–857. [CrossRef] [PubMed]
5. Celkova, L.; Doyle, L.S.; Campbell, M. NLRP3 Inflammasome and Pathobiology in AMD. *J. Clin. Med.* **2015**, *4*, 172–192. [CrossRef] [PubMed]
6. Martin, F.D.; Maguire, G.M.; Ying, G.; Grunwald, E.J.; Fine, L.S.; Jaffe, G.J. Ranibizumab and Bevacizumab for Neovascular Age-Related Macular Degeneration. *N. Engl. J. Med.* **2011**, *364*, 1897–1908. [PubMed]
7. Doyle, S.; Mulfaul, K.; Fernando, N.; Chirco, K.; Connolly, E.; Ryan, T.; Ozaki, E.; Brennan, K.; Maminishkis, A.; Salomon, R. TLR2 bridges

oxidative damage and complement-associated pathology and is a therapeutic target for age-related macular degeneration. *Investig. Ophthalmol. Vis. Sci.* **2018**, *59*, 3475.

8. Sarah, D.L.; Campbell, M.; Ozaki, E.; Robert, S.G.; Mori, A.; Paul, K.F.; Gwyneth, F.J.; Kiang, A.-S.; Marian, H.M.; Ed, C.L.; et al. NLRP3 has a protective role in age-related macular degeneration through the induction of IL-18 by drusen components. *Nat. Med.* **2012**, *18*, 791–798.
9. Kosmidou, C.; Efstathiou, E.N.; Hoang, V.M.; Notomi, S.; Konstantinou, K.E.; Hirano, M.; Takahashi, K.; Maidana, E.D.; Tsoka, P.; Young, L.; et al. Issues with the Specificity of Immunological Reagents for NLRP3: Implications for Age-related Macular Degeneration. *Sci. Rep.* **2018**, *8*, 461. [CrossRef]
10. The Age-Related Eye Disease Study Research Group. The effect of five-year zinc supplementation on serum zinc, serum cholesterol and hematocrit in persons randomly assigned to treatment group in the age-related eye disease study: AREDS Report No. 7. *J. Nutr.* **2002**, *132*, 697–702. [CrossRef]
11. Wong, P.C.; Rinaldi, A.N.; Ho, E. Zinc deficiency enhanced inflammatory response by increasing immune cell activation and inducing IL6 promoter demethylation. *Mol. Nutr. Food Res.* **2015**, *59*, 991–999. [CrossRef]
12. Winiarczyk, M.; Winiarczyk, D.; Michalak, K.; Kaarniranta, K.; Adaszek, Ł.; Winiarczyk, S.; Mackiewicz, J. Dysregulated Tear Film Proteins in Macular Edema Due to the Neovascular Age-Related Macular Degeneration Are Involved in the Regulation of Protein Clearance,

Inflammation, and Neovascularization. *J. Clin. Med.* **2021**, *10*, 3060. [CrossRef]

13. Nordgaard, L.C.; Berg, M.K.; Kapphahn, J.R.; Reilly, C.; Feng, X.; Olsen, W.T.; Ferrington, D.A. Proteomics of the Retinal Pigment Epithelium Reveals Altered Protein Expression at Progressive Stages of Age-Related Macular Degeneration. *Investig. Ophthalmol. Vis. Sci.* **2006**, *47*, 815–822. [CrossRef]
14. Yao, J.; Liu, X.; Yang, Q.; Zhuang, M.; Wang, F.; Chen, X.; Hang, H.; Zhang, W.; Liu, Q. Proteomic analysis of the aqueous humor in patients with wet age-related macular degeneration. *Proteomics. Clin. Appl.* **2013**, *7*, 550–560. [CrossRef]
15. Anderson, G.M.D.; Ablonczy, Z.; Koutalos, Y.; Spraggins, J.; Crouch, K.R.; Caprioli, M.R.; Schey, K.L. High Resolution MALDI Imaging Mass Spectrometry of Retinal Tissue Lipids. *J. Am. Soc. Mass Spectrom.* **2014**, *25*, 1394–1403. [CrossRef]
16. Wills, K.N.; Sadagopa Ramanujam, M.V.; Kalariya, N.; Lewis, R.J.; van Kuijk, F.J.G.M. Copper and zinc distribution in the human retina: Relationship to cadmium accumulation, age, and gender. *Exp. Eye Res.* **2008**, *87*, 80–88. [CrossRef]
17. Erie, C.J.; Good, A.J.; Butz, J.A.; Pulido, J.S. Reduced Zinc and Copper in the Retinal Pigment Epithelium and Choroid in Age-related Macular Degeneration. *Am. J. Ophthalmol.* **2009**, *147*, 276–282.e1. [CrossRef]
18. Erie, C.J.; Butz, A.J.; Good, A.J.; Erie, A.E.; Burritt, F.M.; Cameron, J.D. Heavy Metal Concentrations in Human Eyes. *Am. J. Ophthalmol.* **2005**, *139*, 888–893. [CrossRef]

19. Sang, P.J.; Ju, L.H.; Se, W.J.; Se, K.W.; Kyu, H.P. Five heavy metallic elements and age-related macular degeneration: Korean National Health and Nutrition Examination Survey, 2008–2011. *Ophthalmology* **2015**, *122*, 129–137.
20. Mayer, M.; Frederik, J.G.M. Whole blood selenium in exudativeage-related maculopathy. *Acta. Ophthalmol. Scand.* **1998**, *76*, 62–67.
21. [CrossRef]
22. Heesterbeek, J.T.; Rouhi-Parkouhi, M.; Church, J.S.; Lechanteur, T.Y.; Lorés-Motta, L.; Kouvatsos, N.; Clark, J.S.; Bishop, N.P.; Hoyng, B.C.; den Hollander, I.A.; et al. Association of plasma trace element levels with neovascular age-related macular degeneration. *Exp. Eye Res.* **2020**, *201*, 108324. [CrossRef]
23. Aranaz, M.; Costas Rodriguez, M.; Lobo, L.; González-Iglesias, H.; Vanhaecke, F.; Pereiro, R. Pilot study of homeostatic alterations
24. of mineral elements in serum of patients with age-related macular degeneration via elemental and isotopic analysis using ICP-mass spectrometry. *J. Pharm. Biomed. Anal.* **2020**, *177*, 112857. [CrossRef] [PubMed]
25. Biesemeier, A.; Yoeruek, E.; Eibl, O.; Schraermeyer, U. Iron accumulation in Bruch's membrane and melanosomes of donor eyes with age-related macular degeneration. *Exp. Eye Res.* **2015**, *137*, 39–49. [CrossRef] [PubMed]
26. Jünemann, M.G.A.; Stopa, P.; Michalke, B.; Chaudhri, A.; Reulbach, U.; Huchzermeyer, C.; Schlötzer-Schrehardt, U.; Kruse, E.F.; Zrenner, E.; Rejdak, R. Levels of Aqueous Humor Trace Elements in

Patients with Non-Exsudative Age-related Macular Degeneration: A Case-control Study. *PLoS ONE* **2013**, *8*, e56734. [CrossRef]

27. Aberami, S.; Nikhalashree, S.; Bharathselvi, M.; Biswas, J.; Sulochana, N.K.; Coral, K. Elemental concentrations in Choroid-RPE and retina of human eyes with age-related macular degeneration. *Exp. Eye Res.* **2019**, *186*, 107718. [CrossRef] [PubMed]
28. Erie, C.J.; Good, A.J.; Butz, J.A. Excess Lead in the Neural Retina in Age-Related Macular Degeneration. *Am. J. Ophthalmol.* **2009**,
29. *148*, 890–894. [CrossRef] [PubMed]
30. Rodríguez-Menéndez, S.; Fernández, B.; García, M.; Álvarez, L.; Luisa Fernández, M.; Sanz-Medel, A.; Coca-Prados, M.; Pereiro, R.; González-Iglesias, H. Quantitative study of zinc and metallothioneins in the human retina and RPE cells by mass spectrometry-based methodologies. *Talanta* **2018**, *178*, 222–230. [CrossRef] [PubMed]
31. Gibbons, L.; Ozaki, E.; Greene, C.; Trappe, A.; Carty, M.; Coppinger, A.J.; Bowie, G.A.; Campbell, M.; Doyle, S.L. SARM1 Promotes Photoreceptor Degeneration in an Oxidative Stress Model of Retinal Degeneration. *Front. Neurosci.* **2022**, *16*, 852114. [CrossRef] [PubMed]
32. Capelo-Martínez, J. *Emerging Sample Treatments in Proteomics*; Springer International Publishing AG: Cham, Switzerland, 2019.
33. Norris, L.J.; Caprioli, R.M. Analysis of Tissue Specimens by Matrix-Assisted Laser Desorption/Ionization Imaging Mass Spectrometry in Biological and Clinical Research. *Chem. Rev.* **2013**, *113*, 2309–2342. [CrossRef]
34. Chughtai, K.; Heeren, R.M.A. Mass Spectrometric Imaging for Biomedical Tissue Analysis. *Chem. Rev.* **2010**, *110*, 3237–3277.

35. [CrossRef]
36. Sasaki, Y.; Kakita, H.; Kubota, S.; Sene, A.; Lee, J.T.; Ban, N.; Dong, Z.; Lin, B.J.; Boye, L.S.; DiAntonio, A.; et al. SARM1 depletion rescues NMNAT1-dependent photoreceptor cell death and retinal degeneration. *eLife* **2020**, *9*, e62027. [CrossRef]
37. Ozaki, E.; Gibbons, L.; Neto, G.N.; Kenna, P.; Carty, M.; Humphries, M.; Humphries, P.; Campbell, M.; Monaghan, M.; Bowie, A.; et al. SARM1 deficiency promotes rod and cone photoreceptor cell survival in a model of retinal degeneration. *Life Sci. Alliance* **2020**, *3*, e201900618. [CrossRef] [PubMed]
38. Aydin, E.; Cumurcu, T.; Ozugurlu, F.; Ozyurt, H.; Sahinoglu, S.; Mendil, D.; Hasdemir, E. Levels of iron, zinc, and copper in aqueous humor, lens, and serum in nondiabetic and diabetic patients: Their relation to cataract. *Biol. Trace Elem. Res.* **2005**, *108*, 33–41. [CrossRef] [PubMed]
39. Limbeck, A.; Galler, P.; Bonta, M.; Bauer, G.; Nischkauer, W.; Vanhaecke, F. Recent advances in quantitative LA-ICP-MS analysis: Challenges and solutions in the life sciences and environmental chemistry. *Anal. Bioanal. Chem.* **2015**, *407*, 6593–6617. [CrossRef] [PubMed]
40. Šala, M.; Šelih, S.V.; van Elteren, J.T. Gelatin gels as multi-element calibration standards in LA-ICP-MS bioimaging: Fabrication of homogeneous standards and microhomogeneity testing. *Analyst* **2017**, *142*, 3356–3359. [CrossRef] [PubMed]
41. Doble, A.P.; de Vega, G.R.; Bishop, P.D.; Hare, J.D.; Clases, D. Laser Ablation–Inductively Coupled Plasma–Mass Spectrometry Imaging in Biology. *Chem. Rev.* **2021**, *121*, 11769–11822. [CrossRef]

42. Volland, S.; Esteve-Rudd, J.; Hoo, J.; Yee, C.; Williams, D.S. A comparison of some organizational characteristics of the mouse central retina and the human macula. *PLoS ONE* **2015**, *10*, e0125631. [CrossRef]
43. Elizabeth Rakoczy, P.; Yu, T.J.M.; Nusinowitz, S.; Chang, B.; Heckenlively, J.R. Mouse models of age-related macular degeneration.
44. *Exp. Eye Res.* **2006**, *82*, 741–752. [CrossRef]

Chapter 4

Joshua Millar[1], Luke Gibbons[2], Catia Costa[3] , Ella Schneider[3] , Johanna von Gerichten[4], Melanie J. Bailey[4], Susan Campbell[1], Catherine Duckett[1], Sarah Doyle[2] and Laura M. Cole[1*]:

Analytica: Multimodal Imaging of Metals in a Retinal Degeneration Model to Inform on Ocular Disease

1. Centre for Mass Spectrometry Imaging, Biomolecular Research Centre, Sheffield Hallam University, Sheffield S1 1WB, UK
2. Immunobiology Research Group, Department of Clinical Medicine, Trinity College Institute of Neuroscience (TCIN), School of Medicine, Trinity College Dublin (TCD), D02 R590 Dublin 2, Ireland

Author Contribution: J. Millar conducted all ICP-MS analysis, sample preparation & data processing, and informed on the acquisition of PIXE experiments on-site at the UKNIBC

Other Contributions: Luke Gibbons sectioned & mounted the mouse ocular tissue used in this study; Catia Costa *et al.* at the UKNIC were responsible for the operation of the ion beam analysis suite and conducted data processing in conjunction with the author

Abstract

The metallome has been involved in the pathological investigation into ocular tissue for decades; however, as technologies advance, more information can be ascertained from individual tis- sue sections that were not previously possible. Herein, a demonstration of complementary techniques has been utilized to describe the distribution and concentrations of essential metals in both wildtype (WT) and *Rho*dopsin (*Rho*$^{-/-}$) ocular tissues. The multimodal approach described is an example of complementary datasets that can be produced when employing a multifaceted analytical approach. Heterogenous distributions of copper and zinc were observable within both WT and *Rho*$^{-/-}$ tissue by laser ablation inductively coupled plasma mass spectrometry (LA-ICP-MS), and the distributions of further trace elements notoriously problematic for ICP-MS analysis (phosphorous, Sulfur, chlorine, potassium, calcium, iron, and aluminum) were analysed by particle-induced X-ray emission (PIXE).

1.0. Introduction

As our populations begin to age, the global prevalence of blindness is rising, and with it demands for eye health services.[1] Though many causes of visual impairment may be treated, age-related macular degeneration, one of the most prevalent ocular diseases, has a poor prognosis. Patients with age-related macular degeneration, a disease that accounts for 8.7% of blindness worldwide, can only receive treatment if they are within the 15% of age- related macular degeneration (AMD) patients that have ‘wet’ AMD.[2,3] The remainder, those with dry AMD, have only preventative measures to rely on.[4] Whilst age, genetics, and

environmental factors such as workplace exposure or smoking have been linked to the onset of AMD, the pathology is still poorly understood.

The innate immune system has been heavily associated with AMD in recent years, with some reports suggesting a role of the inflammasome and, more broadly, chronic inflammation as a marker or cause of AMD. These findings are closely associated with the cellular senescence that happens alongside physiological dysregulation in aging, resulting in a buildup of extracellular matrix and debris from dead and dying cells, known as damage- associated molecular patterns (DAMPs), which, through activation of pattern recognition receptors (PRRs), activate the innate immune response.[5,6] Evidence of a feedback loop of this mechanism results in chronic inflammation in the ocular tissue, producing reactive oxygen species (ROS), which must be eliminated.

For as long as two decades, postulations that essential trace elements could be associated with the dysregulation that occurs in AMD have been reported in the literature.[7,8] In 1999, the Age-Related Eye Disease Study (AREDS) supported the idea that the supple- mentation of zinc (and copper to prevent hypocupremia) could help decrease the risk of the onset of AMD.[7,8] These propositions build on a wealth of literature that describes the close relationship of essential metals such as zinc and copper on ocular physiology, namely, their involvement as co-factors for superoxide dismutase and the regulation of oxidative stress. In 1995, Newsome et al. recorded zinc deficiency in those suffering from AMD, reporting a 9% decrease in zinc, and a 45% decrease in soluble zinc in aged eyes; however, they observed a significant increase in the activity of superoxide dismutase.[9] Additionally, Wong et al. reported an enhanced PRR-mediated

inflammatory response caused by a zinc deficiency in aged mice [10]. Inductively coupled plasma mass spectrometry (ICP-MS) studies have been able to confirm the results found in the AREDS trials,[11] noting the changes that occur in zinc and copper in the diseased and aged eye. In addition, studies into other essential elements have shown the changes to the metallome (Cd, Co, Cu, Fe, Mn, Se, and Zn) that can occur in ocular disease.[12]

Essential elements such as chlorine, sulfur, and phosphorus have seldom been anal- ysed in ICP-MS studies due to polyatomic interferences that occur with endogenous elements in an argon-based ICP-MS plasma.[13] Chlorine, however, has been implicated in AMD, with Chuang et al. showing mice with chloride intracellular channel 4 (CLIC4) deficient RPE cells ($RPE^{\Delta Clic4}$) exhibiting all the hallmarks of dry AMD, linking the CLIC4 deficiency to dysregulation of lipid metabolism and, ultimately, drusenogenesis.[14] These findings are indicative of the importance of the wider metallome and the constrictions that individual methodologies can impart to metallomic studies.

ICP-MS can offer detection limits at around 10 pg mL^{-1}, increasing to around 1 ppt

for modern laser ablation (LA)-ICP-MS. This means at a spot size of 10 µm, LA-ICP-MS can be used for the production of MS images of elements in quantities less than 1 ppm in concentration.[15,16] ICP-MS is, however, subject to many factors that affect performance, such as polyatomic interferences, and elemental fractionation. Furthermore, when coupled to LA, it can suffer heavily from matrix effects, whereby more volatile material form aerosols more readily and is disproportionately represented in the ion images formed. Despite this, the past

two decades have produced a wealth of data relating to the relative concentrations and distributions of metals within ocular tissue.[7,11,17-19]

The MeV ion beam analysis (IBA) technique particle-induced X-ray emission (PIXE) is subject to much less interference and is not hindered by matrix effects in biological samples.[20] This allows not only for the analysis of previously complicated elements such as sulfur, phosphorus, and chlorine. Additionally, X-ray spectra are collected together with backscattered particle spectra, which is used to determine the sample matrix composition. Although the “total IBA” approach quantitative analysis can be conducted without the need for complex analytical standards as in LA-ICP-MS.[21] Consequently, the inherent problems faced by more one-dimensional studies can be overcome through the combination of complementary techniques within a multimodal workflow.

The ocular metallome has clear points of interest for the development of the under- standing of ocular pathology. Information gained from wildtype (WT) mouse tissue can

help to describe the ocular metallome in detail and inform on decisions in future research. In ocular research, rhodopsin knockout (*Rho*$^{-/-}$) tissue has long been used as a model of retinitis pigmentosa (RP), offering an insight into the structural and physiological changes that can occur as part of retinal degeneration, with homozygous mice exhibiting a complete lack of rod outer segments (OS), leading to subsequent degradation of cones and the prevention of the phototransduction cascade.[22] When studied alongside WT tissue, the structural changes that occur in a *Rho*$^{-/-}$ tissue could be indicative of the wider ocular metallome and how these changes may occur in retinal degeneration. Likewise, changes within *Rho*$^{-/-}$ tissue

can inform on the viability of the *Rho*$^{-/-}$ tissue in future studies of the ocular metallome.

In this study, the changes that occur within the *Rho*$^{-/-}$ mouse model have been investigated using a quantitative LA-ICP-MSI and PIXE.

2.0. Materials & Methods

2.1. Chemicals

The following materials were used: traceCERT® Multielement Standard Solution 6 for ICP (Merck Group, Darmstadt, Germany) HNO_3 (CAS 7697-37-2) (VWR, Poole, UK), Gelatin (Merck Group, Darmstadt, Germany), and Masson's trichrome (methyl blue) stain kit (Atom Scientific, Hyde, UK) carboxymethylcellulose (CAS 9004-32-4) (Merck Group, Darmstadt, Germany).

2.2. Tissue Collection

WT and Rho−/− mouse ocular tissue were obtained from Trinity College Dublin, Ireland. Ocular tissues were embedded in carboxymethylcellulose (CMC) prior to snap freezing. Sections of the ocular tissues were taken at 5 µm.

2.3. Masson's Trichrome Staining

Serial sections of both the WT and Rho−/− sections analysed by LA-ICP-MSI were stained using a Masson's trichrome (methyl blue) stain kit (Atom Scientific,

Hyde, UK) by staining the sections in Weigart's haematoxylin for 20 min, followed by differentiation in 1% acid alcohol (99:1 EtOH:HCl). Following rinsing and blueing in water, a further stain with ponceau fuchsin was conducted for 5 min prior to rinsing and the differentiation step in water and phosphomolybdic acid for 15 min; a final stain was conducted in methyl blue for 5 min, as per the manufacturer's instructions.

2.4. Preparation of Calibration Arrays

Matrix-matched calibrants for use with LA-ICP-MSI were prepared by serial dilution with 1% HNO_3 of ICP Standard Solution 6 (Merck Group Darmstadt, Germany) to obtain 1–50 ppm solutions. These solutions were mixed 50:50 with 20% gelatin before 15 µL of each were prepared in wells created by fixing 4 mm washers in an epoxy resin. The standards were then allowed to dry in a vacuum desiccator overnight at room temperature.

2.5. LA-ICP-MS

LA-ICP-MS experiments were conducted using an ImageBio266 laser ablation unit coupled to a NexION 350X ICP-MS. The laser spot size was set to 10 µm, and the repetition rate of the laser was set to 500 Hz. The laser power was operated at 37%, resulting in a sample fluence of ~3.8 Jcm^{-1}. The ICP-MS was operated in standard mode, utilizing 5 sweeps and a dwell time of 10, 20, and 20 ms for ^{24}Mg, ^{63}Cu, and ^{66}Zn.

2.6. PIXE

WT and Rho−/− tissue were analysed at the National Ion Beam Centre at the University of Surrey. A 2.5 MeV (nominal beam energy) H^+ beam at normal incidence was focused to a diameter <2 μm using a magnetic quadrupole triplet lens type OM-150 (Oxford Microbeams Ltd., Oxford, UK). X-rays induced by the beam were detected by a silicon drifted detector (SDD) with an active area of 80 mm^2 and mounted at a central angle of 135° to the beam direction in the horizontal plane with a variable sample-to-detector distance of 425 mm. The X-ray detector was fitted with a 130 μm beryllium foil. Elastically backscattered protons were detected using a 150 mm^2 ULTRA-series passivated implanted planar silicon (PIPS) detector (ORTEC, Wokingham, UK). The detector angle was 155° ± 0.2, and the distance between the centre of the nanobeam chamber and the detector entrance was 52.5 ± 0.2 mm. Both detectors were fitted with a sampling cone to stop signals from the chamber from reaching the detectors.

3.0. Results

The retinal structure is a highly privileged and highly conserved part of the ocular anatomy. Any disruption to this otherwise balanced and organized structure can cause issues for those who experience it. Elements within ocular tissue have been observed to localize discreetly within the retinal structure, conforming to the existing anatomy. The observation of elements within the retina, or the changes that occur to the elements within the ocular tissue can be descriptive of important pathophysiological mechanisms within the eye.

3.1. WT and Rho−/− Retinal Anatomy

Healthy mouse ocular tissue is highly structured and can be segmented into distinct layers. Figure 1 shows the choriocapillaris/RPE (CC/RPE) layer, the outer segment (OS) and inner segment (IS); the outer layers, the outer nuclear layer (ONL) and outer plexiform layer (OPL); and the inner layers, the inner nuclear layer (INL) and inner plexiform layer (IPL). The choriocapillaris is responsible for the transport of nutrients from the blood to the eye, and the other layers are key to visual function. Rods and cones function by transforming light into electrical signals, allowing the brain to transform these signals into vision. In ocular diseases such as AMD, these rods and cones are degraded by invading neovasculature in wet AMD and harmful buildups of extracellular matter known as drusen in dry AMD. The ONL and OPL, which contain the rods and cones responsible for vision, can be seen distinctly in Figure 1b. Rho−/− tissue can be seen in Figure 1. The Rho−/− tissue can be seen to have degraded this layer of the ocular tissue, leaving only the INL and the IPL intact. These structural changes that occur within the layers of the retina are severe but represent the degradation that occurs within the ocular tissue of those who have ocular degenerative diseases such as AMD, diabetic retinopathy, retinal pigmentosa, and other similar diseases.

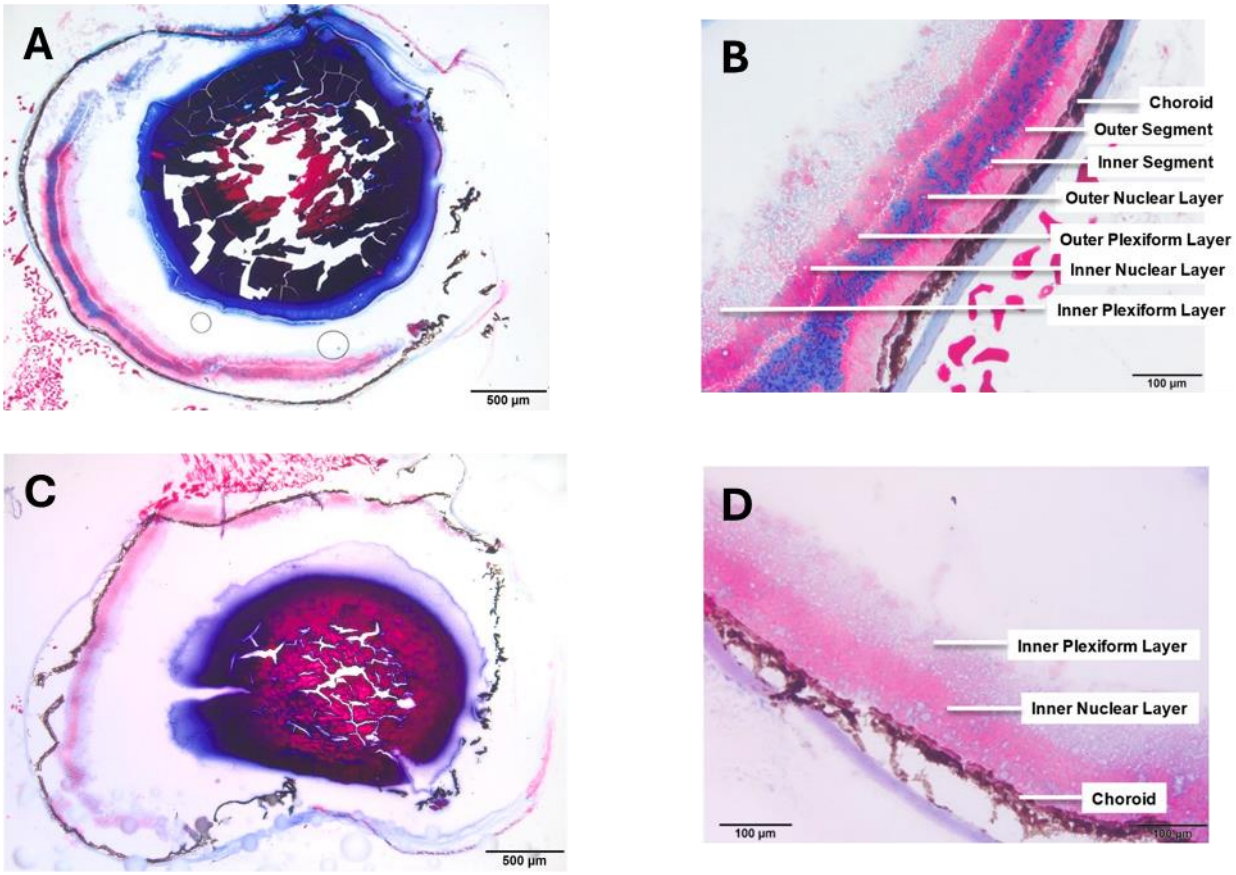

Figure 1 Masson's trichrome (methyl blue) stains of wildtype mouse ocular tissue; (a) 20× view of the whole ocular tissue section and (b) 4× view of the retinal microanatomy. Rho−/− mouse ocular tissue; (c) 20× view of the whole ocular tissue section and (d) 4× view of the degraded retinal microanatomy.

3.2. LA-ICP-MSI

3.2.1. Wildtype Cu

^{63}Cu is one of the key trace metals that constitute a class of essential trace elements for ocular function. Paired with zinc, copper can be critical for the clearance of ROS in ocular tissue.[10,23] Utilizing a previously described method for the quantification of biological tissue by LA-ICP-MS.[19] WT and Rho−/− tissue were analysed alongside the calibration standards at a spot size of 10 µm to

obtain high-resolution spatial characterizations of ^{63}Cu within mouse ocular tissue. Figure 2 shows the distribution of copper throughout the ocular tissue. The copper observed was largely present within all anatomical regions of the tissue, with the exception of the vitreous humor. The relative concentration, however, appeared heterogenous, with copper localizing specifically to a number of substructures of the eye, being in the highest quantity within the ciliary bodies, followed by the iris, retina, lens, and cornea, respectively. Within the retinal region, copper was observed to be most prominent in the choroid/RPE region and formed distinct bands within the retinal layers, allowing the segmentation of the retina into at least six layers of varying width. Quantitative data was produced using 250 µm wide regions of interest (ROI) placed within the substructures of the ocular anatomy by using Masson's trichrome stains of the tissue to ascertain the substructures of the microanatomy. The ROI analysis, produced in Iolite 4, allowed for the quantification of an element within a region.[24-26] Quantitative analysis showed that the concentrations ranged from just over 0.5 ppm down to just above 0.01 ppm. It also showed that the copper was in its highest quantities in the choriocapillaris, followed by the OPL, IS, INL, IPL, and OS, respectively (Figure 2).

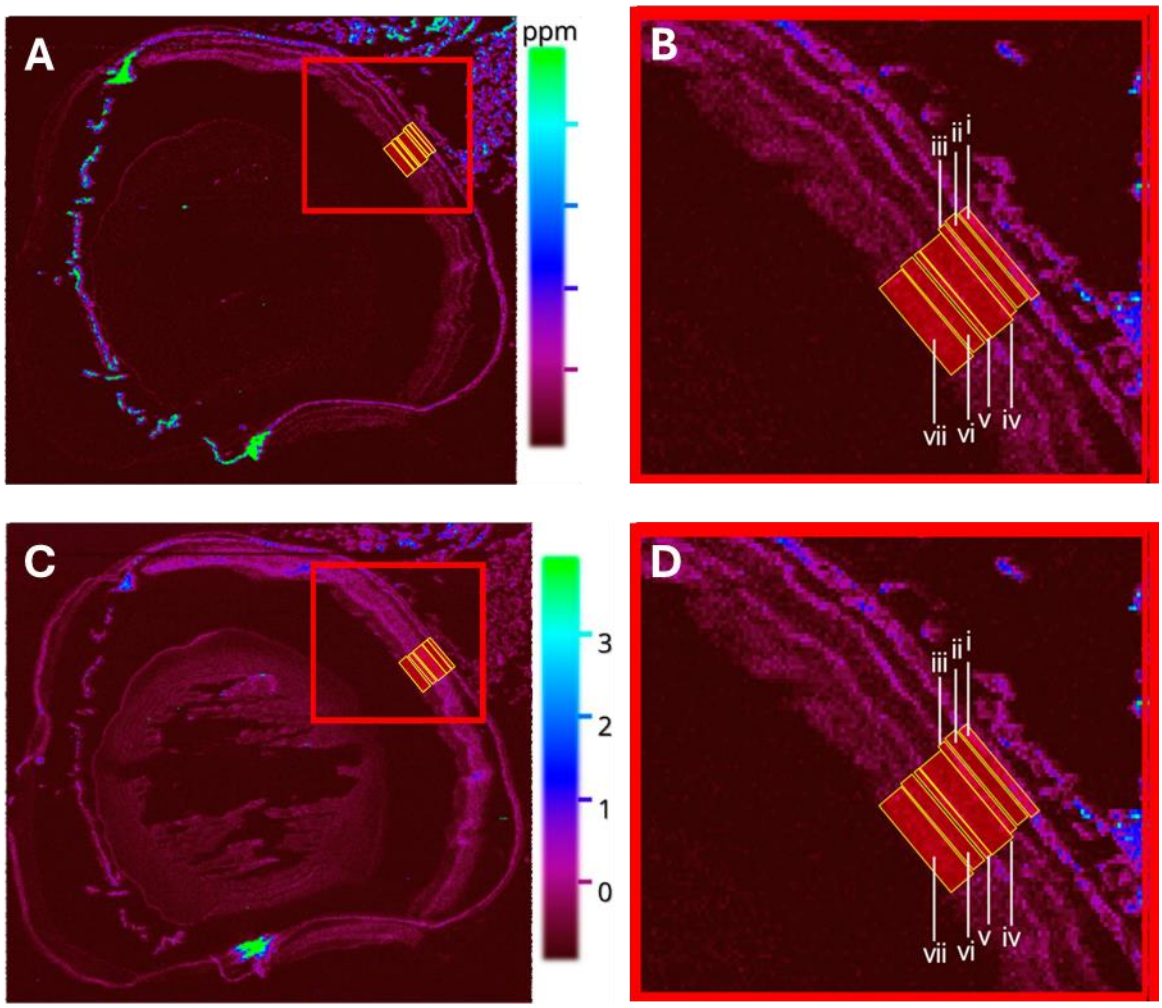

Figure 2 (a) Distribution of ^{63}Cu in WT mouse ocular tissue, with each region of interest (ROI) within the retinal layers highlighted (red). (b) A zoomed view with the portions (i) choriocapillaris (CC),(ii) outer segments (OS), (iii) inner segments (IS), (iv) outer nuclear layer (ONL), (v) outer plexiform layer (OPL), (vi) inner nuclear layers (INL), and (vii) inner plexiform layer (IPL). (c) Distribution of ^{66}Zn in WT mouse ocular tissue, with each region of interest (ROI) within the retinal layers highlighted (red). (d) A zoomed view with the portions (i) CC, (ii) OS, (iii) IS, (iv) ONL, (v) OPL,

(vi) INL, and (vii) IPL.

3.2.2. Wildtype ^{63}Zn

^{66}Zn is another key element in the prevention of chronic inflammation through the upregulation of superoxide dismutase. Additionally, as previously mentioned, Zn has been observed to change as a function of age and is closely linked to AMD with AREDS 2 supplements containing a daily dose of 80 mg. Like copper, ^{66}Zn was observed within wildtype ocular tissue at a spatial resolution of 10 µm, allowing for the resolution of multiple layers within the ocular tissue. Like copper, ^{66}Zn was seen to be present within the majority of the substructures of the ocular anatomy. Unlike copper, there was less heterogeneity observed within the structures in terms of concentration. Only four distinct regions within the retina were able to be observed, but by using the coordinates for each layer found in the copper and Masson's trichrome imaging, the same ROI analysis took place for ^{66}Zn within the retinal tissue. The quantitative analysis showed a range of 0–3 ppm, which is up to 3-fold higher than that observed for copper. ROI analysis showed that the INL, OPL, and ONL were highest in concentration followed by CC, IS IPL, and OS.

The INL, OPL, and ONL were observed to be indistinguishable but otherwise had similar relative concentrations between layers as in the Cu images.

These observed concentration changes between the CC and the rest of the tissue architecture are in agreement with previous studies of this kind, as Erie et al. described an elevated level of both copper and zinc within the CC/RPE when compared to the 'retina' in a study from 2009, which was concurrent with a 2008 study by Wills et al.[23,27]

3.2.3. Rho$^{-/-}$ ^{63}Cu

Using the same quantitative and data analysis techniques as with the wildtype tissue, Rho−/− tissue was analysed by LA-ICP for both ^{66}Cu and ^{66}Zn. The copper images, like those observed in the characterization of Rho−/− tissue in Figure 1, show depletion of the OS and a complete lack of rod outer segments (OS), leading to subsequent degradation of cones, leaving only the INL and the IPL intact. The ^{63}Cu images show that other than in the retina, the distribution of copper has remained unchanged, with varying amounts of copper throughout the ocular tissue, with additional quantities in the iris and ciliary body. The retinal substructures can only be segmented into three substructures: the CC, an inner layer (INL), and an outer layer (IPL) (Figure 3). By segmenting the Rho−/− retina into three substructures, the copper and zinc observed were seen to be quite variable between replicates (Figure 4c,d), but they were generally seen to have high levels of ^{66}Zn in the CC and lower levels in the inner layers, with this difference been less pronounced in ^{63}Cu. This difference in relative concentrations between the CC and the other layers within the retina is consistent with that observed in the WT tissue. Additionally, there are few notable changes to the concentration of the ^{63}Cu and ^{66}Zn in the Rho−/− tissue. It has previously been reported that forms of ocular degeneration, and the aged retina, can lead to an elevated level of zinc and copper in aged tissue; likewise, a reduction of these elements has been observed in the AMD tissue. The results herein show how degeneration of the outer segments as part of a Rho−/− tissue type does not inherently affect the concentrations of zinc and copper within the retinal substructures that remain.

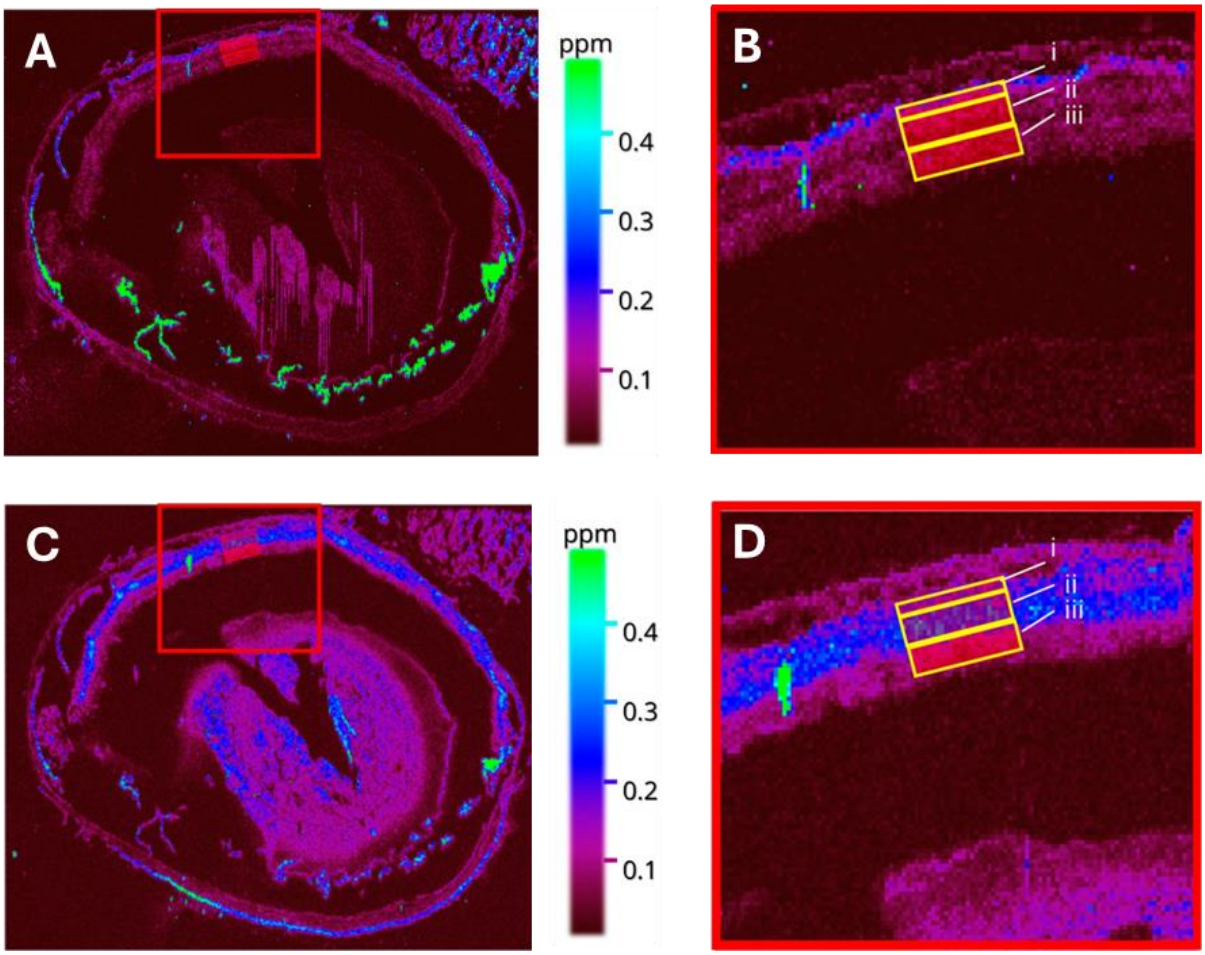

Figure 3 (a) Distribution of 63Cu in Rho−/− mouse ocular tissue, with each region of interest (ROI) within the retinal layers highlighted (red). (b) A zoomed view with the portions (i) choriocapillaris (CC), (ii) inner nuclear layer (INL), (iii) inner plexiform layer (IPL), (c) Distribution of 66Zn in Rho−/− mouse ocular tissue, with each region of interest (ROI) within the retinal layers highlighted (red). (d) A zoomed view with the portions (i) CC, (ii) INL, and (iii) IPL.

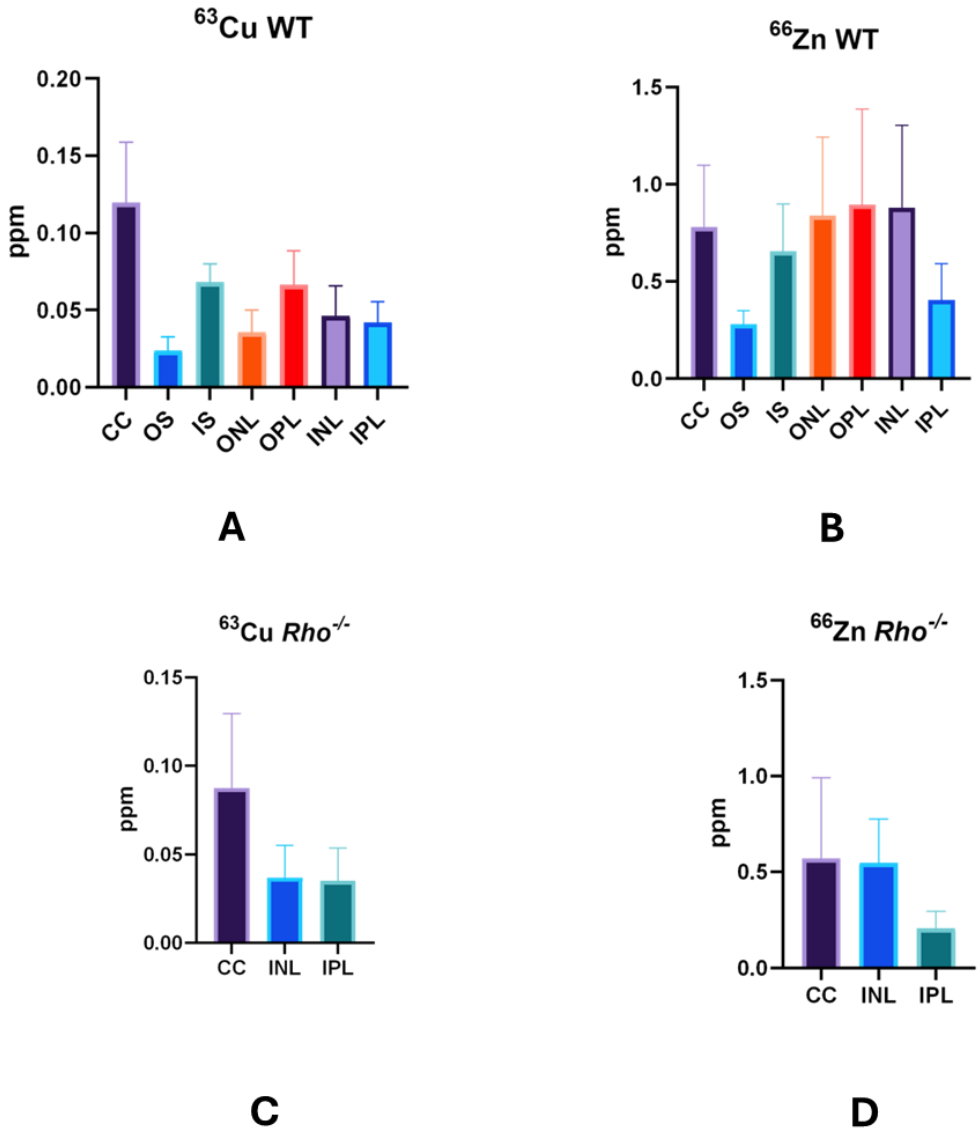

Figure 4 (a) Concentration values (ppm) of copper within a WT ocular tissue. (b) Concentration values (ppm) of Zn in a WT ocular tissue. (c) Concentration values (ppm) of copper within a Rho−/− ocular tissue. (d) Concentration values (ppm) of Zn in a Rho−/− ocular tissue.

3.3. PIXE

3.3.1. Phosphorus

Elements such as phosphorus (^{31}P) have interferences when analysed by an argon plasma in ICP-MS such as $^{14}N^{16}O^{1}H+$, $^{15}N^{15}N^{1}H+$, $^{15}N^{16}O+$, $^{14}N^{17}O+$, $^{13}C^{18}O+$, and $^{12}C^{18}O^{1}H+$ at 31 atomic mass units (amu).[13] This means that phosphorous is virtu- ally incompatible with argon plasma sources, as an ICP will allow the production of these nitrogen and oxygen-containing interferences from the atmosphere. Unlike ICP-MS, IBA techniques, namely, PIXE, rely on the production of characteristic X-rays, with few interferences for the PKα line. Figure 5 shows 1 mm^2 images produced from the ocular retina of mice by PIXE. Figure 5a shows how phosphorus is distributed within this ocular tissue. Like with the LA-ICP images, a clear demarcation between the retinal layers can be made; utilizing an H+ beam focused to < 2 µm, the spatial resolution achieved was superior to that of LA-ICP-MS.

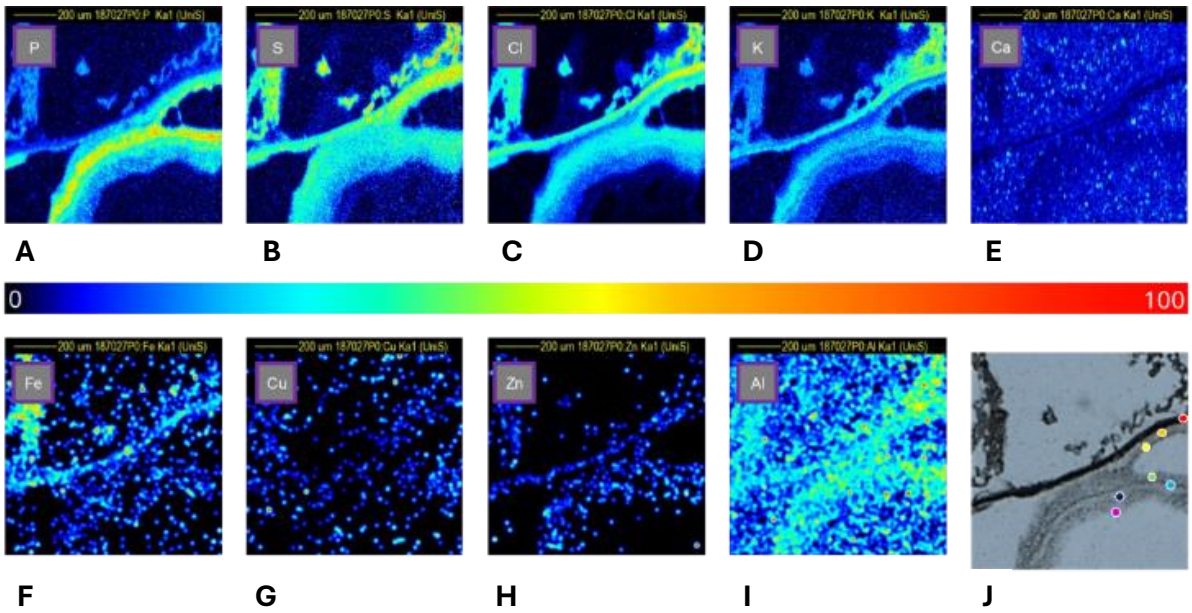

Figure 5 PIXE data detailing the retinal microanatomy of WT tissue: (a) phosphorous, (b) sulfur, (c) chlorine, (d) potassium, (e) calcium, (f) iron, (g)

copper, (h) zinc, and (i) aluminum. (j) Optical image with the choroid (red), outer segment (orange), inner segment (yellow), outer nuclear layer (green), outer plexiform layer (blue), inner nuclear layer (indigo), and inner plexiform layer (violet).

In wildtype tissue, the phosphorus can be seen to localize distinctly in retinal substructures, with the highest quantities in the ONL, followed by the OPL, OS, and then the inner retinal layers (IPL and INL), which share similar concentrations to the CC.

Elevated phosphorus in the OS can be attributed to phosphatidyl-pyridinium bis-retinoid (A2PE), a precursor for A2E, which is formed in the OS.[28] However, the majority of phosphorous observed can be attributed to the nuclei in the ONL, where they are as- sociated with the high density of nucleic acids, something previously observed in ocular tissue.[7]

The Rho−/− tissue was again able to demonstrate differences in tissue architecture

when observed using PIXE analysis. The Rho−/− tissue showed a similarly high level of phosphorus in the INL, followed by the CC and the IPL (Figure 6a). The images show, despite the lack of observable OPL and ONL regions, that the relative concentrations of the remaining layers are consistent.

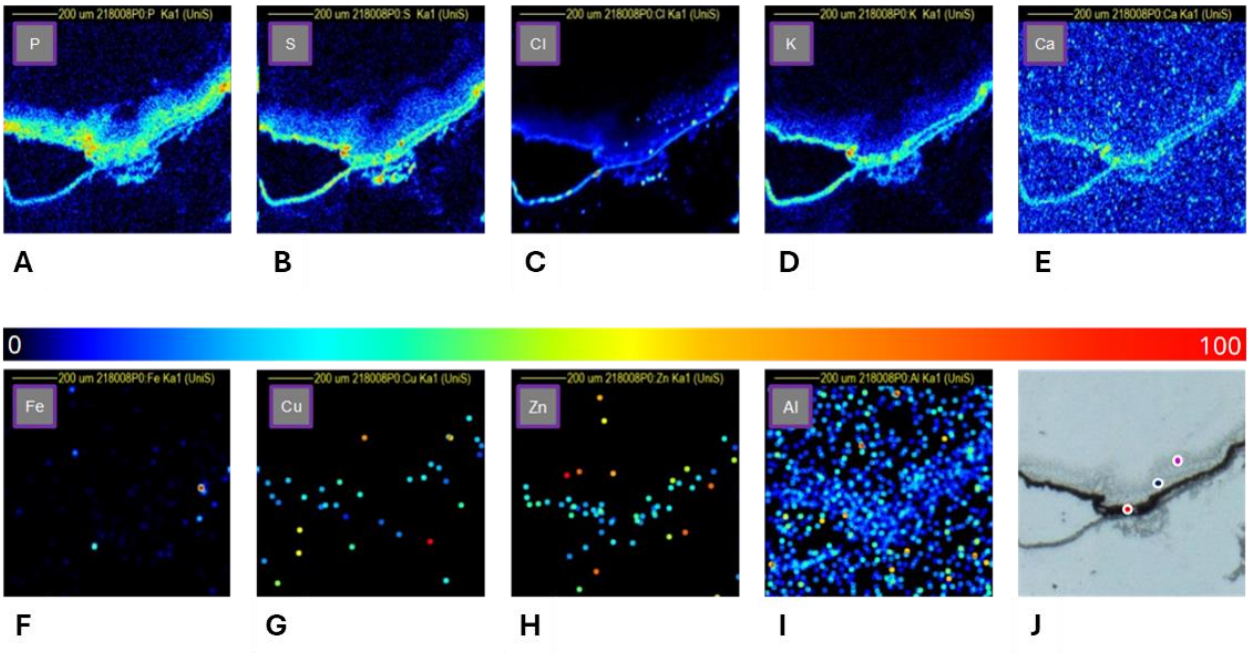

Figure 6 PIXE data detailing the retinal microanatomy of Rho−/− tissue: (a) phosphorous, (b) sulfur, (c) chlorine, (d) potassium, (e) calcium, (f) iron, (g) copper, (h) zinc, and (i) aluminum. (j) Optical image with the choroid (red), inner nuclear layer (indigo), and inner plexiform layer (violet).

3.3.2. Sulphur

Sulphur, like phosphorus, can be closely associated with the presence of proteins in structures with sulphide bonds. Sulphur is subject to polyatomic interferences when analysed by ICP with an argon plasma. Interferences from nitrogen and oxygen ($^{15}N^{18}O^{+}$, $^{14}N^{18}O^{1}H^{+}$) can cause increased levels of background noise. PIXE data (Figure 5b) exhibits the relatively homogenous distribution of sulphur within the tissue, with an increased level of sulphur in the CC and a gradual decrease in abundance moving through the OS, IS, ONL, OPL, INL, and IPL. Due to its relatively high abundance, and homogeneity, it offers a basis to determine when the beam is on or off the tissue in further PIXE analysis.

Sulphur within the Rho−/− is also able to exhibit organizational changes within the tissue. The image (Figure 6b) shows elevated sulphur in the CC, followed by a diffuse structure marking the presence of the IPL and INL. This homogeneity is observed within the IPL and INL of the WT tissue, which, like Rho−/−, has the highest amount of sulphur within the CC.

3.3.3. Chlorine

Chlorine, like phosphorus, is an essential element found abundantly in the natural world and, like phosphorus, encounters issues with polyatomic interferences from the atmosphere when analysed by an argon plasma. The ^{35}Cl isotope (~76%) possesses the same mass as $^{16}O^{18}O^{1}H+$, and the ^{37}Cl isotope (~24%) possesses the same mass as $^{36}Ar^{1}H+$, resulting in problematic analysis when using an argon plasma ICP-MS for analysis.[13] However, chlorine has an important role in human anatomy and specifically in the retinal cycle. Chlorine is present in Ca-activated chloride channels. Chloride channels are vital for ocular function, with some involved in the control of transmitter release in the dark. Additionally, chloride intracellular channel 4 (CLIC4) is a cytosolic protein involved in the innate immune response that regulates chlorine concentration. Previously, $RPE^{\Delta Clic4}$ mice have been shown to exhibit functional and pathological hallmarks of AMD, highlighting the perceived importance of monitoring chlorine levels within the structure of the eye.

The Cl observed within WT tissue (Figure 5c) can clearly be separated into a CC, with the highest concentration, the OS, with a lower concentration the outer

layers, and the inner layers of the ocular tissue, which have higher and lower concentrations, respectively, but lower concentrations than the CC overall. The Rho−/− tissues once again exhibit structural changes through the lack of OSs and the depletion of the outer layers, leaving the less abundantly populated inner layers, in addition to a relatively high concentration of CC (Figure 6c).

3.3.4. Potassium

Potassium is a common essential element found within most extracellular matrices and plays a key role in the phototransduction pathways responsible for vision.[29,30] Potassium, with isotopes at 39 (93.08%), 40 (0.01%), and 41 (6.91%), has some of the most problematic interferences in $^{38}Ar^{1}H+$, $^{40}Ar+$, and $^{40}Ar^{1}H+$, respectively.[13] This makes analysis by ICP with argon plasma extremely problematic. By using PIXE, potassium data from both WT and Rho−/− tissue can be ascertained. The PIXE data (Figure 5d) show potassium to be most prevalent in the CC, ONL, and INL. This, except for the more notable absence in the OPL, is a similar distribution to that of chlorine. As potassium has increased concentrations intracellularly, these results are concurrent with potassium being highly concentrated in the areas that have the highest cellular density. For potassium, once again, only the inner layers and the CC are directly observable within Rho−/− tissue, with little change in the distribution of potassium (Figure 6d). What remains is that the CC and the inner layers appear to have quite a high contrast in concentration in comparison to the WT data.

3.3.5. Calcium

Calcium is an essential trace element closely linked with some of the other elements aforementioned.[29,30] It has a key role within the visual cycle through modulation of the cGMP-gated channels and cGMP itself.[31] Calcium has been associated with ocular diseases such as age-related macular degeneration for some time, though its role is less clear. As part of AREDS, the National Institute for Health (NIH) showed that calcium supplementation could reduce the risk of the onset of AMD.[32] Likewise, reports of elevated levels of calcium in drusen deposits have been reported in AMD patients.[33] The distribution of calcium (Figures 5e and 6e) within ocular tissue is less distinguishable due to seemingly low levels of calcium above the background. This is because the background levels can be attributed to interferences from the PET slide on which the tissue is mounted. In spite of this, elevated levels of calcium could be observed within the CC of the WT and Rho−/− sections. This area within the CC, where Brusch's membrane (BrM) has its interface with the RPE, is incidentally where the calcium-filled deposits of drusen arise.

3.3.6. Iron

Iron, another element that is impaired by polyatomic interferences within an argon plasma, namely, with $^{40}Ar^{16}O+$ (=^{56}Fe), is also of interest in ocular disease.[13] It acts as a cofactor in processes such as oxygen transport, membrane biogenesis, and maintenance of the visual cycle; more specifically, iron is essential for RPE65 activity. Iron is also heavily involved with certain mechanisms of inflammation; the Fenton reaction ($Fe^{2+} + H_2O_2 \rightarrow Fe^{3+} + HO\cdot + OH^-$), for example, produces ROS, which can occur as a by-product of exogenous iron accumulation, which is

a phenomenon that can cause retinal degeneration.[12,34,35] These data indicate that seemingly low levels of iron can be observed predominantly in vasculature outside of the retinal anatomy, likely as part of haemoglobin, and when observed within the anatomy can be seen to be discretely localized to the CC/RPE of the ocular tissue (Figures 5f and 6f).

3.3.7. Copper

PIXE has an inferior limit of detection (ppm range) than ICP-MS, which regularly detects elements in the ppb range.[16,36,37] As a result, the copper observed in the tissue by ICP (~1.5 ppm) is at the lower end of PIXE detection limits, which were ~10 ppm across the 1 mm^2 analysed. In Figures 5g and 6g, the images can be seen to be sparsely populated by data points as a result.

3.3.8. Zinc

Like copper, zinc remains a problematic element given that it has a <3 ppm range according to the LA-ICP-MS data (Figure 2). The data presented in the PIXE analysis were not able to obtain meaningful conclusions due to this lack of sensitivity. Unlike copper, due to its slightly higher endogenous concentration, the difference between on and off tissue was able to be determined (Figures 5h and 6h).

3.3.9. Aluminium

Similarly, aluminium had a poorer signal-to-noise ratio than previously analysed elements. The aluminium can be used to determine between on and off tissue,

yet further information could not be ascertained from the images (Figures 5i and 6i).

3.4. Quantitative PIXE

PIXE analyses can be made to be quantitative without the need for matrix-matched standards. In contrast with LA-ICP-MS, this quantitative ability is compromised by matrix effects experienced in LA-ICP. The quantitative data of WT tissue showed that the endogenous elements phosphorus, sulphur, chlorine, potassium, and calcium were in significantly higher quantities than that of copper and zinc. Chlorine was seen to be in its highest concentration in the CC, where it also exceeded the concentrations of P, S, K, and Ca. Phosphorus was seen to be the highest within the ONL, followed by chlorine, sulphur, and potassium. The highest level metal in the INL was, however, sulphur by a factor of two. The third region (Figure 7b), which described the PET slide on which the slides were analysed, was, however, indicative of the interferences that can be seen in PIXE analysis. The Ca images (Figures 6e and 7e), which were relatively indiscriminate, can be explained by the high presence of Ca within the PET film as seen in Figure 7. The quantitative data show that Ca is not homogenously distributed, yet the signal-to-noise ratio remains too low for discerning structural features. Iron, copper, zinc, and aluminium were in low abundance and were thereby unable to be quantified accurately (Figure S1).

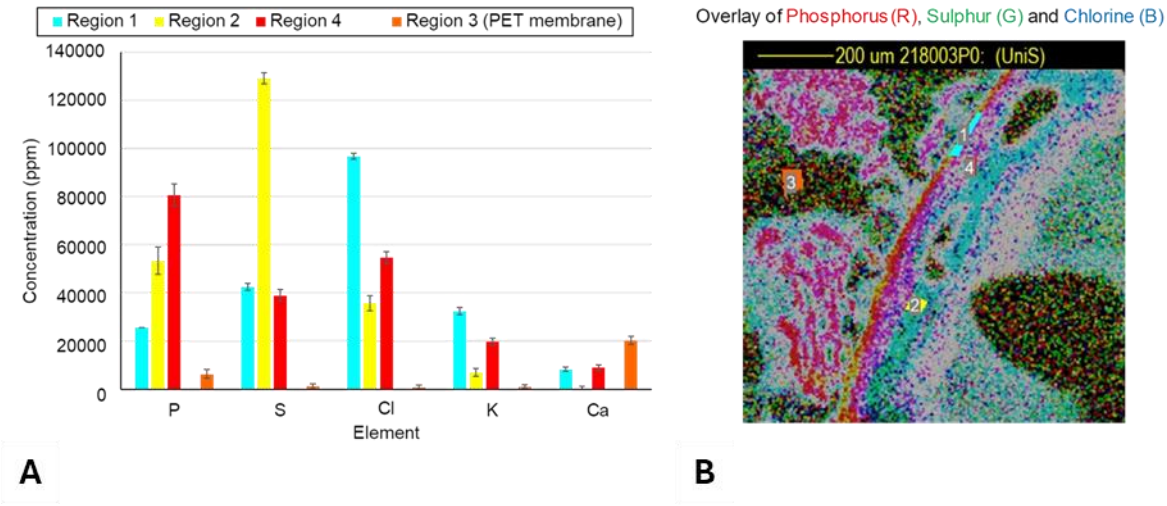

Figure 7 . Quantitative PIXE data exhibiting the concentrations of the elements phosphorus, sulphur, chlorine, potassium, and calcium. (a) Concentrations (ppm) of the regions of interest (ROI) within a wildtype (WT) tissue. (b) An image of the corresponding WT tissue section ROIs; (1) chorio-capillaris (CC) (2) outer nuclear layer (ONL) (3) polyethylene terephthalate (PET) (4) outer/inner segment (OS/IS).

4.0. Discussion & Conclusion

The use of LA-ICP-MS in the exploration of ocular pathology has been able to offer unique insights into the metallome of WT ocular tissue in the past, though it has been at the mercy of matrix effects and polyatomic interferences that LA-ICP-MS is notoriously susceptible to. This body of work comprises a combination of quantitative LA-ICP-MSI and PIXE analysis and has comprehensively described the metallome of not only elements amenable to ICP-MS analysis such as copper and zinc, but also to the wider metallome excluded by studies confined to ICP-MS analysis such as phosphorus, sulphur, chlorine, potassium, calcium, and iron.

Additionally, the datasets herein include a widely used retinal degeneration model, Rho−/−, which has described the structural changes that occur within Rho−/− tissue from the perspective of the metallome. This study has demonstrated the changes that occur to the metal species within Rho−/− tissue and how the changes to the structure affect the distribution of essential elements. With a wider understanding of not only the WT metallome but that of Rho−/− tissue as well, this study contributes to the wider understanding of ocular tissue and how elements from across the periodic table behave in the retina.

From the essential elements measured within WT ocular tissue, it can be seen that there is a highly organized structure within the mouse retina.[38] The distributions of these elements, however, are not uniform to one another, some elements remain relatively homogenous through different layers within the retina, whereas copper can be seen to vary in concentration distinctly between each identifiable layer within the retina. The existence of this complex relationship between structure function and the wider metallome is poorly understood; however, the high spatial resolution imaging of these structures may help to inform ocular physiology and pathology in the future. In addition, the ocular tissue from the Rho−/− mice demonstrated the structural changes that have occurred as a result of the deletion of rhodopsin. The retinal tissue of Rho−/− mice has reduced structural organization and is missing layers, namely, the outer segments. In LA-ICP- MS and PIXE images, these structural changes can be seen to occur but do not affect the distribution or relative concentrations of the metals observed. These data, however, were purely qualitative; so, should further quantitative work be undertaken in the future, some physiological as well as

structural changes may be observed through mapping elemental concentrations in Rho−/− tissue.

The metallome is a widely explored yet poorly understood part of ocular pathology, yet methodologies and techniques for the characterization of such tissue have become increasingly more accessible in recent years. In addition, the use of multimodal work- flows has greatly benefitted the field of metallomics, with PIXE and LA-ICP-MS as prime examples of complimentary datasets, utilizing the sensitivity of ICP and the robustness and spatial resolution of PIXE. These data demonstrate a foundation by which future studies relating to the ocular metallome may build, utilizing more complex sample sets and eventually progressing to patient tissue.

5.0. References

1. Anbesu, J.; et al. Trends in prevalence of blindness and distance and near vision impairment over 30 years: An analysis for the Global Burden of Disease Study. *Lancet Glob. Health* **2021**, *9*, e130–e143. [CrossRef] [PubMed]
2. Papadopoulos, Z. Recent Developments in the Treatment of Wet Age-related Macular Degeneration. *Curr. Med. Sci.* **2020**,
3. *40*, 851–857. [CrossRef]
4. Celkova, L.; Doyle, S.L.; Campbell, M. NLRP3 Inflammasome and Pathobiology in AMD. *J. Clin. Med.* **2015**, *4*, 172–192. [CrossRef]
5. The Age-Related Eye Disease Study Research Group. The effect of five-year zinc supplementation on serum zinc, serum cholesterol and

hematocrit in persons randomly assigned to treatment group in the age-related eye disease study: AREDS Report No. 7. *J. Nutr.* **2002**, *132*, 697–702. [CrossRef] [PubMed]

6. Rock, K.L.; Latz, E.; Ontiveros, F.; Kono, H. The Sterile Inflammatory Response. *Annu. Rev. Immunol.* **2009**, *28*, 321–342. [CrossRef]
7. Guo, H.; Callaway, J.B.; Ting, J.P. Inflammasomes: Mechanism of action, role in disease and therapeutics. *Nat. Med.* **2015**,
8. *21*, 677–687. [CrossRef]
9. Pålsgård, E.; Ugarte, M.; Rajta, I.; Grime, G. The role of zinc in the dark-adapted retina studied directly using microPIXE. *Nucl. Instruments Methods Phys. Res. Sect. B Beam Interactions Mater. Atoms* **2001**, *181*, 489–492. [CrossRef]
10. Randomized, A. Placebo-Controlled, Clinical Trial of High-Dose Supplementation With Vitamins C and E, Beta Carotene, and Zinc for Age-Related Macular Degeneration and Vision Loss: AREDS Report No. 8. *Arch. Ophthalmol.* **2001**, *119*, 1417–1436.
11. Newsome, D.A.; Miceli, M.V.; Tate, D.J.; Alcock, N.W.; Oliver, P.D. Zinc content of human retinal pigment epithelium decreases with age and macular degeneration, but superoxide dismutase activity increases. *J. Trace Elem. Exp. Med.* **1996**, *8*, 193–199. [CrossRef]
12. Wong, C.P.; Rinaldi, N.A.; Ho, E. Zinc deficiency enhanced inflammatory response by increasing immune cell activation and inducing IL6 promoter demethylation. *Mol. Nutr. Food Res.* **2015**, *59*, 991–999. [CrossRef]
13. Ugarte, M.; Osborne, N.N. Recent advances in the understanding of the role of zinc in ocular tissues. *Metallomics* **2014**, *6*, 189–200.
14. [CrossRef] [PubMed]

15. Jünemann, A.G.; Stopa, P.; Michalke, B.; Chaudhri, A.; Reulbach, U.; Huchzermeyer, C.; Schlötzer-Schrehardt, U.; Kruse, F.E.; Zrenner, E.; Rejdak, R. Levels of Aqueous Humor Trace Elements in Patients with Non-Exsudative Age-related Macular Degeneration: A Case-control Study. *PLoS ONE* **2013**, *8*, e56734. [CrossRef]
16. May, T.W.; Wiedmeyer, R.H. A table of polyatomic interferences in ICP-MS. *At. Spectrosc.* **1998**, *19*, 150–155.
17. Chuang, J.Z.; Yang, N.; Nakajima, N.; Otsu, W.; Fu, C.; Yang, H.H.; Lee, M.P.; Akbar, A.F.; Badea, T.C.; Guo, Z.; et al. Retinal pigment epithelium-specific CLIC4 mutant is a mouse model of dry age-related macular degeneration. *Nat. Commun.* **2022**, *13*, 374. [CrossRef]
18. Trueman, C. *Encyclopedia of Analytical Science*, 2nd ed.; Worsfold, P., Townshend, A., Poole, C., Eds.; Elsevier: Oxford, UK, 2005;
19. pp. 171–181.
20. Limbeck, A.; Galler, P.; Bonta, M.; Bauer, G.; Nischkauer, W.; Vanhaecke, F. Recent advances in quantitative LA-ICP-MS analysis: Challenges and solutions in the life sciences and environmental chemistry. *Anal. Bioanal. Chem.* **2015**, *407*, 6593–6617. [CrossRef]
21. Ugarte, M.; Osborne, N.N.; Brown, L.A.; Bishop, P.N. Iron, zinc, and copper in retinal physiology and disease. *Surv. Ophthalmol.*
22. **2013**, *58*, 585–609. [CrossRef] [PubMed]
23. Aberami, S.; Nikhalashree, S.; Bharathselvi, M.; Biswas, J.; Sulochana, K.N.; Coral, K. Elemental concentrations in Choroid-RPE and retina of human eyes with age-related macular degeneration. *Exp. Eye Res.* **2019**, *186*, 107718. [CrossRef]
24. Millar, J.; Ozaki, E.; Campbell, S.; Duckett, C.; Doyle, S.; Cole, L.M.

Multiomic Mass Spectrometry Imaging to Advance Future Pathological Understanding of Ocular Disease. *Metabolites* **2022**, *12*, 1239. [CrossRef]

25. Greenhalgh, C.J.; Karekla, E.; Miles, G.J.; Powley, I.R.; Costa, C.; De Jesus, J.; Bailey, M.J.; Pritchard, C.; MacFarlane, M.; Pringle, J.H.; et al. Exploration of Matrix Effects in Laser Ablation Inductively Coupled Plasma Mass Spectrometry Imaging of Cisplatin-Treated Tumors. *Anal. Chem.* **2020**, *92*, 9847–9855. [CrossRef]
26. Jeynes, C.; Bailey, M.J.; Bright, N.J.; Christopher, M.E.; Grime, G.W.; Jones, B.N.; Palitsin, V.V.; Webb, R.P. "Total IBA"–Where are we? *Nucl. Instrum. Methods Phys. Res. Sect. B Beam Interact. Mater. At.* **2012**, *271*, 107–118. [CrossRef]
27. Jaissle, G.B.; May, C.A.; Reinhard, J.; Kohler, K.; Fauser, S.; Lutjen–Drecoll, E.; Zrenner, E.; Seeliger, M.W. Evaluation of the Rhodopsin Knockout Mouse as a Model of Pure Cone Function. *Investig. Ophthalmol. Vis. Sci.* **2001**, *42*, 506–513.
28. Wills, N.; Ramanujam, V.S.; Kalariya, N.; Lewis, J.; van Kuijk, F. Copper and zinc distribution in the human retina: Relationship to cadmium accumulation, age, and gender. *Exp. Eye Res.* **2008**, *87*, 80–88. [CrossRef] [PubMed]
29. Petrus, J.A.; Chew, D.M.; Leybourne, M.I.; Kamber, B.S. A new approach to laser-ablation inductively-coupled-plasma mass- spectrometry (LA-ICP-MS) using the flexible map interrogation tool 'Monocle'. *Chem. Geol.* **2017**, *463*, 76–93. [CrossRef]
30. Paton, C.; Hellstrom, J.; Paul, B.; Woodhead, J.; Hergt, J. Iolite: Freeware for the visualisation and processing of mass spectrometric data. *J. Anal. At.*

Spectrom. **2011**, *26*, 2508. [CrossRef]

31. Woodhead, J.D.; Hellstrom, J.; Hergt, J.M.; Greig, A.; Maas, R. Isotopic and Elemental Imaging of Geological Materials by Laser Ablation Inductively Coupled Plasma-Mass Spectrometry. *Geostand. Geoanalytical Res.* **2007**, *31*, 331–343. [CrossRef]
32. Erie, J.C.; Good, J.A.; Butz, J.A.; Pulido, J.S. Reduced Zinc and Copper in the Retinal Pigment Epithelium and Choroid in Age-related Macular Degeneration. *Am. J. Ophthalmol.* **2009**, *147*, 276–282.e1. [CrossRef]
33. Boyer, N.P.; Higbee, D.; Currin, M.B.; Blakeley, L.R.; Chen, C.; Ablonczy, Z.; Crouch, R.K.; Koutalos, Y. Lipofuscin and N- retinylidene-N-retinylethanolamine (A2E) accumulate in retinal pigment epithelium in absence of light exposure: Their origin is 11-cis-retinal. *J. Biol. Chem.* **2012**, *287*, 22276–22286. [CrossRef] [PubMed]
34. Bito, L.Z.; DiBenedetto, F.E.; Stetz, D. Homeostasis of the retinal micro-environment: I. Magnesium, potassium and calcium distributions in the avian eye. *Exp. Eye Res.* **1982**, *34*, 229–237. [CrossRef]
35. Mannu, G.S. Retinal phototransduction. *Neurosciences* **2014**, *19*, 275–280. [PubMed]
36. Nakatani, K.; Chen, C.; Yau, K.; Koutalos, Y. *Advances in Experimental Medicine and Biology*; Springer USA: Boston, MA, USA, 2002;
37. pp. 1–20.
38. Tisdale, A.K.; Agrón, E.; Sunshine, S.B.; Clemons, T.E.; Ferris, F.L.; Chew, E.Y. Association of Dietary and Supplementary Calcium Intake With Age-Related Macular Degeneration: Age-Related Eye Disease Study Report 39. *Arch. Ophthalmol. (1960)* **2019**, *137*, 543–550.

[CrossRef]

39. Flinn, J.M.; Kakalec, P.; Tappero, R.; Jones, B.; Lengyel, I. Correlations in distribution and concentration of calcium, copper and iron with zinc in isolated extracellular deposits associated with age-related macular degeneration. *Metallomics* **2014**, *6*, 1223–1228. [CrossRef]
40. Wong, R.W.; Dchimene, R.; Hahn, P.; Green, W.R.; Dunaief, J.L. Iron Toxicity as a potential factor in AMD. *Retina* **2007**, *27*, 997–1003. [CrossRef] [PubMed]

6.0. *Supplementary Material*

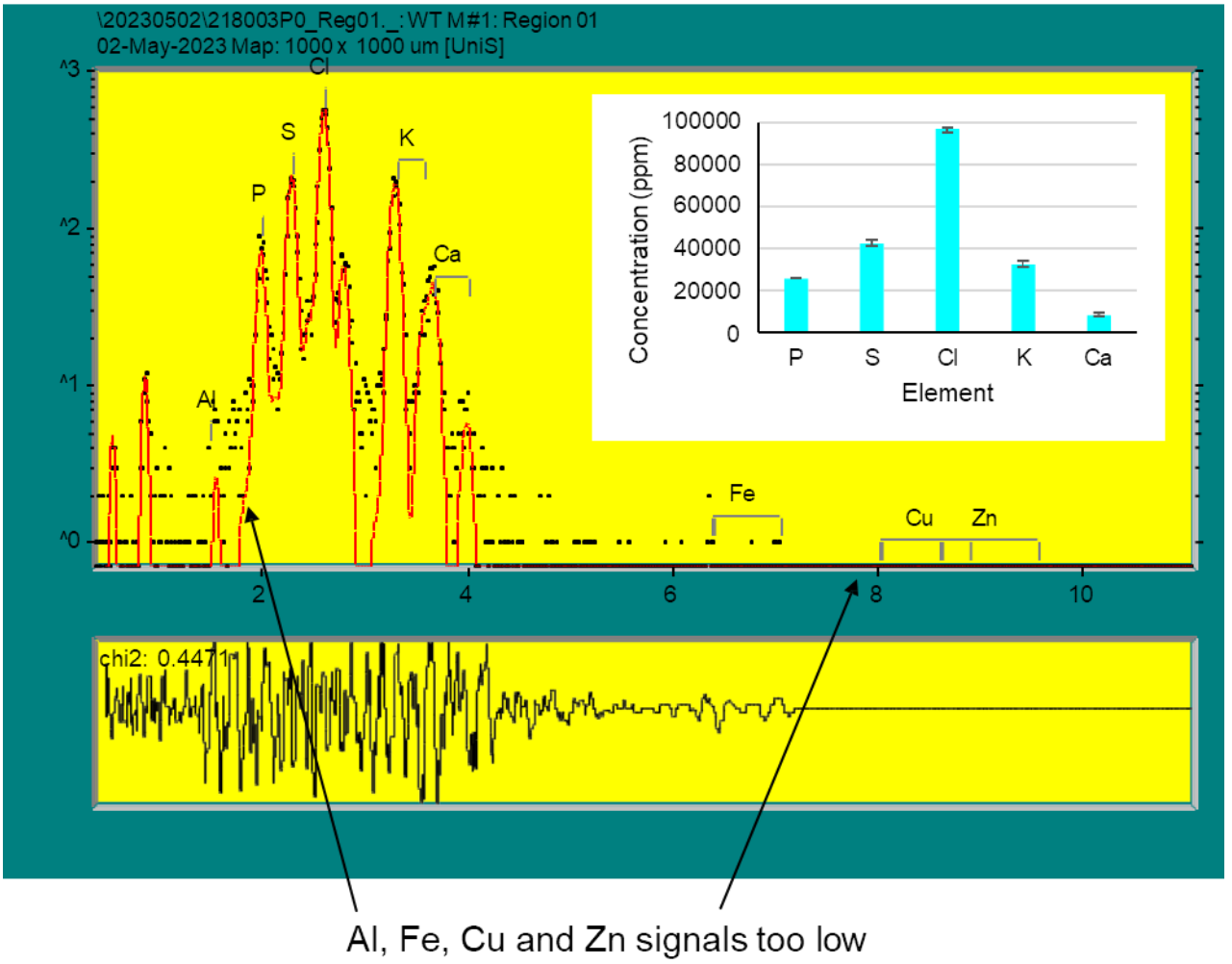

Figure S1 PIXE Spectrum showing insufficient sensitivity for quantification of Al, Fe, Cu , and Zn

Chapter 5

Joshua Millar, Ema Ozaki [2], Susan Campbell [1], Catherine Duckett [1], Sarah Doyle [2] and Laura M. Cole [1]*

A multimodal characterisation of ocular 'omics'

1. Centre for Mass Spectrometry Imaging, Biomolecular Research Centre, Sheffield Hallam University, Sheffield S1 1WB, UK
2. Immunobiology Research Group, Department of Clinical Medicine, Trinity College Institute of Neuroscience (TCIN), School of Medicine, Trinity College Dublin (TCD), D02 R590 Dublin 2, Ireland

Author Contribution: J. Millar conducted all analysis, sample preparation & data processing

Other Contributions: E. Ozaki sectioned & mounted the mouse ocular tissue used in this study

Abstract

Eye conditions are a complex class of diseases that affect billions of the population worldwide. The study of ocular disease in the pursuit of therapeutics is a multimodal and multidisciplinary effort spanning generations. Ocular 'omics' as part of bioanalytical science may demonstrate a beneficial tool within ophthalmology. Here, demonstration of a workflow that utilises multiple techniques in sequence is optimised to build a platform for multimodal ocular 'omics'. Starting with the least destructive technique, this study demonstrates how the use of desorption electrospray ionisation (DESI) and matrix assisted laser desorption ionisation (MALDI) mass spectrometry imaging techniques can be used to generate multitudes of datasets from single pieces of tissue. By exploring the field of metabolomics and lipidomics through DESI and peptidomics using MALDI in both mouse and human tissue, the study herein sets out the inception of a multidisciplinary approach in bioanalytical science to ocular disease.

1.0. Introduction

Ocular 'omics' may hold the key to future directions of pathology within the field of ophthalmology. For decades research into ocular disease has resided in the fields of genetics and immunology, these methodologies have been crucial in finding proteins and targets of interest within the field of ocular pathology.[1] In recent years, more and more studies involving the genetic and proteomic pathology of ocular disease have begun to coalesce around the doctrine

describing chronic inflammation and the wider influence of the innate immune system as a major cause of disease within ocular tissue.[2-5]

One of the major biological systems thought to be involved with age -related macular degeneration (AMD) is the innate immune system. The innate immune system is one of the first lines of defence against foreign bodies and helps serve to recruit immune cells to clear infection and is crucial for clearance of dead cells and extracellular debris.[2] In diseases such as AMD, the innate immune system can have a protective role. The innate immune system employs a number of proteins to conduct these protective processes, a major class of which are known as pattern recognition receptors (PRRs).[3-6] As the disease state produces inflammatory material such as drusen and buildup of extracellular matter, the PRRs react to the damage associated molecular patterns (DAMPs) and pathogen associated molecular patterns (PAMPs) produced in the diseased tissue and elicit an inflammatory response.[3,6] However, some postulate that selected proteins within the innate immune system do not have protective roles and rather can be detrimental to those suffering with AMD.[2,7-13] One theory to support this suggests that the over-reaction from PRRs in the innate immune system can lead to chronic inflammation, which on turn can cause further damage to the affected regions. These PRRs, and their associated proteins have been seen as crucial to further the understanding of how the innate immune system functions.[3-6,12-22]

1.1. TLR2

Notably, toll-like-receptors (TLRs) and related proteins have been seen to have some involvement in the pathways that cause the onset of diseases such AMD. TLRs are a part of the wider innate immune system, the downstream signalling of which forms a key part of the immune and inflammatory response, In 2004

Kindzelskii *et al.* noted the protective role of TLRs, namely TLR 2 and 4 against infection in the anterior region of the eye.[23] In addition, Güven *et al.* exhibited the TLR2-rs5743708 polymorphism caused individual to carry a four times greater risk of having AMD in later life.[2] Furthermore, West *et al.* and Fujimoto *et al.* were able to link choroidal neovascularisation, as found in wet AMD, to be mediated by TLR2, and Mulfaul *et al.* was able to link retinal degeneration to TLR2.[2,7,8,11,24] Considering the role that TLR2 and other TLRs have in innate immunity, and the perceived protective role of TLR2 in inflammation, the association of TLR2 with ocular pathology leaves adequate scope for further exploration into the role of TLR2 in AMD pathogenesis.

1.2. SARM1

Sterile alpha and TIR motif–containing 1 (SARM1), is an adaptor protein for toll-like receptors, and has a role in the regulation of downstream signalling pathways of TLRs. It has been known to be one of the key domains involved in axon degeneration, in response to injury as part of an immune response.[25] SARM1 has been implicated in a variety of diseases, such as amyotrophic lateral sclerosis, traumatic brain injury, and chemotherapy induced peripheral neuropathy, where its activation may play a crucial role.[26] Additionally, SARM1 has been found to be expressed in the retina and has been reported to have a pro-degenerative role within the photoreceptor layer of a retinal degeneration model, with SARM1 deficiency exhibiting a protective role for retinal degeneration.[27] Thought to be activated as a metabolic sensor, SARM1 consumes NAD^+, which in turn can lead to metabolic collapse and cell death.[25-27] As such, SARM1 has been identified as a potential therapeutic target.

1.3. NLRP3

NOD-like receptor protein 3 (NLRP3) is a key protein within the innate immune system, and is essential for the formation of the inflammasome.[3,4,15,28-34] The literature relating to NLRP3 and its association with AMD is still however limited, and only recently have breakthroughs relating to what may be a crucial role for NLRP3 in AMD pathology and future therapeutics. Like other PRRs, NLRP3 acts as a receptor that responds to 'danger' associated signals, and in turn produces the inflammatory response, a role which has been used to associate NLRP3 with AMD pathology. Tseng *et al.* were able to show an upregulation of NLRP3 in the progression of geographic atrophy (GA) and wet AMD, indicative of an inflammatory response in AMD.[30] In addition, Liao *et al.* were able to link NLRP3 with retinal degeneration induced by reactive oxygen species (ROS), suggesting further that the suppression of NLRP3 may be beneficial to ameliorate retinal degeneration.[34] Tarallo *et al.* also exhibited that genetic or pharmacological inhibition of NLRP3 would help to combat AMD onset through the reduction of Alu RNA accumulation implicated in GA AMD.[29] However, in 2012 *Doyle et al.* were able to show NLRP3 provided a protective role for the ocular anatomy by eliciting this immune response in the presence of drusen, one of the symptomatic manifestations of AMD.[29] This work, specifically that of Doyle *et al.* and Tarallo *et al.* which helped to further the understanding of ocular pathology, however was seemingly questioned, with Kosmidou *et al.* citing insufficient immunological specificity being the reason to argue against the role of NLRP3.[35] The paper suggested that due to the lack of reagent specificity, there may be reason to doubt the expression of NLRP3 within the human retina at all. Whilst further immunological studies have been conducted in spite of this proposal by Kosmidou *et al.*, without the use of another technique to study NLRP3, disproving

the hypothesis put forward by Kosmidou *et al.* could prove difficult. The production of data in the pursuit of pathological understanding and novel therapeutics must however exist without compromise. Consequently, the methods developed within this study aimed to conceive a method of observing NLRP3 within human ocular tissue without the need for immunological reagents and help to bolster advances within the ophthalmologic field of research.

1.4. Mouse Models

Mouse models are an established method for studying pathology in biological, medical and analytical sciences as they can be genetically modified, have a relatively short maturation period and are economically viable for many studies. However, though the use of mice in ocular pathology is equally well established, the use of mouse models in the study of macular degeneration can be disputed.[1,36] As nocturnal creatures, mice have less exposure to UV, a key producer of reactive oxygen species in the retinal cycle, which are species thought to contribute to AMD, amongst other diseases. [37] Additionally, mice crucially lack a macula; however there is good evidence to suggest that the parallels between physiological processes within the eyes of both mice and humans, as well as disease associated genes, is relatively strong, and information can be gathered from mice to inform on human ocular pathology.[1,36,38] For example, processes that result from ageing have been observed in mice, and the retinal degeneration genes have been identified within mice. [1,38] Moreover, some of the key symptoms and indicators of AMD have been observed in mice, such as drusen formation, the thickening of the Brusch's membrane (BrM), choroidal neovascularisation and regional RPE dropout.[1]

1.5. Human Tissue Studies

Though the effects can be life-changing, AMD is not considered to be a life-threatening disease. [39,40] As a result, enucleation is not used as a treatment as with other diseases such as uveal melanoma.[41] As such, few AMD patients lose their eye surgically, relying on post-mortem donations for use in biomedical research. However, post-mortem ocular tissue donations are relatively rare, with one study citing the majority of non-donations being as a result of family wishes (48%).[42] These issues, alongside medical exemptions result in a global undersupply of ocular tissue for use in research. Consequently, there have been relatively few pathological investigations into AMD with human tissue, and even fewer that use a sufficient number of participants to inform on AMD within the human population.

1.6. Mass Spectrometry

Using the different categories of '-omics' such as proteomics, lipidomics, metabolomics and metallomics, untargeted mass spectrometry (MS) has long been a crucial utility for biomarker discovery. Increasingly advanced technologies in mass spectrometry have allowed for the development of spatial '-omics', with recent studies citing spatial resolutions of 10µm in DESI-MSI, 5 µm and lower in MALDI analysis[43,44], and in sub micrometre scales in SIMS.[45,46] The discovery of not only key biomarkers in tissues, but their spatial geometry at sub structural levels has caused a shift in the way that MSI is applied to biomarker discovery. In addition to the advances in spatial characterisation of tissue, the field of untargeted '-omics' has benefitted greatly from the increase in mass resolution permitted by modern instruments. With untargeted analyses, many studies are by default constrained to use untargeted approaches for discovery exclusively;

relying later on targeted approaches to verify findings. Though this is still standard practice, the increased mass resolutions have transformed previously dubious tentative identifications into increasingly substantial discoveries. Recently, the virtues of these advancements have been combined, as increasingly diminishing dwell times in modern instruments has allowed for the routine MS imaging of biological tissues at low spatial resolutions, at mass resolutions of 200,000 fwhm in timeframes typical of standard-resolution imaging instrumentation.[47]

Multimodal approaches have been exhibited in numerous studies in the past few decades.[46,48,49] 'True' multimodal approaches that utilise the same sections as opposed to serial sections share the benefits of other multimodal approaches, for MSI, the ability to gain spatial information about multiple classes of compounds offers a potential to revolutionise the approach to untargeted biomarker discovery within mass spectrometry imaging.

1.7. DESI

Desorption electrospray ionisation (DESI) has become one of the most significant soft ionisation technologies within the field of mass spectrometry imaging (MSI). By employing a fine stream of electrostatically charged droplets onto tissue, the creation of secondary ions occurs within the tissue surface with minimal damage to the tissue.[50-52] DESI is most suited to the analysis of smaller species such as lipids and metabolites, and in the past has been used for the investigation of drug distributions within tissues. Consequently, DESI has provided a significant utility for the investigation of lipidomics and metabolomics, with multiple studies taking advantage of its soft ionisation capabilities.[48,51,53] The soft nature of the ionisation of DESI lends it to use in the early stages of the multimodal approach, allowing

for DESI images to be acquired prior to analysis by more destructive techniques or even histological staining and imaging.

1.8. MALDI

MALDI-MSI has long been a staple of mass spectrometry imaging, and over the past four decades has provided key spatial information about key species within tissue, from small molecules to intact proteins. Amongst the '-omics' possible by MALDI-MSI, peptidomics has also been one of the key branches of MALDI analysis.[54-57] Key to peptidomics is sample preparation and preservation. Often this means that once sectioned, tissues destined for peptidomics by MALDI analysis must be vacuum sealed and stored at -80 °C, or immediately put through washing steps. Additionally, through tryptic digestion, matrix application and analysis, it must be ensured that the tissue remains hydrated. For a true multimodal approach, wherein multiple soft ionisation techniques are combined, the virtues of DESI make direct analysis prior to MALDI sample preparation possible. However, due to the complex requirements for peptidomics, DESI imaging must take place in conditions that support the ongoing hydration of the tissue by exposing the tissue for limited amounts of time within ambient conditions. Alongside a sealed chamber for acquisition, reduced duty cycles, and corresponding increased scan rates, DESI analysis can take place in a relatively short window, immediately prior to MALDI sample preparation. Consequently, there was an opportunity to combine the two approaches, and allow for multiple analytical techniques to be combined in order to gain a rich, multidimensional dataset from the same tissues, in the hope that richer datasets could lead to better conclusions about ocular pathology.

2.0. Methods

2.1. Instrumentation & Parameters

2.1.1. Sample Materials

Mouse tissue was obtained from Department of Clinical Medicine, School of Medicine, Trinity College Dublin. Sectioned mouse tissue was obtained from Department of Clinical Medicine, School of Medicine, Trinity College Dublin, where mice were raised and culled in conditions that adhere to the principles laid out by the internal ethics committee at TCD, and all relevant national licences were obtained before commencement of all studies before being processed & sent to Shefield Hallam University Human samples were obtained from AMSBIO (Abingdon, UK) and Accio Biobank (Newmarket, UK). Trypsin was obtained from Promega (Southampton, UK). Acetonitrile, methanol, ethanol, chloroform. and glacial acetic acid were obtained from Fisher Scientific (Loughborough, UK). α-hydroxycinnamic acid (CHCA), trifluoroacetic acid (TFA), and octyl-α/β-glucoside (Oc/Glc) were obtained from Sigma Aldrich (Gillingham, UK). Xtra adhesive poly-lysine slides were obtained from Leica Biosystems (Newcastle, UK).

2.1.2. Washing

Wash steps were performed on ocular tissue by submerging slides of tissue in 50ml of freshly prepared solvents in starting with 70% EtOH (1min), followed by 90% EtOH (1 min), $CHCl_3$ (30s) and 90:9:1 EtOH:gAcOH:H_2O (1 min)

2.1.3. Enzymatic Digests

First, 20 µg/mL of MS-grade trypsin (Promega, Southampton, UK) was prepared in 50 mM NH4HCO3 with 0.1% octyl-α-β-glucoside applied to the tissue via the use of sequencing grade trypsin. Then, 15 layers of 45 °C trypsin were applied at 10 psi N_2 pressure and at 20 $\mu L min^{-1}$ using an HTX M3+ Sprayer (HTX Imaging, Chapel Hill, NC, USA). Following application, the samples were placed in a

humidity chamber containing 50% methanol before incubation overnight at 37 °C. On removal, the samples were allowed to reach room temperature before matrix application.

2.1.4. Matrix Application

A matrix consisting of 5 $mgmL^{-1}$ α-cyano-hydroxycinnamic acid (CHCA) was prepared in a 50% acetonitrile solution with 0.01% TFA. It was then sonicated and syringe-filtered prior to application using an HTX M3+ (HTX Imaging, Chapel Hill, NC, USA) at 80 °C, using a solvent flow rate of 100 $\mu Lmin^{-1}$ and a N_2 pressure of 10 psi, in 8 layers.

Following matrix application, the samples were either used in MALDI analysis immediately or placed into slide mailers, vacuum sealed and stored at -80 °C for a maximum of 1 week.

2.1.5. MALDI-MSI

For MALDI analysis, a Waters Corporation Multi Reflecting Time-of-Flight (MRT) was used. The instrument was operated in MRT mode, wherein the flight path was over 47 m and the resolution was 200,000 FWHM. The 2 kHz laser was operated at 1 kHz and was attenuated with 2 ND filters. The primary variable filter was applied at a laser intensity of 300 arbitrary units, and the secondary fixed filter was engaged. The laser was rastered over the sample at 125 μms^{-1}, utilizing a 25 µm step size. A quad profile and a set of transfer radiofrequencies was set for optimum transmission of the analytes between 700 and 2500 Da, and the scan rate was set to 0.1 s.

2.1.6. DESI-MSI

For DESI-MSI, a second Waters Corporation MRT was used with a DESI-XS source fitted. The instrument was operated in MRT mode. For analysis, a DESI solvent of 98% methanol was used, with 200 pgμL^{-1} leucine enkephalin (LeuEnk) as an internal standard. DESI images were acquired using a flow rate of 2 μLmin^{-1}, a spot size of 30 μm and a scan time of 0.1 seconds.

2.1.7. Data Handling & Analysis

Data acquisition and processing were conducted using MassLynx version 4.2, HDI version 1.7, (Waters Corporation, Wilmslow, UK) and SCiLS Lab MVS version 2022b Pro (Bruker GmbH, Bremen Germany). For DESI analysis, a continuous lock mass correction (CLMC) was applied, using LeuEnk as an internal standard. Partial least squares (PLS) and principal component analysis (PCA) were conducted with MetaboAnalyst 5.0. *In silico* digests were performed using the PeptideMass tool provided by UniProt and cross-references with the UniProtKB the SwissProt Databases.

3.0. Results and Discussion

3.1. DESI Optimisation

DESI is a relatively new technique, having been proposed by Cooks *et al.* in 2004. Since then there have been numerous advancements in the capabilities of DESI-MSI. Notably the sprayer head used to deposit solvent onto tissue as part of DESI experiments has been greatly improved and the streams of solvent deposited can be controlled with much higher accuracy than previously.[58] Consequently, an investigation into the highest achievable spatial resolution without detriment to signal intensity was conducted using a lipidomic profile of human ocular tissue. Figure 2 shows the different pixel sizes applied to the same ocular tissue in

different regions. The ion images, formed from m/z 782 (PC 36:4) shows how a reduction of solvent flow rate in combination with a decreased scan rate can improve the ability to spatially resolve lipids within tissues. Additionally, the image shows examples of oversampling in lower pixel size images. To increase the spatial resolution achieved, the solvent supply was reduced to a flow rate of 1 $\mu Lmin^{-1}$ and parameters in (Figure 1) were altered. For increased spatial resolution d_1 can be reduced, to a height of 0.5-1mm from the surface of the sample, reducing the diameter of the spray incident on the sample. Figure 2 shows how the acuity of the m/z images can increase with parameters set to decrease spot size. The images also demonstrate the loss of signal achieved from a reduction in flow rate and spot size. This relative reduction is a direct result of decreased ionisation efficiency as the incident solvent has a reduced incident velocity and the surface area per pixel is reduced.

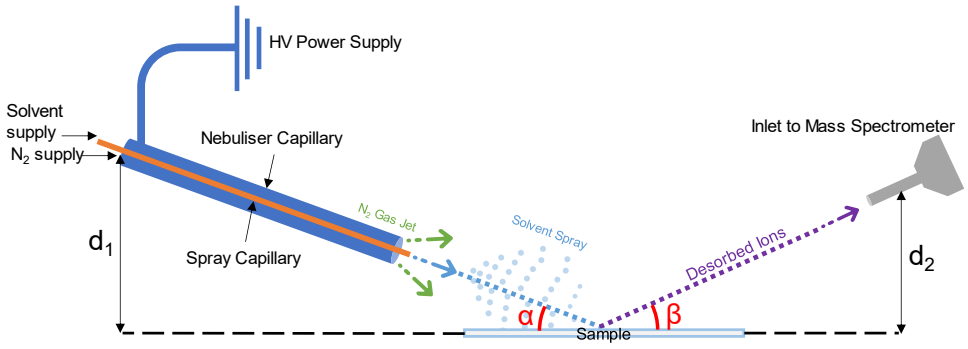

Figure 1 A schematic of a desorption electrospray ionisation source (DESI) and the incident angle of the source (α) the angle of the transfer line (β) the cone height (d_1) and the inlet height (d_2).

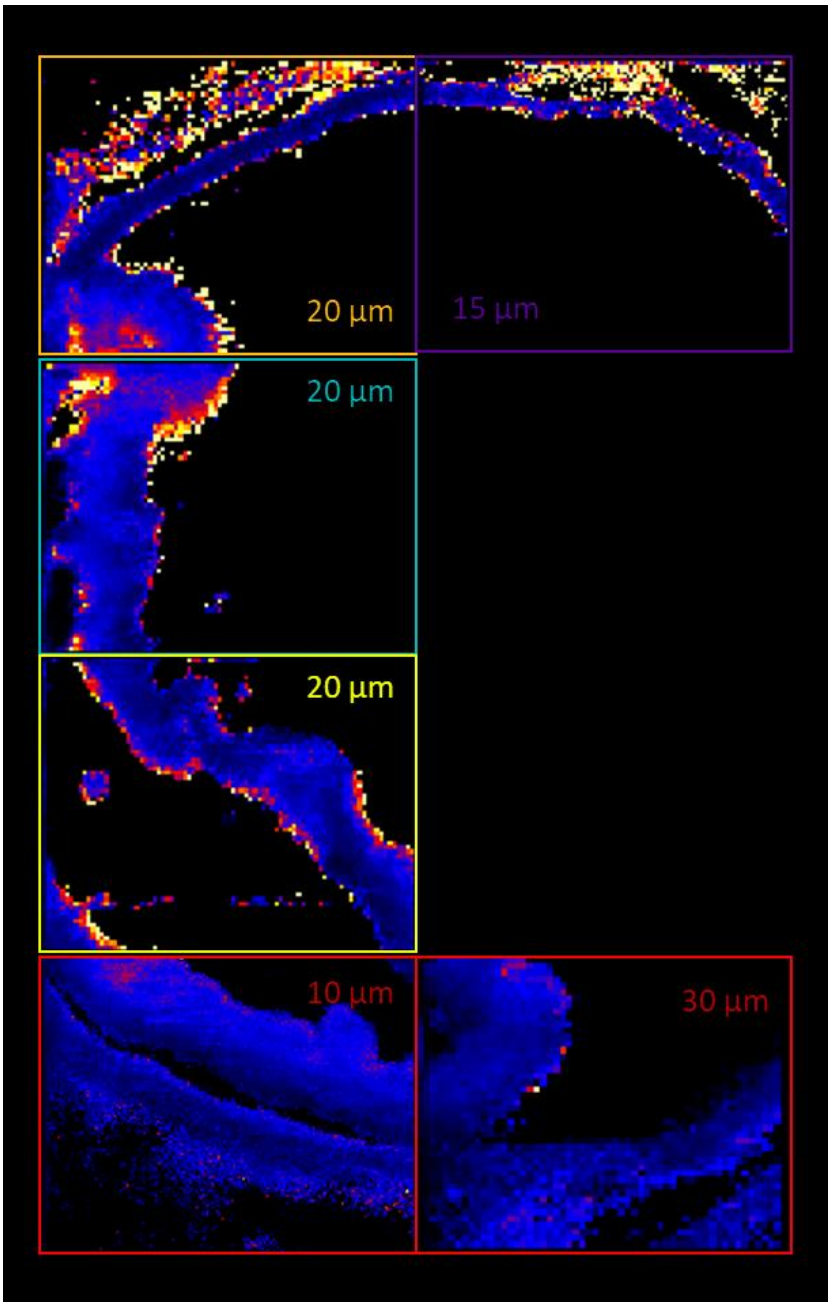

Figure 2 DESI-MSI images of a human ocular tissue, showing the m/z ion 782, normalised to total ion chromatogram acquired at varying pixel sizes, exhibiting the effect of different pixel sizes on the quality of images. Higher levels of detail can be found in the smaller pixel size images, however larger pixel sizes show higher intensities.

3.2. Analysis of WT and transgenic ocular tissues by DESI

In order to assess the capabilities of DESI for future lipid and metabolomic studies with the innate immune system, a study involving three tissue types was devised.

The tissues consisted of a wildtype (WT), and two knockouts which had species relating to the innate immune system deleted; *SARM1*$^{-/-}$ and *TLR2*$^{-/-}$. For each tissue type, 3 animals were utilised, and from each animal, six technical replicates were produced. For maximum transmission of ionised species, and efficiency of data production, a pixel size of 30 µm and a solvent flow rate of 2 µlmin^{-1} was used.

With a total of 54 DESI images acquired, MetaboAnalyst was used to conduct partial least squares (PLS) and principal component analysis (PCA) on the DESI mass spectra of the ocular tissues. In order to refine the statistical model, High Definition Imaging software (HDI v1.7) was used to create regions of interest containing only the ocular tissue, as to remove any signals produced by the surrounding embedding media. In order to ascertain what could be considered 'on-tissue' a pilot study using a Uniform Manifold Approximation and Projection (UMAP) on representative images from each tissue group. The UMAP, performed by MSI Segmentation software (v2.1 Waters Software Labs) allowed the tissue to be distinguished from the embedding media (Figure 3).

Figure 3 A schematic illustrating the process of segmentation performed by the Uniform Manifold Approximation and Projection (UMAP)

Following the export of the ROIs, the images were grouped by tissue type and put through data reduction schemes prior to PLS analysis. The PCA data (Figure 4) showed that the deletion of SARM1 and TLR2 in the tissue provided few differences between the knockouts and the WT. Using PLS to determine differences (Figure 5) the loadings from PC1 and PC2 were used to define m/z values of significance. The data showed the most differences from the WT were exhibited by the *SARM1*$^{-/-}$ tissue types. One example of a high scoring ion was m/z 760.5858, which, when compared to the Human Metabolome Database (HMDB), was tentatively identified as PE-NMe2(20:1(11Z)/15:0) (∆0.920344 ppm). PE-NMe2(20:1(11Z)/15:0) is a phosphatidylethanolamine, which has been speculated to be associated with α-synuclein homeostasis, the disruption of which is responsible for the dysregulation that can lead to amyloid build-up in diseases such Parkinson's disease. [59] As amyloid build-up may play a role in drusen build-up, the detection of phosphatidylethanolamines in ocular tissue could prove useful in future studies. In this particular case there was a perceived heightened concentration of PE-NMe2(20:1(11Z)/15:0) within the *SARM1*$^{-/-}$ tissue type.

Further analysis of the PLS-DA data also saw an increase of another phospholipid within *SARM1*$^{-/-}$ tissues. It was found that PC(20:5(6E,8Z,11Z,14Z,17Z)-OH(5)/P-18:1(9Z)) was found to be heightened in *SARM1*$^{-/-}$ tissues. Whilst this phospholipid is involved in a variety of metabolic processes, one of the most notable characteristics of this species is that it is oxidised. An increased incidence of phospholipids that are in their oxidised state within certain tissue types could indicate that the deletion of a protein, in this case SARM1, is increasing the incidence of oxidative processes. Oxidation and lipid

peroxidation are closely associated with the dysregulation of the innate immune system, and furthermore, the chronic inflammation associated with age-related ocular diseases such as AMD.

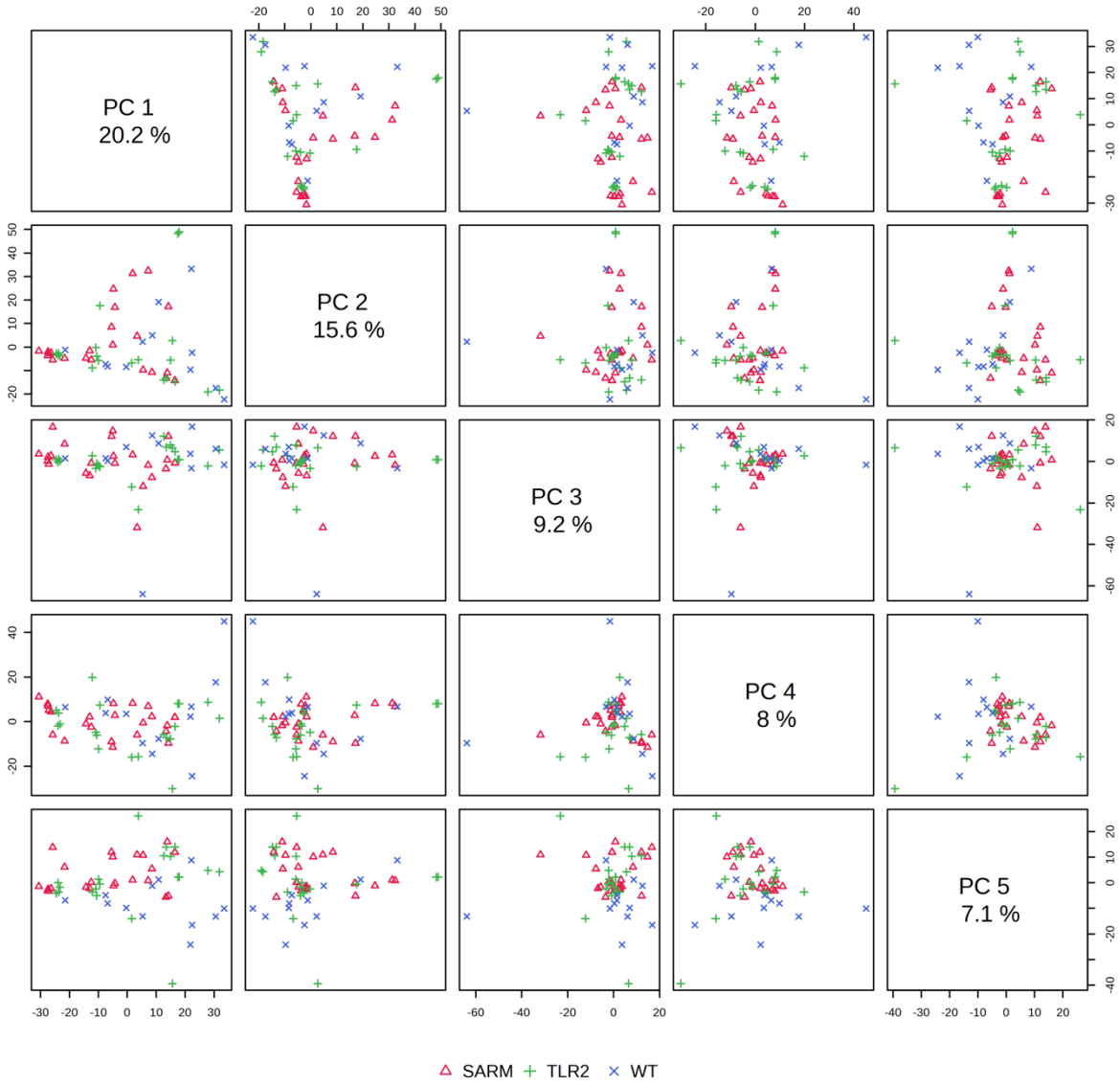

Figure 4 The top five principal components found in an unsupervised principal component analysis (PCA) of WT (blue [x]), SARM1$^{-/-}$ (red [Δ]), and TLR2$^{-/-}$ (green[+])tissue types.

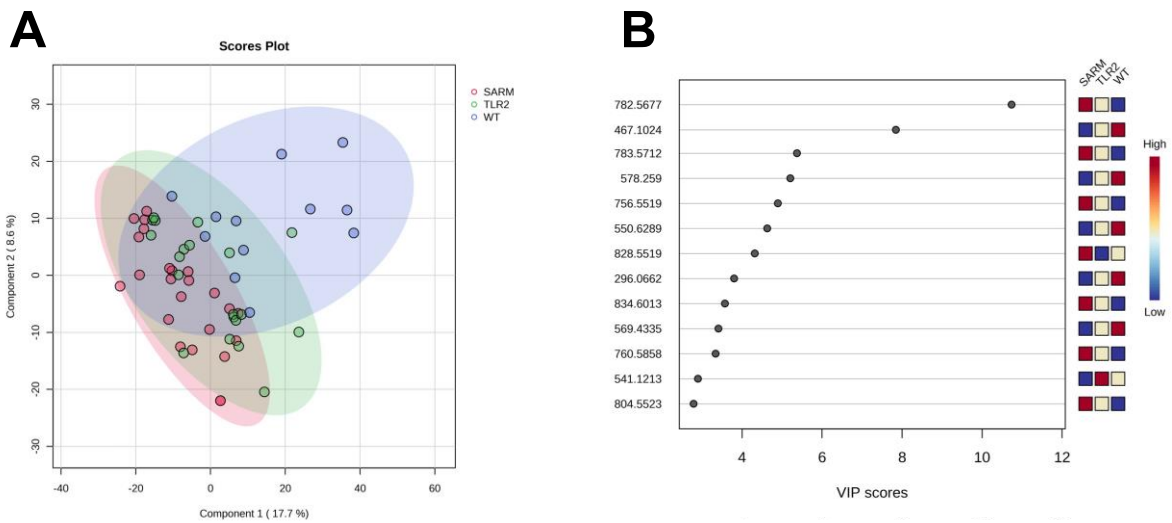

Figure 5 (A) A 2D scores plot created from a partial least squares discriminant analysis (PLS-DA) analysing WT, SARM1$^{-/-}$, and TLR2$^{-/-}$ tissue types (B) the variable importance in projection (VIP) scores of a selection of m/z values identified by PLS-DA, and three-colour scales representing the relative intensities of the ion in each tissue type.

The datasets gathered from the three tissue types exhibit the complexity of ocular tissues. Whilst there is known differences between the tissues, the deletion of singular proteins is minute in comparison to the complexity of the wider ocular anatomy. Consequently, the differences in the tissues, as seen in Figure 5A are relatively small. The observable differences however may hold key data that could help with unravelling the complexities involved in ocular pathology.

3.3. MALDI

The successful analysis of mouse ocular tissue for the detection of key peptides relating to the innate immune system has been previously described. [60] In addition the combination of peptidomics by MALDI imaging and metallomics by LA-ICP-MS has been demonstrated in tandem using the same tissue. With the expense of mouse model tissues and the scarcity of human samples, the ability

to get multiple datasets from singular tissues has always been coveted, with multimodal imaging using MSI and histology being commonplace. With the advancement of soft ionisation techniques such as DESI, the combination of DESI and MALDI is possible. Figure 6 shows the ions observed in a mouse ocular tissue in a DESI-MSI experiment investigating lipidomics, in addition to a MALDI image from the same tissue section investigating peptidomics. With the ability to conduct statistical analysis of large groups of ocular tissue through metabolomics and lipidomics by DESI-MSI, and peptidomics by MALDI-MSI on the same tissue sections, the field of pathology stands to gain the ability to produce multifaceted datasets from single tissue sections. Given the relative stability of the metallomic landscape within ocular tissue, the additional DESI step is unlikely to have detrimental effects to the multimodal MALDI/LA-ICP-MS approach, meaning three dimensions of high-resolution imaging could be achieved from single tissues.

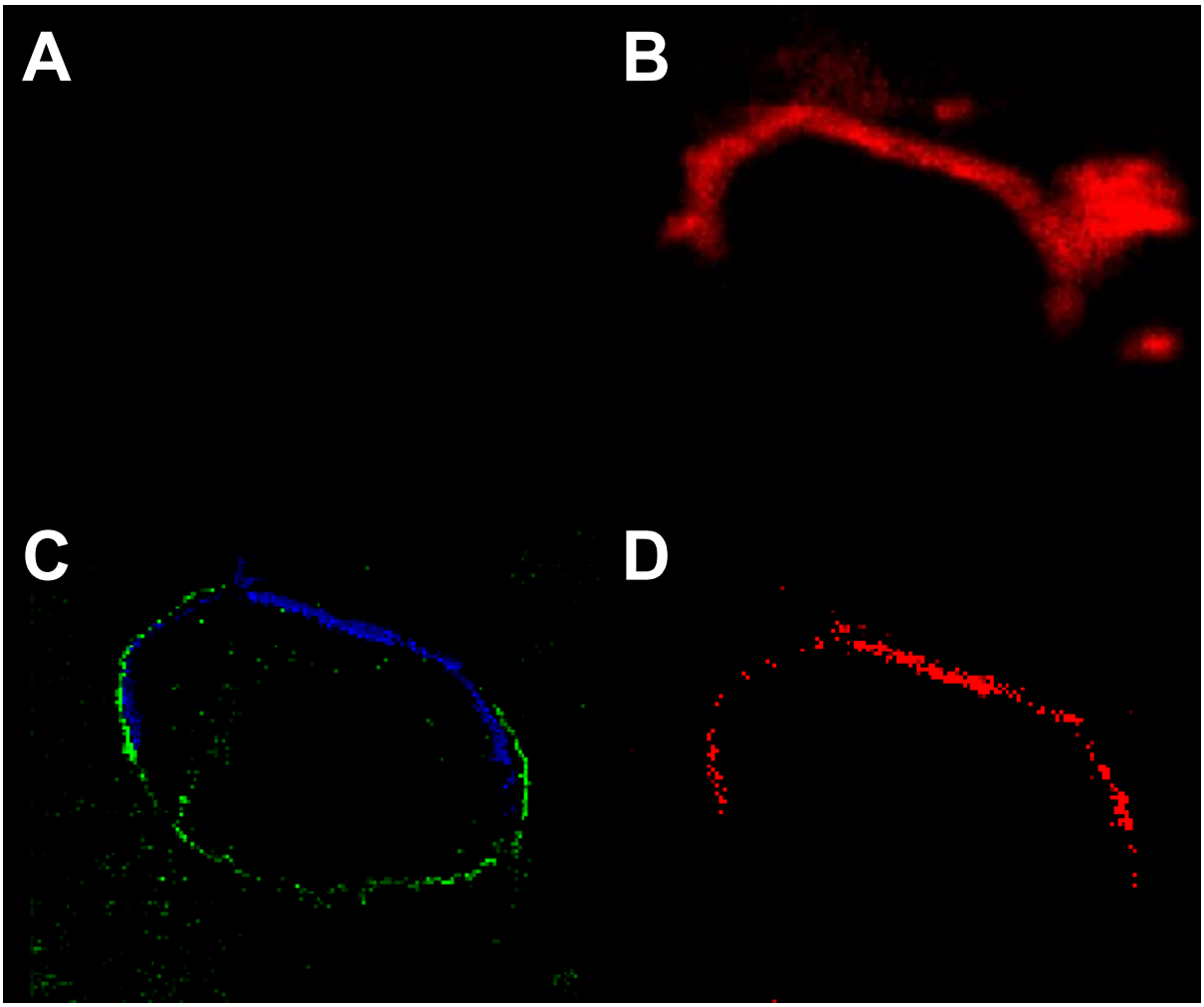

Figure 6 MSI images produced using DESI and MALDI. (A) 30 µm DESI image of an endogenous phosphocoline m/z 782 (PC 36:4) (B) 30 µm DESI image of an endogenous phosphocoline PC(18:1(9Z)-O(12,13)/22:1(13Z)) (C) 25 µm MALDI image of histone (AGLQFPVGR) in blue. (D) 25 µm MALDI image of TLR3 (LDLSSNPLK). All images produced within the figure are from two experiments performed on the same TLR2$^{-/-}$ tissue.

3.4. Preliminary Human Studies

The importance of human tissue for the use in studies has already been greatly accentuated as part of this study. Furthermore, the crucial nature of the presence of NLRP3 within the human retina has been stressed in the literature surrounding

AMD. [29-31,34] This study, whilst limited in its ability to sample from large populations of human tissues, and was limited to healthy tissues, aimed to present some preliminary work with human tissue. Analysis was performed on retinal sections of human tissue that had undergone a tryptic digest, as described above. By utilising a 25 μm spatial resolution, peptides expressed within retinal tissue could be correlated to specific regions of the retinal microanatomy. With the aim to characterise the peptides relating to the proteins within the innate immune system, the MALDI-MRT was tuned to allow transmission of the masses in the range of 700-2500 Da. Through this method, multiple masses within the peptide range were found to localise discretely within the retinal regions of the ocular tissue (Figure 7). Using an in silico digest to compare masses of interest that fit these criteria, one mass, m/z 971.5626, was found to be close to the theoretical value of a peptide from NLRP3 (m/z 971.5632, position 544-552, sequence TNVPGSRLK) this tentative identification, which has a mass error of -0.6 parts per million (ppm) is an extremely close match for the peptide and thereby the mass is likely to be associated with NLRP3. Due to modern advances, high spatial and mass resolution mass spectrometry images can be acquired in timescales previously reserved for acquisitions that prioritise one or the other. As such the tentative identifications found in Figure 8 can be identified within a high mass tolerance and can be distinctly localised to discrete structures within the human retina.

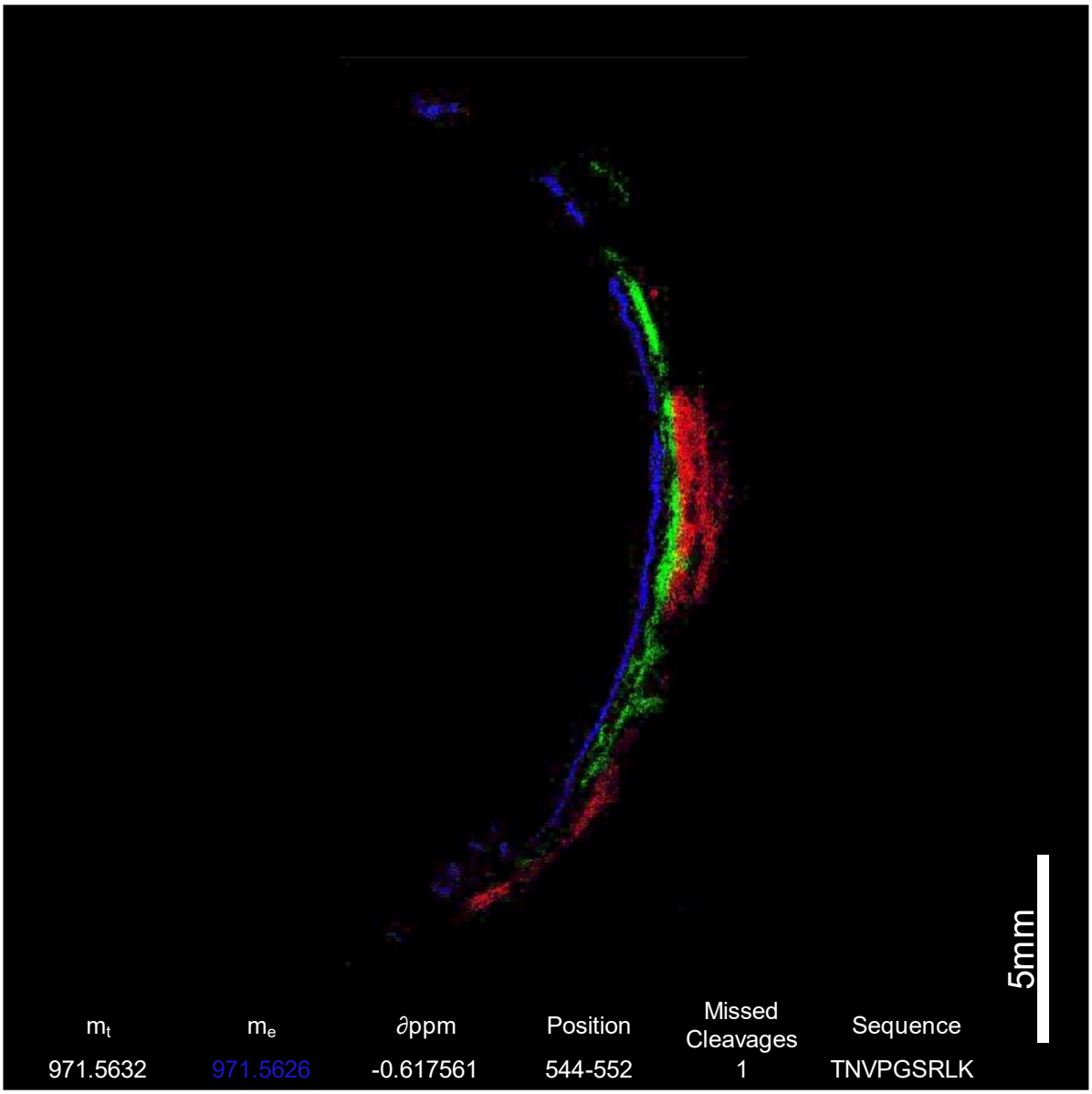

Figure 7 A 25 µm MALDI MS image of a healthy human retina containing NLRP3 (blue) within the retina, as well and two contrasting ions within choroid (green) and the sclera (red)

4.0. Conclusion

The objective of this work was to support the ophthalmologic research into diseases such as age-related macular degeneration in addition to informing on the wider field of ocular disease. The work presented is a compendium of methodologies and workflows that can be utilised in future for the investigation of

ocular tissue.[60,61] Herein these methodologies have been demonstrated, utilising their power to show the rich datasets that can be obtained from ocular tissue. DESI-MSI has been shown as a powerful technique for the analysis of different ocular tissues, with slight changes between different mouse models being observed, such as the increased presence of oxidised species in transgenic tissues. Additionally, the DESI-MSI can be demonstrated to be an incredibly soft analysis technique, allowing MALDI-MSI, a particularly unforgiving technique in terms of sample preparation, to be used in sequence with the analysis successfully, showing the presence of peptides such as histone and tentative identifications of TLR3 proteins within ocular tissue that has been analysed by DESI. MALDI was also able to begin to potentially rectify unresolved disputes within the literature about the presence of NLRP3 within the human retina by exhibiting a tentative identification of an NLRP3 peptide within human tissues.[35] The data herein, whilst significant in its own right, is suited to be held as a foundation for further research into ophthalmology by MSI. The multimodal approach utilised herein may, in future help to answer some of the questions surrounding ocular disease and its intricacies. The ability to use DESI in tandem with MALDI analysis furthers the field's desire to make the field of mass spectrometric '-omics' multimodal and multifaceted.[49,60-63] The ability to obtain multiple datasets from the same tissue may be key in the future for identifying proteins of interest, and indeed the identification of drug targets. In addition, the preliminary work put into human ocular tissue not only provides an insight into the power of ocular MSI, but also may aid in the protection of significant advances in ocular disease pathology from dubiety from the wider research community.

5.0. References

1 P. Elizabeth Rakoczy, M. J. T. Yu, S. Nusinowitz, B. Chang and J. R. Heckenlively, Mouse models of age-related macular degeneration *Experimental eye research,* 2006, **82**, 741–752.

2 M. Güven, B. Batar, T. Mutlu, M. Bostancı, M. Mete, C. Aras and M. Ünal, Toll-Like Receptors 2 and 4 Polymorphisms in Age-Related Macular Degeneration *Curr. Eye Res.,* 2016, **41**, 856–861.

3 K. Kaarniranta and A. Salminen, Age-related macular degeneration: activation of innate immunity system via pattern recognition receptors *J. Mol. Med.,* 2009, **87**, 117–123.

4 H. Guo, J. B. Callaway and J. P. Ting, Inflammasomes: mechanism of action, role in disease and therapeutics *Nature medicine,* 2015, **21**, 677–687.

5 K. L. Rock, E. Latz, F. Ontiveros and H. Kono, The Sterile Inflammatory Response *Annual Review of Immunology,* 2009, **28**, 321–342.

6 A. Kauppinen, J. Paterno, J. Blasiak, A. Salminen and K. Kaarniranta, Inflammation and its role in age-related macular degeneration *Cell Mol. Life Sci.,* 2016, **73**, 1765–1786.

7 S. Doyle, K. Mulfaul, N. Fernando, K. Chirco, E. Connolly, T. Ryan, E. Ozaki, K. Brennan, A. Maminishkis and R. Salomon, TLR2 bridges oxidative damage and complement-associated pathology and is a therapeutic target for age-related macular degeneration *Invest. Ophthalmol. Vis. Sci.,* 2018, **59**, 3475.

8 X. Z. West, N. L. Malinin, A. A. Merkulova, M. Tischenko, B. A. Kerr, E. C. Borden, E. A. Podrez, R. G. Salomon and T. V. Byzova, Oxidative stress induces angiogenesis by activating TLR2 with novel endogenous ligands *Nature (London),* 2010, **467**, 972–976.

9 H. Wu, C. Zhao, Q. Xie, J. Xu and G. Fei, TLR2-Melatonin Feedback Loop Regulates the Activation of NLRP3 Inflammasome in Murine Allergic Airway Inflammation *Frontiers in immunology,* 2020, **11**, 172.

10 B. L. Fiebich, C. R. A. Batista, S. W. Saliba, N. M. Yousif and A. C. P. de Oliveira, Role of Microglia TLRs in Neurodegeneration *Frontiers in cellular neuroscience,* 2018, **12**, 329.

11 K. Mulfaul, E. Ozaki, N. Fernando, K. Brennan, K. R. Chirco, E. Connolly, C. Greene, A. Maminishkis, R. G. Salomon, M. Linetsky, R. Natoli, R. F. Mullins, M. Campbell and S. L. Doyle, Toll-like Receptor 2 Facilitates Oxidative Damage-Induced Retinal Degeneration *Cell reports (Cambridge),* 2020, **30**, 2209–2224.e5.

12 K. Mai, J. J. Chui, N. Di Girolamo, P. J. McCluskey and D. Wakefield, Role of toll-like receptors in human iris pigment epithelial cells and their response to pathogen-associated molecular patterns *Journal of inflammation (London, England),* 2014, **11**, 20.

13 A. Klettner and J. Roider, Retinal Pigment Epithelium Expressed Toll-like Receptors and Their Potential Role in Age-Related Macular Degeneration *International journal of molecular sciences,* 2021, **22**, 8387.

14 K. Dolasia, M. K. Bisht, G. Pradhan, A. Udgata and S. Mukhopadhyay, TLRs/NLRs: Shaping the landscape of host immunity *International reviews of immunology,* 2017, **37**, 3–19.

15 A. C. Shaw, D. R. Goldstein and R. R. Montgomery, Age-dependent dysregulation of innate immunity *Nature reviews. Immunology,* 2013, **13**, 875–887.

16 C. Monaco, S. M. Gregan, T. J. Navin, B. M. J. Foxwell, A. H. Davies and M. Feldmann, Toll-Like Receptor-2 Mediates Inflammation and Matrix Degradation in Human Atherosclerosis *Circulation,* 2009, **120**, 2462–2469.

17 M. K. Vidya, V. G. Kumar, V. Sejian, M. Bagath, G. Krishnan and R. Bhatta, Toll-like receptors: Significance, ligands, signaling pathways, and functions in mammals *International reviews of immunology,* 2017, **37**, 20–36.

18 Y. Zhu, B. Dai, Y. Li and H. Peng, C5a and toll-like receptor 4 crosstalk in retinal pigment epithelial cells *Molecular vision,* 2015, **21**, 1122–1129.

19 K. A. Cavassani, M. Ishii, H. Wen, M. A. Schaller, P. M. Lincoln, N. W. Lukacs, C. M. Hogaboam and S. L. Kunkel, TLR3 is an endogenous sensor of tissue necrosis during acute inflammatory events *The Journal of experimental medicine,* 2008, **205**, 2609–2621.

20 A. O. Edwards, D. Chen, B. L. Fridley, K. M. James, Y. Wu, G. Abecasis, A. Swaroop, M. Othman, K. Branham, S. K. Iyengar, T. A. Sivakumaran, R. Klein, B. E. K. Klein and N. Tosakulwong, Toll-like Receptor Polymorphisms and Age-Related Macular Degeneration *Investigative ophthalmology & visual science,* 2008, **49**, 1652–1659.

21 Y. Cho, J. J. Wang, E. Y. Chew, F. L. Ferris III, P. Mitchell, C. Chan and J. Tuo, Toll-like Receptor Polymorphisms and Age-Related Macular Degeneration: Replication in Three Case-Control Samples *Investigative ophthalmology & visual science,* 2009, **50**, 5614–5618.

22 A. C. Shaw, A. Panda, S. R. Joshi, F. Qian, H. G. Allore and R. R. Montgomery, Dysregulation of human Toll-like receptor function in aging *Ageing research reviews,* 2011, **10**, 346–353.

23 A. L. Kindzelskii, V. M. Elner, S. G. Elner, D. Yang, B. A. Hughes and H. R. Petty, Toll-Like Receptor 4 (TLR4) of Retinal Pigment Epithelial Cells Participates in Transmembrane Signaling in Response to Photoreceptor Outer Segments *The Journal of General Physiology,* 2004, **124**, 139–149.

24 T. Fujimoto, K. Sonoda, K. Hijioka, K. Sato, A. Takeda, E. Hasegawa, Y. Oshima and T. Ishibashi, Choroidal Neovascularization Enhanced by Chlamydia pneumoniae via Toll-like Receptor 2 in the Retinal Pigment Epithelium *Investigative ophthalmology & visual science,* 2010, **51**, 4694–4702.

25 J. Gerdts, E. J. Brace, Y. Sasaki, A. DiAntonio and J. Milbrandt, SARM1 activation triggers axon degeneration locally via NAD+destruction *Science (American Association for the Advancement of Science),* 2015, **348**, 453–457.

26 L. Gibbons, E. Ozaki, C. Greene, A. Trappe, M. Carty, J. A. Coppinger, A. G. Bowie, M. Campbell and S. L. Doyle, SARM1 Promotes Photoreceptor Degeneration in an Oxidative Stress Model of Retinal Degeneration *Frontiers in neuroscience,* 2022, **16**, 852114.

27 E. Ozaki, L. Gibbons, N. G. Neto, P. Kenna, M. Carty, M. Humphries, P. Humphries, M. Campbell, M. Monaghan, A. Bowie and S. L. Doyle, SARM1 deficiency promotes rod and cone photoreceptor cell survival in a model of retinal degeneration *Life science alliance,* 2020, **3**, e201900618.

28 C. Franceschi, P. Garagnani, P. Parini, C. Giuliani and A. Santoro, Inflammaging: a new immune–metabolic viewpoint for age-related diseases *Nature reviews. Endocrinology,* 2018, **14**, 576–590.

29 L. D. Sarah, M. Campbell, E. Ozaki, G. S. Robert, A. Mori, F. K. Paul, J. F. Gwyneth, Anna-sophia Kiang, M. H. Marian, C. L. Ed, A. J. O. Luke, G. H. Joe and P. Humphries, NLRP3 has a protective role in age-related macular degeneration through the induction of IL-18 by drusen components *Nat. Med.,* 2012, **18**, 791–798.

30 W. A. Tseng, T. Thein, K. Kinnunen, K. Lashkari, M. S. Gregory, P. A. D'Amore and B. R. Ksander, NLRP3 Inflammasome Activation in Retinal Pigment Epithelial Cells by Lysosomal Destabilization: Implications for Age-Related Macular Degeneration *Invest. Ophthalmol. Vis. Sci.,* 2013, **54**, 110.

31 V. Tarallo, Y. Hirano, B. Gelfand, S. Dridi, N. Kerur, Y. Kim, W. Cho, H. Kaneko, B. Fowler, S. Bogdanovich, R. C. Albuquerque, W. Hauswirth, V. Chiodo, J. Kugel, J. Goodrich, S. Ponicsan, G. Chaudhuri, M. Murphy, J. Dunaief, B. Ambati, J. Ambati, Y. Ogura, J. Yoo, D. Lee, P. Provost, D. Hinton, G. Núñez, J. Baffi and M. Kleinman, DICER1 Loss and Alu RNA Induce Age-Related Macular Degeneration via the NLRP3 Inflammasome and MyD88 *Cell,* 2012, **149**, 847–859.

32 L. Celkova, S. L. Doyle and M. Campbell, NLRP3 Inflammasome and Pathobiology in AMD *Journal of clinical medicine,* 2015, **4**, 172–192.

33 S. M. Man and T. Kanneganti, Regulation of inflammasome activation *Immunological Reviews,* 2015, **265**, 6–21.

34 Y. Liao, H. Zhang, D. He, Y. Wang, B. Cai, J. Chen, J. Ma, Z. Liu and Y. Wu, Retinal Pigment Epithelium Cell Death Is Associated With NLRP3 Inflammasome Activation by All-trans Retinal *Investigative ophthalmology & visual science,* 2019, **60**, 3034–3045.

35 C. Kosmidou, N. E. Efstathiou, M. V. Hoang, S. Notomi, E. K. Konstantinou, M. Hirano, K. Takahashi, D. E. Maidana, P. Tsoka, L. Young, E. S. Gragoudas, T. W. Olsen, Y. Morizane, J. W. Miller and D. G. Vavvas, Issues with the Specificity of Immunological Reagents for NLRP3: Implications for Age-related Macular Degeneration *Scientific reports,* 2018, **8**, 461–12.

36 S. Volland, J. Esteve-Rudd, J. Hoo, C. Yee and D. S. Williams, A comparison of some organizational characteristics of the mouse central retina and the human macula *PloS one,* 2015, **10**, e0125631.

37 P. D. Kiser, M. Golczak and K. Palczewski, Chemistry of the Retinoid (Visual) Cycle *Chemical Reviews,* 2014, **114**, 194–232.

38 L. Harkema, S. A. Youssef and A. de Bruin, Pathology of Mouse Models of Accelerated Aging *Veterinary pathology,* 2016, **53**, 366–389.

39 D. F. Kiernan, S. M. Hariprasad, I. M. Rusu, S. V. Mehta, W. F. Mieler and R. D. Jager, EPIDEMIOLOGY OF THE ASSOCIATION BETWEEN

ANTICOAGULANTS AND INTRAOCULAR HEMORRHAGE IN PATIENTS WITH NEOVASCULAR AGE-RELATED MACULAR DEGENERATION *Retina (Philadelphia, Pa.),* 2010, **30**, 1573–1578.

40 J. Mitchell and C. Bradley, Quality of life in age-related macular degeneration: a review of the literature *Health and Quality of Life Outcomes,* 2006, **4**, 97.

41 V. M. L. Cohen, M. J. Carter, A. Kemeny, M. Radatz and I. G. Rennie, Metastasis-free survival following treatment for uveal melanoma with either stereotactic radiosurgery or enucleation *Acta ophthalmologica Scandinavica,* 2003, **81**, 383–388.

42 M. Bracher, B. C. Madi-Segwagwe, E. Winstanley, H. Gillan and T. Long-Sutehall, Family refusal of eye tissue donation from potential solid organ donors: a retrospective analysis of summary and free-text data from the UK National Health Service Blood and Transplant Services (NHS-BT) National Referral Centre (1 April 2014 to 31 March 2017) *BMJ Open,* 2021, **11**, e045250.

43 J. Yang, J. L. Norris and R. Caprioli, Novel vacuum stable ketone-based matrices for high spatial resolution MALDI imaging mass spectrometry *Journal of mass spectrometry.,* 2018, **53**, 1005–1012.

44 M. Kompauer, S. Heiles and B. Spengler, Atmospheric pressure MALDI mass spectrometry imaging of tissues and cells at 1.4-μm lateral resolution *Nature methods,* 2017, **14**, 90–96.

45 S. Ma, Y. Leng, X. Li, Y. Meng, Z. Yin and W. Hang, High spatial resolution mass spectrometry imaging for spatial metabolomics: Advances, challenges, and

future perspectives *TrAC, Trends in analytical chemistry (Regular ed.),* 2023, **159**, 116902.

46 M. Angelo, S. C. Bendall, R. Finck, M. B. Hale, C. Hitzman, A. D. Borowsky, R. M. Levenson, J. B. Lowe, S. D. Liu, S. Zhao, Y. Natkunam and G. P. Nolan, Multiplexed ion beam imaging of human breast tumors *Nature medicine,* 2014, **20**, 436–442.

47 D. A. Cooper-Shepherd, J. Wildgoose, B. Kozlov, W. J. Johnson, R. Tyldesley-Worster, M. E. Palmer, J. B. Hoyes, M. McCullagh, E. Jones, R. Tonge, E. Marsden-Edwards, P. Nixon, A. Verenchikov and J. I. Langridge, Novel Hybrid Quadrupole-Multireflecting Time-of-Flight Mass Spectrometry System *Journal of the American Society for Mass Spectrometry,* 2023, **34**, 264–272.

48 L. E. Flint, G. Hamm, J. D. Ready, S. Ling, C. J. Duckett, N. A. Cross, L. M. Cole, D. P. Smith, R. J. A. Goodwin and M. R. Clench, Characterization of an Aggregated Three-Dimensional Cell Culture Model by Multimodal Mass Spectrometry Imaging *Analytical chemistry (Washington),* 2020, **92**, 12538–12547.

49 K. J. Zemaitis, A. M. Izydorczak, A. C. Thompson and T. D. Wood, Streamlined Multimodal DESI and MALDI Mass Spectrometry Imaging on a Singular Dual-Source FT-ICR Mass Spectrometer *Metabolites,* 2021, **11**, 253.

50 H. Awad, M. M. Khamis and A. El-Aneed, Mass Spectrometry, Review of the Basics: Ionization *Applied spectroscopy reviews,* 2015, **50**, 158–175.

51 Takáts Takáts, W. Wiseman, G. Gologan and C. Cooks, Mass Spectrometry Sampling Under Ambient Conditions with Desorption Electrospray Ionization *Science,* 2004, **306**, 471–473.

52 A. T. Jackson, J. P. Williams and J. H. Scrivens, Desorption electrospray ionisation mass spectrometry and tandem mass spectrometry of low molecular weight synthetic polymers *Rapid communications in mass spectrometry,* 2006, **20**, 2717–2727.

53 Z. Miao and H. Chen, Direct Analysis of Liquid Samples by Desorption Electrospray Ionization-Mass Spectrometry (DESI-MS) *J Am Soc Mass Spectrom,* 2009, **20**, 10–19.

54 M. R. Groseclose, M. Andersson, W. M. Hardesty and R. M. Caprioli, Identification of proteins directly from tissue: in situ tryptic digestions coupled with imaging mass spectrometry *Journal of mass spectrometry.,* 2007, **42**, 254–262.

55 P. Zhang, D. Kirby, C. Dufresne, Y. Chen, R. Turner, S. Ferri, D. P. Edward, J. E. Eyk and R. D. Semba, Defining the proteome of human iris, ciliary body, retinal pigment epithelium, and choroid *Proteomics (Weinheim),* 2016, **16**, 1146–1153.

56 P. M. Angel, K. Norris-Caneda and R. R. Drake, In Situ Imaging of Tryptic Peptides by MALDI Imaging Mass Spectrometry Using Fresh-Frozen or Formalin-Fixed, Paraffin-Embedded Tissue *Current Protocols in Protein Science,* 2018, **94**, e65–n/a.

57 C. Keller, P. Wei, B. Wancewicz, T. L. Cross, F. E. Rey and L. Li, Extraction optimization for combined metabolomics, peptidomics, and proteomics analysis of gut microbiota samples *Journal of mass spectrometry.,* 2021, **56**, e4625–n/a.

58 E. Claude, M. Towers and E. Jones, in *Imaging Mass Spectrometry*, ed. L. M. Cole, Springer US, New York, NY, 2023, p. 41–54.

59 E. Calzada, O. Onguka and S. M. Claypool, Phosphatidylethanolamine Metabolism in Health and Disease *International Review of Cell and Molecular Biology,* 2016, **321**, 29–88.

60 J. Millar, E. Ozaki, S. Campbell, C. Duckett, S. Doyle and L. M. Cole, Multiomic Mass Spectrometry Imaging to Advance Future Pathological Understanding of Ocular Disease *Metabolites,* 2022, **12**, 1239.

61 J. Millar, L. Gibbons, C. Costa, E. Schneider, J. von Gerichten, M. J. Bailey, S. Campbell, C. Duckett, S. Doyle and L. M. Cole, Multimodal Imaging of Metals in a Retinal Degeneration Model to Inform on Ocular Disease *Analytica,* 2023, **4**, 264–279.

62 L. M. Cole, J. Handley, E. Claude, C. J. Duckett, H. S. Mudhar, K. Sisley and M. R. Clench, Multi-Modal Mass Spectrometric Imaging of Uveal Melanoma *Metabolites,* 2021, **11**, 560.

63 B. Heijs, S. Holst, I. H. Briaire-de Bruijn, G. W. van Pelt, A. H. de Ru, P. A. van Veelen, R. R. Drake, A. S. Mehta, W. E. Mesker, R. A. Tollenaar, J. V. M. G. Bovée, M. Wuhrer and L. A. McDonnell, Multimodal Mass Spectrometry Imaging of N-Glycans and Proteins from the Same Tissue Section *Analytical chemistry (Washington),* 2016, **88**, 7745–7753.

Chapter 6

Discussion

Discussion

1.0. Background

Investigations into ocular pathology are long established within the research community, however it has only been in the past decade or so where investigations from the Doyle lab group, at Trinity College Dublin have highlighted some of the fundamental proteins and pathways involved in the pathology of AMD, namely the innate immune system and its associated proteins. More recently, mass spectrometry (MS) at Sheffield Hallam University has been used in the pursuit of clarity around ocular pathology, utilising matrix assisted laser desorption ionisation and inductively coupled plasma mass spectrometry imaging (MSI). In addition to multimodal MSI investigations into uveal melanoma, collaborations with Trinity College Dublin have been fruitful in the investigations of AMD.[1-3]

2.0. Innate immunity and inflammation in AMD

Doyle *et al.* had pioneered new research into AMD, linking inflammation to ocular pathology, providing evidence to support innate immune proteins involvement in ocular pathology. In 2020, Ozaki *et al.* provided evidence to support that SARM1 deficiency could promote photoreceptor cell survival.

Doyle *et al.* had pioneered research into the innate immune system in relation to AMD, showing clear links to immune dysregulation and

symptoms similar to that of AMD.[4-9] Studies however reached a critical stage when a study by Doyle *et al.* highlighted the importance of NLRP3 in initiating an inflammatory response to drusen components, providing a protective role in AMD.[4] This paper built on previous research linking the inflammasome to AMD, and helped build a case for the involvement of NLRP3 in AMD pathology, however the major share of the work was called into question in a paper by Kosmidou *et al.*[10] In the study, Kosmidou *et al.* drew attention to the fact that the work by Doyle *et al*. conflicted with that of Tarallo *et al.*, who had suggested that it was NLRP3 deletion that had a protective role in AMD.[10-12] Furthermore, Kosmidou postulated that the results found in each of the studies may have been misguided, and that the contradictory results were in fact the direct result of insufficient reagent specificity in the experimental design, even postulating that NLRP3 may not even be expressed in the human retina.[10] This perceived discrepancy in the literature laid the path for the introduction of a validatory method to be used in conjunction with immunological methods, providing scope for the necessity of analytical techniques such as those used in this body of work to be used in ocular research.

3.0. Elemental analysis

Separately, metals have been identified as being of major importance in ocular pathology. For example in AMD, it is thought that the exposure to non-essential elements such as cadmium and lead are responsible for the increased incidences of AMD in smokers.[13-18] From 1992 to 2001, the National Eye Institute, part of the National Institute for Health (NIH),

funded the Age-Related Eye disease study (AREDS). AREDS highlighted the importance of essential metals in the homeostasis of ocular tissue, and how any disruption of this could lead to issues in later life, recommending supplementation of zinc to help prevent AMD.[13,19,20] In addition, the pathways highlighted by Doyle *et al.* are intrinsically linked to the inflammatory pathway, and it is of note that reactive oxygen species are cleared in a manner dependent on zinc and copper containing superoxide dismutase, and that a zinc deficiency caused immune dysregulation and the production of pro-inflammatory species in aged mouse models.[21,22]

Imaging of metals has been an ever-evolving field, with LA-ICP-MSI emerging as a relatively accessible and high-resolution imaging technique.[23] Imaging of the ocular metallome has been demonstrated in the past, studying the spatial distribution of various elements in the context of ocular disease, and furthermore there have been successful quantitative studies of the ocular metallome in the context of AMD.[21,24-27] Quantitative imaging however has been less accessible, with techniques such as micro particle induced X-ray emission (μPIXE) holding the best quantitative abilities, and fewer strategies being employed by laser ablation inductively coupled plasma mass spectrometry (LA-ICP-MS).[21,24-30]

4.0. Approaches to AMD Pathology

The literature surrounding AMD, and the methods used to study it had highlighted that there had been significant advances made in the field,

however there was still scope for further investigations into AMD pathology. Furthermore, advances in mass spectrometry imaging, and other related techniques provided adequate scope to improve upon existing investigations into the characterisations of ocular tissue. The existing work into AMD had been limited, and spatial resolution of the proteomic, lipidomic and metabolomic species relating to AMD was even more uncommon. [31-36] The metallomic studies into ocular disease have, however, been much more established. There have been examples of quantitative studies into essential and non-essential elements within ocular tissue in the context of ocular disease, as well as spatial characterisations of metal species within the ocular metallome. There have, however, been few studies that combine the quantitative studies with spatially resolved ones, and even fewer that utilise a multimodal approach.

This study however was able to demonstrate the power of high-resolution quantitative imaging of metals in biological tissue and was able to demonstrate the utility of such techniques to the unique field of ocular pathology. In addition, the multidisciplinary approach utilised here allowed a novel, multimodal dataset to be obtained from ocular tissue that helped to marry multiple techniques and demonstrate how future work could use the same multimodal approach to further understanding of ocular disease.

5.0. Initial Optimisation

The first study in this body of work (Millar *et al.*, Chapter 2) focused on the preliminary steps in developing a method for the analysis of peptides relating to proteins within the innate immune system and related pathways by MALDI-MSI, and the development of a quantitative methodology for the mass spectrometry imaging of metals within ocular tissue, (using LA-ICP-MSI to be performed in sequence with the MALDI analysis). Porcine ocular tissue, and mouse ocular tissue were used as material to test the viability of the MALDI-MSI methodology for the analysis of tryptic peptides relating to the pathology of AMD. The study aimed not only to detect the species, but to provide spatial data to correlate the proteomics to regions within the ocular anatomy. Consequently, a sequence of strategies was devised from existing imaging methodologies to ensure that spatial peptidomics was possible within the ocular tissue. The steps within the methodology, which included the removal of salts and lipids, the on-tissue digestion and the application of matrix were employed to enhance the peptide signals available from the tissue. With microstructures within ocular anatomy in divisions smaller than 20 µm, the conservation of the localisation of the analytes was crucial to the success of the experiment.

As such, each step within the methodology had to ensure minimal disruption of the species of interest within the tissue. Wash steps, inspired by works including that of Angel *et al.* Norris *et al.* and Chughtai *et al.*[37-39] were used to remove interfering ions from the tissues, were developed, and saw significant reductions in the presence of

phosphocholine lipid species, and through the removal of species that could cause analytes suppression. Additionally, the inclusion of a reagent to promote protonation, and prevent tissue drying to improve tryptic digestion. A wash method was devised that saw significantly higher detection of tryptic peptides within the ocular tissue. The target proteins of this study were often membrane-bound, making them notoriously difficult to access by enzymes.[40] However, it has been widely reported that the inclusion of detergents can improve the efficacy of a tryptic digest by helping to mobilise species within the tissue, whilst still allowing the conservation of the spatial distribution of the analytes.[41,42]

As a result, multiple surfactants were trialled to determine their efficacy for tryptic digestion in MALDI-MSI. The use of OcGlc, a commercially available surfactant saw a significant increase in the intensity of peptides within MALDI images. The OcGlc not only provided an increase in sensitivity for a peptide from histone, but also increased the observed intensity of TLR peptides. In addition to surfactants as enzyme additives, the use of an additive was trialled within the MALDI matrix itself, as the use of basic compounds such as aniline can improve sensitivity and selectivity of methods through the suppression of background peaks.[43] The study highlighted the importance of some of the intricacies of sample preparation prior to MSI experiments. MSI often involves special considerations for sample preparation over solution or profiling based experiments, and the detection of tryptic peptides can be especially challenging, particularly when the proteins of interest are less accessible. As there are limited studies utilising MS to study PRRs, and to date no

publications referencing the detection of peptides from PRRs by MALDI-MSI, it was crucial to optimise a MALDI imaging workflow in the context of PRR peptides within ocular tissue for the success of this study. The optimisation conducted aided the ability for the detection and spatial characterisation of peptides related to the innate immune system.

Whilst the study showed that the use of surfactants such as octyl-α-β-glucoside were seen to improve detection of peptides, a more targeted approach for the membrane bound species could have been taken. Use of more potent reagents for the mobilisation of inaccessible species have been trialled in the past, notably with similarly membrane bound species.[34] 1,1,1,3,3,3-hexafluoropropanol (HFIP) is a strong solvent, that in relatively small quantities can aid the solubilisation of membrane bound protein such as TLR4. In the past, HFIP has been used in the solubilisation of proteins to improve peptide signal from membrane bound proteins. In addition, the use of HFIP for the solubilisation of the membrane bound aquaporin AQP0 in ocular tissue has been successful.[44-46] In solution, the use of OcGlc, as utilised in this study (Millar *et al.* Chapters 2,3,5) was shown to give clean, good quality spectra, allowing the target protein and its peptides to be observed. When HFIP was employed by Redeby *et al,* however, there was an increase in sensitivity by 10-fold.[44-46] The use of experimental organic solvents within the literature could have further benfitted this study. The use of detergents has been widely reported in MALDI-MSI and its ability to help the mobilisation of species without extreme instances of delocalisation. HFIP, and other organic solvents are less well characterised for the use

in MSI experiments but nonetheless introduce a potential avenue to explore in relation to sample preparation for unique classes of proteins, that has been left unexplored within this study.

In addition, the use of aniline, a compound that helps form an ionic liquid matrix when added to CHCA, that helps to suppress interference from CHCA adducts, was explored as part of the matrix preparation procedure in this study (Millar *et al.*, Chapter 2). The use of aniline proved to be a useful addition to the study, with no distinguishable reduction of image quality, the aniline additive managed to greatly reduce the observed intensity of CHCA adduct ions. The use of matrix additives is common, with many utilising organic acidic compounds such as TFA, as in this study, or use of formic acid to promote protonation. There is however a subdivision of literature surrounding MALDI matrices that encourages the use of a multitude of matrix combinations and matrix additives, in addition to the use of different solvent compositions, and matrix application techniques in pursuit of improved detection of different analytes when using MALDI. Further experiments in future exploring more combinations of matrices and solvent compositions may be a viable option to improve further the work herein.

6.0. Optimisation of a multimodal workflow

As a further nuance of MALDI sample preparation, the use of a robotic sprayer has been widely reported for the successful application of both enzyme and matrix for improved conservation of analyte localisation. In this work, the use of a HTX Imaging (Chapel Hill NC, USA) M3+ sprayer

was used as a benchmark on which to build a suitable methodology (Millar *et al.*, Chapter 3). This study benefited greatly from the advancements in technology that have taken place in MALDI imaging sample preparation and taking advantage of the unique capabilities of commercial robotic sprayers such as the M3+, the work explored the use of high flow rates of matrix to improve the co-crystallisation of analytes by allowing the dissolution of the analyte on the tissue surface. This perceived improvement of analyte co-crystallisation has been made possible by a combination of high application temperatures and a volatile organic matrix solvent, which allows the spatial localisation of the species in the microstructures of the tissues, to be conserved, whilst improving analyte detection. In the past, use of sublimation apparatus, airbrushes, and acoustic multi-spotters have been used in a similar way to deposit matrix without mobilising the species in the tissue, however the relatively dry application methods cannot produce similar efficacies when it comes to analyte dissolution.

With advancements in technology, there is room within the space of MALDI-MSI sample preparation to push the boundaries of the sample preparation procedures, and in future, it could be beneficial for a further exploration of the use of different matrices and matrix solvents in order to achieve analyte sensitivity and spatial resolution that would have previously been unachievable. Within the scope of this study, significant steps have been made to improve the efficacy of the described protocols, however there may be room for further development into a highly targeted

sample preparation strategy for MALDI-MSI of peptides relating to ocular disease.

As discussed, the conservation of the 2D arrangement of analytes within biological tissue is crucial for the success of an MSI experiment, but the labelled ‘success’ of a methodology is defined by other factors. Work at the start of this project (Millar *et al.* Chapter 2) was performed using the MALDI source on a Waters Corporation (Wilmslow, UK) SYNAPT G2-HDMS, which had a theoretical laser spot size of 45 µm and was operated at a spot and pixel size of 50 µm. However, the latter part of this project used a Waters Corporation Multi Reflecting Time-of-Flight (MRT) instrument, fitted with a µMALDI source, with a theoretical spot size as low as 15 µm.[47] Therefore, previously successful methodologies for sample preparation that were once considered viable for the conservation of spatial resolution could be considered inadequate. When operating the µMALDI source, this study (Millar *et al.* Chapters 3 and 5) utilised a spot size larger than the minimum spot size of 15 µm, and instead used a spot size of 25 µm. Using these parameters, in combination with the optimised HTX M3+ trypsin and matrix application, high spatial resolution images of key species relating to AMD and ocular disease such as SARM1 and NLRP3 were observed within ocular tissue and were used to divide the retinal anatomy into up to 3 distinct regions.

However, in ocular tissue, the microstructures within the tissue are confined within 10-20 µm layers (Millar *et al.* Chapter 4; Figure 1), and there is at least 7 distinguishable layers within the mouse retina at this

resolution. Therefore, by utilising a higher spatial resolution, and a smaller pixel size, further subdivisions of the ocular anatomy could be made as part of a MALDI-MSI experiment. For this study the chosen spot size of 25 µm was elected as a compromise, allowing for improved sensitivity given the diminished abundance of the target analytes.

The relatively increased spot size not only afforded larger tolerances within sample preparation, allowing for high flow rate matrix application, but also improved sensitivity within the MALDI source, as larger spot sizes have been shown to improve ion yield.[48] There are examples of investigations into ocular tissue that have achieved much higher spatial resolutions, though the studies in question often target more abundant species, such as lipids and metabolites, that are compatible with high-resolution matrix application techniques such as sublimation.[31,32,49] The work presented herein (Millar *et al.* Chapters 3,5) represents some of the highest spatial resolution peptide imaging ongoing within ocular research using MALDI-MSI, nonetheless, it is possible that in the in future there is room for the application of a higher resolution MALDI-MSI methodology to be applied to peptidomics within ocular tissue.

In addition to high spatial resolution, the change of instrument to the MRT allowed for routine analysis to be conducted at a mass resolution of ≥200,000 FWHM, as opposed to the mass resolution of 40,000 FWHM offered by the SYNAPT G2-HDMS. High mass resolution analysis is routinely conducted within the field of MALDI-MS, and more recently, combinations of the MassTech (Columbia, MD, USA) AP-MALDI source

and high mass resolution instruments such as the ThermoFisher (Waltham, MA, USA) Exploris 480 have achieved mass resolutions of 240,000 FWHM in MALDI imaging experiments. However, due to instrument constraints, scan times of up to 200 ms were necessary to achieve the mass resolutions within an imaging experiment, prolonging the overall experiment time, making some high mass resolution imaging experiments untenable. [50] With the launch of the MRT, which can perform MALDI imaging at a scan rate of 100 ms, there has been a shift that has encouraged high spatial and high mass resolution imaging. This study (Millar *et al.* Chapters 3,5) has demonstrated the ability for MALDI in the acquisition of peptide imaging data from ocular tissues using the minimum scan time allowed by the instrumentation, demonstrating that high mass resolution and high spatial resolution MALDI imaging experiments can be conducted in a timely manner. These advances in the configuration of imaging instrumentation, and experiments such as those described herein (Millar *et al.* Chapters 3,5) should aid the shift within the field of MALDI mass spectrometry imaging into a space wherein high mass and high spatial resolution images are more common.

Despite the targeted nature of the sample preparation for the MALDI experiments, the MS experiments described in Millar *et al.* Chapters 2,3,5 were inherently untargeted approaches to bottom-up proteomics. This approach allowed for the exploration of the wider proteome, whilst using targeted data analysis to extract information about key proteins and processes from the experimental data. Whilst these experiments can cause issues such as high data volumes and issues with interferences,

some of the experiments described (Millar *et al.* Chapter 3) provided an insight into possibilities surrounding future work into ocular pathology. A MALDI experiment using a tryptic digest on ocular tissue (Millar *et al.* Chapter 3) was able to detect the instance of copper chaperone for superoxide dismutase (CCS) within retinal tissue. Though the detection of this species may seem insignificant, the work detailed here (Millar *et al.* Chapters 3,4), and in the wider literature imply that there is significant importance that can be attributed to the antioxidant processes and wider homeostatic roles of essential metals such as zinc and copper within ocular pathology.[13,21,22,51]

Detection of species such as CCS (Millar *et al.* Chapters 3) was not an intended result of the work herein, but it introduces a compelling argument for the construction of an imaging strategy that could combine the work exhibited within the literature, and the studies within Millar *et al.* Chapters 3,4 relating to zinc and copper distribution within the healthy and diseased eye, and the works investigating the role of the inflammatory pathways and the wider innate immune system (Millar *et al.* Chapters 2,3,5). There has been a distinct interest in the role of copper/zinc superoxide dismutase (SOD1) in the anti-inflammatory processes that may be dysregulated as a result of, or as the root of age-related macular degeneration. Developments in metal imaging have shown (Millar *et al.* Chapters 2,3) that the spatial characterization and quantification of metal species can be achieved at high spatial resolutions and at relatively low limits of detection. Crucial however to the utility of these data is the form in which the essential elements are inhabiting. If

for example, there is an increase in zinc concentration within the diseased eye, the utility of that information is entirely dependent on that zinc accumulating as free zinc, or as part of a complex. For example, if there is an elevated presence of zinc in its antioxidant form as a complex with SOD1 within the diseased eye, it could be perceived as a response to the inflammation, which may in turn help or hinder the diseased state of the tissue. However, if the elevated levels of zinc were in fact a direct result of accumulation of free zinc, there is a high chance that the zinc would exacerbate the diseased state, as 'free' or loosely bound metal ions are known to exert toxic effects in biology.[52] The detection of metal complexes as part of an imaging experiment however can prove to be difficult, as few imaging ionisation techniques can preserve the non-covalent interactions once the species enter the gas phase.

Two strategies have been used to date to conduct native mass spectrometry imaging, liquid extraction surface analysis (LESA), which can give a spatial resolution of 400 - 1000µm, and nano desorption electrospray ionisation (nano-DESI) which has been demonstrated at a spatial resolution of as low as 10µm. However, it is nano-DESI that in 2022 demonstrated the imaging of a protein-metal complex by MSI at a spatial resolution of 200 µm.[53] This technology alone has the potential to revolutionise the mapping of the non-covalent interactions of protein-metal complexes, however, in combination with the metal imaging capabilities demonstrated within this body of work (Millar *et al.* Chapters 2,4), there is a real potential to fuel a new field of research within ocular pathology.

7.0. Investigation of Essential Elements

The metallomic aspect of this work was rooted in the developments in ocular research previously conducted at Sheffield Hallam University, and its multimodal investigations into uveal melanoma, and the high-resolution approach used for the analysis of cell aggregates.[1,54] The metallomic research conducted at SHU has utilised a LA-ICP-MS platform, and has historically used a New Wave Research (Bozeman MT, USA) 193 nm laser ablation unit coupled to a Perkin Elmer (Seer Green, UK) NexION 350X ICP-MS. This work was not an exception, however benefitted from not only an updated laser ablation system; the Elemental Scientific Lasers (Bozeman MT, USA) ImageBio266 laser ablation system, but also the use of an ion beam analysis (IBA) centre at the National Ion Beam Centre (NIBC) at the University of Surrey (UoS).

Metal species have long been of interest within pathology, and more specifically within ocular pathology, however due to the complexity and heterogeneity of ocular tissue, little research has been conducted that was able to distinguish the elemental characteristics of different anatomical substructures of ocular tissue. In addition, few studies have adequately compared tissue types by LA-ICP-MSI.

Laser ablation ICP-MSI is an extremely robust and relatively inexpensive technique for the analysis of metals.[55] Due to sensitivity issues, the spatial resolution achievable by LA-ICP-MSI in recent years has been

poorer, but as demonstrated in Millar *et al.* Chapter 1, there have been significant developments in the resolution and sensitivity achievable by modern LA-ICP-MS instruments. The ImageBio266 is an LA unit designed specifically for the creation of metal images from biological tissue. The 266nm laser benefits the analysis of biological tissue by allowing the user to operate with little concern of ablating the glass beneath the biological tissue. [56] In addition, it also benefits from a square spot size, helping to avoid further artefacts from the experiment. In addition, the analyte plume is created and extracted in a fast moving He atmosphere allowing for good sensitivity even at small spot sizes. [57]

The study set out to create a semi-quantitative strategy for the quantitative analysis of elements within healthy and transgenic ocular tissue to further the understanding of the elemental changes that occur as a result of retinal degeneration. The aim of the studies undertaken was to determine the viability of the analysis of metals of interest. In the literature, essential elements such as selenium[58-60], phosphorus[27,61], iron[27,52,62-68], copper[13,20,52,62,67,69-72] and zinc[13,20,21,24,51,52,62,69-71,73-80] have all been highlighted as having key importance for age-related macular degeneration and ocular disease. The ICP-MS system at SHU is a single quadrupole NexION 350X. As a single quadrupole system, there are certain isotopes of trace elements that are extremely difficult to detect (Table 1). Selenium is one of the hardest to detect, as with a mass of 80 amu, has an interfering peak with the dimer of argon ($^{40}Ar_2^+$). This is problematic, as argon (^{40}Ar) is used to supply the source of the ICP-MS and can become ionised and detected alongside selenium. Additionally,

as a single quadrupole mass analyser is only capable of selecting single m/z per mass scan, it is unable to distinguish between the two species. Using a single quadrupole, there are however strategies that can be used to help mitigate background noise created by interfering polyatomic species. The NexION 350X however can utilise kinetic energy discriminatory (KED) mode in which incident gas helps to filter polyatomic interferences though probability of collision. In this study, (Millar *et al*. Chapter 2) the utility of KED mode for the effective detection of iron. The experiment showed a 5,000-fold reduction in noise levels, and the apparent detection of ^{56}Fe where previously undetectable. There was however, a significant reduction in overall signal, with an almost 100-fold reduction in the signal of copper from tissues when using the KED gas. This loss of signal is a result of the lack of specificity permitted by KED mode, which relies on the principle that larger, polyatomic species are more likely to be inhibited by an incident gas due to their higher collisional cross section.

Due to already low levels of elements that were crucial to this study such as copper and zinc, further studies within this project did not utilise the KED technology for problematic elements. This reduction in sensitivity is one of the issues associated with the non-specificity of strategies such as KED, and whilst KED was one of the most important steps for the avoidance of spectral interferences for ICP-MS systems, the introduction of reaction cells that utilised reaction gases scope that ICP-MS can attain.[81] Reaction cells have the ability to selectively react to either the analyte or the interference. This reaction gas, typically ammonia, oxygen

or hydrogen is able to alter the mass to charge ratio of the analyte by changing the charge state or the mass of the polyatomic molecule. Whilst more targeted than a collision gas within KED strategy, reaction gases can cause side reactions, and more interferences can be produced within the reaction cell. For this reason, the introduction of triple quadrupole ICP-MS systems has revolutionised the capabilities of ICP source. By selection of single m/z values in in the first quadrupole (Q1) the reaction in the collision cell (Q2) can be made exclusively with ions of a certain m/z value, and likewise, Q3 can be used to select for a specific m/z for detection.

The use of multiple quadrupoles for the selection of elements can be useful when dealing with particularly problematic species such as iron or calcium, however even with the resolving power afforded by modern ICP-MS instruments, there is still a need for reaction gases. The use of reaction gases can introduce multiple issues, notwithstanding the need to wait for the gases to enter and exit the collision cell. This extra period of time extends the dwell time, which can be detrimental when conducting imaging experiments, and in addition can be problematic when used in conjunction with transient signals such as those given by LA units. As a consequence, there may be some use for a triple quad ICP in conjunction with the LA-ICP system, especially in analysing regions of interest, but imaging experiments may not be viable.

Focusing on the key elements identified in the literature, a strategy for the quantitative imaging of copper and zinc was conceived (Millar *et al.*

Chapter 3). This strategy, based on hydrogels, was designed to allow the comparison of elemental concentrations within ocular tissue, and was applied in a study that compared wildtype (WT) and transgenic mouse ocular tissue (Millar *et al.* Chapter 4). Sagittal sections of the ocular tissue were used to characterise the concentration and distribution of copper and zinc in the retinal microanatomy, as well as the lens, cornea, and ciliary bodies of the eye. To model the changes that occur within a diseased state, the same experiments were conducted on WT and rhodopsin knockout (*rho*$^{-/-}$) tissues, which exhibit a lack of rods, and subsequent degradation of the retinal substructures. Utilising the quantitative strategy developed in Millar *et al.* Chapter 3, the loss of these substructures was visualised, and by using semi-quantitative techniques, the concentration of copper and zinc was characterised. The experiment was able to show a high spatial resolution characterisation of the effects of a diseased state on the metals within ocular tissue, Additionally, by utilising region of interest (ROI) analysis, the concentrations of individual substructures of the retina could be interrogated in a semi-quantitative manner. Though the results yielded showed little change in concentrations when looking at the same substructure between samples, the methodology had proven its utility for the characterisation of metals within ocular tissue. By applying this method to different disease models within mice, or indeed to study the diseased state in human samples, more information surrounding the metallomics of ocular disease could be ascertained.

By exclusively analysing the elements readily detectable by a single quad ICP-MS the study could have been perceived as insular. Through collaboration with the University of Surrey, and the United Kingdom National Ion beam Centre (UKNIBC), some of the work completed herein was conducted using ion beam analysis (IBA), and specifically the use of micro-particle induced X-ray emission (μPIXE). Despite remaining relatively unchanged for a number of years, PIXE remains an extremely powerful technique, but the complexity, footprint, and the need for expertise to conduct PIXE analysis, PIXE remains relatively inaccessible.

As a result, few studies can benefit from the wide capabilities offered by PIXE. With spatial resolutions as low as 1μm, and the ability to image all elements between ^{24}Mg and ^{238}U without the effects of polyatomic interferences, PIXE could be an essential tool for the study of ocular disease. The studies herein (Millar *et al.* Chapter 3) utilised the power afforded by PIXE to analyse wildtype and transgenic ocular tissue, and the metallomic changes that occurred in *rho*$^{-/-}$. By using PIXE, in addition to copper and zinc, which were analysed by LA-ICP-MSI; phosphorous, sulphur, chlorine, potassium, calcium, iron, and aluminium zinc and copper were able to be characterised within WT and *rho*$^{-/-}$ ocular tissue. Data from the PIXE was able to show that the metals not characterised by ICP; phosphorous, sulphur, chlorine, potassium, calcium, iron, and aluminium, were in fact similarly localised within the ocular tissue to that of copper and zinc observed by LA-ICP-MS.

Table 1 A table of isotopes, and their corresponding polyatomic interferences, observed when analysing them by ICP-MS. The full list has been compiled by by May et al. *the elements listed here are those which are considered relevant to this study, and the isotopes listed are the most abundant.*

Isotope	Interference	Ref
^{111}Cd	$^{95}Mo^{16}O^{+}$,$^{94}Zr^{16}O^{1}H^{+}$, $^{39}K_{2}{}^{16}O_{2}{}^{1}H^{+}$	82
^{112}Cd	$^{40}Ca_{2}{}^{16}O_{2}$, $^{40}Ar_{2}{}^{16}O_{2}$, $^{96}Ru^{16}O^{+}$	
^{27}Al	$^{12}C^{15}N^{+}$, $^{13}C^{14}N^{+}$, $^{14}N_{2}$ spread, $^{1}H^{12}C^{14}N^{+}$	
^{31}P	$^{14}N^{16}O^{1}H^{+}$, $^{15}N^{15}N^{1}H^{+}$, $^{15}N^{16}O^{+}$, $^{14}N^{17}O^{+}$, $^{13}C^{18}O^{+}$, $^{12}C^{18}O^{1}H^{+}$	
^{32}S	$^{16}O2^{+}$, $^{14}N^{18}O^{+}$, $^{15}N^{17}O^{+}$, $^{14}N^{17}O^{1}H^{+}$, $^{15}N^{16}O^{1}H^{+}$, $^{32}S^{+}$	
^{35}Cl	$^{16}O^{18}O^{1}H^{+}$, $^{34}S^{1}H^{+}$, $^{35}Cl^{+}$	
^{39}K	$^{38}Ar^{1}H^{+}$	
^{40}Ca	$^{40}Ar^{+}$	
^{56}Fe	$^{40}Ar^{16}O^{+}$, $^{40}Ca^{16}O^{+}$, $^{40}Ar^{15}N^{1}H^{+}$, $^{38}Ar^{18}O^{+}$, $^{38}Ar^{17}O^{1}H^{+}$, $^{37}Cl^{18}O^{1}H^{+}$	
^{57}Fe	$^{40}Ar^{16}O^{1}H^{+}$, $^{40}Ca^{16}O^{1}H^{+}$, $^{40}Ar^{17}O^{+}$, $^{38}Ar^{18}O^{1}H^{+}$, $^{38}Ar^{19}F^{+}$	
^{63}Cu	$^{31}P^{16}O2$ +, $^{40}Ar^{23}Na$+, $^{47}Ti^{16}O$+, $^{23}Na^{40}Ca$+, $^{46}Ca^{16}O^{1}H^{+}$, $^{36}Ar^{12}C^{14}N^{1}H^{+}$, $^{14}N^{12}C^{37}Cl^{+}$, $^{16}O^{12}C^{35}Cl^{+}$	
^{66}Zn	$^{50}Ti^{16}O^{+}$, $^{34}S^{16}O_{2}{}^{+}$, $^{33}S^{16}O_{2}$ $^{1}H^{+}$, $^{32}S^{16}O^{18}O^{+}$, $^{32}S^{17}O_{2}{}^{+}$, $^{33}S^{16}O^{17}O^{+}$, $^{32}S^{34}S^{+}$, $^{33}S_{2}{}^{+}$	
^{80}Se	$^{40}Ar_{2}{}^{+}$, $^{32}S^{16}O_{3}$ $^{+}$	

Neither methodology was able to show downstream effects on metal concentration from the deletion of rhodopsin, however both were able to exhibit the discreet layers in which essential elements are localised in the highly structured retinal layers, and how that changed in the *rho*$^{-/-}$ tissue. The µPIXE was not only able to characterise the distribution of these elements but was able to provide quantitative data without the need for matrix matched standards. This ability to image and quantify elements without any further sample preparation or calibrant optimisation, and the relatively indiscriminate number of elements available for analysis is a demonstration of the power of µPIXE and IBA techniques. The concentrations observed of zinc and copper by ICP-MS however were not validated due to their low abundance being below the limit of quantification by µPIXE, which remains one of the most substantial drawbacks of PIXE when comparing it to LA-ICP-MS.

Nevertheless, the combination of these two complementary techniques is an exemplary demonstration of how a multimodal workflow can provide powerful datasets, in future, the use of the LA-ICP-MSI quantifications and imaging strategy, used in conjunction with IBA could prove to be a formidable suite of technology in the efforts to inform on ocular pathology. Future work using diseased mouse tissues, larger cohorts, or even human healthy and diseased tissue could be crucial for the further understanding of metallomic based ocular pathology.

8.0. Further Development of a multimodal workflow

With the apparent significance assigned to the function, and dysregulation of the innate immune system, and the benefits of multimodal workflow, an experiment combining the two concepts was conceived, and executed (Millar *et al.* Chapter 4). Using the MALDI imaging protocol outlined in Millar *et al.* Chapters 2-3, proposed proteomic data would be obtained from ocular tissue that had been genetically modified to lack innate immune proteins; *SARM1*$^{-/-}$, and *TLR2*$^{-/-}$. It had already been demonstrated that the use of LA-ICP-MSI immediately following MALDI analysis was demonstrable. In order to add further dimensions to the dataset, and further utilise the ocular tissue as a valuable resource, a further imaging technique was added to the workflow. DESI-MSI, as described previously (Millar *et al.* Chapter 1) was an ideal candidate for the use within the workflow. With the extremely 'soft' nature of DESI, the imaging could be undertaken prior to MALDI analysis, obtain information about the lipids & metabolites prior to the wash step as part of the MALDI sample preparation.

The results from DESI showed that the differences between WT, *SARM1*$^{-/-}$, and *TLR2*$^{-/-}$ tissue were relatively minimal, with low scores within statistical analysis. The analysis did however show some analytes of interest differing in some of the tissues. Key to demonstrating the success of the proposed workflow however was the successful subsequent MALDI imaging that took place. The work (Millar *et al.* Chapter 4) was able to demonstrate the successful imaging of peptides within the ocular

tissue from a sample that had been used in a DESI-MSI analysis previous to the sample preparation step.

With multiomic capabilities such as those demonstrated here becoming ever more prevalent, there are lipidomic and peptidomic studies that have demonstrated the utility of multiomic workflows that combine two facets of data.[83-85] With the developed imaging workflows herein, there is adequate scope for lipidomic, peptidomics, and metallomic data to be combined to produce intensely rich datasets from single tissues. With the right experimental design, and use of diseased tissue, or mouse models similar to those used in this study, multiple exploratory studies could be undertaken to inform on ocular pathology in a potentially revolutionary way. The ability to see the lipidomic, peptidomic, and metallomic changes that occur in a disease state could provide context to the changes that are observed in diseases such as age-related macular degeneration.

Key to the success of such a study however would be a unique combination of data reduction schemes, as though rich datasets can be informative, without the proper processing, the results can be meaningless. With the growth and evolution of machine learning, and in combination with pathway identification software, sense could be made from complex ocular -omic data produced from the proposed workflow.

9.0. Final Conclusion

The work presented as part of this PhD aimed to develop and apply a multimodal and multiomic imaging workflow (Figure 1) to inform on the

pathology of age-related macular degeneration and aid the pursuit to understand ocular physiology and pathology. Within this work, DESI-MSI, MALDI-MSI, LA-ICP-MSI, and µPIXE have been employed to work towards this goal. The study has shown that imaging of ocular tissue can be extremely informative, and that the new high spatial resolutions achieved by modern imaging techniques has a unique ability to co-register species of interest to the ocular anatomy. The detection of peptides related to the innate immune system and wider AMD pathology could aid in the understanding of how age-related macular degeneration can affect the proteomic landscape of ocular tissue. This study showed how these peptides could be monitored spatially. There has also been demonstrated a shift in the capabilities of modern techniques in the workflow created whereby three analytical techniques can be used in sequence to get three different datasets. The MALDI imaging work done in this work has shown that high resolution peptidomics can be a useful asset in the arsenal of a pathological investigation, and that with future developments, more meaningful conclusions can be drawn from observations within the ocular proteome. Work from Trinity College Dublin has been verified by the work done as part of this study (Millar *et al.* Chapter 4) and further insight into the effects of innate immune proteins within ocular tissue has been explored.

In addition, the metallomic investigations have initiated extremely high spatial resolution quantitative imaging workflows that stand to provide greater detail and context to the decades of research into the ocular metallome. Many studies have attempted to characterise the ocular

metallome, though few have attempted quantitative spatial characterisations of metals in ocular disease. The methods developed as part of this study, when applied to a retinal degeneration model were able to exhibit the intracacies and details of the ocular metallome, and demonstrate the utility of metal imaging for ocular pathology. Through experiments that yield results such as those found here, incremental steps can be made in the effort to identify biomarkers and pursue therapeutic targets within the field of ocular pathology.

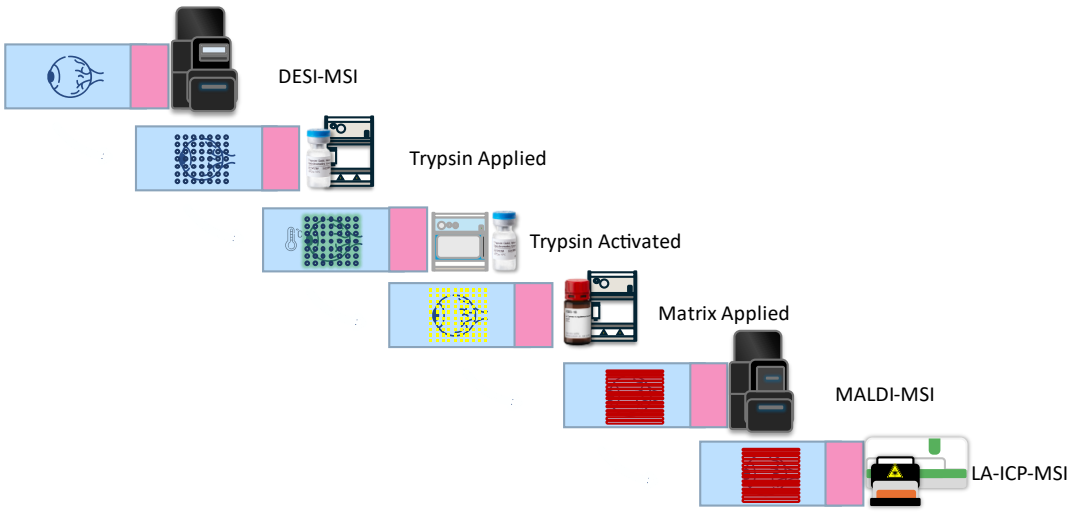

Figure 1 Multimodal workflow proposed for obtaining multiomic data from single tissues using multimodal imaging platform

Though the work presented here as part of this project has been an insightful exploration into the application of mass spectrometry imaging with ocular tissue, there is still a need for further use of mass spectrometry imaging within ocular pathology. Multiomics in ocular pathology remains in its infancy, yet the combination of techniques within a multimodal workflow can not only optimise the quantity and quality of datasets obtained from single tissues but can provide unique insights into

the cross-talk between otherwise discrete field of pathology. In addition, with the insights into the ocular metallome and proteome, there is potential for MSI to inform on new therapeutic targets, as well as in the development of new therapies.

The work presented as part of this PhD is an extensive investigation into the powerful suite of analytical techniques available to biosciences, and how when employed in an informed and collaborative manner can benefit fields of research, in this case the field of ocular pathology. The research demonstrated here is a highly novel approach to ocular pathology investigations and as such it may be beneficial should studies like the work described here be used as a foundation for further novel research in ocular pathology.

10.0. References

1 L. M. Cole, J. Handley, E. Claude, C. J. Duckett, H. S. Mudhar, K. Sisley and M. R. Clench, Multi-Modal Mass Spectrometric Imaging of Uveal Melanoma *Metabolites,* 2021, **11**, 560.

2 J. Millar, E. Ozaki, S. Campbell, C. Duckett, S. Doyle and L. M. Cole, Multiomic Mass Spectrometry Imaging to Advance Future Pathological Understanding of Ocular Disease *Metabolites,* 2022, **12**, 1239.

3 J. Millar, L. Gibbons, C. Costa, E. Schneider, J. von Gerichten, M. J. Bailey, S. Campbell, C. Duckett, S. Doyle and L. M. Cole, Multimodal Imaging of Metals in a Retinal Degeneration Model to Inform on Ocular Disease *Analytica,* 2023, **4**, 264-279.

4 L. D. Sarah, M. Campbell, E. Ozaki, G. S. Robert, A. Mori, F. K. Paul, J. F. Gwyneth, Anna-sophia Kiang, M. H. Marian, C. L. Ed, A. J. O. Luke, G. H. Joe and P. Humphries, NLRP3 has a protective role in age-related macular degeneration through the induction of IL-18 by drusen components *Nat. Med.,* 2012, **18**, 791-798.

5 L. Celkova, S. L. Doyle and M. Campbell, NLRP3 Inflammasome and Pathobiology in AMD *Journal of clinical medicine,* 2015, **4**, 172-192.

6 S. Doyle, K. Mulfaul, N. Fernando, K. Chirco, E. Connolly, T. Ryan, E. Ozaki, K. Brennan, A. Maminishkis and R. Salomon, TLR2 bridges oxidative damage and complement-associated pathology and is a therapeutic target for age-related macular degeneration *Invest. Ophthalmol. Vis. Sci.,* 2018, **59**, 3475.

7 K. Mulfaul, E. Ozaki, N. Fernando, K. Brennan, K. R. Chirco, E. Connolly, C. Greene, A. Maminishkis, R. G. Salomon, M. Linetsky, R. Natoli, R. F. Mullins, M. Campbell and S. L. Doyle, Toll-like Receptor 2 Facilitates Oxidative Damage-Induced Retinal Degeneration *Cell reports (Cambridge),* 2020, **30**, 2209-2224.e5.

8 E. Ozaki, L. Gibbons, N. G. Neto, P. Kenna, M. Carty, M. Humphries, P. Humphries, M. Campbell, M. Monaghan, A. Bowie and S. L. Doyle, SARM1 deficiency promotes rod and cone photoreceptor cell survival in a model of retinal degeneration *Life science alliance,* 2020, **3**, e201900618.

9 L. Gibbons, E. Ozaki, C. Greene, A. Trappe, M. Carty, J. A. Coppinger, A. G. Bowie, M. Campbell and S. L. Doyle, SARM1 Promotes Photoreceptor

Degeneration in an Oxidative Stress Model of Retinal Degeneration *Frontiers in neuroscience,* 2022, **16**, 852114.

10 C. Kosmidou, N. E. Efstathiou, M. V. Hoang, S. Notomi, E. K. Konstantinou, M. Hirano, K. Takahashi, D. E. Maidana, P. Tsoka, L. Young, E. S. Gragoudas, T. W. Olsen, Y. Morizane, J. W. Miller and D. G. Vavvas, Issues with the Specificity of Immunological Reagents for NLRP3: Implications for Age-related Macular Degeneration *Scientific reports,* 2018, **8**, 461-12.

11 V. Tarallo, Y. Hirano, B. Gelfand, S. Dridi, N. Kerur, Y. Kim, W. Cho, H. Kaneko, B. Fowler, S. Bogdanovich, R. C. Albuquerque, W. Hauswirth, V. Chiodo, J. Kugel, J. Goodrich, S. Ponicsan, G. Chaudhuri, M. Murphy, J. Dunaief, B. Ambati, J. Ambati, Y. Ogura, J. Yoo, D. Lee, P. Provost, D. Hinton, G. Núñez, J. Baffi and M. Kleinman, DICER1 Loss and Alu RNA Induce Age-Related Macular Degeneration via the NLRP3 Inflammasome and MyD88 *Cell,* 2012, **149**, 847-859.

12 L. D. Sarah, M. Campbell, E. Ozaki, G. S. Robert, A. Mori, F. K. Paul, J. F. Gwyneth, Anna-sophia Kiang, M. H. Marian, C. L. Ed, A. J. O. Luke, G. H. Joe and P. Humphries, NLRP3 has a protective role in age-related macular degeneration through the induction of IL-18 by drusen components *Nat. Med.,* 2012, **18**, 791-798.

13 A Randomized, Placebo-Controlled, Clinical Trial of High-Dose Supplementation With Vitamins C and E, Beta Carotene, and Zinc for Age-Related Macular Degeneration and Vision Loss: AREDS Report No. 8 *Arch. Ophthalmol.,* 2001, **119**, 1417-1436.

14 A. Repić, P. Bulat, B. Antonijević, M. Antunović, J. Džudović, A. Buha and Z. Bulat, The influence of smoking habits on cadmium and lead blood levels in the Serbian adult people *Environmental science and pollution research international,* 2020, **27**, 751-760.

15 J. THORNTON, R. EDWARDS, P. MITCHELL, R. A. HARRISON, I. BUCHAN and S. P. KELLY, Smoking and age-related macular degeneration: a review of association *Eye (London),* 2005, **19**, 935-944.

16 C. Rubio Armendáriz, T. Garcia, A. Soler, Á J. Gutiérrez Fernández, D. Glez-Weller, G. Luis González, A. H. de la Torre and C. Revert Gironés, Heavy metals in cigarettes for sale in Spain *Environmental research,* 2015, **143**, 162-169.

17 E. W. Wu, D. A. Schaumberg and S. K. Park, Environmental cadmium and lead exposures and age-related macular degeneration in U.S. adults: The National Health and Nutrition Examination Survey 2005 to 2008 *Environmental research,* 2014, **133**, 178-184.

18 E. Damar Güngör, F. Yülek, U. Serkant, Y. Toklu, A. Hocaoğlu and Ş Şimsek, Blood lead and cadmium in age related macular degeneration in a Turkish urban population *Journal of trace elements in medicine and biology,* 2018, **48**, 16-19.

19 Age-Related Eye Disease Study Research Group, *A randomized, placebo-controlled, clinical trial of high-dose supplementation with vitamins C and E, beta carotene, and zinc for age-related macular degeneration and vision loss: AREDS report no. 8*, 119, United States, 2001.

20 The Age-Related Eye Disease Study Research Group, The effect of five-year zinc supplementation on serum zinc, serum cholesterol and hematocrit in persons randomly assigned to treatment group in the age-related eye disease study: AREDS Report No. 7 *The Journal of nutrition,* 2002, **132**, 697-702.

21 C. P. Wong, N. A. Rinaldi and E. Ho, Zinc deficiency enhanced inflammatory response by increasing immune cell activation and inducing IL6 promoter demethylation *Molecular Nutrition & Food Research,* 2015, **59**, 991-999.

22 D. A. Newsome, M. V. Miceli, D. J. Tate, N. W. Alcock and P. D. Oliver, Zinc content of human retinal pigment epithelium decreases with age and macular degeneration, but superoxide dismutase activity increases *The journal of trace elements in experimental medicine,* 1996, **8**, 193-199.

23 C. A. Heinrich, T. Pettke, W. E. Halter, M. Aigner-Torres, A. Audétat, D. Günther, B. Hattendorf, D. Bleiner, M. Guillong and I. Horn, Quantitative multi-element analysis of minerals, fluid and melt inclusions by laser-ablation inductively-coupled-plasma mass-spectrometry *Geochimica et cosmochimica acta,* 2003, **67**, 3473-3497.

24 S. Rodríguez-Menéndez, B. Fernández, M. García, L. Álvarez, M. Luisa Fernández, A. Sanz-Medel, M. Coca-Prados, R. Pereiro and H. González-Iglesias, Quantitative study of zinc and metallothioneins in the human retina and RPE cells by mass spectrometry-based methodologies *Talanta,* 2018, **178**, 222-230.

25 T. N. Abduljabbar, B. L. Sharp, H. J. Reid, N. Barzegar-Befroeid, T. Peto and I. Lengyel, Determination of Zn, Cu and Fe in human patients' serum using micro-sampling ICP-MS and sample dilution *Talanta (Oxford),* 2019, **204**, 663-669.

26 M. Šala, V. S. Šelih and J. T. van Elteren, Gelatin gels as multi-element calibration standards in LA-ICP-MS bioimaging: fabrication of homogeneous standards and microhomogeneity testing *Analyst (London),* 2017, **142**, 3356-3359.

27 R. Pamphlett, S. Cherepanoff, L. K. Too, S. Kum Jew, P. A. Doble and D. P. Bishop, The distribution of toxic metals in the human retina and optic nerve head: Implications for age-related macular degeneration *PloS one,* 2020, **15**, e0241054.

28 C. Jeynes, M. J. Bailey, N. J. Bright, M. E. Christopher, G. W. Grime, B. N. Jones, V. V. Palitsin and R. P. Webb, “Total IBA” – Where are we?*Nuclear instruments & methods in physics research. Section B, Beam interactions with materials and atoms,* 2012, **271**, 107-118.

29 C. J. Greenhalgh, E. Karekla, G. J. Miles, I. R. Powley, C. Costa, J. de Jesus, M. J. Bailey, C. Pritchard, M. MacFarlane, J. H. Pringle and A. J. Managh, Exploration of Matrix Effects in Laser Ablation Inductively Coupled Plasma Mass Spectrometry Imaging of Cisplatin-Treated Tumors *Analytical chemistry (Washington),* 2020, **92**, 9847-9855.

30 G. W. Grime, O. B. Zeldin, M. E. Snell, E. D. Lowe, J. F. Hunt, G. T. Montelione, L. Tong, E. H. Snell and E. F. Garman, High-Throughput PIXE as

an Essential Quantitative Assay for Accurate Metalloprotein Structural Analysis: Development and Application *Journal of the American Chemical Society,* 2020, **142**, 185-197.

31 D. Anderson, Z. Ablonczy, Y. Koutalos, J. Spraggins, R. Crouch, R. Caprioli and K. Schey, High Resolution MALDI Imaging Mass Spectrometry of Retinal Tissue Lipids *J. Am. Soc. Mass Spectrom,* 2014, **25**, 1394-1403.

32 D. M. G. Anderson, W. Lambert, D. J. Calkins, Z. Ablonczy, R. K. Crouch, R. M. Caprioli and K. L. Schey, Imaging MS of Rodent Ocular Tissues and the Optic Nerve *Methods in molecular biology (Clifton, N.J.),* 2017, **1618**, 15-27.

33 H. E. Bowrey, D. M. Anderson, P. Pallitto, D. B. Gutierrez, J. Fan, R. K. Crouch, K. L. Schey and Z. Ablonczy, Imaging mass spectrometry of the visual system: Advancing the molecular understanding of retina degenerations *Proteomics. Clinical applications,* 2016, **10**, 391-402.

34 A. C. Grey, P. Chaurand, R. M. Caprioli and K. L. Schey, MALDI Imaging Mass Spectrometry of Integral Membrane Proteins from Ocular Lens and Retinal Tissue *Journal of proteome research,* 2009, **8**, 3278-3283.

35 C. L. Nordgaard, K. M. Berg, R. J. Kapphahn, C. Reilly, X. Feng, T. W. Olsen and D. A. Ferrington, Proteomics of the Retinal Pigment Epithelium Reveals Altered Protein Expression at Progressive Stages of Age-Related Macular Degeneration *Investigative ophthalmology & visual science,* 2006, **47**, 815-822.

36 B. A. Boughton, O. R. B. Thomas, N. J. Demarais, D. Trede, S. E. Swearer and A. C. Grey, Detection of small molecule concentration gradients in ocular tissues and humours *Journal of mass spectrometry.,* 2020, **55**, e4460-n/a.

37 J. L. Norris and R. M. Caprioli, Analysis of Tissue Specimens by Matrix-Assisted Laser Desorption/Ionization Imaging Mass Spectrometry in Biological and Clinical Research *Chemical reviews,* 2013, **113**, 2309-2342.

38 P. M. Angel, K. Norris-Caneda and R. R. Drake, In Situ Imaging of Tryptic Peptides by MALDI Imaging Mass Spectrometry Using Fresh-Frozen or Formalin-Fixed, Paraffin-Embedded Tissue *Current Protocols in Protein Science,* 2018, **94**, e65-n/a.

39 K. Chughtai and R. M. A. Heeren, Mass Spectrometric Imaging for Biomedical Tissue Analysis *Chemical reviews,* 2010, **110**, 3237-3277.

40 O. Vit, P. Man, A. Kadek, J. Hausner, J. Sklenar, K. Harant, P. Novak, M. Scigelova, G. Woffendin and J. Petrak, Large-scale identification of membrane proteins based on analysis of trypsin-protected transmembrane segments *Journal of proteomics,* 2016, **149**, 15-22.

41 E. Patel, M. R. Clench, A. West, P. S. Marshall, N. Marshall and S. Francese, Alternative Surfactants for Improved Efficiency of In Situ Tryptic Proteolysis of Fingermarks *J. Am. Soc. Mass Spectrom,* 2015, **26**, 862-872.

42 E. Patel, in *Imaging Mass Spectrometry*, ed. nonymous , Springer New York, New York, NY, 2017, p. 77-84.

43 C. Calvano, S. Carulli and F. Palmisano, Aniline/a-cyano-4-hydroxycinnamic acid is a highly versatile ionic liquid for matrix-assisted laser desorption/ionization mass spectrometry *Rapid communications in mass spectrometry,* 2009, **23**, 1659-1668.

44 T. Redeby and A. Emmer, Membrane protein and peptide sample handling for MS analysis using a structured MALDI target *Analytical and bioanalytical chemistry,* 2005, **381**, 225-232.

45 J. Franck, R. Longuespée, M. Wisztorski, A. Van Remoortere, R. Van Zeijl, A. Deelder, M. Salzet, L. McDonnell and I. Fournier, MALDI mass spectrometry imaging of proteins exceeding 30,000 daltons *Medical science monitor,* 2010, **16**, BR293-BR299.

46 D. B. Thibault, C. J. Gillam, A. C. Grey, J. Han and K. L. Schey, MALDI Tissue Profiling of Integral Membrane Proteins from Ocular Tissues *J Am Soc Mass Spectrom,* 2008, **19**, 814-822.

47 M. R. Eveque-Mourroux, P. J. Emans, A. Boonen, B. S. R. Claes, F. G. Bouwman, R. M. A. Heeren and B. Cillero-Pastor, Heterogeneity of Lipid and Protein Cartilage Profiles Associated with Human Osteoarthritis with or without Type 2 Diabetes Mellitus *Journal of proteome research,* 2021, **20**, 2973-2982.

48 H. Qiao, V. Spicer and W. Ens, The effect of laser profile, fluence, and spot size on sensitivity in orthogonal-injection matrix-assisted laser desorption/ionization time-of-flight mass spectrometry *Rapid communications in mass spectrometry,* 2008, **22**, 2779-2790.

49 A. Venkatraman, G. Hochart, D. Bonnel, J. Stauber, S. Shimmura, L. Rajamani, K. Pervushin and J. S. Mehta, Matrix-Assisted Laser Desorption Ionization Mass Spectrometry Imaging of Key Proteins in Corneal Samples from Lattice Dystrophy Patients with TGFBI-H626R and TGFBI-R124C Mutations *Proteomics. Clinical applications,* 2019, **13**, e1800053-n/a.

50 A. Tran, I. A. Monreal, E. Moskovets, H. C. Aguilar and J. W. Jones, Rapid Detection of Viral Envelope Lipids Using Lithium Adducts and AP-MALDI High-Resolution Mass Spectrometry *Journal of the American Society for Mass Spectrometry,* 2021, **32**, 2322-2333.

51 F. van Kuijk J.G.M., S. W. McPherson and H. Roehrich, Enhanced Detection of Sub-Retinal Pigment Epithelial Cell Layer Deposits in Human and Murine Tissue: Imaging Zinc as a Biomarker for Age-Related Macular Degeneration (An American Ophthalmological Society Thesis) *Trans. Am. Ophthalmol. Soc.,* 2017, **115**, T3.

52 Ugarte, Marta, DPhil, FRCOphth, N. N. Osborne PhD, L. A. Brown PhD and Bishop, Paul N., FRCOphth, PhD, Iron, zinc, and copper in retinal physiology and disease *Survey of ophthalmology,* 2013, **58**, 585-609.

53 E. K. Sisley, O. J. Hale, I. B. Styles and H. J. Cooper, Native Ambient Mass Spectrometry Imaging of Ligand-Bound and Metal-Bound Proteins in Rat Brain *Journal of the American Chemical Society,* 2022, **144**, 2120-2128.

54 L. E. Flint, G. Hamm, J. D. Ready, S. Ling, C. J. Duckett, N. A. Cross, L. M. Cole, D. P. Smith, R. J. A. Goodwin and M. R. Clench, Characterization of an Aggregated Three-Dimensional Cell Culture Model by Multimodal Mass

Spectrometry Imaging *Analytical chemistry (Washington),* 2020, **92**, 12538-12547.

55 I. Konz, B. Fernández, M. L. Fernández, R. Pereiro and A. Sanz-Medel, Laser ablation ICP-MS for quantitative biomedical applications *Anal Bioanal Chem,* 2012, **403**, 2113-2125.

56 T. Van Acker, S. J. M. Van Malderen, L. Colina-Vegas, R. K. Ramachandran and F. Vanhaecke, Selective ablation of biological tissue and single cells on a glass substrate by controlling the laser energy density of nanosecond 193 nm laser radiation *Journal of analytical atomic spectrometry,* 2019, **34**, 1957-1964.

57 L. Elemental Scientific Lasers, The TwoVol3 Ablation Cell for ESL Platform 2018, .

58 W. J. Bettger, Zinc and selenium, site-specific versus general antioxidation 1993, **71**, 721-724.

59 X. Wang, Z. Wang, H. Gao, G. Danscher and L. Huang, Localization of ZnT7 and zinc ions in mouse retina—Immunohistochemistry and selenium autometallography 2006, **71**, 91-96.

60 S. Zampatti, F. Ricci, A. Cusumano, L. T. Marsella, G. Novelli and E. Giardina, Review of nutrient actions on age-related macular degeneration 2014, **34**, 95-105.

61 T. Léveillard, N. J. Philp and F. Sennlaub, Is Retinal Metabolic Dysfunction at the Center of the Pathogenesis of Age-related Macular Degeneration?2019, **20**, 762.

62 A. Lau, H. Tan and Y. Xu, Epigenetic Effects of Dietary Trace Elements *Curr Pharmacol Rep,* 2017, **3**, 232-241.

63 A. Biesemeier, E. Yoeruek, O. Eibl and U. Schraermeyer, Iron accumulation in Bruch's membrane and melanosomes of donor eyes with age-related macular degeneration 2015, **137**, 39-49.

64 T. N. Abduljabbar, B. L. Sharp, H. J. Reid, N. Barzegar-Befroeid, T. Peto and I. Lengyel, Determination of Zn, Cu and Fe in human patients' serum using micro-sampling ICP-MS and sample dilution 2019, **204**, 663-669.

65 P. Hahn, Maculas affected by age-related macular degeneration contain increased chelatable iron in the retinal pigment epithelium and Bruch's membrane.(Archives of Ophthalmology)(Author Abstract) 2003, **290**, 2525.

66 T. J. Heesterbeek, M. Rouhi-Parkouhi, S. J. Church, Y. T. Lechanteur, L. Lorés-Motta, N. Kouvatsos, S. J. Clark, P. N. Bishop, C. B. Hoyng, A. I. den Hollander, R. D. Unwin and A. J. Day, Association of plasma trace element levels with neovascular age-related macular degeneration 2020, **201**, 108324.

67 E. Aydin, T. Cumurcu, F. Ozugurlu, H. Ozyurt, S. Sahinoglu, D. Mendil and E. Hasdemir, Levels of iron, zinc, and copper in aqueous humor, lens, and serum in nondiabetic and diabetic patients: Their relation to cataract 2005, **108**, 33-41.

68 J. M. Flinn, P. Kakalec, R. Tappero, B. Jones and I. Lengyel, Correlations in distribution and concentration of calcium, copper and iron with zinc in isolated extracellular deposits associated with age-related macular degeneration 2014, **6**, 1223-1228.

69 J. C. Erie, J. A. Good, J. A. Butz and J. S. Pulido, Reduced Zinc and Copper in the Retinal Pigment Epithelium and Choroid in Age-related Macular Degeneration 2009, **147**, 276-282.e1.

70 A. G. M. Jünemann, P. Stopa, B. Michalke, A. Chaudhri, U. Reulbach, C. Huchzermeyer, U. Schlötzer-Schrehardt, F. E. Kruse, E. Zrenner and R. Rejdak, Levels of Aqueous Humor Trace Elements in Patients with Non-Exsudative Age-related Macular Degeneration: A Case-control Study 2013, **8**, e56734.

71 N. K. Wills, V. M. Sadagopa Ramanujam, N. Kalariya, J. R. Lewis and F. J. G. M. van Kuijk, Copper and zinc distribution in the human retina: Relationship to cadmium accumulation, age, and gender 2008, **87**, 80-88.

72 Hajare Q, Mehdi K. Kayser-Fleischer ring in Wilson's disease. The Pan African medical journal. 2018;30:137.

73 F. Virgili, R. Ambra, J. McCormack, Ellen E.A. Simpson, D. Ciarapica, L. Barnaba, E. Azzini and A. Polito, Genetic Polymorphisms and Zinc Status: Implications for Supplementation in Metabolic Diseases *Curr.Pharm.Des.,* 2018, **24**, 4131-4143.

74 M. Maywald and L. Rink, Zinc homeostasis and immunosenescence 2015, **29**, 24-30.

75 M. Ugarte and N. N. Osborne, Recent advances in the understanding of the role of zinc in ocular tissues 2014, **6**, 189-2.

76 J. P. Sang, H. L. Ju, J. W. Se, W. K. Se and H. P. Kyu, Five heavy metallic elements and age-related macular degeneration: Korean National Health and Nutrition Examination Survey, 2008-2011 2015, **122**, 129-137.

77 P. Pao, E. Emri, S. B. Abdirahman, T. Soorma, H. Zeng, S. M. Hauck, R. B. Thompson and I. Lengyel, The effects of zinc supplementation on primary human retinal pigment epithelium 2018, **49**, 184-191.

78 H. Haase and L. Rink, The immune system and the impact of zinc during aging 2009, **6**, 9.

79 M. A. Aras and E. Aizenman, Redox Regulation of Intracellular Zinc: Molecular Signaling in the Life and Death of Neurons 2011, **15**, 2249-2263.

80 N. K. Wills, V. M. Sadagopa Ramanujam, N. Kalariya, J. R. Lewis and F. J. G. M. van Kuijk, Copper and zinc distribution in the human retina: Relationship to cadmium accumulation, age, and gender 2008, **87**, 80-88.

81 D. P. Bishop, D. Clases, F. Fryer, E. Williams, S. Wilkins, D. J. Hare, N. Cole, U. Karst and P. A. Doble, Elemental bio-imaging using laser ablation-triple quadrupole-ICP-MS 2016, **31**, 197-22.

82 T. W. MAY and R. H. WIEDMEYER, A table of polyatomic interferences in ICP-MS 1998, **19**, 150-155.

83 H. I. Wettersten, A. A. Hakimi, D. Morin, C. Bianchi, M. E. Johnstone, D. R. Donohoe, J. F. Trott, O. A. Aboud, S. Stirdivant, B. Neri, R. Wolfert, B.

Stewart, R. Perego, J. J. Hsieh and R. H. Weiss, Grade-Dependent Metabolic Reprogramming in Kidney Cancer Revealed by Combined Proteomics and Metabolomics Analysis 2015, **75**, 2541-2552.

84 C. Keller, P. Wei, B. Wancewicz, T. L. Cross, F. E. Rey and L. Li, Extraction optimization for combined metabolomics, peptidomics, and proteomics analysis of gut microbiota samples 2021, **56**, e4625-n/a.

85 H. Jin, P. Goossens, P. Juhasz, W. Eijgelaar, M. Manca, J. M. H. Karel, E. Smirnov, C. J. J. M. Sikkink, B. M. E. Mees, O. Waring, K. van Kuijk, G. E. Fazzi, M. J. J. Gijbels, M. Kutmon, C. T. A. Evelo, U. Hedin, M. J. A. P. Daemen, J. C. Sluimer, L. Matic and E. A. L. Biessen, Integrative multiomics analysis of human atherosclerosis reveals a serum response factor-driven network associated with intraplaque hemorrhage 2021, **11**, e458-n/a.

Chapter 7

Oral Presentations and Poster Presentations

Oral Presentations

British Mass Spectrometry Society Annual Meeting, Sheffield, UK – September 2021

International Mass Spectrometry Society Annual Meeting, Colorado Springs (Virtual) – October 2021

British Mass Spectrometry Society Imaging Symposium , Sheffield, UK – May 2022

American Society of Mass Spectrometry Annual Conference, Minneapolis, USA – June 2022

RSC Biennial National Atomic Spectroscopy Symposium, Manchester, UK – June 2022

British Mass Spectrometry Society Imaging Annual Conference , Sheffield, UK – September 2022

Poster Presentations

OurCON

IMSS3 International Mass Spectrometry Society 3rd Annual Conference – 2021

ASMS American Society of Mass Spectrometry – Annual Conference – 2020, 2021

BMSS British Mass Spectrometry Society Annual Conference – 2020, 2021

BMSS British Mass Spectrometry Society Imaging Symposium – 2022

European Winter Conference on Plasma Spectrochemistry -2023

American Society of Mass Spectrometry – 2023